

Dissertation ETH number 21142

# **Controlled Crystallization of Complex Confectionery Fats.**

A dissertation submitted to

ETH Zurich

for the degree of

Doctor of Sciences

presented by

Daniel Ehlers

Dipl.-Ing. University of Karlsruhe (TH), Germany

born 9<sup>th</sup> April 1982

citizen of Germany

accepted on the recommendation of

Prof. Dr.-Ing. Erich J. Windhab, Examiner

Prof. Dr. Gregory R. Ziegler, Co-Examiner

Dr. William Hanselmann, Co-Examiner

2012

Copyright © 2012 Daniel Ehlers  
Laboratory of Food Process Engineering (ETH Zurich)  
All rights reserved.

## **Controlled Crystallization of Complex Confectionery Fats.**

ISBN: 978-3-905609-57-8

Food Process Engineering series no. 50

*Published and distributed by:*

Laboratory of Food Process Engineering  
Institute of Food, Nutrition and Health  
ETH Zurich  
ETH Zentrum, LFO  
8092 Zurich  
Switzerland  
<http://www.fpe.ethz.ch/>

*Printed in Switzerland by:*

ETH Reprozentrale Hönggerberg  
HIL C45  
8093 Zurich  
Switzerland



*To me.*



# Acknowledgements

Von August 2008 - Juni 2013 habe ich mein Doktoratsstudium auf dem Gebiet der Fettkristallisation und Schokolade durchgeführt. Während und neben der Arbeit habe ich dabei natürlich nicht nur Daten und Fakten gesammelt, sondern mit vielen Menschen zusammengearbeitet und diskutiert, denen ich an dieser Stelle danken möchte.

Mein Dank gilt als erstem Herrn Prof. Windhab, für sein Vertrauen in mich zunächst als Doktoratsaspiranten und anschliessend während meiner gesamten Doktorandenzeit an der ETH. Es war sehr hilfreich und vor allem lehrreich die Details und die Fokussierung in den Forschungsprojekten auf Basis eigener Vorschläge mit ihm zu diskutieren und ausarbeiten zu können.

I would also like to express my special thanks to Prof. Ziegler for being the Co-Examiner of this thesis. His advice from outside of ETH and from a well known scientist in the field of chocolate and fats was very helpful to examine this piece of work carefully in terms of uniqueness and professional interest.

Ein grosser Dank für die Übernahme des Korreferats, aber vor allem im Hinblick auf das Gelingen der schriftlichen Arbeit gebührt Dr. William Hanselmann. Es war teilweise hart, aber auf jeden Fall nötig, seine Kritik zu diskutieren und das Skript dementsprechend zu überarbeiten. Mit mir muss man manchmal Geduld haben. Und William hatte sie.

Für die (V)Erarbeitung vieler meiner Daten war unser Technikerteam unerlässlich. Ich danke Dani und Jan für die Bauteile, Bruno für praktische Hard- und Software, Bigler für seine Ideen, wie man etwas auseinander oder zusammenbekommt und „wo was wohnt“. Ohne Bernie und seinen Ölfilter (V1-4.0) wäre die Auswertung der Röntgenstreuexperimente bei weitem nicht so übersichtlich durchzuführen gewesen. Hierfür, wie auch für jegliche computertechnische Unterstützung und seine (Fast-) Geduld beim Jassen danke ich ihm an dieser Stelle sehr herzlich. Natürlich darf an dieser Stelle auch Jean-Claude (ISG) nicht fehlen. Er war ebenfalls stets zugegen wenn der Mac nicht so wollte, wie gewünscht. Die Schoggi-Pausen, Skate Nights und Roller-Treffen waren darüberhinaus sehr amüsant.

Da in unserer Gruppe trotz MiWeWi niemand ein SOP für einen Do-it-yourself-Teilchenbeschleuniger verfasst hat, danke ich ebenfalls dem gesamten PSI Swiss Light

Source Team, im Besonderen Frau Dr. Fabia Gozzo und Michael Lange. Die prinzipielle Unterstützung während der 24x7-Studien ist zwar einerseits Teil ihrer Arbeit, andererseits ist aber die Art und Weise eine sehr grosse Hilfe bei der Umsetzung der geplanten Experimente gewesen.

Natürlich wurden viele Rohdaten und Auswertungen, nicht von mir persönlich, sondern stattdessen unter meiner Betreuung erarbeitet. Eine Anzahl an Studenten haben im Rahmen ihrer HiWi-, Bachelor- oder Master-Arbeit engagiert geforscht und somit ebenfalls zum Gelingen dieser Arbeit beigetragen. Deshalb einen grossen Dank an Euch alle: Agnes, Cornelia, Judith, Lea, Adrian, Andi, Emanuel, Jussi und Lukas.

Viele Stunden habe ich auch im Büro verbracht, in dem man ja zum Glück nicht alleine sitzt. Wir sind zwar Naturwissenschaftler, aber Maschinen sind wie eben auch nicht. Es war ein unheimlich grosses Vergnügen, diese Zimmergspönlü über die Jahre an meiner Seite gewusst zu haben: Theo, Duxi, Fabian und Marianne.

Unsere VT-Gruppe ist bekanntlich nicht so klein. Trotzdem hat jeder einzelne einen Anteil an der hervorragenden Arbeitsatmosphäre und der auch damit abhängigen Performance unseres Labors. Ich kann mich sehr glücklich schätzen, ein kleiner Teil davon gewesen zu sein und mich stellvertretend für alle bei Helen, Varvi, Chriggi, Cornelia, Rühli, Heiko, Urs und Res für die schöne, gemeinsame Zeit an der ETH bedanken. Ich hoffe, viele weiterhin auch ausserhalb vom Science-Week Wochenende und dem Sommerfest zu sehen!

Weil sich ein Labor auch nicht von selbst organisiert, zahllose Formulare einzureichen und Deadlines einzuhalten sind, ist es mir ein grosses Anliegen an dieser Stelle vor allem unserer Sekretärin Anna Emslander meine Hochachtung auszusprechen.

Die letzten Jahre sind vor allem möglich gewesen, weil meine Familie trotz vieler Luftkilometer auch schon im Studium in Karlsruhe im Kopf immer bei mir war. Natürlich erarbeitet man sich selber hier und da Chancen. Aber all die wichtigen Kleinigkeiten, die man schon zuhause vorgelebt bekommen hat, waren und sind in meinen Augen nicht minder wichtig auf dem Weg durch das Arbeitsleben. Und da ist auch ein Doktorat keine Ausnahme.

5 Jahre ist eine lange Zeit. Aber Katja und ich sind trotz unzähliger Bahnkilometer immer noch da. Ich bin Dir unendlich dankbar! Infolgedessen haben wir auch eine Zweitausbildung als SBB- und DB- Zugansager genossen:

Prochain arrêt Ulm - next stop Ulm...

Zürich, im Juli 2013

# Table of Contents

<b>Acknowledgements</b>	<b>v</b>
<b>Notation</b>	<b>ix</b>
<b>Abstract</b>	<b>xvii</b>
<b>Zusammenfassung</b>	<b>xix</b>
<b>1. Introduction</b>	<b>1</b>
<b>2. Background</b>	<b>5</b>
2.1. Confectionary Fats . . . . .	5
2.1.1. Chemical . . . . .	6
2.1.2. Physical . . . . .	9
2.2. Chocolate Processing . . . . .	20
2.2.1. Precrystallization . . . . .	21
2.2.2. Moulding . . . . .	24
2.2.3. Cooling . . . . .	25
2.2.4. Spray Chilling - Prilling . . . . .	28
<b>3. Materials, Processes and Methods</b>	<b>31</b>
3.1. Materials . . . . .	31
3.1.1. Vegetable Fats . . . . .	31
3.1.2. Confectionery Masses . . . . .	34
3.2. Processes . . . . .	34
3.2.1. Seed Production . . . . .	34
3.2.2. Precrystallization . . . . .	38
3.2.3. Moulding . . . . .	41
3.2.4. Cooling . . . . .	43
3.2.5. Spray Chilling . . . . .	45
3.3. Methods . . . . .	46
3.3.1. Melting Characteristics . . . . .	46
3.3.2. Solid Fat Content . . . . .	47
3.3.3. Solidification Kinetics . . . . .	49

3.3.4. Contraction . . . . .	51
3.3.5. Analytical Shear Application . . . . .	55
3.3.6. X-Ray Crystallography . . . . .	56
3.3.7. Temper Analysis . . . . .	62
3.3.8. Mould Detachment . . . . .	62
3.3.9. Texture Analysis . . . . .	66
3.3.10. Fat Bloom Analysis . . . . .	67
3.3.11. Confocal Laser Scanning Microscopy . . . . .	68
3.3.12. Particle Size Analysis . . . . .	69
3.3.13. Powder Flow Property . . . . .	70
<b>4. Nucleation and Crystallization Kinetics of Fats</b>	<b>71</b>
4.1. Shear Induced Nucleation and Crystal Growth . . . . .	71
4.1.1. Reduction of Nucleation Time . . . . .	71
4.1.2. Polymorphism of Crystallizing Fats under Shear . . . . .	74
4.2. Quantitative Seed Effects on Solidification . . . . .	93
4.2.1. Crystallization Kinetics . . . . .	94
4.2.2. Contraction Kinetics . . . . .	104
<b>5. Knowledge Transfer to Industrial Cooling Concepts</b>	<b>115</b>
5.1. Structure Density of Cocoa Butter . . . . .	115
5.2. Cooling Limits for Praline Production . . . . .	122
5.3. Seed Powder Processing . . . . .	139
<b>6. Conclusions</b>	<b>151</b>
<b>Bibliography</b>	<b>155</b>
<b>Appendix</b>	<b>167</b>
<b>A. Methods</b>	<b>169</b>
<b>B. Results</b>	<b>173</b>

# Notation

## Latin Letters

Symbol	Unit	Definition
$a^*$	-	chromatic component from green to red (HUNTER scaling)
$A$	$m^2$	surface
$A_1$	$m^2$	cross-sectional area of a rod-like crystal grain
$A_2$	m	thickness of a plate-like crystal
$A_3$	m	shape factor of a spherical crystal, $4\pi/3$
$b^*$	-	chromatic component from blue to yellow (HUNTER scaling)
$c$	-	concentration by mass fraction
$c_{\text{light}}$	m/s	speed of light, $2.998 \cdot 10^8$ m/s <sup>a</sup>
$C$	Pa	compression (or bulk) modulus
$c_d$	-	drag coefficient
$c_p$	J/(g K)	specific heat capacity for p=const.
$d$	mm, cm	diameter
$d_{\text{XRS}}$	nm	distance of crystallographic planes (d-spacing)
$D$		place holder for a group of variables of $t_{\text{ind}}$
$D^*$		place holder for a group of variables of $t_{\text{ind}}$
$D_1$		place holder for $A_1 \dot{I} N_0$ in Avrami's 1D equation
$E$	J	energy
$E_{\text{mod}}$	Pa	elastic modulus
$E_{\text{beam}}$	keV	x-ray beam energy
$\dot{E}_{\text{diss}}$	$J/(m^3 s)$	volumetric energy dissipation by frictional heat per time
$f_{\text{NMR}}$	-	extrapolation factor of SFC evaluation by NMR
$f$	Hz	frequency
$ff_c$	-	characteristic flowability of a bulk soild
$F^*$		place holder for a group of variables of $t_{\text{ind}}$
$g_{\text{abs}}$	1/min	absolute growth rate

continued on next page

## Notation

Symbol	Unit	Definition
$g_{\text{rel}}$	1/min	relative growth rate
$G$	J	Gibb's free energy
$G'$	Pa s	storage modulus
$G''$	Pa s	loss modulus
$h$	Js	Planck constant, $6.626 \cdot 10^{-34}$ Js) <sup>a</sup>
$h_{\text{plain}}$	m	thickness of overflowing plain
$H$	J	enthalpy
$k_A$	1/s	rate constant of <i>Approximate Avrami Equation</i>
$k_{\text{NMR}}$	-	averaged slope of solid signal domain (NMR)
$k_B$	J/K	Boltzmann constant, $1.381 \cdot 10^{-23}$ J/K <sup>a</sup>
$\dot{l}$	m/s	one dimensional growth rate of crystal grain
$l$	m	one dimensional length of a crystal grain
$L$	m	characteristic length
$L^*$		luminance (HUNTER scaling)
$m$	kg	mass
$m_A$	-	exponent of <i>Approximate Avrami Equation</i>
$n$	1/min	rotation frequency
$N$	-	number density of crystal grains
$o_{\text{NMR}}$	-	digital offset factor (NMR)
$p$	bar	pressure
$p_A$	-	probability of crystal growth per unit time
$\dot{Q}$	J/s	heat flux
$r$	m	radius
$R_{\text{US}}$	-	fraction of reflected ultrasound energy
$R^2$	-	coefficient of determination
$s$	°C/min	slope value of temperature vs. time
$s_{\text{HT}}$	m	representative length for heat transfer
$S$	J/K	entropy
$t$	s, min	time
$t_1$	s	spin-grid relaxation time (NMR)
$t_2$	s	spin-spin relaxation time (NMR)
$T$	K, °C	temperature
$T_{\text{US}}$	-	fraction of transmitted ultrasound energy
$\Delta T_{\text{sub}}$	K, °C	absolute value of supercooling temperature difference (subcooling)
$v$	m/s	velocity
$v_{\text{grain}}$	$m^3$	volume of a single crystal grain
$v_{\text{mol}}$	$m^3$	molecular volume

continued on next page



---

Symbol	Unit	Definition
$V$	$m^3$	volume
$V_e$	$m^3$	volume of crystal grains
$\dot{V}$	ml/min	volume flow rate
$x_{10,3}$	$\mu m$	particle diameter, 10%-percentile of volume distribution
$x_{50,3}$	$\mu m$	particle diameter, 50%-percentile of volume distribution, median value
$x_{90,3}$	$\mu m$	particle diameter, 90%-percentile of volume distribution
$z$	-	dimensionless time
$Z$	$(kg)/(m^2s)$	acoustic impedance

---

## Greek Letters

Symbol	Unit	Definition
$\alpha$	W/K	heat transfer coefficient
$\alpha$	-	crystal form
$\beta$	-	crystal form
$\beta'$	-	crystal form
$\Delta_{\text{span}}$	-	span of a particle size distribution
$\eta$	Pa s	viscosity
$\gamma$	-	crystal form
$\gamma^*$	mN/m	interfacial tension
$\dot{\gamma}$	1/s	shear rate
$\Theta$	°	scattering angle
$\kappa$	-	adiabatic exponent
$\lambda$	W/(m K)	heat conduction coefficient
$\lambda$	nm	wave length
$\xi$	%	relative, oscillatory deformation
$\nu$	Hz	atomic vibration frequency
$\rho$	$g/cm^3$	mass density
$\sigma$	J/m <sup>3</sup>	free energy of solid- liquid interface
$\sigma_1$	kPa	consolidation stress
$\sigma_c$	kPa	unconfined yield strength
$\sigma_{\text{pre}}$	kPa	normal preshear stress
$\sigma_{\text{sh}}$	kPa	normal shear stress

---

continued on next page

---



---

<sup>a</sup>Tipler and Mosca (2003)

## Notation

Symbol	Unit	Definition
$\tau$	min	characteristic time, Avrami kinetic
$\tau_{\text{pre}}$	kPa	preshear stress
$\tau_{\text{sh}}$	kPa	shear stress
$\phi$	°	deformation angle
$\omega$	rad/s	angular frequency of oscillation
$\omega_{\text{rot}}$	rad/s	angular velocity of rotation

## Indices

Symbol	Definition
<b>subscripts</b>	
act	activation
approx	approximated
ave	average
choc	chocolate
cond	conduction (heat)
cool	cooling
cor	correction
crit	critical value
cryst	main crystallization
end	endset
f	fusion, melting
g	gas
hom	homogeneous
i	inner
inc	incorporation
ind	induction
inf	inflection
lam	laminar
liq	liquid
m	molar
melt	melting
meta	metastable
max	maximal
min	minimal value
n	nozzle
continued on next page	

---

Symbol	Definition
o	outer
pre	pre-conditioning
prod	product
rel	relativ
ripe	ripening
s	surface
start	starting value
sol	solvent
stor	storage
sup	supercooling
trans	transfer (heat)
tot	total
turb	turbulent
US	ultrasound
v	volumetric

---

## Dimensionless Numbers

Symbol	Definition
$Bi$	Biot number
$Nu$	Nusselt number
$Oh$	Ohnesorge number
$Pr$	Prandtl number
$Re$	Reynolds number
$We$	Weber number
$WI$	whiteness index

---

## Abbreviations

Symbol	Definition
III	crystal form of cocoa butter
1D	one dimensional
2D	two dimensional
2L	$\equiv$ -2, long spacing stacking, fatt acid bilayer
3D	three dimensional
3L	$\equiv$ -3, long spacing stacking, fatt acid trilayer
C <sub>6</sub>	caproic acid
C <sub>8</sub>	caprylic acid
C <sub>10</sub>	capric acid
CB	cocoa butter
CBR	cocoa butter replacer
CDF	center depositing filling
CLSM	confocal laser scanning microscopy
CO	cocos oil
d.p.	dripping point
DSC	differential scanning calorimetry
DSP	digital signal processor
H	hexanoic acid
H <sub>⊙</sub>	hexagonal carbon chain packing in crystals
HO	hazelnut oil
HPLC	high performance liquid chromatography
NMR	(pulsed) nuclear magnetic resonance
L	lauric acid
LA	Laurina <sup>®</sup> fat
Li	Linoleic acid
ls	long spacing
m.a.	melting area
m.p.	melting point
M	myristic acid
M1	method 1 of contraction evaluation
M2	method 2 of contraction evaluation
O <sub>⊥</sub>	orthorhombic carbon chain packing in crystals
OOO	triglyceride of by combination of O-O-O
PIDS	polarization intensity differential scattering
PK	palm kernel oil
PKS	palm kernel stearin
continued on next page	

---

Symbol	Definition
PM	palm mid fraction
PO	palm oil
POP	triglyceride of by combination of P-O-P
POS	triglyceride of by combination of P-O-S
PS	palm stearin
PSD	particle size distribution
PSI	Paul Scherrer Institute
PSS	palm super stearin
ss	short spacing
S	stearic acid
Sat	saturated fatty acid
SD	standard deviation
SOS	triglyceride of by combination of S-O-S
SFC	solid fat content
SH	sample holder
SSHE	scraped surface heat exchanger
T <sub>  </sub>	triclinic carbon chain packing in crystals
TA	texture analysis
US	ultrasound
Unsat	unsaturated fatty acid
WB	water bath
XRD	x-ray diffraction
XRPD	x-ray powder diffraction
XRS	x-ray scattering

---



# Abstract

The crystallization characteristics of natural, vegetable fats used in the confectionery industry, vary strongly as a result of their triglyceride composition. Predictions of polymorphic behavior, nucleation times, crystallization kinetics and contraction ability are not possible so far for these systems, not to mention for binary or ternary mixtures. Nevertheless, detailed knowledge of these properties is crucial for an optimal processing of chocolate products containing fats as the continuous and structuring phase. Besides product quality, process efficiency is also of interest in this context.

In this work the effect of designed crystal seeds on the crystallization properties of lauric and non-lauric confectionery fats was investigated. The individual seed suspensions were produced by the concept of high shear crystallization.

The nucleation time as well as the polymorphic transformation period from an  $\alpha$  to a  $\beta'$  state is consistently reduced as a function of the applied shear rate. With respect to a relevant process time, further transformation into the  $\beta$  form is temperature controlled. The lauric fats coconut, palm kernel and palm kernel stearin are  $\beta'$  stable only. Supplementary, high shear conditions guarantee the generation and stabilization of rather small crystal seeds.

Fat specific seeding of molten fat by small amounts of corresponding seed suspension results in direct crystal growth of the most stable polymorphic structure even at gentle supercooling conditions. Uncontrolled nucleation is thereby inhibited. An universal correlation of supercooling temperature difference to representative crystal growth rate is evident for lauric as well as non-lauric fats. The absolute contraction ability is predominantly a function of the final solid fat content. The volume density of crystalline fat increases up to 10 % compared to liquid fat. High stable forms show the most dense structuring. Therefore, the contraction progression of seeded fats is not only accelerated and homogenized by a controlled number density of seed crystals, but also slightly enhanced.

By inline monitoring of the crystallization process in a cooling tunnel (forced convection), the delay of filling to shell crystallization for praline systems produced by One-Shot moulding becomes evident. It exists a minimum crystallization temperature to preserve the polymorphic quality of cocoa butter based products. The inline detection of the product-mould detachment process is possible by a revised version of

an ultrasound based in-house development, *DetachLog V2.0*. It reveals the contraction deficit for nucleation based solidification by low stable crystals of cocoa butter. The successful production of high quality seed powder by spray-chilling (*prilling*) of concentrated seed suspension provides a third option for precrystallization besides conventional tempering and suspension seeding. The powder is different to commercial products, as it is thermodynamically stable directly after production and contains a significant amount of the most stable  $\beta^{VI}$  crystals, reflecting the advantages of the seed suspension over the conventional tempering method. Especially for small enterprises and confectioners the application of powder seeds can be of practical and economical interest, since the application of powder is more flexible than a single tempering device.

In general, the crystallization and contraction kinetics of confectionery fats are triggered by the supercooling temperature difference and the corresponding solid fat content, respectively. Fat specific suspension seeding is beneficial not only in terms of crystallographic stabilization, but also with respect to crystallization kinetics (cooling time reduction) and structure density (contraction, fat bloom stability) of the final crystal network. The optimal amount of seed material should be seen as a function of the subsequent cooling conditions. It can be quantified by inline analysis and can be well adjusted by the concept of suspension seeding. Industrial cooling periods can be further reduced by consideration of this interdependency. High amounts of seed crystals will enable the application of stronger cooling conditions at a consistent quality level. In addition the maximization of a feasible cooling air speed is of major importance, to improve heat transfer. It was confirmed to be less critical in terms of internal product temperature gradients (polymorphism) and the risk of condensation than a simple reduction of the cooling air temperature.



# Zusammenfassung

Die Kristallisationseigenschaften der in der Schokoladenindustrie verwendeten, natürlichen Pflanzenfette variieren als Resultat ihrer komplexen Triglyceridzusammensetzung. Der Polymorphismus, die Nukleationszeit, die Kristallisationskinetik und das Kontraktionsverhalten sind für diese Reinfette derzeit nicht berechenbar. Folglich sind auch die Eigenschaften von Fettmischungen nur experimentell bestimmbar. Nichtsdestoweniger ist die Kenntnis dieser Eigenschaften notwendig, um den Herstellungsprozess von Schokoladenprodukten zu optimieren, die Fett als kontinuierliche und somit strukturgebende Matrix beinhalten.

In dieser Arbeit wurde der Effekt von gezielt hergestellten Impfkristallen auf die Kristallisationseigenschaften von laurischen und nicht-laurischen Schokoladenfetten untersucht. Die fettspezifischen Impfkristallsuspensionen wurden mittels Hochshear-kristallisation hergestellt.

Die Nukleationszeit von  $\alpha$ -Kristallen und deren Transformation in eine stabilere  $\beta'$  Struktur werden mit steigender Scherrate stetig verkürzt. Um relevante Prozesszeiten zu erreichen, kann die weitere Transformation in die hochstabile  $\beta$ -Form durch eine gezielte Temperaturerhöhung induziert werden. Laurische Fette wie Kokos, Palmkern und Palmkernstearin sind  $\beta'$  stabil. Rein kristallographisch ist in diesen Fällen keine Temperaturreifung notwendig.

Neben der Kinetikbeschleunigung bewirkt Hochshearung auch die Bildung und Stabilisierung von vergleichsweise kleinen Impfkristallen. Bereits bei geringen Impfmengen und Unterkühlungstemperaturen bewirkt das spezifische Animpfen von Fetten ein direktes Kristallwachstum der stabilsten Kristallstruktur. Gleichzeitig wird eine unkontrollierte Nukleation unterbunden. Eine allgemeingültige Korrelation von Unterkühlungstemperatur und relativem Kristallwachstum ist sowohl für laurische, als auch für nicht-laurische Fette festzustellen. Das Kontraktionsverhalten ist hauptsächlich eine Funktion des erreichten Festfettgehalts. Die Volumendichte von kristallinem Fett ist bis zu 10 % höher im Vergleich zu flüssigem Fett. Darüberhinaus weisen die stabilsten Kristallformen die höchsten Einzelstrukturichten auf. Der Kontraktionsverlauf von Fetten wird durch Animpfen daher nicht nur beschleunigt und homogenisiert, sondern auch leicht verstärkt.

Die zeitliche Verzögerung der Füllungskristallisation gegenüber der Schokoladenhülle von Pralinensystemen, die im *One-Shot* Verfahren hergestellt werden, kann durch inline Messungen nachgewiesen werden. Die Hauptkristallisation von Kakaobutter basier-

ten Produkten sollte oberhalb der kritischen Schmelztemperatur der niedrigstabilen  $\alpha$ -Kristalle stattfinden, um die Bildung der gewünschten, hochstabilen Strukturen sicherzustellen. Das Ablösen der Praline von der Form während des Kühlvorgangs kann ebenfalls inline durch die überarbeitete Version einer Ultraschall basierten Messtechnik (*DetachLog V2.0*, Eigenentwicklung der ETH Zürich) bestimmt werden. Die Ergebnisse bestätigen ein Kontraktionsdefizit des Produkts bei zusätzlicher Nukleation von instabilen Kristallkeimen durch Unterschreiten der vorab erwähnten, minimalen Kristallisationstemperatur.

Das Einmischen von Impfpulver ist eine dritte Möglichkeit der Vorkristallisation neben klassischem Temperieren und dem Animpfen mit frisch hergestellter Kristallsuspension. Mittels Tieftemperatur-Sprühkristallisation (*prilling*) einer konzentrierten Impfkristallsuspension kann ein hochwertiges Kakaobutter-Impfpulver hergestellt werden, dass sich durch eine sofortige Kristallstabilität direkt nach der Produktion und einer erhöhten Temperaturstabilität gegenüber kommerziellen Pulvern auszeichnet. Dieses Produkt könnte vor allem für kleine Betriebe aus praktischen und ökonomischen Gründen interessant sein, weil die Anwendung von Impfpulver wesentlich flexibler ist als die Produktion einer einzelnen Temperiermaschine.

Allgemein werden die Kristallisations- und Kontraktionskinetiken der untersuchten Schokoladenfette durch die Unterkühlungstemperatur der Schmelze und den erzielten Festfettgehalt bestimmt. Das Impfen mittels fettspezifischer Kristallsuspensionen verbessert nicht nur die Kristallstrukturstabilität, sondern beschleunigt zusätzlich die Kinetiken (Kühlzeitverkürzung) und erhöht die Strukturichte (Kontraktion, Fettreifstabilität). Die Impfkristallkonzentration sollte als Funktion der anschliessenden Unterkühlung angesehen werden. Sie kann durch inline Messungen bestimmt und durch die Anwendung der Impftechnik auf einfache Weise angepasst werden. Es wird vermutet, dass industrielle Kühlzeiten durch Anwendung der Messtechnik und unter Berücksichtigung dieser gegenseitigen Beziehung reduziert werden können. Dass Maximieren einer unkritischen Luftgeschwindigkeit im Kühltunnel ist für diesen Zweck ein wichtiger Punkt, um den Wärmeübergang zu verbessern. Bei vergleichbaren Gesamtkühlzeiten bis zum Formablösen führt diese Beschleunigungsmassnahme generell zu einer weniger kritischen Erniedrigung der äusseren Produkttemperaturen und zu einer geringeren Erhöhung des produktinternen Temperaturgradienten als eine einfache Absenkung der Kühlungstemperatur.

# 1. Introduction

Vegetable fats have a wide range of application in the food, but also in the pharmaceutical and cosmetic industry. They are used as stabilizer, thickener, creamer and as carrier for agents and flavors. Protective embedding and enhanced bioavailability of hydrophobic active agents are convincing properties of fats for their application in fat and emulsion systems and are therefore often used in nutritive foods but also creams and lotions. Within the dairy, pastry and confectionery industry for instance, fats and oils can depict different structure-property relationships. Milk fat suspended by small amounts in a continuous water phase (o/w-emulsion) as in drinks or regular milk cream, influences the viscosity and thereby mouth feeling. By further increase of the fat content, a yield stress can be reached (e.g. mayonnaise products). The fat is also essential for the structure of whipped dairy products. In this case, the firmness is achieved by integration of air resulting in additional interface stabilized by micro fat particles.

In butter or margarine the water stays for the disperse and the fat for the continuous phase (w/o-emulsion). The solid fat content (SFC) of the fat phase is rather high resulting in plastic to rigid properties. The SFC is thereby a function of temperature as the triglyceride mixture of the fat has a melting range instead of a melting point in contrast to chemically pure systems. However, process realization can be also crucial as in the case of puff pastry margarines. A good plasticity is desired to ensure deformable and continuous fat layers during multiple folding and rolling of the initial dough-fat-dough composition. For this purpose, the fat crystal network should be rather a highly concentrated crystal suspension directly after production. This is usually realized by a network disruption after crystallization by the use of pin-mixers. The application of low temperature extrusion is an alternative, where crystallization and plasticizing are coupled. Nevertheless, for slow crystallization kinetics during production, rigid fat crystal bridges may form during post crystallization on storage. Furthermore crystalline solid-solid transformation processes of unstable polymorphs lead also to crystal clustering as a side-effect. In both cases, the plasticity is lost prior to the final application of the margarine in the puff pastry process.

Within the confectionery industry, process development engineers deal with similar boundary conditions for the manufacturing of chocolate and chocolate products, whereas the final goal may differ. The integrative term *structure density* implies properties on multiple dimensions. Molten dark chocolate is a fat based suspension out of cocoa butter (CB), sugar, cocoa particles and the emulsifier lecithin. Similar

to the margarine fat, the cocoa butter exhibits crystallization kinetics as a function of cooling temperature. Moreover, this fat shows polymorphic behavior resulting in six crystalline subcell structures. The quality characteristics surface gloss, *snap* (fracture sound), melting and storage stability of chocolate are related to the presence of the specific crystal form  $\beta^V$ . This polymorphic form can not be directly achieved at cooling out of the complete melt on a productive time scale. Therefore precrystallization is generally carried out either by classical tempering of the whole chocolate mass or by seeding with a cocoa butter crystal suspension (CBCS). Seeding is a rather novel concept in terms of industrial realization (Zeng, 2000). Crystallization into the  $\beta^V$  subcell structure results in several advantages as indicated before. Regarding crystallization kinetics, the nucleation time is bypassed as seed crystals are already existing in both cases of precrystallization technique. The  $\beta$  form features the highest volume densities. Hence, the absolute contraction is optimal in terms of product detachment from the mould during cooling. Finally this structure is thermodynamically more stable than a  $\beta'$  (named  $\beta^{IV}$  for cocoa butter) or  $\alpha$  form. Thereby the development of fat bloom by crystallographic transformation into the most stable  $\beta^{VI}$  form is delayed. For filled products, such as pralines, bloom can be also induced by migration of filling oils into the chocolate shell. In this case, the oil destabilizes the cocoa butter crystals. Finally the migrated triglycerides recrystallize on the products surface and are therefore visible regardless of their crystallographic structure. The more stable and the more dense the crystal network of the chocolate shell, the slower the migration of the filling oils (Motwani *et al.*, 2011). In general, the presence of cocoa butter  $\beta^V$ -seed in chocolate yields in reduced cooling times, increased contraction ability, a homogeneous crystallization of the fat network, desired melting characteristics and a delay of fat bloom development compared to non-seeded masses.

The term *precrySTALLIZATION* is used in this work as a general term for the generation or addition of seed crystals in a fat based sample. Precrystallization processes for cocoa butter based products are successfully applied since several decades from a practical point of view. The structural effects were also investigated qualitatively on a scientific level. However, the quantification of the seeding effects on kinetics and their interpretation for a production process has not been carried out in detail. Cocoa butter is the best analyzed of the confectionery fats. Consequently, no comprehensive concept exists so far to categorize in detail all fats applied in the confectionery industry within this context.

The objective of this work is therefore to perform qualitative and quantitative investigations on the crystallization characteristics of representative, confectionery fats as effected by compatible seed application. The fats of interest are: cocos, palm kernel, palm kernel stearin, palm, palm mid fraction, palm stearin fractions and cocoa butter.

---

The production of seed material is based on the concept of high-shear crystallization. Therein, it is further of interest to gain insight into the crystallographic development of confectionery fats nucleating out of the melt. In the context of combined chocolate products, the crystallization as well as contraction kinetics of single fats and their divergence are of importance. These informations are essential for a sustainable optimization of the process steps moulding and cooling of filled products in terms of product quality and process efficiency.

This work is split into two major parts. On one hand, suitable analysis methods on a lab scale are applied on pure natural fat systems for detailed characterization of the controlled nucleation and solidification kinetics of several fats including crystallographic determinations. On the other hand, these findings are complemented and validated by investigations on a pilot plant production scale with pure cocoa butter as well as chocolate masses. Moulding was realized by *One-Shot* technology. Cooling was performed by controlled air convection. Thereby the universal validity of laboratory findings for representative process equipment including its boundary conditions is assessed. Finally, the production of storable seed powder by a spray-chilling (*prilling*) process is explained by the example of cocoa butter.



## 2. Background

### 2.1. Confectionary Fats

Confectionary fats are a specified class of the bigger pool of edible fats and oils. The most prominent member is cocoa butter, based on its convenient material properties: melting range, hardness and homogeneous polymorphic uniqueness. The latter can be a problem at the same time as shown later. The fat is obtained from the seeds of the cocoa tree *Theobroma cacao*. It is cultivated along the equator mainly up to 20° latitude in Africa, Central and South America as well as Asia and Oceania. The Ivory Coast is the world's largest producer with 34 %, followed by Ghana (18.5 %) and Indonesia (13.5 %). The world production of cocoa beans was steadily raised from 0.8 Mt/a around 1950 to 3.58 Mt/a in 2009 (Rohsius *et al.*, 2010). With an average content of 56 %, the cocoa butter production is calculated to 2.0 Mt/a. An additional boost was observed from the 1980's on. Growth rate was around 9 %/a from thereon. Other vegetable fats used in the confectionary industry are mainly chosen to partly replace, completely substitute or supplement the cocoa butter to achieve similar or slightly different properties in the mouth feeling. Some synonyms of these classes in common use are listed in Timms (2003a). They will be summarized by the term *non-cocoa butter fats* within this work. Palm oil plays the most important role besides illipé, sal and shea butter (Talbot, 2009). It is obtained from the mesocarp of the oil palm (*Elais guineensis* and *Elais olifera*). Its main growing areas are Malaysia and Indonesia with 50 % and 33 % of the world total production of 23.5 Mt/a (Timms, 2003a). The fat can be fractionated, re-blended and esterified into several fat products. They have a high content of the saturated palmitic but also of the unsaturated oleic acid and are therefore a candidate for replacing cocoa butter. These fats are generally called *non-lauric*. Finally fat of the palm kernel together with coconut oil represent by far the most important lauric fats. As the name implies, these fats are high in the short-chained lauric acid and generally low in unsaturated acids in addition. Coconut oil is obtained from the nut of the coconut palm (*Cocos nucifera*). While the annual production of palm kernel oil increased naturally with the oil palm cultivation up to 3 Mt/a, the coconut oil production stayed rather constant on the 1970's level (Timms, 2003a).

## 2. Background

---

In the following subchapters the most important properties of a confectionery fat and the fat specific differences with respect to the presented work are highlighted from a physico-chemical point of view.

### 2.1.1. Chemical

In general, confectionery fats contain mainly triglycerides (triacylglycerols) and small amounts of diglycerides, monoglycerides, free fatty acids, and phospholipids. The triglyceride composition and first of all the fatty acid distribution are crucial for the physical properties of the fat product. Within cocoa butter, stearic (S) and oleic acid (O) with 35 % each and palmitic acid (P) with 26 % represent already >95 % of the total fatty acid distribution (Chaiseri and Dimick, 1989; Foubert *et al.*, 2004). This results in a triglyceride composition strongly dominated by Sat-O-Sat (82.5 %, Sat: saturated), followed by Sat-OO (8.5 %), Sat-Li-Sat (4.5 %, Li: linoleic) and OOO (5 %) in an international average. Consistently, an unsaturated fatty acid is situated in the middle position of the glyceride backbone (>98 %). More details are given in the Table 2.1 and is provided by (Talbot, 2009; Timms, 2003a).

Crude palm oil shows also high amounts of palmitic (45 %) and oleic acids (40 %) similar to cocoa butter (Che Man *et al.*, 1999; Gunstone, 2011). However, the fraction of stearic acid (5 %) is very low and even topped by the linoleic acid (10 %), representing a double-unsaturated carbon chain. Consequently the combination in triglycerides is no longer comparable to cocoa butter. The spread of different combinations is therefore increased, headed by POP/PPO (29 %), POO (23 %) and PLO (10 %). Furthermore, the general uniformity of Sat-Unsat-Sat (saturated-unsaturated-saturated) is no longer given. Even though the main melting range is conform to the requirements for a cocoa butter replacer, the physical properties differ tremendously based on triglyceride composition. A stearin fraction is obtained by a fractionation process (Braipson-Danthine and Gibon, 2007; Che Man *et al.*, 1999; Deffense, 1985). This can be repeated at higher temperatures to achieve a better purity of the high temperature stable triglycerides, here namely PPP. The effect of palm fractionation on the triglyceride composition is shown in Table 2.1.

For lauric fats not only the triglyceride compositions is diverse but also the fatty acid distribution is bigger (Fig. 2.2, see also Laureles *et al.*, 2002). Furthermore, the averaged chain length of the fatty acids shifts from 16-18 for the non-lauric to 12-14 for the lauric fats. The differences between coconut and palmkernel oil are rather small (Ibrahim *et al.*, 2003; Pantzaris and Basiron, 2002). Logically, lauric acid dominates with 48 %, followed by myristic (17 %) acid. The most significant difference of palm kernel and coconut oil is stated for the oleic acid (18:1). The content in palm kernel is doubled (15 %) on the lack of caprylic (8:0) and capric acid (10:0) relative to coconut oil. In general, melting range of these fat crystals is reduced for lower fatty acid chain



Table 2.1.: Triglyceride composition of palm fats and cocoa butter in mol-%, listed by number of unsaturated fatty acids.

triglyceride type	carbon number	palm		cocoa
		refined Che Man	stearin <i>et al.</i> (1999)	refined Foubert <i>et al.</i> (2004)
Sat <sub>3</sub> :				
PPP	48	5.51	27.16	0.19-0.51
PPS	50	1.06	5.06	0.58-0.95
Sat <sub>2</sub> -Unsat:				
POP	50	29.62	23.36	17.0-19.4
PPO	50			
PLi <sup>a</sup> P	44	9.23	7.18	1.55-2.18
PPLi	44			1.36-2.18
POS	52	4.9	3.85	38.6-41.7
SOS	54			23.8-26.3
SOA	56			1.05-1.34
PLiS	46			2.46-3.10
MPLi	42	2.20	2.22	
Sat-Unsat <sub>2</sub> :				
POO	52	23.26	9.4	1.8-5.96
PLiO	46	9.68	4.53	0.32-0.51
SOO	54	2.24	2.47	2.09-7.0
Unsat <sub>3</sub> :				
OOO	54	4.40	2.14	<1.51
sum		92.10	87.57	>90.8

<sup>a</sup>linoleic acid

length. Thereby, the maximum melting range of refined lauric fats is lower than for palm fats. On the other hand, this can be observed for an increase of unsaturated chains as well. In this case the palm kernel oil finally has a slightly enhanced melting range (m.p. 28 °C) compared to coconut oil (m.p. 25 °C). Beyond this, a fractionation process to palm kernel stearin can be performed for palm kernel oil, yielding enhanced fractions of trisaturated triglycerides containing lauric and myristic acid (Tang *et al.*, 1995). Thereby the melting range is designed towards the region of well crystallized cocoa butter (Calliauw *et al.*, 2005).

## 2. Background

---

Table 2.2.: Triglyceride composition of lauric fats in mol-%; listed by carbon number (mean values), most representative TAG types indicated (Bezard, 1971; Tang *et al.*, 1995).

triglycerides		coconut	palm kernel	
carbon number	type	refined	refined	stearin
28	C <sub>6</sub> <sup>a</sup> C <sub>10</sub> <sup>b</sup> L	0.8	0.6	0.1
	C <sub>8</sub> <sup>c</sup> C <sub>8</sub> L			
30	C <sub>8</sub> C <sub>10</sub> L	3.5	1.3	0.5
	C <sub>6</sub> LL			
32	C <sub>8</sub> LL	13.4	6.3	3.3
34	C <sub>8</sub> LM	17.1	8.4	6.5
	C <sub>10</sub> LL			
36	LLL	19.1	23.3	27.5
38	LLM	16.5	17.0	24.8
40	LLP	10.2	9.8	15.2
	LMM			
42	LLS <sup>d</sup>	7.3	9.1	9.2
	LMP			
44	LMS	4.1	6.6	5.2
46	LPS	2.5	5.1	3.0
48	LSS	2.1	5.8	2.4
	MPS			
50	MSS	1.5	2.3	0.9
	PPS			
52	PSS	1.2	2.2	0.7
54	SSS	0.7	0.5	0.7
sum		100.0	98.3	100.0

---

<sup>a</sup>caproic acid

<sup>b</sup>capric acid

<sup>c</sup>caprylic acid

<sup>d</sup>S means Stearic+Oleic (=C18) in this table only:

## 2.1.2. Physical

### Crystallography

**Basics:** Triglycerides in the solid state are aligned in crystalline structures. Lutton (1950) reviewed the knowledge about the subcell packing from mono- up to triglycerides. Larsson followed this route, further refining the nomenclature especially for triglyceride systems (Larsson, 1966, 1972). In general, classification of the main crystal structures into  $\alpha$ ,  $\beta'$  and  $\beta$  with increasing temperature stability is based on the orientation of the *zigzag* planes of the carbon chain parallel to each other (short-spacing). They correspond to hexagonal ( $H_{\odot}$ ), orthorhombic ( $O_{\perp}$ ) and triclinic ( $T_{\parallel}$ ) arrangements (Garti and Sato, 2001; Sato, 2001). These are three out of the 7 crystal systems generally discussed in the field of crystallography (Hammond, 2009). Each of the 14 *Bravais*-lattices is allocated to one of the 7 classes. Their practical identification is based on the x-ray diffraction or scattering intensity pattern in the wide angle region (short spacing values). If the melting temperature of each polymorphic form of the fat sample is known in advance, determination of the present crystallographic structure can be alternatively performed by differential scanning calorimetry (DSC). In the review of natural fat polymorphism from D'Souza *et al.* (1990) based on x-ray analysis,  $\alpha$  is correlated to a single short spacing peak around 0.415 nm and  $\beta'$  either to two strong peaks around 0.380 nm and 0.420 nm or to three around 0.371 nm, 0.397 nm and 0.427 nm (Malssen *et al.*, 1996). Finally  $\beta$  is stated with a short spacing peak pattern, matching neither the criteria of  $\alpha$  nor of  $\beta'$  and an additional very strong peak around 0.460 nm. The variance in natural fatty acids, their compositions into a triglyceride, their mixture within a natural fat and finally fat blending results in an innumerable quantity of theoretical fat products that show differences in the polymorphic variance and stability as a function of cooling rate, final temperature, time, pressure and impurities (Fredrick *et al.*, 2008; Gibon *et al.*, 1986; Guth *et al.*, 1989; Koyano *et al.*, 1989; Langevelde *et al.*, 1999; Mechelen *et al.*, 2008a,b, 2006; Sato *et al.*, 1989).

**Cocoa Butter:** Wille and Lutton (1966) published six polymorphic forms of cocoa butter. Different approaches for the nomenclature of these forms were published over the years, so that a mixture of these is commonly used today (Tab. 2.3). They all differ from the definitions by crystallographers (see column Malssen, 1994). Nevertheless they are used for the discussion of cocoa butter in this work to avoid confusion for the reader, while we followed the crystallographic specifications for the non-cocoa butter fats.

## 2. Background

Table 2.3.: An overview of the nomenclature for the cocoa butter polymorphs in literature, including related melting peak points (m.p.) or melting areas (m.a.).

Wille, 1966	Dimick, 1987	Lovegren, 1976	van Malssen, 1994	own measure
name m.p.	m.a.	name m.p.	name m.a.	name m.a.
I 17.3	13.1 → 17.6	VI 13.0	$\beta'_3$ -5 → 5	$\gamma$ <18
II 23.3	17.5 → 19.9	V 20.0	$\alpha$ 17 → 22	$\alpha$ 18 → 22
III 28.0	22.4 → 24.5	IV 24.5	$\beta'_2 - 2$ 20 → 27	III 22 → 27
IV 27.5	26.4 → 27.9	III 25.0	$\beta'_1 - 2$	$\beta^{IV}$ 27-30
V 33.8	30.7 → 34.4	II 30.0	$\beta_2 - 3$ 39 → 34	$\beta^V$ 30 → 34
VI 36.3	33.8 → 34.1	I 33.5	$\beta_1 - 3$	$\beta^{VI}$ > 34

While short spacings give information about the parallel alignment of the carbon chains, long spacings describe their stacking into a double-chain (2L) or triple-chain length (3L) in the third dimension of space (Langevelde *et al.*, 2001a). In the nomenclature this detail is introduced by the suffix  $-2$  or  $-3$  to the corresponding characters. For cocoa butter, a switch from 2L to 3L is observed for the transformation from  $\beta'$  to  $\beta$  (Wille and Lutton, 1966). An overview of long and short spacing value is given in Table 2.4.

Table 2.4.: Long and short spacings of the cocoa butter polymorphs by x-ray powder and scattering analysis, reviewed in literature; vw: very weak, w: weak, m: medium, s: strong, vs; very strong.

polymorph	long spacing <sup>a</sup>	short spacing <sup>b</sup>
cryst. author nm	nm	nm
$\beta'_3$ $\gamma$	5.38	0.417(s), 0.387(m)
$\alpha$ $\alpha$	4.87 → 5.1	0.42(vs)
$\beta'_2 - 2$ III	4.5 → 5.0	0.42vs, 0.387vw
$\beta'_1 - 2$ $\beta^{IV}$		0.432(s), 0.413(s), 0.388(w), 0.375(m)
$\beta_2 - 3$ $\beta^V$	6.6	0.538(m), 0.513(w), 0.422(w), 0.398(s), 0.387(w), 0.373(s), 0.365(s)
$\beta_1 - 3$ $\beta^{VI}$	6.48	0.537(m), 0.509(vw), 0.453(vs), 0.421(vw), 0.401(w), 0.384(m), 0.367(s)

<sup>a</sup>Langevelde *et al.* (2001a)

<sup>b</sup>Larsson (1994)

Visually, fat bloom denotes the whitish surface of a chocolate with the parallel loss of gloss (James and Smith, 2009; Nopens *et al.*, 2008; Sonwai and Rousseau, 2008). It is not a microbiological problem but still a significant problem for the confectionery industry (Juul, 2010; Rohm *et al.*, 2007). Fat bloom on pure chocolate is a product of  $\beta^{VI}$  development on the products surface (Cebula and Ziegleder, 1993; Peschar *et al.*, 2004; Sonwai and Rousseau, 2006). The structure is based on crystalline modifications mainly of POP and SOS triglycerides (Minato *et al.*, 1997; Sato *et al.*, 1989). Its formation out of the  $\beta^V$  form is diffusion controlled (Malssen *et al.*, 1999). Direct crystallization into the  $\beta^{VI}$  form has not been observed so far. Fat bloom is also a result of oil migration in filled products such as pralines, generally accelerating this development or leading to non-cocoa butter fat crystals and the product surface after migration (Manning and Dimick, 1985; Motwani *et al.*, 2011; Ziegleder and Schwingshandl, 1998; Ziegleder *et al.*, 1996a,b).

**Non-cocoa butter:** For palm fat, as for all non-cocoa butter fats, less investigations by XRD or XRS are found in literature compared to cocoa butter. Furthermore, the polymorphic situation of these fats is more complex, since the triglycerides are less compatible. Fractionation by different polymorphic structures can occur. In combination with the fluctuation of the triglyceride composition by the fats origin, this results in less concordance of published data. D’Souza *et al.* (1990) states, that palm oil is merely  $\beta'$  stable, but also  $\beta$  fractions are denoted. The short spacings below 0.4 nm of the reviewed publications differ. The variance in palm oil origin, refining process, and temperature treatment may led to these differences. Generally, the existence of a lower stable  $\beta'_2$ , a higher stable  $\beta'_1$  and a  $\beta$  fraction was stated by Yap *et al.* (1989) and Braipson-Danthine and Gibon (2007). Both authors also investigated palm stearin fats, whereas Yap identified only a slightly increased ability towards the  $\beta$  formation, while Braipson-Danthine published data of complete transformation processes as function of temperature. The latter confirmed equivalent findings by Sonoda *et al.* (2004). The diffraction of palm kernel fat was investigated by Riiner (1970) and Jin *et al.* (2008). The  $\beta'$  stable fat shows short spacing peak values that differ significantly from the regular pattern presented above. However, the crystallographic background of this deviation could not be found in the literature. In contrast, the other lauric fat, coconut oil, does follow the general trend (also Riiner, 1970).

In a review by Ghotra *et al.* (2002), coconut and palm kernel oil are even listed as generally  $\beta$  stable fats, which is challenged by the author. The heterogenous picture of the non-cocoa butter diffraction data in literature points out, that the boundary conditions, chemical composition, cooling temperature and storage time are important factors for the microstructural development of these fats. Table 2.5 gives a short summary of published diffraction data of non-cocoa butter fats.

Table 2.5.: Short spacings of non-cocoa butter polymorphs by x-ray powder and scattering analysis, reviewed in literature.

fat	short spacings (nm)		subcell type	conditions	reference
coconut	0.451(w),	0.433(m),	$\beta' > \beta$	22°C, 1 month	Riiner, 1970
	0.412(m),	0.384(s)			
palm kernel	0.444(m), 0.425(s), 0.404(m), 0.384(s)		$\beta'$	22°C, 1 month	Riiner, 1970
palm	0.435(m), 0.420(s), 0.387(s)		$\beta'$	22°C, 1 month	Riiner, 1970
	0.417(s), 0.373(w)		$\beta'_2$	-23°C	Riiner, 1970
	0.417(s), 0.380(w)		$sub - \alpha$	-10°C	Braipson-Danthine, 2007
	0.420(s), 0.388(m)		$\beta'_2$	15°C	Braipson-Danthine, 2007
	0.458(w), 0.418(m), 0.402(w), 0.383(m)		$\beta'_1 > \beta$	35°C	Braipson-Danthine, 2007
	0.435(s), 0.419(s), 0.388(m)		$\beta'$	5°C, 1 day	Yap, 1989
	0.456(vw), 0.434(s), 0.420(s), 0.389(s)		$\beta' > \beta$	5°C, 36 days	Yap, 1989
palm stearin	0.456(w), 0.435(s), 0.420(w), 0.405(w),		$\beta' > \beta$	5°C, 1 day	Yap, 1989
	0.387(s)				
	0.467(m), 0.438(s), 0.424(s), 0.384(m)		$\beta' > \beta$	5°C, 36 day	Yap, 1989
	0.429(m), 0.418(s), 0.405(w), 0.386(m)		$\beta'_1$	25°C	Braipson-Danthine, 2007
	0.456(s), 0.383(m), 0.375(m)		$\beta$	45°C	Braipson-Danthine, 2007

**Shear Crystallization:** Shear affects the crystallization of polymorphic fats in terms of the nucleation as well as transformation period into the next higher polymorphic form (Mazzanti *et al.*, 2003). Furthermore, crystals will be oriented when reaching a critical size and featuring an anisotropic geometry (e.g. platelike, needle like). In the case of cocoa butter, not only a general acceleration of the crystallization procedure is observed (Sonwai and Mackley, 2006; Windhab *et al.*, 1991), but also an effect on the polymorphic forms generated (MacMillan *et al.*, 2002; Padar, 2009). For temperatures  $\geq 20^{\circ}\text{C}$  a direct transformation from a mixed  $\alpha/\text{III}$  state into  $\beta^{\text{V}}$  was reported, bypassing the  $\beta'$  state observed for static conditions. De Graef *et al.* (2009) showed that also palm oil reacts on the application of shear with reduced nucleation and transformation times. As most of the investigations were performed within a rheometer, the crystallization period is additionally monitored by rheological parameters. In principle, the data can provide additional information during further crystal growth even up to the generation of fat crystal networks when using the oscillatory shear mode (De Graef *et al.*, 2007, 2008; Tarabukina *et al.*, 2009).

**Seeding:** In principle, direct crystallization into each of the three main subcell structures is possible from a thermodynamic point of view at certain boundary conditions. In reality, solidification of confectionary products is generally performed at low temperatures ( $5\text{--}15^{\circ}\text{C}$ ). This results in high cooling rates combined with a strong supercooling, leading to high fractions of low stable polymorphs. Therefore, the idea of precrystallization was inevitable to achieve homogeneous and stable product properties. Especially the group of Kiyotako Sato (Hiroshima University, Japan) did research on the field of seed crystal admixing by designed triglyceride systems, focusing on cocoa butter (Hachiya *et al.*, 1989a,b; Koyano *et al.*, 1990; Sato, 2001). The positive crystallographic effect as well as kinetic acceleration was clearly a function of seed concentration. This concept was further refined by combination with the effects of high shear crystallization by Windhab (1999) and successfully translated into an industrial application (Windhab and Zeng, 2000; Zeng, 2000, 2002).

## Crystallization Kinetics

Understanding thermodynamics of crystal nucleation and growth is required to realize the complexity of both mechanisms. Moreover, natural fats consists of inhomogeneous mixtures of triglycerides including impurities such as diglycerides, monoglycerides and free fatty acids, which add further to the complexity. Therefore, the basics described in Himawan *et al.* (2006) and Rousset (2002) are shortly outlined in the first paragraphs prior to the discussion of kinetic models.

## 2. Background

---

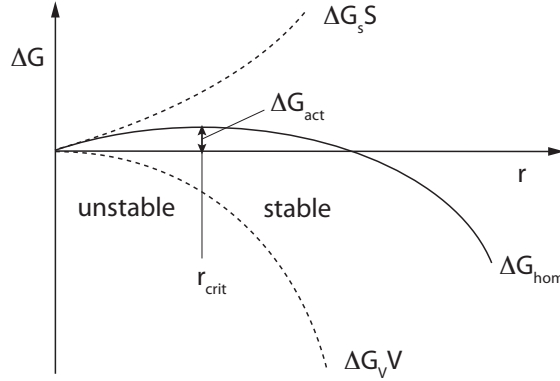


Figure 2.1.: Free Gibbs energy of homogeneous nucleation  $\Delta G_{\text{hom}}$  as function of nuclei radius  $r$ ,  $\Delta G_V$ : volumetric free energy by liquid-solid phase transfer,  $\Delta G_S$ : free energy of solid-liquid interface,  $\Delta G_{\text{act}}$  activation free energy of the present polymorphic form.

Assuming the nucleation of a pure system and homogeneous nucleation, the total change in the Gibbs free energy ( $\Delta G_{\text{hom}}$ ) is dependent on two opposing effects (Fig. 2.1):

$$\Delta G_{\text{hom}} = \Delta G_V V + \Delta G_S S \quad (2.1)$$

where  $V$  and  $S$  are the volume and surface area of the single embryo formed.

On one hand, the Gibbs free energy is reduced due to the volumetric transformation into a solid:

$$\Delta G_V = -\frac{\Delta H_{m,f} \Delta T}{T_f \Delta V_m} \quad (2.2)$$

where  $\Delta H_{m,f}$  is the molar melting enthalpy,  $T_f$  is the temperature of fusion,  $\Delta T$  is the absolute supercooling in relation to  $T_f$  and  $V_m$  is the molar volume solidified.

On the other, the generation of a solid-liquid interface results in a surface free energy ( $\sigma$ ) increasing the overall energy level:

$$\Delta G_S = \sigma \quad (2.3)$$

Consequently, the Gibbs free energy of nucleation is given by

$$\Delta G_{\text{hom}} = -\frac{\Delta H_{m,f} \Delta T}{T_f \Delta V_m} V + \sigma S \quad (2.4)$$



The expression is thereby a function of the embryos radius  $r$  and shows a maximum for

$$r_{\text{crit}} = -\frac{2\sigma}{\Delta G_v} \quad (2.5)$$

at

$$\Delta G_{\text{hom,crit}} = \Delta G_{\text{act}} = -\frac{16\pi}{3} \frac{\sigma^3}{\Delta G_v^2} = \frac{16\pi}{3} \frac{\sigma^3 T_f^2 V_f^2}{\Delta H_{m,f}^2 \Delta T^2}. \quad (2.6)$$

Below this critical radius, triglyceride clusters are unstable, because only a decomposition reduces the absolute free Gibbs energy (Fig. 2.1). Only for  $r \geq r_{\text{crit}}$ , embryos are stable nuclei, so that crystal growth is energetically favored. The nucleation process in reality is not solely homogeneous. Also heterogeneous nucleation occurs by impurities. Secondary nucleation occurs as well by crystal break-up due to shear flow or direct impingement with other crystals or process equipment.

Up to now, only the thermodynamic background of nucleation was explained but not quantified. For the approximation of the nucleation rate  $I_{\text{hom}}$  according to Turnbull and Fisher (1949), the embryo size is assumed to follow a Boltzmann distribution, and is given by:

$$I_{\text{hom}} = N_0 \nu_0 p N_s^0 e^{-\frac{\Delta G_{\text{inc}}}{k_b T}} e^{-\frac{\Delta G_{\text{hom,crit}}}{k_B T}} \quad (2.7)$$

where  $N_0$  is the number of molecules per unit volume,  $\nu_0$  is the atomic vibration frequency,  $p$  is the adsorption probability of a molecule,  $N_s^0$  is the density of sites on a nucleus,  $\Delta G_{\text{inc}}$  is the activation free energy necessary to incorporate a molecule in the crystalline nucleus and  $k_B$  is the Boltzmann constant.

Before a solid embryo or nucleus is formed, a pre-ordering of the triglycerides is assumed (Garti and Sato, 2001). The time from undergoing the melting temperature until the final clustering of an embryo with  $r \geq r_{\text{crit}}$  is called *induction time* (Kenny *et al.*, 1993). While this time is equal to zero for metals due to their high molecular mobility, it can be significant for rather large molecules such as triglycerides. The induction time ( $t_{\text{ind}}$ ) can be approximated according to Buckle (1961) by:

$$t_{\text{ind}} = D e^{\left(\frac{\Delta G_{\text{hom,crit}}}{k_b T}\right)} = \frac{1}{(4\sigma k_B T)^{1/2}} v_{\text{mol}}^{-1/3} h e^{\left(\frac{16\pi\sigma^3 T_f^2 V_m^2}{3k_B T \Delta H_{m,f}^2 \Delta T^2}\right)} \quad (2.8)$$

where  $\nu_m$  is the molecular volume and  $h$  is the Planck constant.

In general, there are two different types of polymorphism. A fat is monotropic, if there exists only one thermodynamically most stable crystal subcell structure. A fat is enantiotropic, if the declaration of the most stable form is a function of temperature and pressure. In most cases, triglycerides exhibit monotropic polymorphism (Fig. 2.2). This scheme also points out, that in principle, a  $\beta$  nucleation is possible, as there

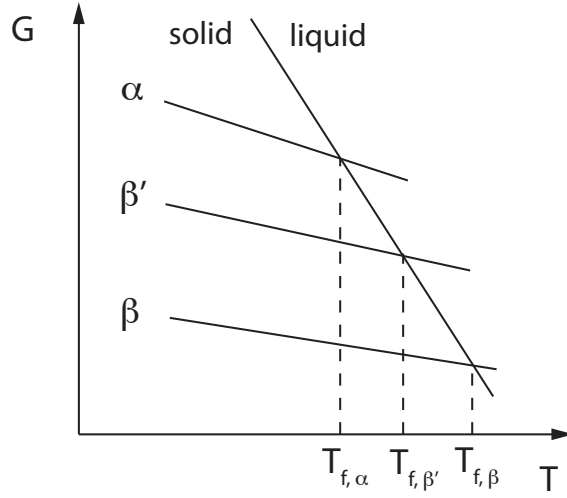


Figure 2.2.: Gibbs free energy as function of temperature by the three main polymorphs of fat crystals with corresponding melting temperature  $T_f$  (adapted from Himawan *et al.*, 2006).

exists a defined temperature range above the melting temperature of  $\beta'$  and below that of  $\beta$ . In reality, these temperatures might overlap due to several triglycerides classes and their mixtures, resulting in transient regions instead of precise melting limits of probably more than one. The nucleation of less stable instead of high stable forms is often observed at rather low temperatures. As shown before, the induction time and the nucleation rate are functions of  $(\sigma^3)/(\Delta H_{m,f}^2 \Delta T^2)$ . Generally, the surface tension of the fat polymorphs vary strongly, following the trend in relative temperature stability:  $\sigma(\alpha) < \sigma(\beta') < \sigma(\beta)$ . This favors the nucleation of lower stable crystals. Melting enthalpy as well as the supercooling temperature difference at a constant temperature increase for higher stable polymorphs. However, their relative increment in combination with the reduced power law value ( $3 \rightarrow 2$ ) is smaller than for the surface tension. Consequently the least stable phase within the present boundary conditions shows the fastest formation kinetics. This conclusion is illustrated in Figure 2.3.

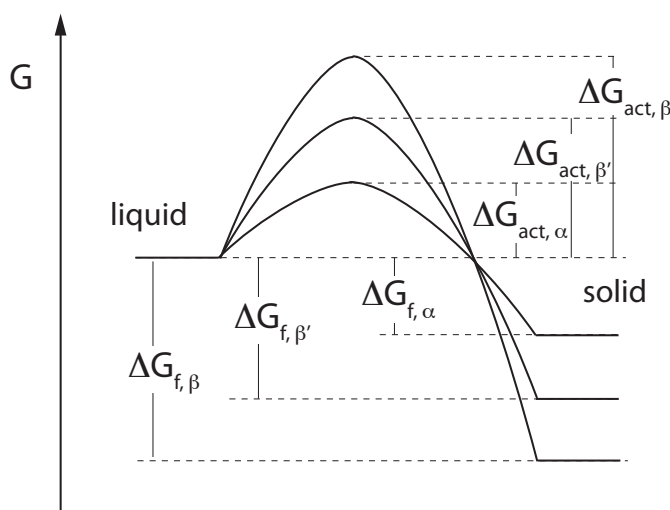


Figure 2.3.: Activation  $\Delta G_{\text{act}}$  and melting free energy  $\Delta G_f$  as function of polymorphic form for  $T < T_{f,\alpha}$  (adapted from Rousset, 2002).

### Kinetic Models:

Avrami developed a deterministic model initially for low molecular weight molecules in the first half of the 19th century (Avrami, 1939, 1940). This theory was widely used in the field of metals (Christian, 2002), polymers (Mandelkern *et al.*, 1954; Sharples, 1966), but also fat systems (Kawamura, 1979; Wright *et al.*, 2000; Ziegler, 1990). The approach includes all three phases of a typical solidification curve on a physical basis: nucleation, main growth and crystal-crystal impingement.

In most cases, not the physically exact models are applied on the experimental data, since there was no parallel proof of 1D, 2D, or 3D crystal growth available during these studies. To overcome this gap, the equations can be consolidated by simplification leading to a general equation of Avrami's theorem. The derived model is more robust, but leads to non-integer values for one of the fitting parameters that is supposed to be an integer, indicating 1D, 2D or 3D growth mechanisms as well as sporadic or instantaneous nucleation. For fat crystallization this was interpreted as simultaneous crystallization of different triglycerides or triglyceride mixtures of diverse kinetics, as well as the parallel existence of 1st order nucleation out of the melt and 2nd order by crystal impingement. Consequently, the values of a successful fit give rather relative information than precise kinetic factors as the original equations do. Moreover, combination of different, coincidental crystallization processes can result in the very same fitting parameters. The physical nonsense of a modification of the approximate equation by Khanna and Taylor (1988) was pointed out by Marangoni (1999). Different to Avrami itself, Marangoni (2005) derived Avrami's approximate equation based on a crystal growth mechanism analogous to mass diffusion. The mathematical expression is identical, but the kinetic constant factor is now seen as

## 2. Background

---

a cumulation of geometric and material properties as well as distinct crystal growth factors. On the other hand, again only integer values for the second fitting parameter are allowed in this approach, bringing back the initial problem of missing information about the morphological development of single crystals without additional effort by an appropriate analysis. Beyond that, the implementation of Fick's law of diffusion is not valid for the third part of crystallization, the crystal-crystal impingement towards the end of the process.

Prior to the idea of Marangoni, Foubert (2003) proposed a differential equation by the assumption of an analogy of chemical reaction and crystallization kinetics. As mainly for all the other authors, Foubert's experimental data was obtained by pNMR and DSC analysis of cocoa butter. In this case, solidification was performed between 19–23°C. The advantage is, that also non-isothermal boundary conditions can be considered by the differential approach. On the other hand, the fitting parameters are still not based on physical parameters of crystallization and polymorphism is not implied. It can only be considered by estimation and implementation of corresponding experimental data. Another approach by an analogous mechanism was initially worked out by Berg and Brimberg (1983) and further developed by Klok *et al.* (2000), based on the kinetics of bacterial growth (Zwietering *et al.*, 1990). As before, this system also lacks in physical meaning of the fitting parameter.

Révérénd *et al.* (2009) optimized a simulation system from Tewkesbury *et al.* (2000), that was influenced by a first approach of Franke (1998). This model is based on the approximate Avrami equation for the crystallization part on one hand, and the general equations for heat transfer on the other (Chap. 2.2.3). It was set up for the holistic simulation of the cooling process of chocolate products. It includes non-isothermal boundary conditions as well as a simplified consideration of the polymorphism. It is seen as the most advanced work on the field of the cooling process simulation of cocoa butter, where its accuracy depends on the quantity and quality of the required DSC data series.

It can be summarized, that the models of Avrami by determination in 1D, 2D and 3D crystal growth are still the best attempts in parameterization of the crystallization kinetics of pure fats on a physically meaningful basis including all three phases: nucleation, main crystal growth and impingement. Nevertheless, the nucleation time has to be determined separately by experimental data or approximation according to Equation 2.8 and potential polymorphism has to be taken into account for the discussion of the fitting results.

The Avrami model is explained in detail by Padar *et al.* (2009) and Foubert (2003). It is based on the hypothesis, that nucleation starts by germ nuclei growth, which already exist in the melt. Their number is controlled by the pretreatment conditions (temperature, pressure, time). Based on this theory of number density, the distribution of germ nuclei in the supercooled melt and its exponentially decrease in time ( $V_e$ ) represents the grain volume for unimpeded growth:

$$V_e = N_0 \int_0^\tau v_{\text{grain}}(\tau, z) e^{-z} dz \quad (2.9)$$

where  $N_0$  is the absolute number of germ nuclei and  $v_{\text{grain}}(\tau, z)$  is the volume of a crystal grain. The characteristic time  $\tau$  is a linear function of  $p_A z$  with the probability  $p_A$  of nuclei growth ( $p_A < 1$ ) and time  $z$ . It was assumed, that the increase of crystal volume is proportional to the volume fraction of the remaining liquid. Furthermore, the crystal volume fraction for the final state in equilibrium is usually less than unity, leading to the following expression for the overall crystal volume ( $V$ ) as function of  $V_e$ :

$$V = V_{\text{max}} (1 - e^{-V_e}) \quad (2.10)$$

where  $V_{\text{max}}$  is the crystal volume in the thermodynamic solid-liquid equilibrium of the present polymorph. Finally a linear growth rate  $\dot{l}$  was assumed, independent of the crystal plane growing. The final equations for 1D (needle like), 2D (plate-like) and 3D (sphere-like) crystal growth are then given by:

$$V = V_{\text{max}} \left[ 1 - e^{-(A_1 \dot{l} N_0 / p_A)(e^{-\tau} - 1 + \tau)} \right] \quad (2.11)$$

$$V = V_{\text{max}} \left[ 1 - e^{-(A_2 \dot{l} N_0 / p_A)(-e^{-\tau} + 1 - \tau + (\tau^2/2))} \right] \quad (2.12)$$

$$V = V_{\text{max}} \left[ 1 - e^{-(A_3 \dot{l} N_0 / p_A)(e^{-\tau} - 1 + \tau - (\tau^2/2) + (\tau^3/6))} \right] \quad (2.13)$$

where  $A_1$  represents the constant cross-sectional area of the needle-like crystal growing,  $A_2$  stands for the thickness of the plate-like crystal growing and  $A_3$  is the shape factor  $4\pi/3$  for a sphere.

The simplified modification is derived by consideration of the two extreme situations  $\tau \rightarrow 0$  and  $\tau \gg 0$  and transcription of the inner, exponential term into its power series, so that:

$$V = V_{\text{max}} (1 - e^{-k_A t_A^{m_A}}) \quad (2.14)$$

where  $k_A$  is a constant and  $m_A$  denotes, whether a 1D, 2D or 3D crystal growth mechanism is most likely. Because sporadic ( $\tau \rightarrow 0$  for  $p_A \rightarrow 0$ ) as well as instantaneous nucleation ( $\tau \gg 0$  for  $p_A \gg 0$ ) can occur, 1D growth is attributed to values of  $1 < m_A < 2$ , 2D to  $2 < m_A < 3$  and 3D to  $3 < m_A < 4$ , respectively. This generalization in Eqn. 2.14 is called *Approximate (Avrami) Equation* in this thesis (adopted by Padar *et al.*, 2009).

### 2.2. Chocolate Processing

A short outline of the process chain of chocolate manufacturing from the bean to the well-flavored chocolate after conching is presented. We will further focus on the final production steps of precrystallization, moulding and cooling. More details are given in Beckett (2009) and Timms (2003a).

The first steps of chocolate processing are carried out directly after harvesting the pods from the cocoa tree. The beans are removed from the pod with parts of the pulp, naturally fermented on a heap. During this phase, wrong treatment by too short or too long fermentation might lead to mold or damage of the shell and will negatively affect the final flavor quality and can not be corrected by subsequent process steps. The beans are sun dried, dispersed either on mats of banana leaves or bamboo laying on the ground (lower quality) or on wooden benches (better quality). Drying can be supported by forced convection via ventilation or artificial drying. Thereafter the beans are bagged and shipped. After separation from stones, metals and other contaminating material, the beans are mostly roasted before they are broken into nibs. The shell material is removed by winnowing. As an alternative, the beans can be also broken prior to roasting to improve the homogeneity of the temperature field. On the other hand, the shell detaches suboptimal prior to roasting and the volatile cocoa flavor notes are no longer preserved by the shell layer during the high-temperature roasting process. The latter might be positive for astringent components but is negative for the desired flavors as well as constitutional compounds such as polyphenols, acting as a natural antioxidant in the human body. The release of undesired, volatile compounds can be further enhanced by additional water stripping at the beginning of the roasting process. Roasting is generally also used as a sterilization step, since temperatures up to  $T_{\max} = 110\text{--}140^\circ\text{C}$  are reached.

The roasted nibs are pre-ground in two steps to approximately  $x < 50\text{ }\mu\text{m}$  in a dry or semi-dry state, respectively, for instance by combination of a hammer mill and a three-roll refiner. In this step the fibrous cell walls are disintegrated and the containing fat (cocoa butter) is released (54 % total mass). The product is then called cocoa liquor or cocoa mass. Either it is pressed down to a fat content of  $\approx 10\text{--}15\%$  to gain pure cocoa butter and is further used as cocoa powder for drinks or other applications, or it is mixed with sugar, additional cocoa butter, emulsifier (usually lecithin) and optionally milk powders (=milk chocolate) to become chocolate. This highly viscous mass is fed to a five-roll refiner. This fine-grinding step yields in a maximal particle size below  $30\text{ }\mu\text{m}$ . On the other hand, particles below  $5\text{ }\mu\text{m}$  should be avoided to keep appropriate flow properties. Two main functions are assigned to the adjacent conching process. First, particles are de-agglomerated by shear and coated with fat and lecithin. Thereby the flow properties of the suspension are improved significantly. Secondly, chocolate flavor is developed and moisture reduced by multiple incorporation and release of air at elevated temperatures ( $T_{\text{conch}} > 40^\circ\text{C}$ )

for hours. The final composition of the chocolate is set by gradual addition of cocoa butter over the long period of conching.

### 2.2.1. Precrystallization

The term *precrystallization* is used in this work as a general term for the generation (*tempering*) or addition (*seeding*) of seed crystals in a fat based sample.

From an engineering point of view, the process steps explained so far can be conducted separately. Starting with the precrystallization, a continuous processing to the final product is compulsory. As explained before (Chap. 2.1.2), cocoa butter is a polymorphic fat and the properties of the  $\beta^V$  form are desired for an optimal organoleptic result (melting, chocolate snap, surface gloss). Precrystallization is either realized by manual hand tempering or industrial tempering of the chocolate. An alternative is given by the addition of specific seed crystals into the molten chocolate. The development and details of all three options are explained in this subsection.

Although straight  $\beta^V$  crystallization is possible at high temperatures from a thermodynamic point of view, it would be very time consuming by slow kinetics and would lead to a coarse macrostructure due to small number of crystal nuclei growing. In contrast, a high number of nuclei of an unstable form ( $\gamma, \alpha$ ) is achieved by strong supercooling under high shear conditions (Mazzanti *et al.*, 2003). During a *ripening step* at temperatures around the melting end set of  $\beta^{IV}$  crystals (Tab. 2.3) the transformation into  $\beta^V$  is optimal. Thereby a high number of small  $\beta^V$  crystal seeds can be achieved.

In former times, only the positive effect but not the crystallographic background nor the function of shear was known in detail. The chocolate was tempered by hand. This concept is still used by traditional confectioners or even industry to produce small batches of handmade chocolate or pralines:

A fraction of the molten chocolate is pretreated on a marble table with a spatula. Thereby the mass is cooled down by the massive block of 20–22°C featuring good heat conduction properties and sheared or *slapped* by hand to initiate crystallization. By observations of the consistency and mass temperature based on his experience, the confectioner evaluates the temper state of the mass. The precrystallized, high viscous chocolate (< 30°C) is then re-mixed into the major chocolate, which has been down to  $\approx 30^\circ\text{C}$ . Due to the reheating, the unstable crystal nuclei are remelted, while  $\beta$  crystals are stable at this temperature. The precrystallized chocolate is ready for moulding and cooling.

The industrial version (conventional tempering machine) of this concept is explained in detail by Windhab (2009). In principle, the procedure is translated by operation in three temperature controlled sequences. The chocolate is continuously pumped and

cooled down in an angular gap by water jackets and scraped of the wall by opposing blades. In a first cooling step, only specific heat is removed for preparation of the second cooling step, where crystal nucleation is achieved by further cooling under shear. A re-heating zone is implemented at the very end instead of a re-mixing unit (see hand tempering). Thereby continuous tempering of the whole mass is achieved. In recent developments of a leading machine manufacturer, the incoming chocolate stream is split into a two disproportionate fractions. Following the concept of hand tempering, the bigger portion is only cooled down by a heat exchanger, while the smaller portion is tempered to a high extend and finally remixed into the main, non-tempered stream. This adaptation improves the energy consumption. Conventional outlet temperatures of dark chocolates are 29–31 °C. The tempering profile for milk chocolates are generally shifted to slightly lower temperatures with increased residence times as function of the milk fat type and amount (Reddy *et al.*, 1996).

The absolute quantification and size determination of conventionally produced seed crystals is not straight forward and highly dependent on the compositions of the suspension (=chocolate or filling mass) and its time-temperature-shear history (Windhab, 2009). The degradation of energy by cooling and reheating of the whole mass is another disadvantage of this concept. Keeping the main goals of a high number of small and  $\beta^V$  stable crystals in mind, a seeding technique with pure fat crystals seems most appropriate for precise and sustainable processing. As reviewed before, high-shear crystallization of cocoa butter at temperatures below 20 °C can be performed, keeping the crystal slurry in a free-flowing state at ripening conditions (Zeng, 2000). A concentrated seed suspension with a solid fat fraction up to 18 % and crystal sizes below 10  $\mu\text{m}$  can be obtained by the following boundary conditions: pure cocoa butter, shear rates up to 6000  $\text{s}^{-1}$ , cooling at 15 °C, ripening at 31–32 °C. As the product is reduced to pure fat, the crystal size is small and the ripening temperature high, even further transformation into the  $\beta^{VI}$  form is observed during ripening. This step is diffusion driven (Malssen *et al.*, 1999) and thereby much slower as the initial conversion into the  $\beta^V$  state. Finally a small amount ( $\approx 0.3\%$ ) of the  $\beta^V/\beta^{VI}$  cocoa butter fat suspension is simply mixed into the molten chocolate (31 °C  $\pm$  3 °C).  $\beta^{VI}$  induce crystal growth in the  $\beta^V$  form only.

While conventional tempering yields in solid fat fraction of 1–4 % (solid/total cocoa butter, Timms, 2003b), cocoa butter suspension seeding results in SFC values  $<0.5\%$  (Zeng, 2002). The volume specific surface area of the seed crystals is increased, as the overall crystal size is reduced by high-shear crystallization. The seed effect of a single crystal is therefore improved and the overall seeding by the bigger number of seed crystals more homogeneous as in conventionally tempered masses. Moreover, the improved stability of the seed suspension by a matured system and a significant fraction of  $\beta^{VI}$  seeds ( $T_{\text{melt}} \geq 34\text{ °C}$ ) is yet another advantage over conventional tempering, where outlet temperature is close to the melting endset of the seeds created. It is claimed to achieve a more dense and finely structured crystal network by application



of the seeding technique (Windhab, 2009). Slightly accelerated crystallization kinetics were confirmed by Mehrle (2007) for the use of seed slurry compared to conventional tempering.

The quality of tempering is generally evaluated by *tempermeter* systems. Instead of time-consuming polymorphic form analysis by x-ray powder diffraction (XRPD) or differential scanning calorimetry (DSC), this method is indirect and empirical. It was developed out of the Shukoff method (Timms, 2003a). A precrystallized chocolate is filled into a cup ( $V \approx 9$  ml), placed into a rack and chilled at temperatures of 7–10 °C, by water or a Peltier cooling element (Talbot 2008). Core temperature is continuously recorded. The latent heat is released by crystallization starting from outside to the inside of the sample. Because of heat accumulation caused by a fast crystallization in relation to local heat conduction, the initial rate of temperature reduction decreases for a certain time. In order to judge the precrystallization quality, the core temperature inflection is evaluated. It is known empirically, that a well-tempered chocolate shows an inflection point with the ideal temperature-time gradient of 0.0 °C/min  $\pm$  0.5 °C/min. Secondly the inflection is expected around 24 °C for dark and 23 °C for milk chocolates. It is important to note, that these values are dependent on chocolate recipe, cooling condition and sample geometry. The tolerable deviation from ideal values is defined individually by the manufacturer. We assume further, that this measuring technique is only suitable for the common cooling boundary conditions applied so far in industry.

Until now, confectionery fillings are conventionally precrystallized only, if a significant amount of cocoa butter ( $c_{\min}(CB) \approx 30\%$ ) is present besides other fats like hazelnut oil. The parameter adjustment for the conventional method is individual for each product. The manufacturer relies on their experience to decide whether a filling still has to be precrystallized and how. No deterministic concept exists to optimize this step. Based on the seeding technique, Zeng (2000) showed that the melting range of  $\beta^{VI}$  seeds is reduced by the presences of nut oils and CBRs. Consequently the seeding temperature has to be reduced according to the fat composition.

Due to economical, but also for more flexibility in textural aspects, fraction of non-cocoa butter fats are further increased. Consequently, these fats become predominant in the mixture. However, experience with these masses in terms of precrystallization with respect to crystallization kinetics, contraction and oil migration is insufficient on a practical but also a scientific level so far. The crucial point for precrystallization of cocoa butter based masses is the fat polymorphism, namely its  $\beta$  stability. Based on literature, at least the fillings containing palm oil or high melting palm oil fraction (palm stearin) are therefore supposed to be precrystallized (Braipson-Danthine and Gibon, 2007; D’Souza *et al.*, 1990; Yap *et al.*, 1989).

### 2.2.2. Moulding

In general, precrystallized chocolate is preconditioned to temperatures of  $29^{\circ}\text{C} < T < 32^{\circ}\text{C}$ . The seeds and the liquid fat did not reach the thermodynamic  $\beta^V$  equilibrium. Therefore the nuclei still grow. The flow properties are sensitive towards temperature fluctuations. *Too high* temperatures result in a quality loss by remelting of the seed crystals accomplished before, that are needed for a homogeneous contraction and storage stability. *Too low* results in an increase of the yield value and the flow curve values while the remaining contraction ability is reduced. This is problematic for the moulding and the de-moulding process. Therefore the time period until moulding is kept rather short (minutes).

Moulding of chocolate bars is realized by simple dispensing via nozzle systems, followed by shakers and optionally scraper blades for excessive material. The nozzles are flexible in diameter, enabling the use even for chocolate with whole hazelnuts or almonds with auxiliary equipment to avoid dripping. In contrast, three different concepts are used for the production of praline systems.

- Conventional
- Frozen Cone<sup>®</sup>(Aasted Mikroverk) / ColeCore<sup>™</sup>(Bühler AG)
- One-Shot

The first two are based on sequentially manufacturing the chocolate shell, insertion of the filling mass and covering with additional chocolate shell mass. A cooling step is required after each step, resulting in long production lines. The difference of these two is located at the very beginning of the shell formation. By conventional moulding, the mould is filled with chocolate up to the rim. The mass partly solidifies during a short period (minutes) at room temperature. Subsequently the mould is flipped, so that excessive chocolate flows off and a highly viscous chocolate layer of fairly uniform thickness remains. Due to the flow properties of viscous masses, the corner sections of the shell geometry are typically rounded off by this method. The first cooling period for an initial solidification follows before the filling and the topping step are executed. To achieve an accurate and uniform shell thickness with high reproducibility, the shell can be formed by a cooled plunger instead (Frozen Cone<sup>®</sup> or Cold Stamp<sup>™</sup>). By this second option of shell forming, the moulds are only filled with the precise volume of the resulting shell geometry. The stamp is cooled down below  $0^{\circ}\text{C}$  and pressed into the mould for a few seconds. Thereby the mass is homogeneously distributed and complex shell geometries (precise shell thickness at multiple angles) can be realized. The shell solidifies first on the inside leading to a contraction off the stamp before

this is pulled back. Even though the cooling conditions for direct contact with the stamp are rather harsh, there is no major quality damage observed in terms of fat bloom stability due to potential, low stable crystal nucleation during this short-term period. On the contrary, an improved surface gloss of the final product is evident at least for a short period (days) compared to conventional moulding. More details of this cold forming technology are given by Walker (2009) and Heller (2000).

For certain chocolate to filling viscosity ratios, pralines can also be formed in a single step using the *One-Shot* or *Single-Shot* technology. The concept is based on a two-phase angular gap nozzle. The chocolate shell mass (angular gap) and the filling (central nozzle) are deposited simultaneously. The two pistons are controlled separately following a product specific velocity profile to achieve a homogeneous shell thickness around the filling. The moulding temperatures of chocolate and filling have to be similar to avoid remelting of the lower tempered mass. Particle additives such as nuts or raisins are not practicable. The advantage of this technique is the reduction of a whole production line to a single deposition and cooling step. Thereby the technical equipment, the required space and the energy consumption are reduced. From a qualitative point of view, the initial migration of filling oils into the chocolate shell is increased, since both masses are still liquid when combined (Rohm *et al.*, 2007; Rohm H., 2005). The oil mobility is improved by an increased temperature compared to the cooled shell in the conventional moulding process. More details of this moulding concept are given in Padar *et al.* (2009) and Heller (2000).

### 2.2.3. Cooling

Generally contact, convection and radiation cooling exist in decreasing order of efficiency. All three are applied in state of the art cooling tunnels. The product is transported on conveyer belts (contact), overflowed by cold air (convection) and additionally affected by cooling plates positioned above (radiation). Regular cooling temperatures are mainly between 10–15°C (Beckett, 2009), while milk chocolates are cooled at slightly lower levels. Usually the tunnel system is split into three successive sections. Only specific heat is removed in the first one at slow air speeds to avoid nucleation of unstable polymorphs (Ziegler, 2001) and the formation of ripples on the product surface. In the second, mostly latent heat is released and cooling at low temperatures and high air speed (preferably turbulent conditions) is performed. Finally, the product is annealed to temperatures above the dew point of the surrounding area to avoid any condensation. Besides tunnels, multi-tier cooling systems are applied. Due to the compact layering of several moulds, the geometric boundary conditions are much more complex to achieve a fast but homogeneous cooling history for each single item.

## 2. Background

---

On one hand, cooling stands for a simple solidification of the moulded product. Ergo, the main goal is the fast removal of specific and especially latent heat of crystallizing masses. On the other hand the fat crystal network developing has to consist of preferably  $\beta^V$  crystals and should generate a homogeneous and sufficient contraction behavior to fulfill the quality characteristics named before: *snap*, smooth melting in the mouth, surface gloss, fat bloom stability. The cooling kinetics of each polymorphic form supercooled compete each other (Fig. 2.2). By the application of tempering techniques,  $\beta^V$  crystals are strongly promoted, because nucleation becomes obsolete for crystal growth. However, unstable forms still nucleate at very low temperatures, since their activation free energy is rather low and their crystalline integration fast (Fig. 2.3). Therefore the cooling conditions have to comply the qualitative limits set by the polymorphic kinetics to assure  $\beta^V$  crystal growth. In this context, not only the cooling temperature but also the air speed has to be considered.

### Theoretical Background

The unsteady temperature profile of an object is obtained by the combination of the conservation of energy (incompressible medium) and the fundamental law of heat conduction by Fourier to the heat equation:

$$c_p \rho \frac{\partial T}{\partial t} = \lambda \nabla^2 T \quad (2.15)$$

where  $c_p$  is the specific heat capacity,  $\rho$  is the density of the product and  $\lambda_{\text{prod}}$  is the heat conduction coefficient of the product. In case of crystallization by supercooling an additional term for heat generation (Franke, 1998) or its integration into an unsteady  $c_{p,\text{eff}}$  term (Tewkesbury *et al.*, 2000) has been proposed in literature. However, the integration of the latent heat is not in the focus of this work, as mainly the period until crystallization start is of interest.

The heat flux  $\dot{Q}$  from a warm product to its environment is generally described by

$$\dot{Q} = kA(T_{\text{prod}} - T_{\text{cool}}) \quad (2.16)$$

where  $A$  denotes the product surface area and  $k$  stands for the overall heat transfer coefficient, defined by:

$$\frac{1}{k} = \frac{1}{\alpha_{\text{HT}}} + \frac{s_{\text{HT,prod}}}{\lambda_{\text{HT,prod}}} \quad (2.17)$$

where  $\alpha$  is the convective heat transfer coefficient,  $s_{\text{HT,prod}}$  is the representative length of the product profile (sphere: radius, plate: half thickness).

The product parameter ( $c_p, \rho, \lambda_{\text{HT}}, \text{prod}$ ) are set by the recipe and the heat transfer area ( $A$ ) as well as the profile depth ( $s_{\text{HT,prod}}$ ) by the product geometry. Only by variation of the heat transfer coefficient  $\alpha_{\text{HT}}$  or the cooling temperature  $T_{\text{cool}}$ , the progression of the temperature gradients can be influenced. The Nusselt number represents the ratio of transferred heat by convection to conduction and is defined by:

$$\text{Nu} = \frac{\alpha_{\text{HT}} L}{\lambda_{\text{HT,air}}} \quad (2.18)$$

where  $L$  is the characteristic length of the cooled product and  $\lambda_{\text{air}}$  is the thermal conductivity of air.

For an overflowed chocolate plate (=tablets), the Reynolds number is given by:

$$\text{Re} = \frac{\rho_{\text{air}} v_{\text{air}} L_{\text{plate}}}{\eta_{\text{air}}} \quad (2.19)$$

where  $\rho_{\text{air}}$  is the density of the air,  $v_{\text{air}}$  is the air velocity,  $L_{\text{plate}}$  is the length of the plate and  $\eta_{\text{air}}$  is the air viscosity. This dimensionless number represents the ratio of inertia forces to viscous forces of the cooling medium (here: air).

Furthermore the Prandtl number represents the ratio of momentum diffusivity (kinematic viscosity) to thermal diffusivity within the air flow:

$$\text{Pr} = \frac{\eta_{\text{air}} c_{p,\text{air}}}{\lambda_{\text{HT,air}}} \approx \text{const} \approx 0.7 \quad (2.20)$$

where  $c_{p,\text{air}}$  is the specific heat capacity and  $\lambda_{\text{HT,air}}$  the heat conduction coefficient of air.

This value is approximately 0.7 for air within a wide range of regular temperatures at atmospheric pressure.

The Nusselt number can be approximated by  $\text{Re}$  and  $\text{Pr}$  for laminar, turbulent and transient condition, so that the dependency on the air flow speed becomes evident ( $\text{Re}_{\text{crit}} = 10^6$  for  $\text{Pr} > 0.6$ ; VDI, 2006):

$$\text{Nu}_{\text{lam}} = \frac{\alpha_{\text{HT}} L}{\lambda_{\text{HT,air}}} = 0.664 \text{Re}^{0.5} \text{Pr}^{1/3} \propto v^{0.5} \quad (2.21)$$

$$\text{Nu}_{\text{turb}} = 0.05 \text{Re}^{0.78} \text{Pr}^{0.42} \propto v_{\text{air}}^{0.78} \quad (2.22)$$

The Biot number represents the ratio of resistance by internal heat conduction to heat transfer dominated by forced convection.

$$\text{Bi} = \frac{\alpha_{\text{HT,air}} s_{\text{HT,prod}}}{\lambda_{\text{HT,prod}}} \quad (2.23)$$

## 2. Background

---

This factor points out that either product properties ( $\lambda_{\text{HT,prod}}$ ,  $s_{\text{HT, prod}}$ ) or the cooling conditions ( $\alpha_{\text{HTair}}$ ) are able to limit the speed of a cooling process until the core temperature of the product center changes.

### 2.2.4. Spray Chilling - Prilling

The conditions during solidification of atomized fats by spray chilling (*prilling*) are extreme from a kinetic point of view. Of course, the basic principles of heat transfer are still valid (Chap. 2.2.3), while the correlations for the overflowed sphere instead of a plate have to be considered (VDI, 2006). The created droplets are small. The temperature gradients and the heat transfer coefficient very high. Consequently, the release of specific and latent heat is accelerated.

The atomization of fluids itself relies on a sufficient relative velocity of the fluid being sprayed and the surrounding gas phase. This can be realized by pressure atomizers (pressure nozzle), air-assist atomizers (two-component nozzle systems) or rotary atomizers. High pressure nozzles are simple systems, but most efficient to achieve very small particles. However, the particle size distribution (PSD) is coupled to the liquid flow rate. Furthermore clogging of the nozzle can occur for shear thickening liquid systems. Both problems are solved by the use of two-component nozzle systems. The liquid flow rate is controlled by a low feed pressure (<10 bar) and the breakup is realized by parallel injection of pressurized air. The junction can be realized externally (external mixing) or internally (internal mixing), which results in a more efficient breakup but also in a back pressure. Generally, such nozzles can handle high viscous fluids, but they are energetically inefficient at the same time (Lefebvre, 1989). To avoid only clogging of shear thickening material, rotary atomizers can be used. Similar to the air-assist systems the maximal shear rate is obtained outside the nozzle due to the centrifugal acceleration. Other concepts exist like ultrasonic systems. However they are rather niche processes and not of interest for the present work. Details of the design and working principles of atomization systems are given in Walzel (2009) and Lefebvre (1989).

The Weber number describes the ratio of the fluid's inertia to surface tension:

$$\text{We} = \frac{\rho_{\text{liq}} v_{\text{rel}}^2 d_{\text{drop}}}{\gamma_{\text{liq}}^*} \quad (2.24)$$

where  $\rho_{\text{liq}}$  is the density of the liquid,  $v_{\text{rel}}$  is the relative velocity,  $d_{\text{drop}}$  is the droplet diameter and  $\gamma_{\text{liq}}^*$  is the interfacial tension of the liquid to air.

A drop breaks up if  $We$  exceeds the critical value of  $8/c_d$ , where  $c_d$  is the drag coefficient (Lefebvre, 1989). This can be achieved by an increase of the relative

velocity. For spraying, the initial droplet diameter is preset by the diameter of the spray nozzle  $d_n$ . The required, velocity difference of the liquid feed and the air is created by the pressure drop of the product itself (pressure nozzle) or of the adjacent air stream (pneumatic nozzle). Ohnesorge (1936) identified the relation of product surface tension, inertia moments and viscosity, to define the type of jet breakup, by the use of the Weber number and the Reynolds number (Eqn. 2.24-2.26).

$$\text{Re} = \frac{\rho_{\text{liq}} v_{\text{rel}} d_n}{\eta_{\text{liq}}} \quad (2.25)$$

$$\text{Oh} = \frac{\sqrt{\text{We}}}{\text{Re}} = \frac{\eta_{\text{liq}}}{\sqrt{\gamma_{\text{liq}}^* \rho_{\text{liq}} d_n}} \quad (2.26)$$

where  $\eta_{\text{liq}}$  is the viscosity of the liquid.

The Ohnesorge number of a specified, Newtonian liquid is a function of the material properties and the nozzle diameter only. Starting at zero speed the categories dripping, jetting, wave breakup and atomization (Walzel, 2009) are therefore crossed by a horizontal shift ( $\text{Oh}=\text{const.}$ ) with increasing velocity (Fig. 2.4). For shear-thinning (and shear thickening) behavior, this shift is superimposed with a reduction (increase) of the Ohnesorge number and an increase (decrease) in Reynolds number.

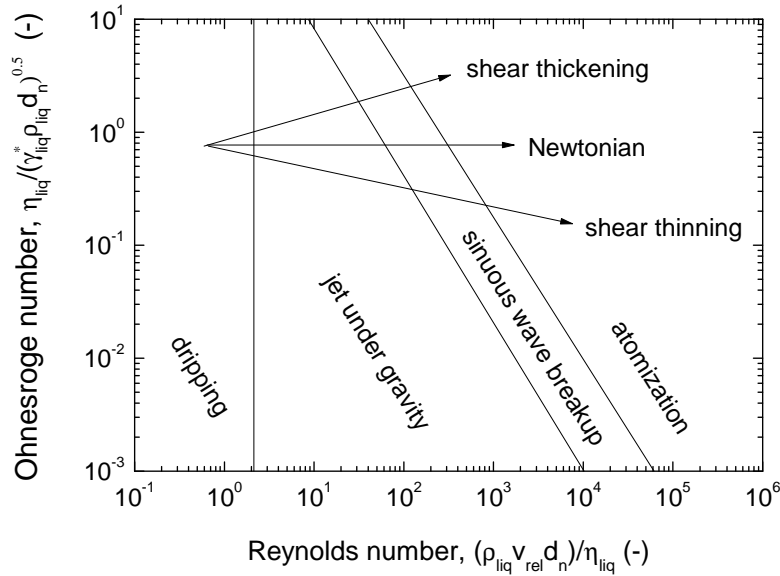


Figure 2.4.: Illustration of Ohnesorge-Reynolds relation for the general classification of jet breakup regimes, arrows indicate the effect of increasing  $v_{\text{rel}}$ ;  $v_{\text{rel}}$ : relative velocity of liquid to air at the nozzle outlet.

## 2. Background

---

Prilling of fat and cocoa butter in particular, was performed by Wagner (1997) and Zeng (2000). Pressure nozzles were used. Apart from the effect on the PSD by variation of the process parameters, the polymorphic quality and stability on storage was of interest. The powder contained a mixture of several crystalline forms and transformation processes were evident on subsequent storage towards the  $\beta$  state. Spraying of a cocoa butter seed slurry did not result in an improvement of the polymorphic quality immediately after the atomization process.



## 3. Materials, Processes and Methods

### 3.1. Materials

#### 3.1.1. Vegetable Fats

Non-cocoa butter vegetable fats were provided by Nutriswiss AG (Lyss, Switzerland) and Florin AG (MuttENZ, Switzerland). Cocoa butter was supplied by Maestrani AG (Flawil, Switzerland) and hazelnut oil from Sabo (Manno, Switzerland). The lauric fat named *Laurina*<sup>®</sup> is a designed fat of lauric components serving as a cocoa butter replacer. Triglyceride composition and SFC as function of temperature are given in Tables 3.1 and 3.2.

Table 3.1.: Fatty acid distribution, content of free fatty acids and trans fatty acids of confectionery fats investigated, in mass-%.

fatty acid	cocos	palm kernel		Laurina <sup>®</sup>	original		mid	palm		super stearin	hazelnut
		original	stearin		PO <sup>b</sup>	PM <sup>b</sup>		PS <sup>b</sup>	PSS <sup>b</sup>		
	CO <sup>a</sup>	PK <sup>a</sup>	PKS <sup>b</sup>	LA <sup>b</sup>							HO <sup>c</sup>
caprylic	C 8:0	7.5	3.9	1.8	1.4	-	-	0	0	-	-
capric	C 10:0	6.0	3.6	2.8	2.0	0.1	-	0	0	-	-
lauric	C 12:0	46.2	48.4	54.8	38.9	0.3	1.1	0.3	0.2	-	-
myristic	C 14:0	17.3	15.8	21.0	15.3	1.1	1.5	1.4	1.2	<0.1	<0.1
palmitic	C 16:0	9.5	8.2	9.5	26.2	42.0	43.8	57.8	74.9	4.5-7.5	4.5-7.5
stearic	C 18:0	2.9	2.5	2.0	3.8	5.8	6.3	5.6	4.9	1.8-3.2	1.8-3.2
oleic	C 18:1	8.3	14.9	7.0	9.3	39.9	37.6	27.6	14.3	77.0-84.0	77.0-84.0
linoleic	C 18:2	2.0	2.5	1.1	1.7	9.1	7.9	6.3	3.4	6.0-14.0	6.0-14.0
linolenic	C 18:3	0.2	0.1	0	0.1	0.2	0.2	0.1	0.1	<0.3	<0.3
arachic	C 20:0	0.1	0.1	0	0.1	0.4	0.4	0.4	0.3	<0.3	<0.3
sum	100.0	100.0	100.0	100.0	98.8	98.9	98.5	99.8	99.3	>89.3	>89.3
free FA	0.02	0.01	0.03	0.03	0.03	0.03	0.03	0.03	0.03	-	-
trans FA	-	-	0	0	0.1	0.1	0.6	0.3	0	<2.0	<2.0

<sup>a</sup>Florin<sup>b</sup>Nutriswiss<sup>c</sup>Sabo

Table 3.2.: Solid fat content by variation of temperature in mass-% as provided by supplier according to official AOCS standards (AOCS, 1999a).

temperature °C	cocos		palm kernel		Laurina®		palm		super stearin	
	CO <sup>a</sup>	original PK <sup>a</sup>	original PKS <sup>b</sup>	LA <sup>b</sup>	PO <sup>b</sup>	mid PM <sup>b</sup>	original PS <sup>b</sup>	mid PM <sup>b</sup>	original PS <sup>b</sup>	mid PM <sup>b</sup>
10	74.1	70.8	-	92.6	47.2	61.2	-	-	-	-
15	58.3	60.0	-	-	-	48.6	-	-	-	-
20	29.8	41.6	81.9	81.8	24.4	28.4	-	-	-	-
25	0.2	17.7	63.8	63.3	-	10.1	-	-	-	-
30	0	0.1	26.9	35.2	9.4	4.3	43.9	87.1	-	-
35	-	0	0	0.7	-	0	-	-	-	-
40	-	-	-	-	-	-	26.3	74.8	-	-
d.p. [°C]	25.1	28.8	33.9	37.0	39.6	32.8	-	-	-	-

<sup>a</sup>Florin  
<sup>b</sup>Nutriswiss

### 3.1.2. Confectionery Masses

For the application trials in Chapters 5.2 and 5.3, dark chocolate and a praline of dark chocolate and nougat filling were used. Both masses were provided by Bühler AG (Uzwil, Switzerland). The ingredient list is shown in in Table 3.3.

Table 3.3.: Recipes of confectionery masses.

ingredient	dark chocolate	nougat filling
-	%	%
cocoa mass	40	-
cocoa powder	-	4
add. cocoa butter	9.58	25.58
sugar	50	38
hazelnut paste	-	22
whole milk powder	-	10
lecithin	0.4	0.4
vanillin	0.02	0.02
total fat	32	43

## 3.2. Processes

### 3.2.1. Seed Production

Using the seed-crystallization technology, condition of initial crystals reacting as nuclei during the final cooling process can be very well determined. Melting characteristics, crystal size, morphology, polymorphic structure and seed amount can be analyzed before mixing into the melt. Seed production was performed batchwise, by the concept of high shear crystallization, followed by a ripening step. Two scale size units were used. The smaller pilot plant scale ( $V \approx 101$ ) was used for non-cocoa butter fats, while the industrial scale ( $V \approx 1501$ ) was employed for cocoa butter.

### Pilot Plant Scale

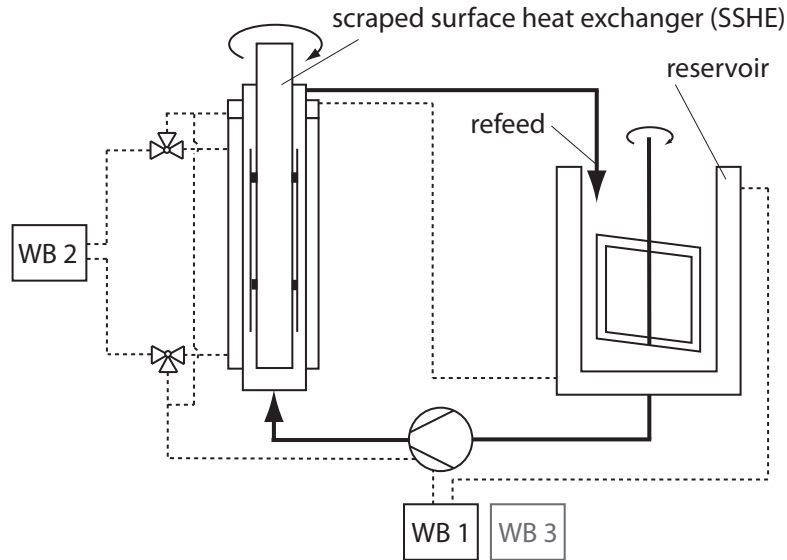


Figure 3.1.: Flow chart and details of seed production on pilot plant scale, WB: water bath.

The pilot plant scale apparatus is based on a scraped surface heat exchanger (SSHE) described by Zeng (2000). It works in a batchwise procedure and consists of two process units (Fig. 3.1). They are temperature controlled by water baths (WB1-WB3) attached to the double-wall designed components. The reservoir contains the molten bulk fat mass. The fat is fed by a temperature controlled eccentric screw pump (NEMO NM 005B, Netzsch Pumpen & Systeme GmbH, Germany) into the crystallization unit. The high shear crystallizer consists of an outer stator ( $d = 62 \text{ mm}$ ) and an inner rotor ( $d = 50 \text{ mm}$ ) equipped with two opposing blades, which scrape at the outer cylinder by rotational control. This results in a ring-shear gap. Pump speed as well as rotor speed are frequency controlled (0–50 Hz, VLT 3006 ST, Danfoss, Denmark). By a three-way valve system and an additional water bath, the temperature control of the core crystallization unit (Scraped Surface Heat Exchanger - SSHE) can be separated from the rest, (outlet of crystallizer, reservoir tank, pump) thereby enabling a fast switch to crystallization temperature when production starts. Since the residence time of the fluid in the crystallization unit is rather low and the temperature difference of incoming fat to set temperature is high, a powerful cooling system has to be used (FPW55 water bath, Lauda-Königshofen, Germany).

Seed production was generally divided into three periods. During a preparation step of 15 minutes, the molten fat ( $T > T_{melt}$ ) was pumped in a loop and all components are heated above fat melting temperature. Production was initiated by starting the scraper blade system. Secondly the pre-heating water bath (WB1,  $T \geq 50^\circ\text{C}$ ) was exchanged by another system (WB3) tempered to ripening temperature. Further, the water circulation for the crystallizing unit was decoupled from the rest and connected to its own system (WB2). For the final ripening period, the temperature was synchronized again by the three-way valve system and the high shear rotor was stopped. Seed material probes were taken from the refeed into the reservoir, for analysis and further experimentats.

Based on Zeng (2000), high shear crystallization was performed at 900 rpm to obtain small crystal sizes. Standard crystallization time was set to 60 min. Corresponding shear rate ( $\dot{\gamma}$ ) is approximated by Equation 3.1 to  $540\text{s}^{-1}$  without taking the shear blades into account.

$$\dot{\gamma} = \frac{2 \cdot \omega_{\text{rot}}}{1 - (r_i/r_a)^2} = \frac{4\pi \cdot n}{60[1 - (r_i/r_o)^2]} \quad (3.1)$$

where  $\omega_{\text{rot}}$  is the angular velocity [rad/s] of rotation,  $r_i$  denotes the radius of the inner rotor  $r_o$  of the outer stator, and  $n$  stands for rotation frequency [ $\text{min}^{-1}$ ].

Crystallization time had to be reduced for palm super stearin, in order to avoid any pipe blockage. The fats investigated and their individual process parameters as well as analytical results of the seed suspensions are listed in Table 3.4.

Table 3.4.: Process parameter for seed production of confectionary fats on a scraped surface heat exchanger (pilot plant scale), melting endset (DSC) of seed suspension listed.

fat	$T_{\text{cryst}}$ °C	$T_{\text{ripe}}$ °C	$SFC_{\text{ripe}}$ %	melting endset °C
PK	20	25.5	5.1	30.0
PKS	28	30.5	8.5	36.8
LA	30	36	5.5	38.6
PM	15	27	8.2	41.0
PSS	45	61	3.0	64.2

## Industrial Scale

Seed production of cocoa butter fat was performed on a *SeedMaster* device (version *ChrystMix*, Bühler AG, Uzwil, Switzerland). It is an scale-up form the pilot plant unit. It is described in more detail by Mehrle (2007). Temperatures during crystallization and ripening, as well as operating times, are adapted to the requirements of the cocoa butter fat. In addition, a modification of reservoir temperature control was implemented by Bühler to optimize processing time and crystal quality. After the crystallization period the reservoir temperature is increased to promote the  $\beta^V$  to  $\beta^{VI}$  transformation process. Production is finished as soon as a critical differential pressure in the loop section is measured, which correlates to a corresponding viscosity (SFC value). Details of the process parameters are displayed in Table 3.5. The final solid fat content after ripening was 8-9%. Since there was no special transformation process observed for non-cocoa butter fats, the final solid fat content was rather constant, whereas in the case of cocoa butter, a slight increase was observed over several hours of ripening. The fraction of  $\beta^{VI}$  crystals reaches a main melting temperature of nearly 36°C as quantified by DSC analysis (Fig. 3.2). Their morphology and size is comparable to the palm based seed crystals.

Table 3.5.: Process parameters of cocoa butter seed production by the industrial *SeedMaster Cryst* device.

stage	$T_{\text{cryst}}$ °C	$T_{\text{tank}}$ °C	$T_{\text{pipe}}$ °C	time period
melting	47	47	47	until melted
crystallization	15	26	32	80min
ripening	-	31	32	$\Delta p \geq \Delta p_{\text{crit}}$

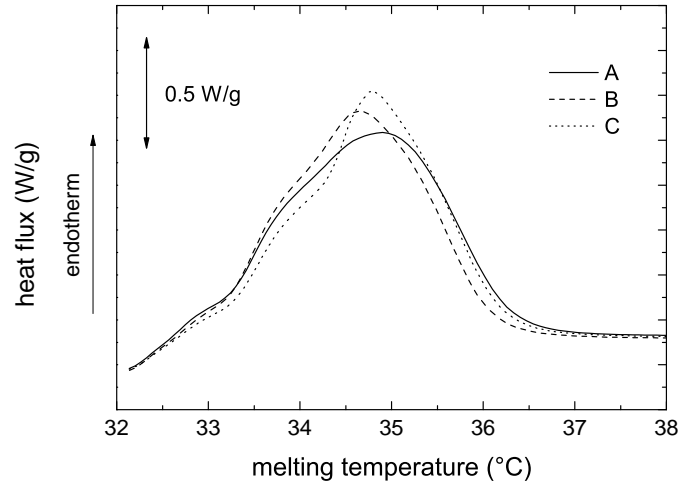


Figure 3.2.: Melting characteristics (triplicate: A, B, C) of cocoa butter seed suspension after several hours of ripening, produced by the *SeedMaster* device.

#### 3.2.2. Precrystallization

##### Conventional Tempering

Conventional tempering was performed only for the application test of cocoa butter powder seeding as a reference. A lab scale 50l temper device was used (Fig. 3.3, AMK50, Aasted Mikroverk, Farum, Denmark). Chocolate was melted over night at 47°C and recirculated for 1 hr before the production was started. Operating temperature profile is outlined in Table 3.6. The tempered chocolate was moulded by hand directly into tablets of 100 g and cooled down to 10°C in a cooling chamber.

Table 3.6.: Temperature parameter for conventional tempering of dark chocolate.

zone type	zone no.	temperature [°C]
re-melting	0	46
pre-cooling	1	29.0
cooling	2	20.5
reheating	3	25.0



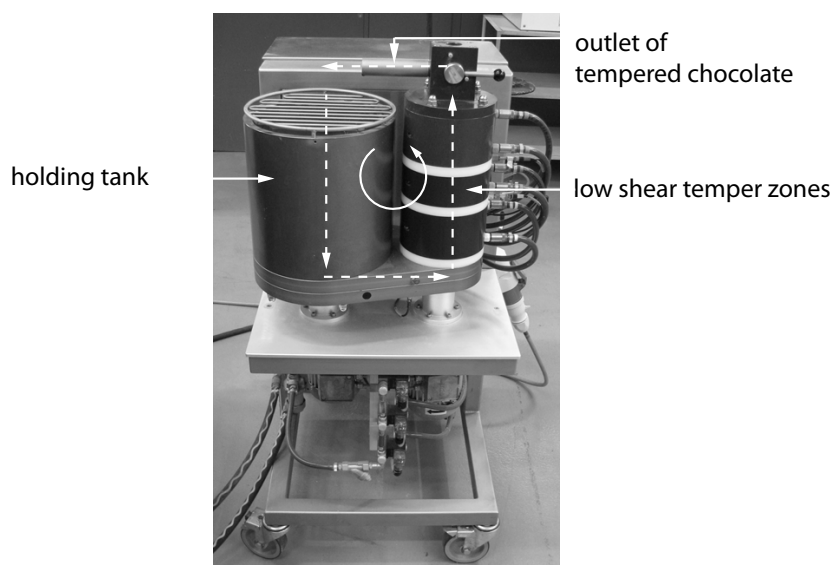


Figure 3.3.: Conventional tempering device operating with a recirculating three-zone system; AMK50, Aasted Mikroverk.

### Bench-Top Tempering

Molten cocoa butter was cooled down from 50 °C to 32.5 °C in a temperature controlled beaker. A cooling step at 22.5 °C was performed while stirring (120 rpm) for 40 min before temperature was raised to 31 °C for 20 min. Temperature history of the fat during processing and final temper seed quality ( $\beta^V$ ) are shown in Figure 3.4.

### Suspension Seeding

Precrystallization by suspension seeding was performed for determination of solidification kinetics by NMR analysis in Chapter 4.2.1 as well as contraction kinetics by the rheometric approach in Chapter 4.2.2. The mixing ratio of melt and seed was adjusted individually to reach an absolute seed concentration of 0.5 %. Fats were melted over night at 50 °C or 70 °C (palm stearin fats) and thermostated within a double jacketed beaker to corresponding ripening temperature of the seed suspension produced by the lab scaled SSHE (non-cocoa butter) or *SeedMaster* (cocoa butter) respectively. Required suspension volume was added successively to the molten fat by a syringe to optimize mixing homogeneity. After 10 min of stirring the seeded fat was immediately used for solidification or contraction analysis. Seeding was performed anew for each set analyzed to guarantee comparability within preparation procedure.

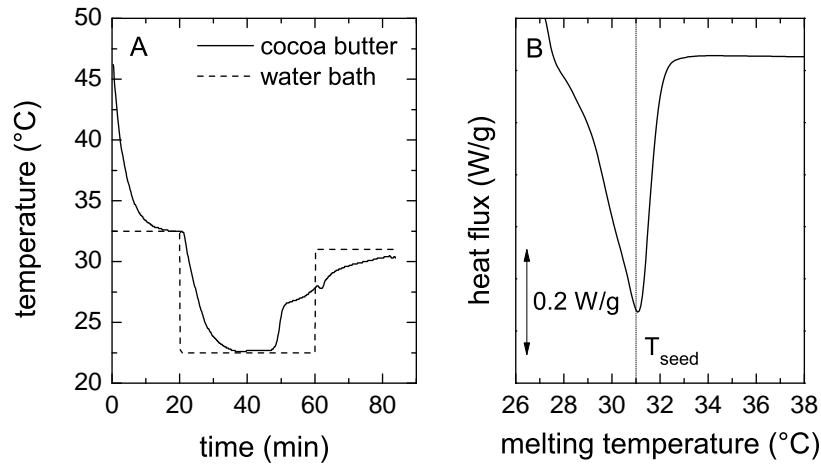


Figure 3.4.: Hand tempering details; A: Temperature control and product temperature progression during processing, B: Melting characteristics of the final hand temper seed after stabilization at 27°C.

Seeding of confectionery masses was performed in the same way. Melting period at 50°C was extended to 24 h. Additionally, the masses were evacuated ( $p = 250$  mbar) to remove entrapped air. Since molten fats are much less viscous compared to molten chocolate, this was not necessary for pure fats. Seed concentration was adjusted to the empirical approach of tempercurve analysis (Chap. 2.2.1). For the present experiments (Chap. 5.2), seed concentrations of 0.5 % for dark chocolate and 1 % for hazelnut filling were determined, resulting in approximately 0.125–0.140 % and 0.185–0.210 % of seed crystals in the fat phase. For pure fat systems seed concentration was elevated to a constant value for each fat to guarantee a sufficient seed amount and to keep comparability.

#### Powder Seeding

Homogeneous mixing of small amounts of powder into a liquid is challenging. One of the reasons is powder agglomeration due to wetting. For application tests with spray-chilled cocoa butter seed powder, a semi-manual method was worked out achieving a reproducible precrystallization state controlled by tempercurve analysis. Melted chocolate was poured into an horizontal double-screwed kneading device (IKAVISC Messknetter, IKA Werke, Staufen, Germany) and cooled down to seeding temperature (31.5°C). The stored powder ( $T_{storage} = 10^\circ\text{C}$ ) was disagglomerated by a sieve and thereby trickled into the chocolate, continuously stirred by low energy input. After 5 min of mixing the tempercurve test was performed and chocolate bars were

moulded. Required amount of seed powder was determined to 0.8 % by tempercurve analysis. Even by approximation of partial remelting of the small fraction of lower stable powder seeds to 30 %, the effective seed crystal amount (SI0.75%) in fat) is increased by factor 5-6 compared to suspension seeding. It reflects the positive seeding effect of a smaller seed crystal size (seed suspension) and the inhomogeneity problems of powder/liquid mixing stated earlier (seed powder).

## Nomenclature

Within this thesis the term *tempered* stands for minor temperature fluctuations during low shear treatment of the mass to be precrystallized as described in Chapters 3.2.2 and 3.2.2. *Seeded* stands for the addition of a crystal seed suspension (Chap. 3.2.2) or powder (Chap. 3.2.2) to the bulk mass (fat or chocolate). *Non-tempered* and *non-seeded* are synonyms for any precrystallization treatment at all, but crystallization out of a perfect melt.

## 3.2.3. Moulding

### Manual

Moulding of single components, such as pure cocoa butter for structure density investigations (Chap. 5.1) or pure chocolate for powder seeding application (Chap.5.3) and cooling experiments (Chap. 5.2), was performed manually. After seeding, the mass was poured gently into the moulds, air bubbles were removed on a vibrating table for approximately 10sec and excessive material was scraped off by a spatula. The period from moulding to start of cooling was kept constant at about 1 min. For pure chocolate pralines used as reference samples in Chapter 5.2, the moulded mass stayed another 3 min at ambient temperature for comparison reasons (see One-Shot).

### One-Shot

The *One-Shot* depositer GKH-ed (Bühler Bindler GmbH, Bergneustadt, Germany) was used (Fig. 3.5 A). A SIMATIC PC FI 10 control panel (Siemens AG, München, Germany) is operating on a Windows 95 PC-system (Microsoft Corp., Redmond, US). Mould design was simplified by combination of a cylinder on top of a half sphere ( $d = 28$  mm, Fig. 3.6). Therefore, the operational mode *center deposit filling* (CDF) could be used. Total volume was 17.5 ml. Chocolate-to-filling volume ratio was set to 45:55 resulting in a shell thickness of  $s_{shell} = 1.75$  mm  $\pm$  0.5 mm. Applied depositing profiles were based on the findings of Padar (2009) and gradually optimized within

### 3. Materials, Processes and Methods

pre-trials (Fig. 3.5 B). Only one praline per shot was produced, leading to a 3.5–4 min depositing time for 30 pralines.

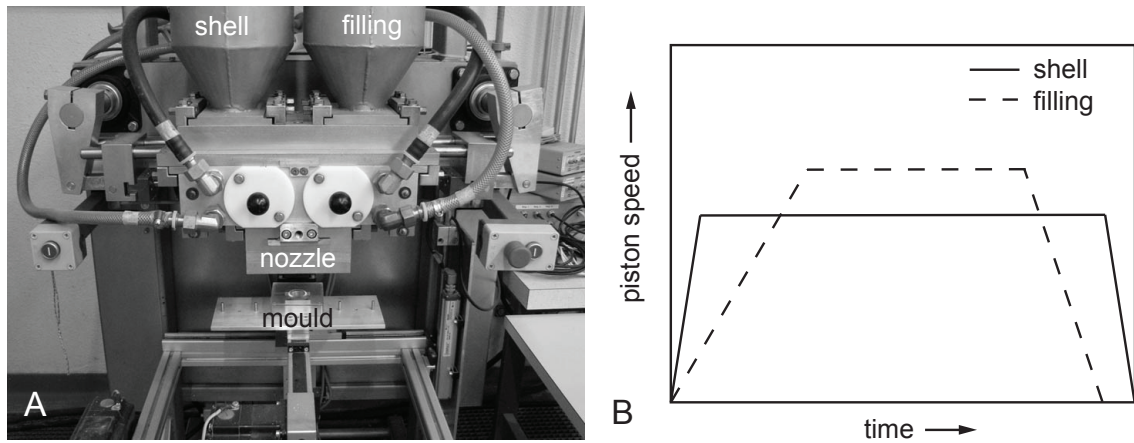


Figure 3.5.: Photography of *One-Shot* equipment (A) and sketch of depositing profile for chocolate shell and filling mass (B).

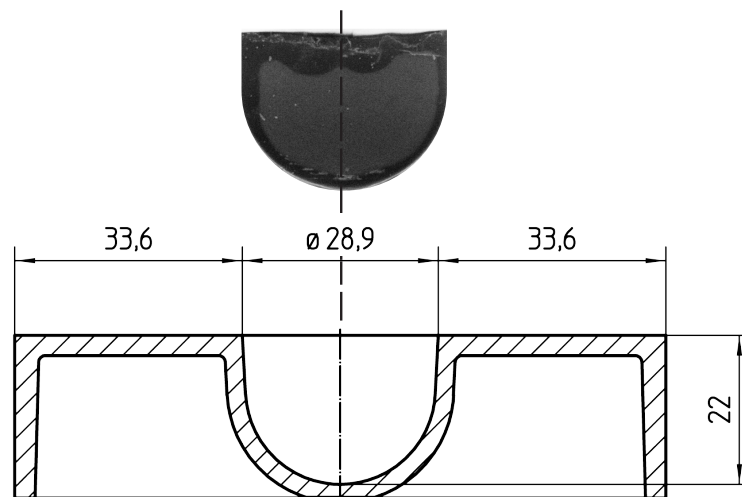


Figure 3.6.: Praline profile and mould geometry of *One-Shot* praline systems produced; dimensions in mm.

### 3.2.4. Cooling

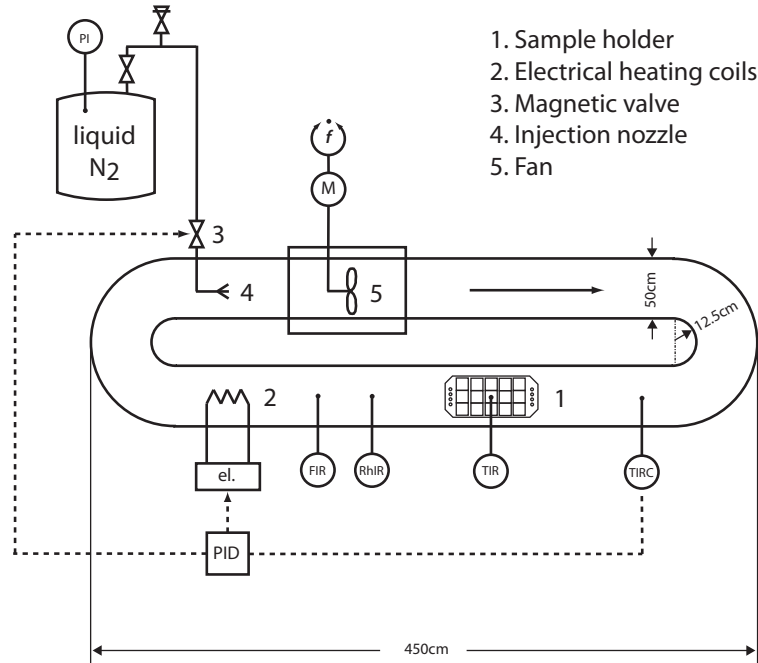


Figure 3.7.: Cross sectional view of praline mould and profile of final praline, distances given in cm.

After moulding, the pralines were loaded on a two level rack (Fig. 3.8). Cooling trials were performed on an ETH workshop made cooling tunnel (Fig. 3.7). It consists of a 4.5 m long oval loop driven by a fan and cooled down to desired temperature by injection of liquid nitrogen out of a 60 l reservoir. An electrical heating system and an automatic control unit are installed for precise temperature regulation.

Product temperature was monitored by thermocouples (k-type, 1 mm, Thermocoax, Suresnes, France) in central mould position of the upper level (A), reflecting local temperatures from the core to the shell region (Fig. 3.9). Detachment (Chap. 3.3.8) was analyzed at an adjacent mould (B). Texture analysis was performed alternately in the first cross row (C) by needle penetration. Local temperatures of the cooling tunnel as well as the product were logged by a LabVIEW program on a central PC unit.

The cooling parameters applied were based on discussions with industrial producers and machine manufacturers resulting in regular values ( $T_{\text{tunnel}} = 12^{\circ}\text{C}$ ;  $v_{\text{tunnel}} = 1 \text{ m/s}$ ,  $3 \text{ m/s}$ ), practical limits ( $T_{\text{tunnel}} = 7^{\circ}\text{C}$ ;  $v_{\text{tunnel}} = 6 \text{ m/s}$ ) and extreme conditions ( $T_{\text{tunnel}} = -10^{\circ}\text{C}$ ) of regular industrial equipment. Four runs were performed for each

parameter set producing 30 pralines per run. The cooling period was 30 min. Re-warming to 7°C ( $\approx 20$  min) was necessary after cooling at  $T_{\text{tunnel}} = -10^\circ\text{C}$  to prevent condensation. Results are presented in Chapter 5.2.

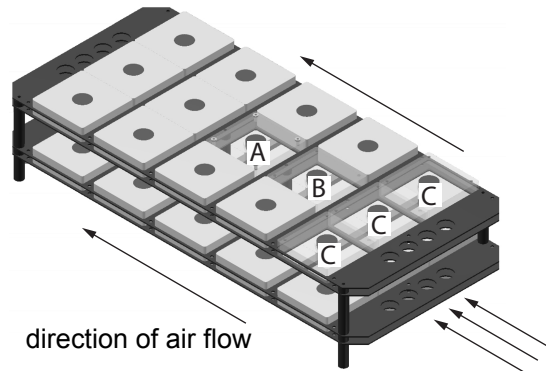


Figure 3.8.: Sketch of mould rack for air cooling experiments., praline positioning of corresponding analysis tool: A - temperature sensors, B - DetachLog, C - needle penetration.

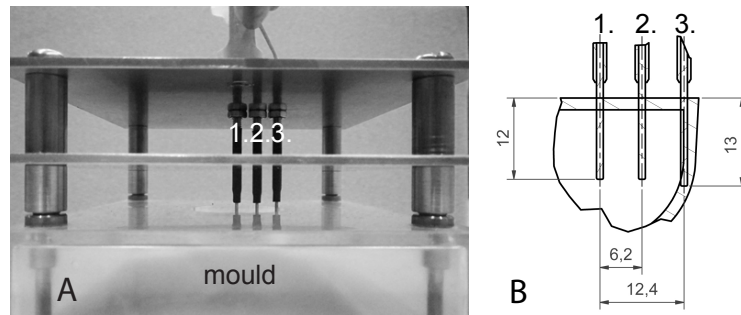


Figure 3.9.: Thermocouple installation for monitoring of local time-temperature history at local praline spots; A - combined with praline mould, B - local alignment, distances in mm.

### 3.2.5. Spray Chilling

The setup for spray chilling of cocoa butter seed suspension is based on a concept by Wagner (1997). An isolated tower with a height of 4.5 m and a diameter of 1 m was cooled down by directly induced liquid nitrogen at several locations at the head room, with a temperature control system regulating the liquid nitrogen feed. Cocoa butter seed suspension was produced on the industrial *SeedMaster* device and transferred to a temperature controlled reservoir. The highly viscous suspension was pumped by a rotary lobe pump (SRU/S1-0005-V08, SSP Pumps, Eastbourne, England) into a double jacket, flexible tube system especially designed for this purpose combined with the two-component nozzle system (Spraying System Co., Pfäffikon, Switzerland). It is also temperature controlled by a double jacketed design (Fig. 3.10).

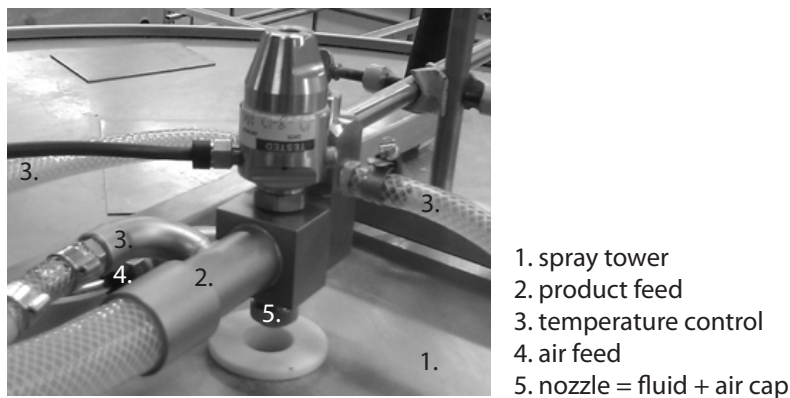


Figure 3.10.: Pneumatic two-component nozzle system for prilling of temperature sensitive fat suspensions.

In contrast to a pressure nozzle design, the process parameters product flow rate and dispersing forces are decoupled, by use of a two-component system. On the other hand, the dispersing air flow had to be preheated to reduce additional energy removal of the product stream directly at the place of dispersion due to expansion effects. Two-component systems consist of an outer air cap for dispersion and the inner fluid cap for the product inlet. Pre-trials showed that a simple A/L-volume ratio of pressurized air (A) to dispersed liquid (L) is not the crucial factor for particle size control (Schroeder *et al.*, 2012). Not the volume flow rate itself but the velocity of the decompressed air causes the effective disruption of the liquid as defined by the Weber number (Eqn. 2.24). Increase of air cap diameter and thereby increased air volume flow at constant feed nozzle diameter and constant air pressure did not reduce particle sizes significantly. Therefore the geometry combination of the two-component nozzle system was kept constant. Based on the tower dimension and the available

pump performance, a fluid cap of  $d = 0.7\text{mm}$  (type 2850) was used in combination with an air cap of  $d_{\text{inner}} = 1.3\text{mm}$ ,  $d_{\text{outer}} = 1.8\text{mm}$  (type 70).

Three series of experiments were performed regarding the process parameter variation of cooling temperature, product flow rate and dispersing air pressure respectively (Appendix, Tab. B.10). The feed pump had to be changed to an eccentric screw pump (EDS 4.2, Hilge GmbH & Co. KG, Bodenheim, Germany) for small product flow rates and for the low viscous melt of the reference trial. The feed pipe had to be conditioned at  $33^{\circ}\text{C}$  to avoid any risk of pipe blocking. Since mainly  $\beta^{VI}$  crystals are present at this stage, the elevated temperature is not destroying seed crystals, but rather enhances process stability. A reference trial with molten cocoa butter at  $50^{\circ}\text{C}$  was performed for direct evaluation of the seed crystal effect. The temperature outlet of expanded, dispersing air was checked to lay between  $30^{\circ}\text{C}$  to  $33^{\circ}\text{C}$ .

## 3.3. Methods

### 3.3.1. Melting Characteristics

For the determination of crystallization and melting characteristics such as phase transition temperature ranges (onset, endset), peak temperatures and melting enthalpy, differential scanning calorimetry (DSC) measurements were performed. A STAR<sup>e</sup> system consisting of a DSC822<sup>e</sup> module and the STAR<sup>e</sup> software version 8.10 (Windows) were used (Mettler Toledo GmbH, Greifensee, Switzerland).

Two aluminum pans ( $V_{\text{pan}}=40\mu\text{l}$ ), each placed on several highly sensitive temperature sensors, are heated or cooled simultaneously with a controlled rate. The reference pan is empty, the sample pan is filled with 5-10mg of product. Sealing of the pan by an aluminum lid is not mandatory, as there is no oxygen sensitivity, evaporation or chemical reaction by the fat sample. If phase transition occurs, temperatures of reference and sample pan differ. The additional heat flux for the compensation of the sample to reference temperature difference is evaluated and recorded. Typical DSC graphs display heat flux values versus sample temperature (dynamic) or time (static). General DIN norms are not appropriate in the case of fat studies, as fat shows rather broad and partially inhomogeneous phase transitions ranges. Therefore the standard parameters were modified for our systems.

For static experiments **without precrystallization**, no special preparation method was needed and the melted samples (generally at  $50^{\circ}\text{C}$ , palm stearin at  $80^{\circ}\text{C}$ ) were placed into the pans using pipettes. For storage tests or direct analysis of pretreated masses, the aluminum pans, lids and tools were tempered to sample temperature. Insulated containers were used to keep samples and pans at the appropriate temperature. Alternatively preparation was performed within a climate chamber. If



not otherwise specified, cooling rate was set to 10°C/min and the heating rate to 5°C/min respectively. Cooling rates were rather high compared to industrial cooling tunnel conditions. They were applied anyhow to avoid recrystallization processes during cooling stage and to check the effect of seed crystals compared to non-seeded samples. The melting rate value was chosen, since it is an appropriate compromise between too slow (transformation inducing) and too fast (curve shift to higher temperatures) treatments. For evaluation of the crystallization/melting curve the characteristic values such as extrapolated melting peak, endset and heat flux integral were used. A horizontal baseline at the heat flux level of  $T = T_{\text{end}} + 5^\circ\text{C}$  was chosen for the parameter evaluation.

**Solid samples** were transferred in a temperature controlled box and prepared on a table by scalpel and spatula at ambient conditions. Sample mass was adjusted prior to analysis and pans were sealed. The DSC melting program generally started with 1 min of equilibration at corresponding storage temperature of the sample prior to melting. Corresponding samples were:

- solidified seed suspensions,
- cocoa butter samples for structure density investigations,
- confectionery products such as plain chocolate, filling masses and specific fat bloom samples of products.

For specific evaluation of fat bloom on confectionary product, only the upper and preferably dull or grey surface layer was scraped off by a scalpel. Filling mass samples of pralines were taken from the central point of the product. Duplicates of two different pralines were performed (4 measures).

**Seed suspensions** were typically sensitive in time and temperature since the probe temperature was within the corresponding melting range. For reduction of preparation time, semi-solid and suspension samples were analyzed without a lid and sample weight was determined after melting analysis.

### 3.3.2. Solid Fat Content

Most of the macroscopic properties of fat crystal networks correlate with the solid fat content, presented as solid fraction of the whole fat content in [-] or [%]. This value can be determined by low resolution, pulsed, nuclear magnetic resonance analysis (NMR). The proton of a hydrogen atom nucleus is spinning and leading thereby to a magnetic dipole moment. By applying an external magnetic field, precession of nuclei are aligning parallel to this field to minimize energy state, resulting in a magnetization vector of distinct magnitude. The resonance frequency of hydrogen protons at a permanent magnetic flux density of 0.47 Tesla is 20MHz (Larmor frequency). By

application of pulsed radio waves of the same frequency, the magnetic vector can be deflected by  $180^\circ$ . By a first relaxation process, a redirection of precession towards the permanent magnetic field occurs. The absolute value of this antiparallel vector is therefore decreasing towards zero and finally increasing up to the starting value of the initial vector. A time-resolved determination of this relaxation process can be carried out by additional, multiple  $90^\circ$ -deflections for separation of permanent and sample specific magnetic vector. Thereby, the so-called spin-grid relaxation time  $t_1$  is determined. Furthermore, a second relaxation time  $t_2$  is describing the spin-spin relaxation process. It is based on the intensity decrease towards zero after every single deflection of  $90^\circ$ . Both intensity curves are fitted with exponential growth and decay functions respectively, for final parameter determination.  $t_1$ - and  $t_2$ -relaxations are dependent on the material itself and its state of aggregation. Generally, a solid phase relaxes much faster than its liquid phase. Quantification of solid fat content is only one of several applications of this particular technique.

Mainly two methods for final quantification exist. In the *indirect* method (AOCS, 1999a), the signal of the liquid fraction at the state of interest is compared with the signal of the complete melt at higher temperatures. In the *direct* method (AOCS, 1999b), as used here, the relaxation signal of the solid is directly compared with the signal of the liquid fraction. A three-point-calibration by the use of paraffin oil-acrylic glass standards is required. Raw signals  $11\ \mu\text{s}$  (for solid) and  $70\ \mu\text{s}$  (for liquid) after the impulse ( $mean_{11}, mean_{70}$ ) are corrected by the calibration factors  $k_{\text{NMR}}$ ,  $f_{\text{NMR}}$  and  $o_{\text{NMR}}$ :

$$SFC_{dir} = \frac{(mean_{11} \cdot k_{\text{NMR}} - mean_{70}) \cdot f_{\text{NMR}}}{(mean_{11} \cdot k_{\text{NMR}} - mean_{70}) \cdot f_{\text{NMR}} + mean_{70}} \cdot 100 \quad (3.2)$$

where  $k_{\text{NMR}}$  stands for the slope value within the solid signal domain,  $f_{\text{NMR}}$  is used for extrapolation of signal value to  $t = 0\ \text{ms}$  and  $o_{\text{NMR}}$  is the digital offset factor, to correct for the non-linearity or offset of the detector.

Measurements were performed on a *Minispec mq20* device (Bruker BioSpin AG, Fällanden, Switzerland). The samples, as well as the probe head, were tempered by an external water bath to the required measurement temperature. A single NMR value displays the average of four evaluation cycles. Calibration was checked every 24 h of use. Measurement errors of less than 0.5 % in SFC are stated. For static measurements, the samples already reached examination temperature well in advance and no specific preparation procedure was needed. For kinetic determinations see section below.

### 3.3.3. Solidification Kinetics

For quantification of crystallization kinetics, a time-resolved progression of the solid fat content at distinct boundary conditions is generally used. The advantages of the NMR-technique are the defined probe geometry, a short period of single analysis and reliable quantification over a wide range of the whole solidification process. The downside is less sensitivity for low values which is important for precise nucleation time determination. DSC analysis is another tool regarding kinetic evaluation. It is very sensitive to small amounts of latent heat release and covers as well the whole range of solidification. For final interpretation, the exact values of melting enthalpy for every single polymorphic structure formed and their relative ratios have to be known additionally. Thereby the DSC method is very time-consuming for achieving overall quantitative solidification kinetics, only.

Since only comparison of series of vegetable fat and a range of crystallization temperature were of interest, the NMR-technique was chosen. For a controlled and reproducible cooling process, the NMR-tubes ( $d_{\text{NMR}} = 10 \text{ mm}$ ) were filled with 5 ml ( $\pm 0.25 \text{ ml}$ ) of sample fat and lined up in a massive, metal sample holder providing effective heat transfer properties. It was placed in a water bath at the set crystallization temperature. To reduce discontinuity of cooling during analysis ( $\Delta t_{\text{NMR}} \approx 10 \text{ s}$ ) multiple sample tubes were handled parallel within a single run. A first series was performed with three replicates and consecutive evaluation every single minute. In cases where the previous analysis was inconsistent in time progression or relative to results of adjacent temperatures, a second rung was performed with 9 samples decreasing the analysis intervall to 20 s.

In general, a final solid fat content range from 0% to 80% was of interest, thereby leading to a cooling temperature range from 5°C to 30°C, depending on the vegetable fat type. Minimum temperature was determined by practical traceability of SFC increase over time. Maximum temperature was defined by incomplete crystallization within a total period of 60 min. Limits were based on measurements of non-seeded samples.

The experiments were performed with several non-seeded and seeded fats (Appendix, Tab. A.1, A.2). Seed was provided by the scraped surface heat exchanger and gently mixed into the molten, pre-cooled fat by an automative stirrer. The seeding temperature was equal to the ripening conditions of the seed production process (Fig. 3.4). Approximately an initial SFC of 0.1 % for a pure fat sample is sufficient for a positive seeding effect of cocoa butter (Zeng, 2000). In the present case, a standardized SFC of 0.5 % for the seeded samples was adjusted based on the SFC-value of pure seed, to guarantee a seeding effect as long as the seed crystals are compatible with the molten fat. Experimental data was fitted by the *Approximate Avrami* equation (Eqn. 2.14) as well as one-, two- and three-dimensional growth equations (Eqn. 2.11-2.13). The quality of the fits is illustrated by the example of Laurina in Figure 3.11.

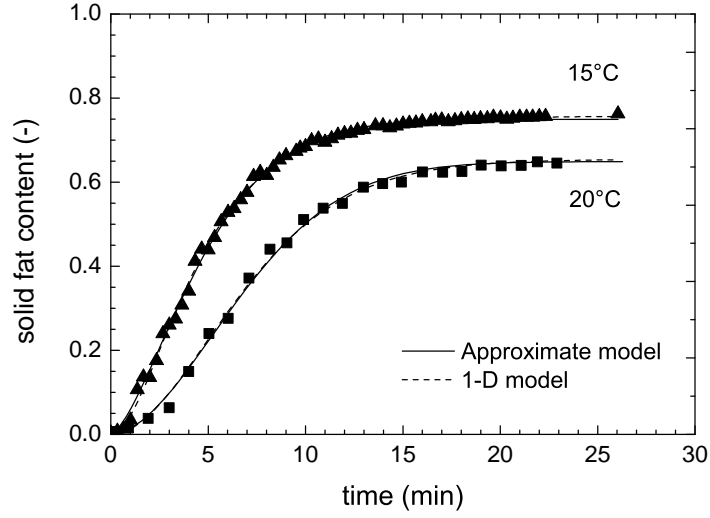


Figure 3.11.: Avrami fit of solidification curves from Laurina cooled from  $T_{start} = 50^\circ\text{C}$  and corrected by  $t_0$ ,  $R_{ave}^2 \geq 0.98$ .

Nucleation time was evaluated based on the restrictions of the minispec sensitivity ( $SFC_{min,NMR} = 0.5\%$ ). The associated time of the last SFC value below this limit was taken as the approximate nucleation phase (*lag time*) and zero point in time for the fittings. Absolute crystal growth rate  $g_{abs}$  was averaged from  $0.25 < SFC(t)/SFC_{max} < 0.75$  (Eqn. 3.3). Furthermore, this value was normalized to  $g_{rel}$  by the maximal SFC reached at corresponding temperature (Eqn. 3.4).

$$g_{abs} = \frac{SFC_{max}(0.75 - 0.25)}{t_{0.75} - t_{0.25}} \quad (3.3)$$

$$\begin{aligned} t_{0.75} &= t(SFC \equiv 0.75 \cdot SFC_{max}) \\ t_{0.25} &= t(SFC \equiv 0.25 \cdot SFC_{max}) \end{aligned}$$

$$g_{rel} = \frac{g_{abs}}{SFC_{max}} \quad (3.4)$$

An additional sample was equipped with a data logging system, recording probe core temperature during crystallization, providing insight into the latent heat release, similar to the principle of a chocolate tempermeter system. For comparison of the crystallization time  $t_{approx}$  without (Eqn. 3.6) and with seed (Eqn. 3.7), the approximated value of seeded samples had to be corrected, since seeding temperature was consist-

ently lower than the starting temperature of non-seeded samples. This correction was defined as time period from cooling start until reaching the seeding temperature of non-seeded samples. Periods of  $1 \text{ min} < t_{\text{cor}} < 2.5 \text{ min}$  were determined.

$$t_{\text{half}} = \frac{\ln 0.5^{-m_A}}{k} \quad (3.5)$$

$$t_{\text{approx, non-seeded}} = t_0 + 2 \cdot t_{\text{half}} \quad (3.6)$$

$$t_{\text{approx, seeded}} = t_0 + 2 \cdot t_{\text{half}} + t_{\text{cor}} \quad (3.7)$$

### 3.3.4. Contraction

Contraction of crystallizing fat is the consequence of a more dense packing of mass on several scales. As explained in 2.1.2, triglycerides are aligned along their fatty acid chains, forming a subcell structure on a molecular scale in the crystalline state. The variation of main subcell structures and potential modifications are dependent on their composition and homogeneity. Furthermore, strong supercooling leads to uncontrolled heterogeneous nucleation of a high number of polymorphic unstable nuclei, which finally interfere with each other after crystal growth. This results in imperfect crystal surface-surface packing, whereas crystal growth or nucleation at very low supercooling conditions leads to much less crystal-crystal interface area and thereby to a more compact structure on a macroscopic scale. Consequently, the density of a fat sample increases leading to volume contraction. In this study, quantification of relative and absolute values of contraction are of interest, as well as time-resolved development of this phenomena during crystallization.

### Archimedes Principle

From a theoretical point of view, a simple displacement setup according to the *Archimedes Principle* is capable of mass density analysis, either for objects of unknown volume or liquids. A balance (Mettler AE163, Mettler Toledo GmbH, Greifensee, Switzerland) with a sensitivity of  $10^{-5} \text{ g}$  is placed on top of a double-jacketed beaker, which is temperature-controlled by a water bath (Fig 3.12). The beaker is filled with demineralized water of known density ( $\rho_{\text{water}}(10^\circ\text{C}) = 0.9997 \text{ g/cm}^3$ ,  $\rho_{\text{water}}(20^\circ\text{C}) = 0.9982 \text{ g/cm}^3$ ). A sample holder made of polyvinylchloride and aluminum was constructed, keeping the probe in central position. It was hooked below the balance. By adjustment of the beaker, the sample was immersed into the liquid up to a marked height on the sample holder. Sample holder mass was determined in air and immersed in water for calibration reasons. For each sample placed on the sample holder, the probe was weighed in air ( $m_{\text{tot, air}}$ ) and subsequently immersed in

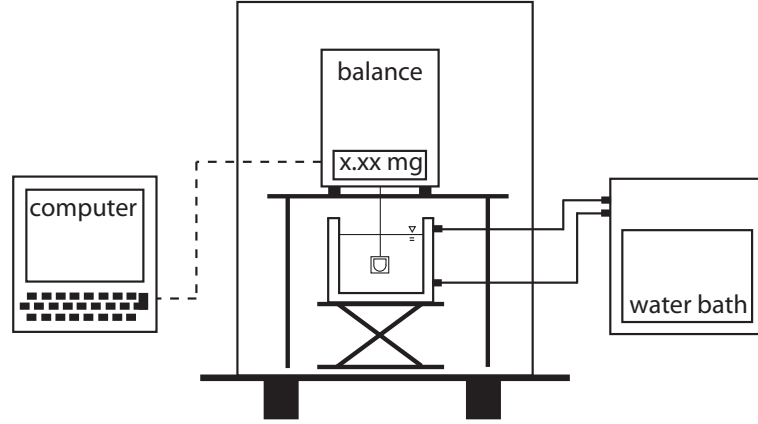


Figure 3.12.: Sketch of density measurements via the Archimedes principle of volume replacement.

water ( $m_{\text{tot, water}}$ ). Finally, sample density was determined according to Equations 3.8-3.10.

$$m_{\text{prod, air}} = m_{\text{tot, air}} - m_{\text{SH, air}} \quad (3.8)$$

$$m_{\text{prod, water}} = m_{\text{tot, water}} - m_{\text{SH, water}} \quad (3.9)$$

$$\rho_{\text{prod}} = \frac{m_{\text{prod, air}} \cdot \rho_{\text{water}}}{m_{\text{prod, air}} - m_{\text{object, water}}} \quad (3.10)$$

where  $m$  stands for the mass and  $\rho$  for volume density. The subscript, *tot* the total value (product + sample holder), *SH* the sample holder, *air* analysis in air and *water* immersed in water.

The setup was validated by analysis of materials of known volume ( $V = 9\text{cm}^3 \pm 0.045\text{cm}^3$ ). Several materials were tested. A maximum error of about 1% was determined for polyvinylchloride. Its density was the closest to cocoa butter of all materials tested. Furthermore, there is a general trend that the accuracy of the method increases with an increase in sample mass. Air bubbles may stick to the surface after immersion and falsify the result towards lower density values. This effect is more pronounced for non-tempered than for tempered or seeded samples. By gentle immersion and soft vibration afterwards, the generation of air bubbles was minimized.

## Tensile Force

Schantz and Linke (2001) presented a new technique for simultaneous quantification of general solidification and horizontal chocolate contraction (2D) by the use of a rheometer. The important feature of the device was a normal force control for experiments with a plate/plate-geometry. Mehrle (2007) adopted this method and expanded the range of evaluated data for contraction of chocolate and chocolate fillings. Absolute values were not congruent with each other. Besides the chocolate recipes, the details in methodological work were also slightly different. However, contraction values of up to 4% for chocolates and 7% for a cocoa butter seed suspension were presented by Mehrle (2007). In this study the contraction of several pure vegetable fats were of interest.

Contraction forces are acting during fat crystallization. Initially a fat suspension and finally a crystal network is formed. The analysis options of a strain-controlled rheometer (Physica MCR300, Anton Paar GmbH, Ostfildern, Germany) were combined for parallel monitoring of both phenomena. A plate-plate geometry ( $d_{\text{plate}} = 25 \text{ mm}$ ), equipped with a Peltier temperature control was used. Prior to sampling, the system was heated to the corresponding sample temperature for 10 min. A sample volume of roughly 0.75 ml was poured on the lower plate geometry. Spare fat was removed after positioning the upper plate to a starting gap value of 1 mm. After 5 min of temperature equilibration, direct cooling to the set temperature was performed, while gap reduction and network formation were monitored. The set-point of normal force was 0.0 N with a hysteresis of 0.5 N. Oscillatory analysis was performed with a constant strain of  $\xi = 10^{-3} \%$  and an angular frequency of  $\omega = 10 \text{ rad/s}$  to analyze structure development ( $G'/G''$ ) simultaneously. These values were tested in preliminary trials, to avoid degradation or modification of the network built up. Measurements were performed in doubles. Duration of a single measurement point was 20 s.

Since the yield stress of liquid fats is rather low and sample would flow off the plates immediately, the surface was modified in two different ways ( $M1$ ,  $M2$ ).  $M1$  (method 1) stands for a rough metal surface profile, while  $M2$  (method 2) denotes the combination of sand paper (P100, Sianor J, SIA Abrasives, Charlotte, US) stuck on regular flat, metal plates. Analysis with  $M1$  worked fine with cocoa butter and palm mid fraction, but was insufficient for fast crystallizing fat types such as palm kernel stearin, Laurina and palm super stearin. For these fats  $M2$  was developed. Test measurements showed that comparison of contraction values between both setups is applicable, but network characteristics have to be discussed separately.  $M2$  results in consistently lower values than  $M1$ , since its depth profile in the z-direction is less pronounced.

Besides the contraction of fat due to temperature dependent dilatation and phase transition, the geometry itself is contracting to a significant extent and therefore

has to be taken into account. The integrated correction by the software *RheoPlus* (Multi3 V3.61, Anton Paar GmbH, Ostfildern, Germany) is generally coupled with the temperature set point of the Peltier elements. Hence, only automated corrections in temperature equilibria are possible. Furthermore, the default value was different to control measurements. Aside from these points, the correction by geometry dilatation depends on the lag-phase of fat contraction. Geometry dilatation prior to any interconnected fat network is not recognized by the system since the sample volume is simply sucked to its center point (horizontal flow), rather than building up any forces in a vertical direction. This fact was demonstrated by analysis with rapeseed oil staying liquid during the whole experiment. The contraction measured was 0 %, but the actual distance between the plates was apparently increased ( $>1$  mm). On one hand, this point is a disadvantage compared to the *Archimedes principle*. Thermal dilatation of the setup (metal plate-plate geometry) can be corrected as explained below. However, the initial contraction by crystallization prior to crystal-crystal interaction can not be quantified further and represents a methodological error. On the other hand, the contraction kinetics can be monitored by the rheometer setup, whereas only final contraction values are obtained by the volume replacement method.

Appropriate calibration measurements were performed by the use of a thin brass plate ( $s(T = 25^{\circ}\text{C}) \approx 150\text{ }\mu\text{m}$ ). For general quantification of the geometry contraction coefficient by thermal dilatation, the brass was pressed between the two profiled plates. A normal force pressure by 1 N ( $\pm 0.2$  N) was applied. The setup was cooled down with a constant cooling rate. With decreasing material temperature, the upper part of the geometry was lowered by the absolute dilatation coefficient of the setup. In a second series, direct cooling to several set temperatures was performed and the final contraction value was calculated. Geometry contraction by gradual and direct cooling were in good agreement (Appendix, Fig. A.1). Furthermore, the normalized contraction development over time for direct cooling was comparable for the temperature range applied during the experiments (Fig. A.2). Thus, a matrix was installed estimating the effective geometry contraction to be corrected as a function of lag-phase (min) and initial cooling temperature difference ( $T_{\text{start}} - T_{\text{cool}}$ ). By this approach, only final contraction values are corrected. Diagrams showing the time-resolved development of gap reduction over cooling time are not corrected and show the original data only. Nevertheless, the time-resolved results do reflect the relative trends to each other.

In a first test series, the effect of fat type and temperature was discovered (Tab. A.3). Temperature ranges were chosen based on fat specific melting and solid fat content profile. Thus, palm super stearin was crystallized at rather high temperatures. SFC was generally determined in parallel for a comprehensive discussion of the results (Chap. 4.2.1). Within a second series, effects of fat specific seed crystals were tested. Seed material was produced by the pilot plant scale SSHE system, apart from cocoa butter seed, produced on the industrial *SeedMaster* device. Information about pro-



duction parameters are given in Table 3.4. For direct comparison, the non-seeded fat was analyzed anew, as the starting temperature  $T_{\text{rip}}$  was lower than for the first test series without seeding. Default cooling temperature of this series was  $T_{\text{cool}} = 15^\circ\text{C}$ . Additional variation of this parameter was performed if necessary (Tab. A.4). Total time of analysis was 30-60 min. Measurements were stopped if:

- contraction was less than 0.5 % after 30 min,
- progression of contraction was less than 0.3 % within the past 5 min,
- 60 min were reached.

By this method, it cannot be distinguished between contraction by thermal dilatation and phase transition. No Information is available about the temperature of the probe during analysis. For a general approximation of the thermal dilatation effect, densities of the fats were determined in a liquid state ( $40^\circ\text{C}$  to  $25^\circ\text{C}$ ). The liquid density as function of temperature was extrapolated to  $5^\circ\text{C}$  for calculation of absolute, thermal dilatation values. It was determined on the basis of an averaged thermal expansion coefficient ( $6.66 \times 10^{-4} \text{ g}/(\text{ml}^\circ\text{C}) \pm 1.66 \times 10^{-5} \text{ g}/(\text{ml}^\circ\text{C})$ ). For an averaged density at  $50^\circ\text{C}$  of  $0.894 \pm 0.0048 \text{ g/ml}$  a thermal, volume dilatation by 0.75 % per  $10^\circ\text{C}$  occurs. However, in reality, the fraction of contraction by thermal dilatation is lower, since it is not detectable by the rheometer during the initial lag phase. It decreases exponentially with increasing lag time as the differential equation for the sample temperature is equivalent to the mathematical structure of the heat equation (Eqn. 2.15).

### 3.3.5. Analytical Shear Application

The effect of shear on the nucleation period of vegetable fats crystallizing was investigated by rotational rheometry (Physica MCR300, Anton Paar GmbH, Ostfildern, Germany). Approximately 13 ml of molten fat ( $T > T_{\text{melt}} + 10^\circ\text{C}$ ) was pre-sheared within a 1 mm gap by a concentric cylinder geometry at  $\dot{\gamma} = 10 \text{ s}^{-1}$  for 10 min. Cooling was performed by a Peltier element at a constant rate of  $-5^\circ\text{C}/\text{min}$  and a variable shear rate ( $\dot{\gamma} = 10, 10^2, 10^3 \text{ s}^{-1}$ ) to the set temperature. The nucleation time (lag time) was defined by the cross section of tangents of the viscosity development, both before and after the initial increase in viscosity over time. Zero-time was defined as the point in time, when reaching the set temperature. Measurements were stopped when reaching a viscosity plateau due to the occurrence of wall slip. In Table 3.7, the fats and temperature parameters are listed. The temperatures chosen correspond to supercooling from  $-5^\circ\text{C}$  to  $-11^\circ\text{C}$  for lauric and  $-8^\circ\text{C}$  to  $-20^\circ\text{C}$  for palm stearin in relation to melting endset temperature. Increased supercooling was necessary for

Table 3.7.: Crystallization temperature for vegetable fats crystallized in the rheometer.

fat type	$T_{pretreat}$ °C	$T_{cryst}$ °C	$T_{f,max}$ °C
CO	50	14, 17, 20	25
PK	50	17, 20, 23	28
PS	65	33, 39, 45	53

palm stearin since it is  $\beta$  stable (Chap. 2.1.2). Besides the effect on nucleation kinetics, the solidified fats were analyzed by XRD for determination of corresponding crystallographic structure.

#### 3.3.6. X-Ray Crystallography

In general, the alignment of crystallographic planes in subcell structures can be determined by x-ray radiation. The scattering of x-rays results in distinct patterns, in accordance to the crystalline subcell geometry. Positive interference is achieved if the plane distance  $d_{XRS}$ , is equivalent to a multiple of the wave length, resulting in an increase of radiation intensity at the corresponding reflection angle of the incident beam. The relationship of scattering angle  $\Theta$  and  $d$  is given by Bragg's Law (Hammond, 2009):

$$d = \frac{n \cdot \lambda}{2 \cdot \sin(\theta)} \quad (3.11)$$

where  $n$  is an integer and  $\lambda$  is the wave length of the x-ray beam. Scattering occurs in reflection as well as transmission mode. The absorption of radiation is a material constant. Furthermore the incident beam energy ( $E_{beam}$ ) and wave length ( $\lambda$ ) are coupled by:

$$E_{beam} = \frac{h \cdot c_{light}}{\lambda} \quad (3.12)$$

where  $h$  is the Planck constant and  $c_{light}$  is the speed of light.

#### Single State - Diffraction

Reflection analysis by the x-ray powder diffraction method (XRPD), requires a planar sample surface and its exact alignment to the incident beam. For fat analysis, a classical preparation by milling and pestling as for mineral powders cannot be performed, due to its liquid fraction and remelting character by friction heat. In a solid or plastic

state, the fat samples have to be cut in small pieces and minced by a scalpel or razor blade as gently as possible to avoid remelting. If produced as a suspension, it is poured into the sample holder. Creation of a planar surface is complicated in the first case, due to coarse particles and sticky sample characteristics. For qualitative analysis, a glass plate can be used for gentle squeezing the material to the exact level of height. Thus, preferred orientation of crystals can occur resulting in an anisotropy. Therefore quantitative evaluations are not recommended for this preparation method. Generally, this effect can be corrected only by a 2-D detector system, where anisotropic states can be determined. The term XRD instead of XRPD is used in this work, if a suspension or plastic sample was analyzed instead of a powder. Since fat usually contracts during crystallization, the operator has to pay attention to horizontal displacements during temperature treatment. This methodological error has to be corrected afterwards by re-calculation of the appropriate diffraction angles. Either the displacement has to be determined or the diffraction patterns are recognizable and stored in a general data base. In this case, its strongest peak serves as correction basis (Spiess *et al.*, 2009).

A D8 advanced X-Ray Diffractometer (Bruker axs GmbH, Karlsruhe, Germany) was used for analysis of processed and solidified samples in equilibrium. The sample was covered by a peltier controlled temperature stage (Fig. 3.13). Only short spacing values can be determined by this tool. A Cu-K $\alpha$ 1-radiation source was used ( $\lambda = 0.15406nm$ ,  $E_{\text{beam}} = 40 \text{ keV}$ ). Samples are rotated for statistical reasons, covering a circular area with a diameter of 6mm. Measuring time was kept short due to reheating effects within the sample stage for analysis at ambient temperature conditions. Furthermore, for freshly crystallized material polymorphic transformation processes had to be avoided. The general settings of the applied XRD method are listed in Table 3.8.

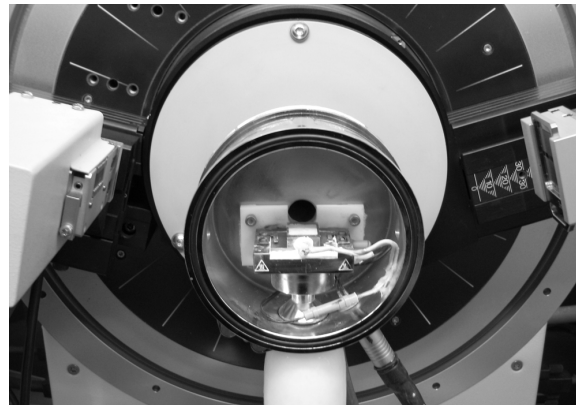


Figure 3.13.: XRD setup with radiation source (left), sample stage including temperature chamber (center) and detector (right).

Table 3.8.: Method parameters of x-ray powder diffraction analysis.

parameter	value
diffraction angle	$18^{\circ} - 25^{\circ}$
step size	$0.02^{\circ}$
time per step	0.8 s
rotation	on

### Kinetics - Synchrotron Radiation Analysis

**Setup:** The drawback of the XRD setup for fat analysis is the duration of a single analysis with a minimum of 5 min at rather low angle resolution. Therefore, kinetic aspects in terms of initial polymorphic form and transformation processes cannot be determined. In addition, the sample is aligned on a stage, where only a thin surface area is penetrated by the x-rays, and no shear forces can be applied during evaluation. The experiments for shear affected crystallization kinetic analysis were performed at the Material Science beamline of the Paul Scherrer Institute (MS X04SA, Villigen, Switzerland). A high beam energy provided by a particle accelerator, enables penetration of adjacent constructing material and still results in high sample diffraction intensities per time step. Conversely, high beam energy leads to a decrease in wave length and thereby to a lower peak resolution on the  $2\Theta$  or d-spacing for a constant detector chip distance. An energy of 17 keV ( $\lambda = 0.072\,93\text{ nm}$ ) was an appropriate compromise. A linear set of detectors was used for analysis. In principle, potential orientation cannot be evaluated in detail by this setup. Nonetheless, anisotropy is indicated by intensity variations of single peaks, if the corresponding reference pattern is known in advance. The general settings of the applied XRS method are listed in Table 3.9.

Table 3.9.: Parameters of synchrotron x-ray scattering analysis.

parameter	value
beam energy	17 keV
wave length	0.072 93 nm
diffraction angle	$0^{\circ} - 20^{\circ}$
angle step size	$0.003\,76^{\circ}$
evaluation time	9 s (series 1) 21 s (series 2)
distance to sample	250 mm

For application of shear, the same rheometer was taken as for all other rheological applications in this thesis (Physica MCR300, Anton Paar GmbH, Ostfildern, Germany). To ensure sufficient radiation of the sample for a high detection intensity and a precise temperature control, a specialized *Searle* geometry was used (Fig. 3.14, workshop ETH Zurich). It is optimized in terms of minimal transmission paths for the x-rays ( $s_{\text{tot}} \leq 1.6 \text{ mm}$ ) and enhanced thermal conductivity by using aluminum as constructing material. The outer stator is double-walled and tempered by water baths. A direct switch from melt to crystallization condition is enabled by an electrical water hose control (Fig. 3.15).

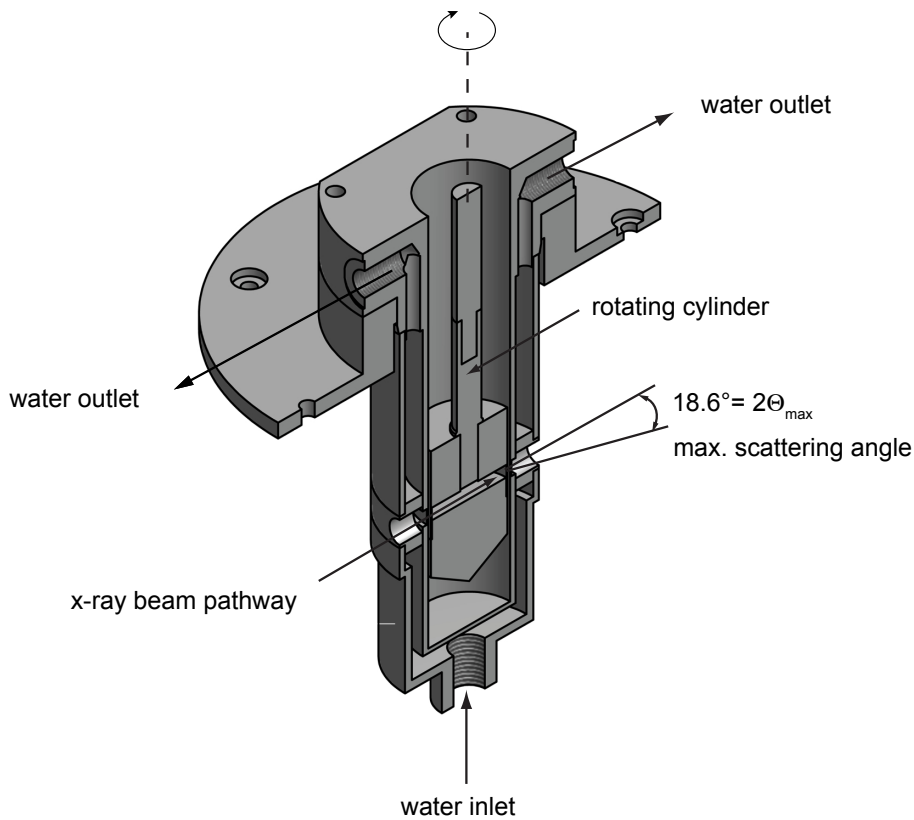


Figure 3.14.: Temperature controlled, rheometric Searle geometry constructed for x-ray scattering experiments; cross-sectional view in 3D.

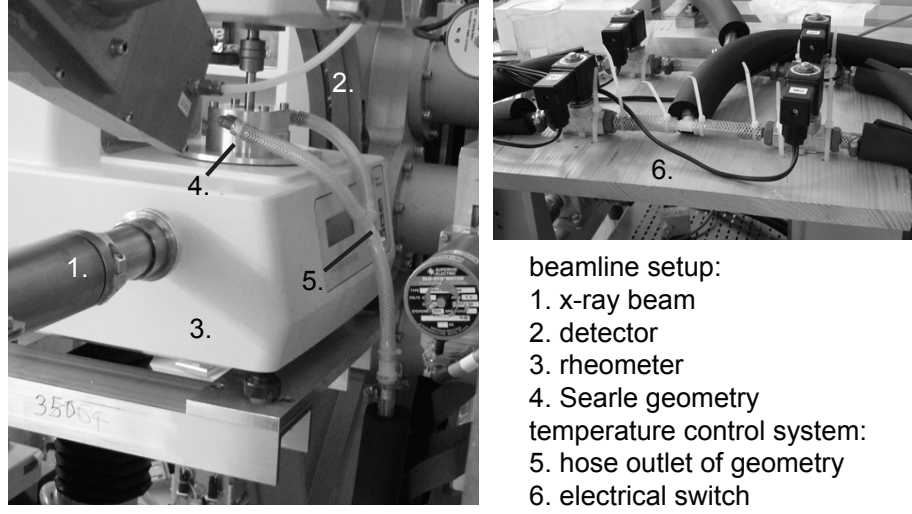


Figure 3.15.: Setup of rheometer in beam line for time-resolved crystallographic monitoring during shear crystallization experiments.

**Experimental Plan:** Two experimental series were performed. In both cases the effect of shear on crystallization kinetics and polymorphic transformation was of major interest. Furthermore, the effect of ripening in terms of polymorphism was determined.

The general sequence of experimental sections for the 1<sup>st</sup> series was the following:

- Pre-conditioning of sample at  $T_{pre} = T_{melt,max} + 10^\circ\text{C}$  for 15 min at  $\dot{\gamma} = 10 \text{ s}^{-1}$ .
- 1<sup>st</sup> crystallization at  $T_{cryst} = T_{melt,end} - 10^\circ\text{C}$  (or  $-20^\circ\text{C}$ ).
- Hold temperature for about 10min after nucleation as observed by significant viscosity increase.
- Switch to ripening temperature at  $T_{ripe} = T_{melt,end} - 2^\circ\text{C}$  and hold for 15 min at  $\dot{\gamma} = 10^{-1}$ .
- 2<sup>nd</sup> crystallization at  $T_{cryst}$ .

For determination of the shear effect in the first series, shear rate was set to  $\dot{\gamma} = 1000 \text{ s}^{-1}$  for high shear application and  $\dot{\gamma} = 10 \text{ s}^{-1}$  for almost static conditions. This is the lowest shear rate giving consistent response with time on the rheometer during 1<sup>st</sup> and 2<sup>nd</sup> crystallization. The experiments were performed with palm kernel, palm mid, palm stearine and palm super stearine fat according to their melting range, as evaluated in advance by differential scanning calorimetry (Appendix, Tab. A.5).

Palm kernel oil showed very fast kinetics in pre-trials, at supercooling of  $-20^{\circ}\text{C}$ . Thus supercooling was set to  $-5^{\circ}\text{C}$   $-10^{\circ}\text{C}$  respectively.

Within the second series, shearing parameters were adapted to practical boundary conditions, specified by application trials on the scraped surface heat exchanger before. Therefore the high shear value was set to  $\dot{\gamma} = 540\text{ s}^{-1}$  (*dynamic*), while *static* conditions were imitated by oscillation analysis ( $\phi = 0.005^{\circ}$ ,  $f = 1\text{ Hz} \equiv 6.28\text{ rad/s} = \omega$ ). Samples were restricted to palm based fats, since transformation into a  $\beta$  structure was more likely than for lauric fats. Furthermore, temperature values were kept constant for all samples.

The general sequence of experimental sections for the 2<sup>nd</sup> series was the following:

- Pre-conditioning of sample at  $T_{\text{pre}} = 70^{\circ}\text{C}$  for 20 min at  $\dot{\gamma} = 10\text{ s}^{-1}$ .
- 1<sup>st</sup> crystallization at  $T_{\text{cryst}} = 25^{\circ}\text{C}$  (or  $20^{\circ}\text{C}$ ), either static or dynamic condition.
- Keep temperature for at least 10 min after nucleation as observed by significant viscosity increase.
- Switch to ripening temperature at  $T_{\text{rip}} = 40^{\circ}\text{C}$  for 15 min at  $\dot{\gamma} = 10\text{ s}^{-1}$ .
- 2<sup>nd</sup> crystallization at  $T_{\text{cryst}} = 20^{\circ}\text{C}$  for 10 min, static condition.

Direct, static crystallization to  $T_{\text{cryst}} = 20^{\circ}\text{C}$  was additionally performed in order to compare non-seeded and seeded conditions, prior to final solidification at  $20^{\circ}\text{C}$  (Appendix, Tab. A.6). While in the 1<sup>st</sup> series refined, pure, natural fats were analyzed, the effect of fat blends was of interest in the 2<sup>nd</sup> series. Palm mid fraction known as a  $\beta'$  stable fat was blended with the  $\beta$  stable palm super stearin at 10 % and 20 %. Unfractionated palm oil, with a general potential of a  $\beta$  structure, was blended with hazelnut oil as destabilizer by the same amounts. In both cases the effect of blending on the generation and ripening of seed crystals under shear and on the crystallographic homogeneity of the subsequent seed crystallization was of interest.

**Data Evaluation:** Within the 1<sup>st</sup> series, rheological data was used only for the evaluation of crystallization induction times (lag times) and the control of a minimal amount of seed crystals during the ripening step. Lag times were determined by the cross section of tangents to the graph (viscosity vs. time) after reaching target temperature (ideally horizontal) and the linear extension of maximal slope value of viscosity progression. As long as viscosity values during ripening were higher than prior to nucleation, seed crystals still existed. If not, the potential seed crystals formed in the first step were remelted during ripening. For the second series, not only induction times, but also structure development during the initial crystallization phase were of interest for monitoring crystallization kinetics ( $G', G''$ ).

Scattering data was pre-processed by a user-written program. After baseline subtraction and use of a moving average mode, the peak patterns were strung into a movie sequence giving a first impression about the crystallographic transformation process over time. In this thesis (printed media), only 3-D waterfall patterns can be shown for exemplification. Furthermore, single spacings of peak pattern were determined by evaluation of local scattering intensities (intensity vs. d-spacing) within the characteristic d-spacing ranges of fat polymorphs. Relative phase development was compared by time-resolved intensities of characteristic short spacings of each polymorph. The crystallographic lag time was determined by the cross section of the tangents before and after the initial increase of the maximal scattering peak intensity over time. Experiments were mostly performed in doubles.

#### 3.3.7. Temper Analysis

The temper quality of cocoa butter based confectionery masses was measured on a MultiTherm<sup>TM</sup> (Bühler AG, Uzwil, Switzerland). It operates with the common aluminum sample cups (Nespresso cups, Nestle, Vevey, Switzerland) and a Peltier cooling system ( $T_{\text{cool}} = 8^{\circ}\text{C}$ ). The integrated indexing of the data evaluation was not used. The data of the temperature inflection point (temperature, slope value) were interpreted according to the confectionery product tested.

#### 3.3.8. Mould Detachment

The detachment of chocolate and chocolate products is based on fat contraction due to crystallization, rather than temperature dilatation. If chocolate is precrystallized correctly and the ratio of absolute contraction to surface area is sufficient, the product detaches from its mould, leading to a good demoulding behavior and the desired surface gloss. Within the thesis of Mehrle (2007), a method for mould detachment based on ultrasound waves was developed by B. Pfister (workshop ETH Zurich, Switzerland). A prototype was successfully tested in the lab and a first version (V1.0) integrated into industrial moulds for chocolate bars.

Hardware, as well as software were improved in the actual version 2.01. Electrostatic charging of the mould was causing system break downs, since the whole setup is incorporated into the mould geometry, which gets charged during the industrial process. Therefore, the hardware including the battery energy source was covered by metal plates. Battery endurance, as well as internal memory space was enhanced, leading to extended operating periods of approximately six hours. Due to a more compact design (now 5 cmx5 cm, before 10 cmx8 cm), the system is adaptable to a bigger variety of mould systems (Fig. 3.16). Finally, the LabView-based application for data evaluation was revised in terms of multiple analysis and user-friendly handling.



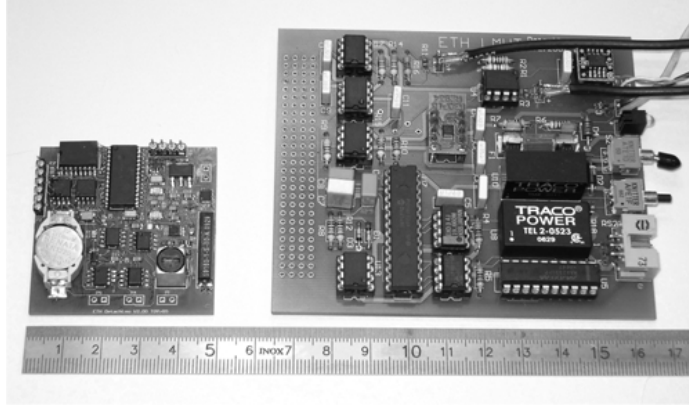


Figure 3.16.: Electrical board of *DetachLog* version 1.0 (right) and 2.01(left).

### Measurement Principles and Setup

The system is based on the physics of ultrasonic wave transfer and reflection at material interfaces, in combination with the damping characteristics of material structure. The impedance ( $Z$ ) is representing a material specific resistance to sound propagation. It depends on ultrasound velocity ( $v_{US}$ ) passing the material and the material density ( $\rho$ , Eqn. 3.13). Velocity in solids (sol) is defined by Equation 3.14, in liquids (liq) by Equation 3.15 and in gases (g) by Equation 3.16 respectively, where  $E_{\text{mod}}$  is the elastic modulus of a solid,  $C$  the compression modulus of a liquid,  $\kappa$  is the adiabatic exponent and  $p_g$  the ambient gas pressure.

$$Z = \rho \cdot v_{US} \quad (3.13)$$

$$v_{US,\text{sol}} = \sqrt{\frac{E_{\text{mod}}}{\rho_{\text{sol}}}} \quad (3.14)$$

$$v_{US,\text{liq}} = \sqrt{\frac{C}{\rho_{\text{liq}}}} \quad (3.15)$$

$$v_{US,\text{g}} = \sqrt{\frac{\kappa p_g}{\rho_g}} \quad (3.16)$$

The ratio of reflected ( $R_{US}$ ) and transmitted ( $T_{US}$ ) sound waves at the interface of material A and B can be calculated according to Equations 3.17-3.19. The bigger the difference in impedance the more energy is reflected.

$$R_{US} = \left( \frac{Z_B - Z_A}{Z_B + Z_A} \right)^2 \quad (3.17)$$

$$T_{US} = \frac{4Z_A Z_B}{(Z_B - Z_A)^2} \quad (3.18)$$

$$R_{US} + T_{US} = 1 \quad (3.19)$$

Even though all physical values given in the equations above are temperature dependent, the most significant effect on impedance is given by the material density. Density ratio of a solid to air is in the magnitude order of  $> 10^4$ . Therefore, the sound waves induced into mould material are mainly reflected at each mould-air interface. If a mould is filled with molten chocolate ( $\rho_{mould}/\rho_{choc} \approx 1$ ), a significant fraction is transmitted into the chocolate. As soon as the chocolate contracts due to cooling crystallization, a thin but effective air layer is generated between the mould material and the chocolate. Consequently, less transmission occurs, and reflection ultimately increases. A second and essential point is the attenuation factor of a material. Besides by divergence of wave frequency and scattering of the signal, attenuation occurs due to intermolecular friction in the shear flow. On a relative scale, this factor is low for solids and high for liquids or gases.

The final parameter of interest is the received amplitude value of a steady ultrasonic wave after passing a mould-chocolate system. Therefore transmitter and transducer are placed diagonal to the bottom of the mould tablet. The signal received is the result of multiple interference of ultrasound waves, reflected and transferred several times at interfaces of chocolate, mould and air.

Since resonance frequency and thereby amplitude height of the transmitter is temperature dependent, in addition to most of material properties mentioned above, detailed interpretation of the amplitude progression with cooling time is not possible so far. Nevertheless the setup is capable of detecting the beginning and the final moment of contraction. Noise was reduced by discrete Fourier transformation to  $f = 40kHz$  (Goertzel, 1958).

Figure 3.17 displays a typical cooling pattern for a chocolate tablet by air cooling. The collected data contains sample core temperature and the received ultrasonic amplitude over time. Important is not the absolute value of amplitude, but the trend. In this case, the recording starts with an empty mould ( $t = -500$  s). After chocolate moulding ( $t = -250$  s), the liquid mass damps (attenuation factor) the signal by energy absorption. When cooling starts ( $t = 0$  s), further damping occurs, before

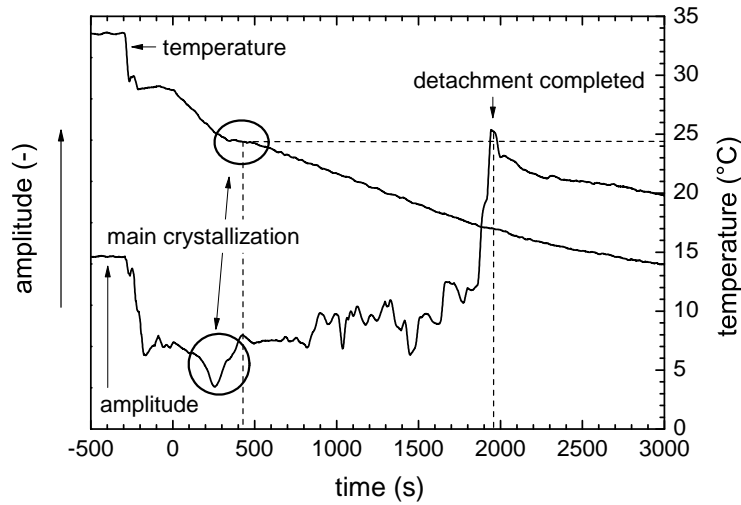


Figure 3.17.: Crystallization of a milk chocolate tablet (300 g) in an air cooler monitored by *DetachLog* technique,  $T_{cool} = 12^{\circ}\text{C}$ .

main crystallization is observed ( $t = 300 \rightarrow 400\text{ s}$ ). Until the moment of complete detachment, the amplitude signal is increasing ( $t = 1950\text{ s}$ ). From this moment, on the chocolate is in contact to the mould only on the bridging parts of the tablet and the ultrasound is merely reflected. Amplitude signal is slightly reduced with ongoing cooling time by temperature effects only. A local maximum of the amplitude represents the precise moment of detachment.

In the case of praline moulds, there are no bridging elements present, lifting the rest of the product. Even though the praline surface is detached from the mould it is but still in contact with the mould material. Thereby not an amplitude maximum, but only a significant kink in the amplitude progression is observed at the moment of detachment. It is therefore approximated by tangent intersection before and after the kink.

## Hardware

The *DetachLog* system consists of a closed aluminium box, containing a Digital Signal Processor (DSP) for data processing and external memory chips (3.18). For industrial use, this box can be mounted into a mould with a minimum depth of 16.5 mm. In general, an ultrasonic ceramic transmitter (type 400ET080, Farnell AG, Wallisellen, Switzerland) and detector (400ER080, Farnell AG) as well as a temperature sensor (PT100-type, Pro-Wave, Electronics. Corp., Chung Hi City, Taiwan) are wired to the box giving sufficient flexibility for positioning. The sensors are glued to the mould

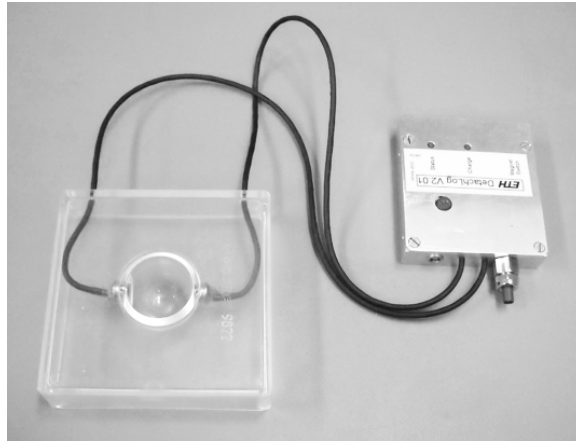


Figure 3.18.: Single praline mould (macrolon®) equipped with the DetachLog system V2.01.

and the thermocouple is stucked through the mould and positioned in the product center. Product temperature cannot be monitored on a single praline mould, as the thermocouple hinders proper detachment and moulding by *One-Shot* technology would not be possible (Chap. 5.2). Therefore, the sensors (k-type,  $d = 1$  mm, Thermocoax, Suresnes, France) were placed to a different praline for detection of the whole span of time-temperature developments (Fig. 3.9). Corresponding signals were recorded by a customized LabView software on an external PC hardware.

#### 3.3.9. Texture Analysis

Texture analysis was performed using a TA.XT2 from Stable Micro Systems (Godalming GB), equipped with a load cell of maximal  $25 \text{ kg} \pm 0.1 \text{ g}$ . Distance accuracy is  $0.1 \text{ mm} \pm 0.0025 \text{ mm}$ . Trigger force was set to  $0.05 \text{ N}$ .

For characterization of the praline solidification process in a cooling channel (Chap. 3.2.4), off-line needle penetration ( $d_{\text{needle}} = 1 \text{ mm}$ ) was performed after certain cooling times ( $t = 2, 5, 10, 15, 20, 30 \text{ min}$ ). Thereby pralines were punctured twice in a radial distance of  $5 \text{ mm}$  from the center point. Measurements started  $5 \text{ s}$  after removal of the praline from the cooling tunnel together with its mould. Penetration was performed with a speed of  $1 \text{ mm/s}$  to a depth of  $7 \text{ mm}$  ( $1/3$  of praline height), from the bottom part of the praline, since it was still moulded upside down. At this part of the praline, chocolate shell had a nonuniform thickness of up to  $5 \text{ mm}$ . Shell hardness was evaluated in a depth of  $3.5 \text{ mm}$ . Double measurements were performed. Storage analysis was conducted differently for assessing the shell and the filling specific values separately. Since the effects of migration during storage on a uniform shell thickness

were of interest, penetration was performed at the top part of the praline without any mould support. The chocolate shell was punctured to a depth of 1 mm at 1 mm/s, to avoid contact with the filling mass. In a second step, the praline was cut horizontally in half and the hardness of the filling mass in the lower part was determined. Samples were punctured four times on two different pralines. The averaged penetration force at a depth of 0.5 mm and corresponding standard deviations are presented.

### 3.3.10. Fat Bloom Analysis

#### DigiEye

Evaluation of fat bloom stability on long-term storage for confectionery products was performed by digital image evaluation (DigiEye, Cromocol Scandinavia AB, Borås, Sweden), using the L-a-b color system (CIELAB definition, Schanda, 2007). The system was applied for praline evaluation on storage (Chap. 5.2). Storage temperature was 23°C. This method is nondestructive. Therefore, a set of pralines of each trial can be evaluated repeatedly for the entire storage period. The light reflections of a defined surface area of the praline top are analyzed. The software is evaluating each pixel separately for the variables luminance ( $L^*$ ), chromatic component on a scale from green to red ( $a^*$ ) and chromatic component from blue to yellow ( $b^*$ ). Whiteness index ( $WI$ ) was calculated by the following, general definition:

$$WI = 100 - \sqrt{(100 - L^*)^2 + a^{*2} + b^{*2}} \quad (3.20)$$

Since chocolate gives a dark background, and fat bloom is correlated to a whitish-grey appearance on the product surface, the whiteness index can be taken as an index for fat bloom development. The higher the value, the more fat bloom has been developed. Within the study, not absolute values but relative differences are discussed. Fresh reference samples showed  $WI$  values of  $25.8 \pm 0.45$ . A critical fat bloom level for customer acceptance was determined by correlation to a human panel judgement to  $WI = 29 - 30$ . Measurements were performed by the Swedish Institute for Food and Biotechnology (SIK, Gothenburg, Sweden).

#### Human Eye

Determination by human eye served as a control of the digital evaluation and is the most common approach in the industry. No defined method exists, so each company developed their own empirical approach. In the present case the test was performed by an industrial panel of Aarhus Karlshamn (AAK, Aarhus, Denmark). Quality scale bar for human assessment ranges from 8 (=top quality) to 1 (=heavily bloomed). Level 4 is the lowest level of acceptance while level 3 is classified as insufficient for further distribution on the market. An impression is given in Figure 3.19. The method is non-destructive.

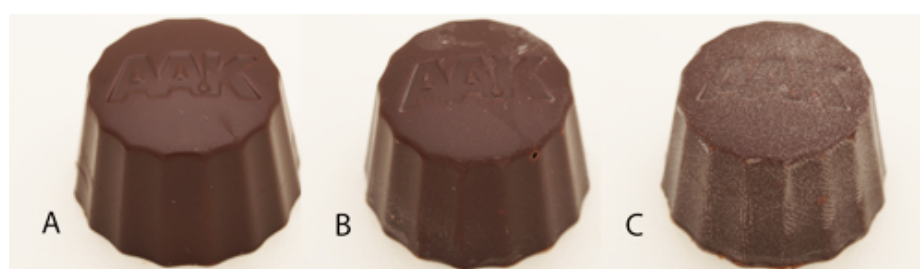


Figure 3.19.: Fat bloom scale bare visualization by sample pralines; A: 8 = perfect, B: 3 = not acceptable, C: 1 = heavily bloomed.

#### 3.3.11. Confocal Laser Scanning Microscopy

Microscopy techniques are often used for fat crystal growth observations such as regular and polarized light microscopy (De Graef *et al.*, 2008; Marangoni, 2003; Narine and Marangoni, 1999b). Also atomic force and scanning electron microscopy can be applied for high resolution surface investigations (James and Smith, 2009; Sonwai and Rousseau, 2008). These methods are restricted to a two-dimensional visualization. In contrast, confocal laser scanning microscopy (CLSM) enables 3-dimensional reconstruction of a food matrix by a series of laser scanned images in different focal planes of the sample (Lorén, 2007). In most applications fluorescent stains have to be introduced into the system for imaging different phases (Rousseau, 2007). If the dye can be added before the structuring takes place, this method is non-destructive. However if the structure has to be stained afterwards, the sample has to be cut at the plane of interest and stained volume area is restricted by the laws of diffusion.

In the present study the pralines were analyzed by a Leica SP5 CLSM (Leica Microsystems GmbH, Wetzlar, Germany). Two objectives with different magnifications were used; an air objective (HC PL FL 10x/0.30) and a glycerol objective (HCX

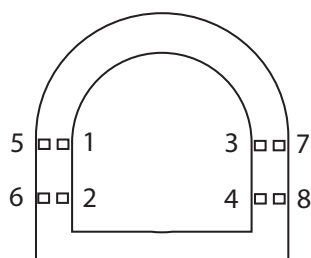


Figure 3.20.: Local spots of praline analyzed by CLSM technique close to shell-filling interface (1-4) and product surface respectively (5-8).

PLAPO 63x/1.30 GLYC CORR CS). Staining had to be performed individually for each storage period. Therefore two dyes were placed on a cling film and left to dry. The pralines were cut vertically in half and cutting face was covered by the prepared cling film. The cocoa particles were stained with *Texas Red* (Invitrogen, Life Technologies, Carlsbad, US), while the fat phase was stained with *BODIPY FL16* (Life Technologies). *BODIPY FL16* is fat soluble, but only in the liquid phase of cocoa butter. Crystalline structures are too dense for dye penetration. To assure good conditions for dye diffusion, the samples were wrapped in play dough and stored for at least 24h at the regular praline storage temperature and humidity. The samples were analyzed at 8 different spots of the praline shell as shown in Figure 3.20. Analysis at the praline top shell area as performed for all other methods applied was not possible due to geometric concerns of the sample holder. The measurements were performed by the Swedish Institute for Food and Biotechnology (SIK, Gothenburg, Sweden).

### 3.3.12. Particle Size Analysis

Fat powder crystals were analyzed by static light scattering technique, including polarization intensity differential scattering technology (PIDS). Since the internal setup of the particle size analyzer (LS 13320, Beckman & Coulter, Nyon, Switzerland; Software: LS5.0428) was not temperature controlled and fat would melt and stick to the sensitive interior equipment during analysis by the use of a regular powder module, the powder was dispersed into methanol prior to analysis. Chawla and Deman (1990) stated that alcoholic solvents are suitable for dispersion of fat crystals. Selection criteria are miscibility with the liquid fat fraction and insolubility of the solid fraction. According to Wagner (1997), methanol is applicable for cocoa butter particles and similar fats of reduced fatty acid chain length. About 2 g of powder were dispersed in 50 ml of solvent ( $T_{\text{solv}} = 10^{\circ}\text{C}$ ) by hand. 10 ml of sample were transferred in a plastic

tube and sonicated for 8 s in order to destroy small agglomerates. After background determination, the sample was dripped into the internal methanol circulation of the system by a pipette up to a PIDS obscuration of  $45\% \pm 5\%$ . Two runs of 90 s were performed per sample analyzed. Duplicates were performed. Hence, the results depict averaged values of four measurements. The software analysis is based on planar projection of spheric particles, resulting in a representative, volume equivalent diameter  $x_3$ . Particle size are illustrated by  $q_3$ -distributions and corresponding characteristic values  $x_{10,3}$ ,  $x_{50,3}$  and  $x_{90,3}$ . The span of this distribution is defined by:

$$\Delta_{\text{span}} = \frac{x_{90,3} - x_{10,3}}{x_{50,3}} \quad (3.21)$$

#### 3.3.13. Powder Flow Property

Characterization of the powder flowability was performed by a ring shear tester (RST-XS, Dr. Dietmar Schulze Schüttgutmesstechnik, Wolfenbüttel, Germany) including internal vane geometries for prevention of wall slip. The equipment was placed inside the climate chamber of the stored powder ( $T=10^\circ\text{C}$ ). The powder was gently filled into an aluminium geometry (type XS-Mr) with a cross section of  $24\text{ cm}^2$  and a volume of  $30\text{ cm}^3$  avoiding uncontrolled preconsolidation. Excessive material was scraped off. After closing with a lid, the probe was presheared at  $\sigma_{\text{pre}} = 2\text{ kPa}$  ( $\equiv \sigma_1 = 3.5\text{ kPa}$ ) until the shear stress ( $\tau_{\text{pre}}$ ) was constant. For a single analysis of the unconfined yield strength ( $\sigma_c$ ) the yield loci ( $\tau_{\text{pre}}$ ) for  $\sigma_{\text{sh}} = 0.4, 1, 1.6\text{ kPa}$  were determined. Measurements were performed in triplicates.

The flowability is expressed by the  $ffc$  value (Eqn. 3.22) according to the classification in Table 3.10. More details about the theory of powder flow properties based on the Mohr stress cycle are given in Schulze (2008).

$$ffc = \frac{\sigma_1}{\sigma_c} \quad (3.22)$$

Table 3.10.: Classification of powder flow characteristics according to Schulze (2008).

$ffc$	flow property
$<1$	not flowing
$1 < x < 2$	very cohesive
$2 < x < 4$	cohesive
$4 < x < 10$	easy flowing
$10 < x$	free flowing



## 4. Nucleation and Crystallization Kinetics of Fats

### 4.1. Shear Induced Nucleation and Crystal Growth

#### 4.1.1. Reduction of Nucleation Time

**Approach:** It is known from literature, that shear can accelerate the nucleation period of crystallizing fat material in addition to supercooling (Bolliger *et al.*, 1998; Maleky and Marangoni, 2008; Sonwai and Mackley, 2006). Nonetheless, boundary conditions exist for both parameters, temperature and shear, regarding a minimal nucleation time. For very low temperatures, the limiting factor is no longer *crystallization pressure* by supercooling, but the structuring kinetics of triacylglyceride molecules creating the nuclei. Conversely, high shear will be counterproductive at temperatures close to the fat melting point, when reheating occurs, resulting from heat dissipation by viscous friction. It counteracts the molecular clustering process of nucleation.

It was of interest to determine the correlation of shear and nucleation time for fat crystallization taking into account the polymorphic structure formed. Based on the findings of Graf (2006), it was tested, whether a crystallographic transformation is the origin of a partial melting temperature increase observed for lauric fats crystallized under high shear conditions. Thus, several fats were crystallized within a concentric cylinder geometry of a rheometer, at defined shear rates and temperatures (Chap. 3.3.5).

**Results:** As can be seen in Figure 4.1, coconut fat showed an exponential decrease in nucleation time with increase of shear rate under isothermal conditions at selected temperatures. Similar results were found for palm kernel fat (data not shown). Supercooling by  $\Delta T_{\text{sup}} = 8^\circ\text{C}$  led to very similar nucleation times (Fig. 4.2) for coconut and palm kernel oil. Cooling temperatures were evaluated based on regular DSC analysis in advance. The melting peak maximum temperature ( $T_{\text{melt,max}}$ ) is the

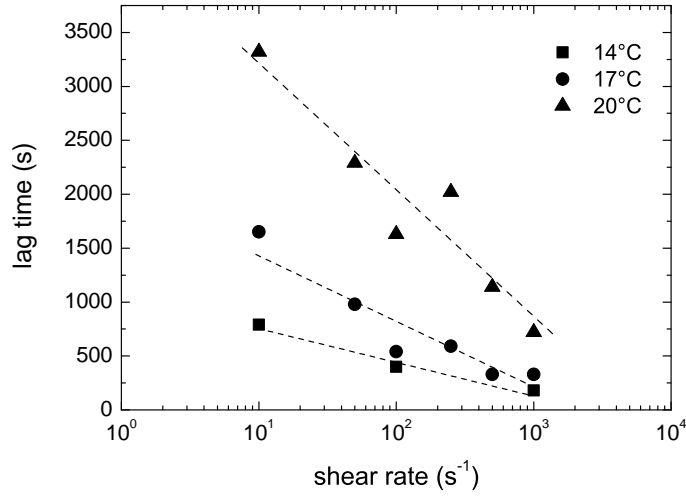


Figure 4.1.: Lag time until crystallization start of coconut fat by isothermal crystallization under shear.

basis of the supercooling temperature difference ( $\Delta T_{\text{sup}}$ ):

$$\Delta T_{\text{sup}} = T_{\text{melt,max}} - T_{\text{cool}} \quad (4.1)$$

The nucleation time of palm stearin was also reduced with increasing shear rate but to a lower extent. The results confirm the exponential correlation of nucleation time and shear rate for fat crystallization also stated by Mazzanti (2005) and MacMillan *et al.* (2002) for cocoa butter (CB) and palm oil (PO). It is assumed that the reduced shear effect for palm stearin is caused by the more dense packing and an increased activation energy of the  $\beta$  polymorphic structure formed compared to  $\beta'$  form of the lauric fats (Fig. 4.3), while the lag time for almost static conditions is comparable. Since pure  $\beta'$  structures were formed as analyzed by XRD for lauric fats (CO, PK), the origin of a slight increase in the melting ranges of shear-crystallized CO and PK, as stated by Graf (2006), is not based on a polymorphic transformation into a  $\beta$  form. A sub-fractionation process within the  $\beta'$  fraction is assumed instead.

It can be summarized that shear rates up to  $1000 \text{ s}^{-1}$  reduced  $\beta'$  nucleation lag times up to 80 % at  $\Delta T_{\text{sup}} = 5$  to  $11^\circ\text{C}$  (CO, PK). The XRD analysis was performed off-line after the crystallization process. Therefore, a potential  $\alpha$  nucleation and further transformation into the  $\beta'$  form during the shear crystallization can not be excluded at this point. The accelerating effect of high shear on nucleation was less pronounced for  $\beta$  stable palm stearin ( $\approx 20\%$  at  $\Delta T_{\text{sup}} = 8^\circ\text{C}$ ).

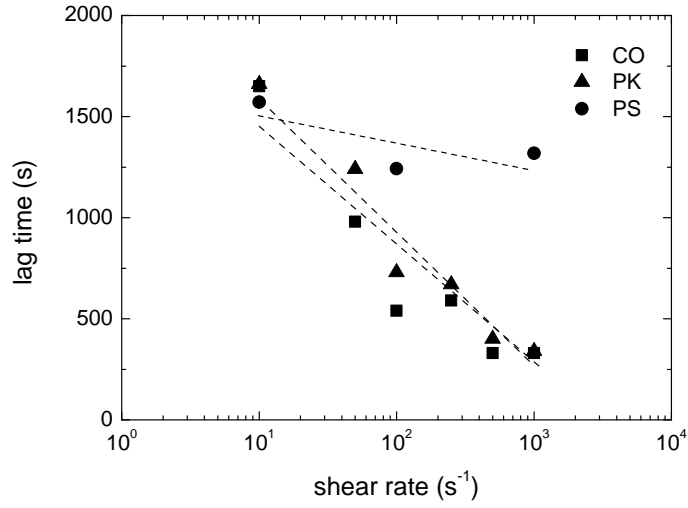


Figure 4.2.: Lag time until crystallization start of coconut (CO), palm kernel (PK) and palm stearin (PS) fats crystallized at  $\Delta T_{\text{sup}} = 8^\circ\text{C}$  under shear.

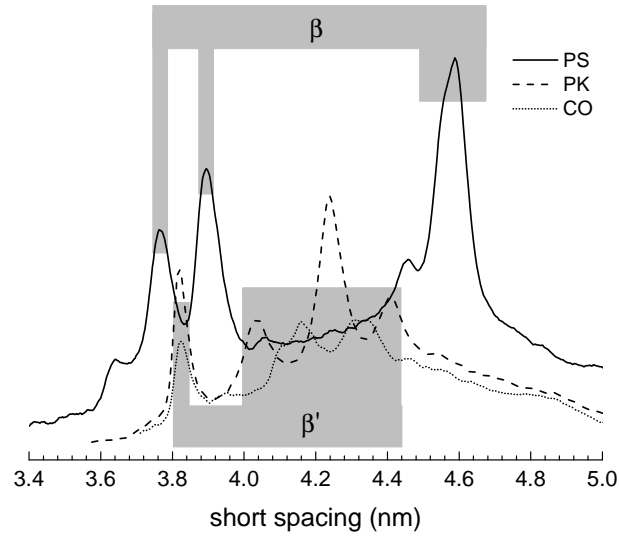


Figure 4.3.: Short spacing patterns (XRD) of coconut (CO), palm kernel (PK) and palm stearin (PS) fats crystallized at  $\Delta T_{\text{sup}} = 8^\circ\text{C}$  under shear ( $\dot{\gamma} = 1000\text{s}^{-1}$ ).

### 4.1.2. Polymorphism of Crystallizing Fats under Shear

The effect of shear and temperature on crystallographic microstructure of vegetable fats were determined by synchrotron radiation (PSI Villigen, Switzerland), as explained in Chapter 3.3.6. Besides the effect of time-resolved analysis, this setup works in transmission, rather than reflection scattering mode (e.g. XRD/XRPD). Moreover, synchrotron radiation reveals real-time structural orientation information of crystallizing fats under shear. General sensitivity, as well as differentiation between the main polymorphic forms ( $\alpha$ ,  $\beta'$ ,  $\beta$ ) was better for long spacing diffraction values (= small angles), while short spacing values (= wide angles) provided additional information about the subcell structuring. Due to geometric aspects, short spacing resolution was up to 100 times higher than for long spacing values. The findings are split into investigations on pure vegetable fats (series 1) and palm based fat blends (series 2).

#### Pure Fats

**Approach:** Palmkernel (PK), palm mid fraction (PM), palm stearin (PS) and palm super stearin (PSS) fats were analyzed while cooled and sheared at  $10\text{ s}^{-1}$  or  $1000\text{ s}^{-1}$ . Crystallographic developments during crystallization without precrystallization, a subsequent ripening step (temperature increase) and finally a second crystallization period were of interest. The intermediate ripening step is important for the polymorphic stabilization of the seed crystals nucleating in the first crystallization step. Thereby a seed crystallization is simulated during the second crystallization step. Results are presented separately for each fat in the following paragraphs. Afterwards, similarities and singularities are summarized.

**Results:** The rheological data are exemplarily discussed for **palm kernel oil**. As known from DSC and NMR kinetic crystallization measurements, the lauric palm kernel fat crystallizes fast, even at low supercooling conditions (Fig. 4.4). Immediate viscosity increase at  $t = 0\text{ s}$ , was caused by the temperature dilatation of the melt. The next level of viscosity increase reflects nucleation and crystal growth. After partial remelting by ripening (viscosity reduction), the second crystallization step is indicated by an instantaneous viscosity rise. The absence of any lag phase during this step confirms a sufficient amount of ripened crystals. They act as seed nuclei in the second crystallization step and thereby accelerate the whole process.

Following focus is set on the polymorphic of the fat systems. The scattering signal of a representative experiment with palm kernel fat is illustrated by the short spacing patterns in Figure 4.5. All peaks correspond to the  $\beta'$  form and were detected directly after nucleation. This monomorphic behavior was independent of the shear rate or

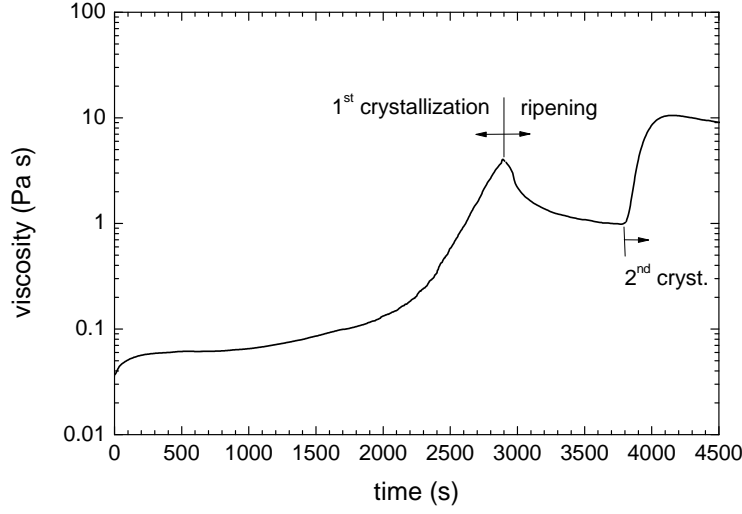


Figure 4.4.: General structural development of palm kernel fat crystallized in a double-stage sequence under low shear ( $\dot{\gamma} = 10 \text{ s}^{-1}$ ) at  $T_{cool} = 23^\circ\text{C}$  ( $\Delta T_{sup} = 5^\circ\text{C}$ ) with intermediate ripening at  $26^\circ\text{C}$  by variation of the applied shear rate during crystallization.

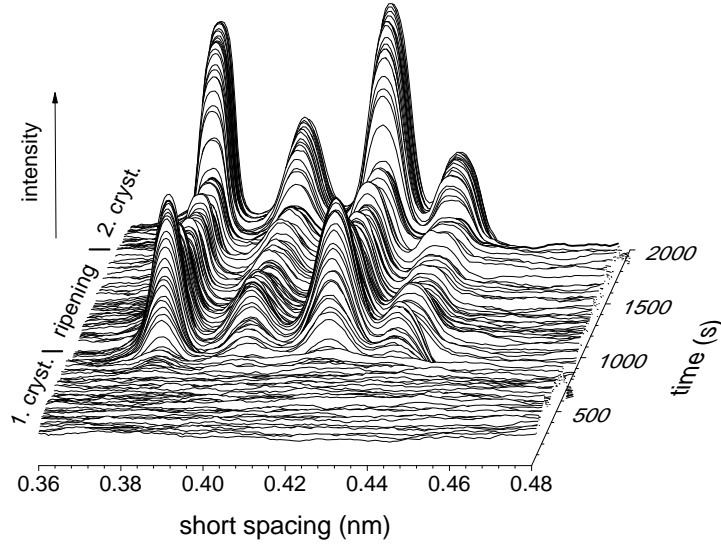


Figure 4.5.: Development of  $\beta'$  short spacing pattern at  $T_{cool} = 18^\circ\text{C}$  ( $\Delta T_{sup} = 10^\circ\text{C}$ ) by application of low shear ( $\dot{\gamma} = 10 \text{ s}^{-1}$ ) including intermediate ripening at  $26^\circ\text{C}$ .

crystallization temperature applied. No evidence for further transformation into a  $\beta$  structure during the ripening step as implied by Ghotra *et al.* (2002) was found.

Short spacing values are based on the parallel packing of carbon chains, whereas long spacings are the result of stacked carbon chains (Chap. 2.1.2). Palm kernel fat shows a strong tendency towards needle like crystallization behavior (Calliauw *et al.*, 2005). Crystal orientation during the second crystallization period was observed in particular for the high-shear regime ( $\dot{\gamma} = 1000 \text{ s}^{-1}$ ). It is assumed, that the carbon chains of the triglycerides are aligned along such a needle, while the needle itself aligns perpendicular to the shear gradient (=parallel to the flow direction). Since the 1D detector system was mounted perpendicular to the direction of flow (Fig. 4.6B), anisotropies due to crystal orientation were indicated by an increase of the peak intensity of the short spacing and a decrease of the long spacing region (Fig. 4.6 A). While short spacing intensities, especially those of the main planes (e.g.  $d=0.383 \text{ nm}$  for the 6-0-0 plane of  $\beta'$ ), increased, long spacing intensity decreased at high shear application during the second crystallization period. The effect was most obvious for strong supercooling conditions, due to an increased concentration of crystals (=increased SFC) within the suspension. Mazzanti *et al.* (2003) observed the same effect for cocoa butter fat amongst other fats crystallized at  $17.5^\circ\text{C}$  and a shear rate of  $1440 \text{ s}^{-1}$ . In this case, the author assumed a platelike morphology of the crystals based on literature (Unruh *et al.*, 2002). Consequently, the crystal plane aligned as well perpendicular to the shear gradient.

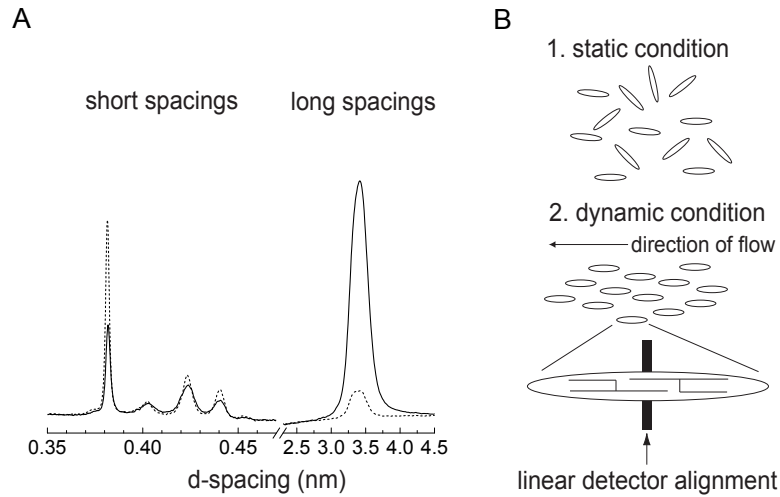


Figure 4.6.: Palm kernel crystal orientation, A:  $\beta'$  x-ray pattern during initial (solid line) and final seed crystallization (dashed line) by application of shear;  $\dot{\gamma} = 1000 \text{ s}^{-1}$ ,  $T_{cool} = 18^\circ\text{C}$  ( $\Delta T_{sup} = 10^\circ\text{C}$ ), B. Schematic orientation of needle-like crystals by application of laminar shear flow.

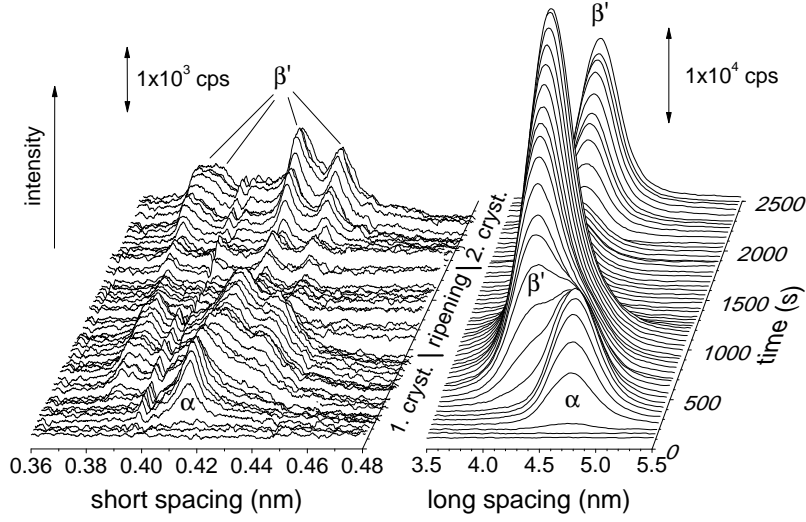


Figure 4.7.: Development of palm fat mid fraction d-spacing patterns crystallized at  $T_{\text{cool}} = 17^\circ\text{C}$  ( $\Delta T_{\text{sup}} = 20^\circ\text{C}$ ) at high shear conditions ( $\dot{\gamma} = 1000 \text{ s}^{-1}$ ) including intermediate ripening at  $35^\circ\text{C}$ .

Different to palm kernel fat, the **palm fat mid fraction** crystallized rather slow. Supercooling by only  $5^\circ\text{C}$  did not result in any crystallization within one hour. At  $\Delta T_{\text{sup}} = 10^\circ\text{C}$ , directly  $\beta'$  long spacing peak values but no short spacings were detected, representing a very low concentration of nuclei crystals. For  $\Delta T_{\text{sup}} = 20^\circ\text{C}$  the  $\alpha$  form was initiated instead (Fig. 4.7). Lag time, as well as transformation period into  $\beta'$  within the first crystallization step, were reduced by application of high shear rates (Fig. 4.8). Minor crystal orientation was observed only at  $\Delta T_{\text{sup}} = 20^\circ\text{C}$  and high shear application (data not shown). Solid fat content of PM at  $17^\circ\text{C}$  ( $\Delta T_{\text{sup}} = 20^\circ\text{C}$ ) is  $\approx 0.5$  and almost equal to the SFC of PK at  $18^\circ\text{C}$  ( $\Delta T_{\text{sup}} = 10^\circ\text{C}$ ). Microscopic images of seed crystals produced on the lab scale shear crystallizer showed a needle-like shape for palm kernel fat (Fig. 4.9), clustered in layers to rather big seed agglomerates ( $5 \times 30 \mu\text{m}$ ). For the palm mid fat fraction the single crystal is rather oval and of smaller size compared to palm kernel seeds. The shape but also the seed crystal size at constant flow profile dimensions are therefore crucial factors for orientation. The more non-spherical and the bigger the crystal (here PK), the better it can be aligned in a simple shear flow.

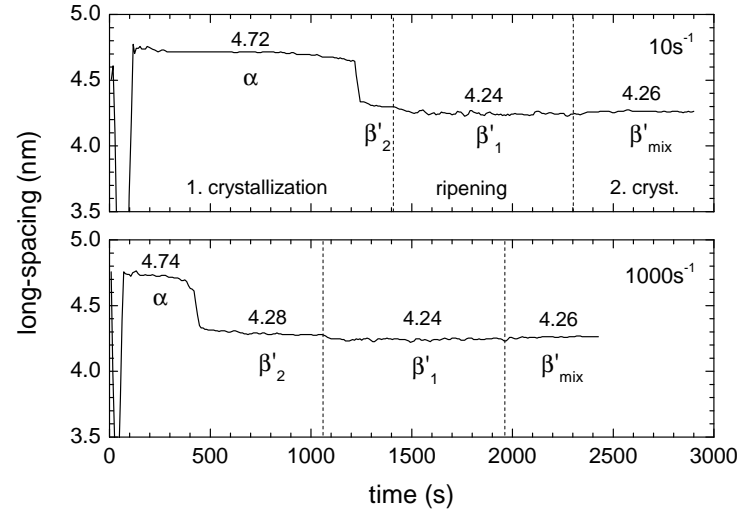


Figure 4.8.: Development of the dominant palm mid fraction long spacing peak value at  $17^\circ\text{C}$  ( $\Delta T_{\text{sup}} = 20^\circ\text{C}$ ) including intermediate ripening at  $35^\circ\text{C}$  for different shear rates.

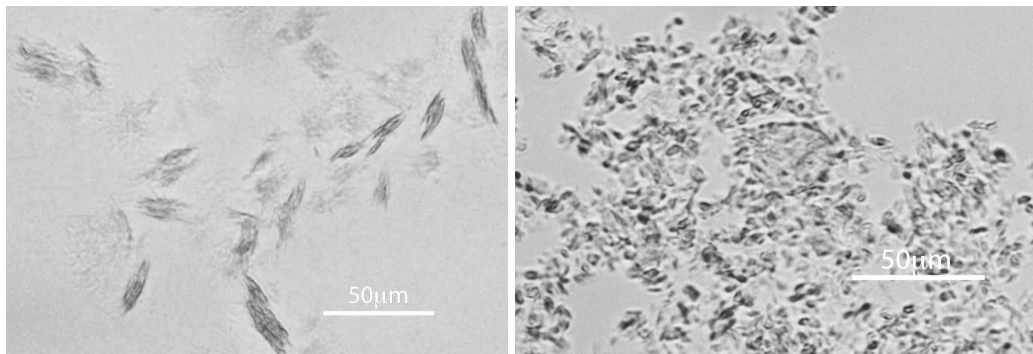


Figure 4.9.: Crystal size and morphology of diluted palm kernel and palm mid fraction seed crystal suspensions produced on the pilot plant scale crystallizer unit;  $\dot{\gamma} = 540 \text{ s}^{-1}$ .



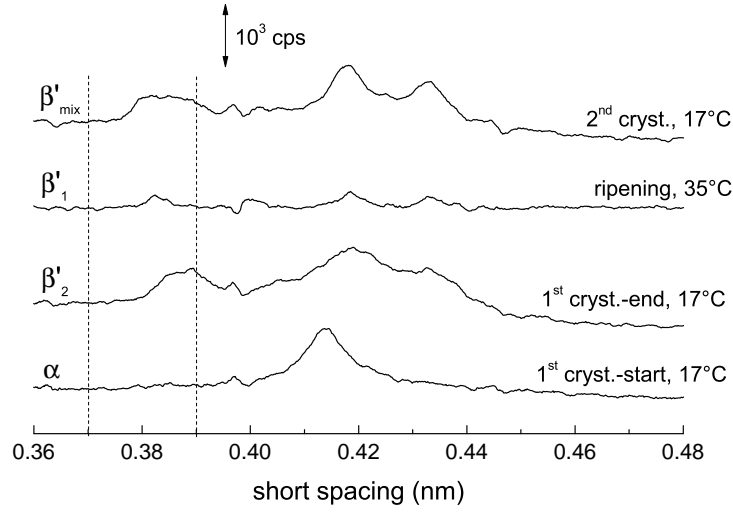


Figure 4.10.: Short spacing x-ray scattering pattern of palm mid fraction, crystallographic modification by temperature cycling;  $\dot{\gamma} = 1000 \text{ s}^{-1}$ .

A minor, but reproducible and consistent modification of the overall stable  $\beta'$  structure of PM was observed due to ripening by a short spacing peak shift between  $d_{\text{XRS}} = 0.37 - 0.39 \text{ nm}$  as indicated in Fig. 4.10. The modification ( $\beta'_{\text{mix}}$ ) compared to the initial crystallization step ( $\beta'_1$ ) can be explained by a fractionation process. The palm fat mid fraction is a mixture of several triacylglycerides. By the intermediate ripening step the molecules may split into two main subfractions, which are both  $\beta'$  stable. This can result in two overlapping peaks of chemically different  $\beta'$  subcell structures after the second crystallization.

Similar to palm mid fraction, **palm stearin** fat crystallized only slightly at  $\Delta T_{\text{sup}} = 10^\circ\text{C}$  and low shear, thus only the long spacing value of a  $\beta'$  structure was detected. For high shear, the nucleation and crystallization kinetics were accelerated, leading to a  $\beta'$  peak pattern not seen before (Fig. 4.11). It consists of five rather narrow peaks between  $0.40 \text{ nm}$  to  $0.44 \text{ nm}$ , instead the two broad peaks analyzed for stronger supercooling and generally reported in literature (Fig. 2.5; D'Souza *et al.*, 1990). This structure is metastable since it was not directly transformed into a  $\beta$  structure by a solid-solid-phase transition during the ripening period ( $52^\circ\text{C}$ ), but was remelting instead. However, a solid-liquid-solid transition into the  $\beta$  form was observed lasting from initial crystallization over the whole ripening period till final crystallization at  $44^\circ\text{C}$ . It is assumed that the ripening period could be shortened, still resulting in a complete transformation. In return, it was not tested, if a solid-solid phase transition occurs within a long time period at crystallization out of the melt. Since the detector

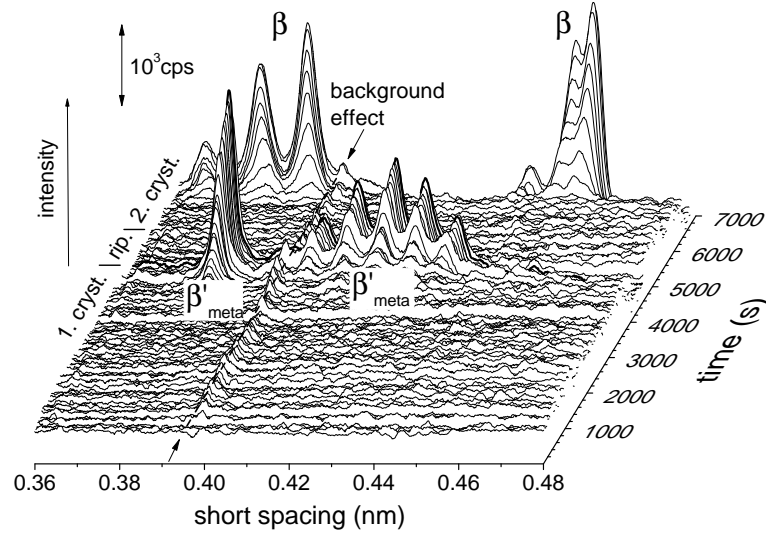


Figure 4.11.: Development of palm stearin short spacing pattern at  $T_{\text{cool}} = 44^{\circ}\text{C}$  ( $\Delta T_{\text{sup}} = 10^{\circ}\text{C}$ ) by application of high shear ( $\dot{\gamma} = 1000 \text{ s}^{-1}$ ) including intermediate ripening at  $52^{\circ}\text{C}$ .

resolution of the synchrotron beamline is more than twenty times higher than that of the laboratory device used for powder diffraction analysis, it was demonstrated that the most characteristic peak for general  $\beta$  determination of fats (4.11,  $d_{\text{XRS}} \approx 0.46 \text{ nm}$ ; D'Souza *et al.*, 1990) is a double peak. The peaks represent the 1-0-0 and 1-0-1 crystallographic planes of the triclinic crystal structure (Mechelen *et al.*, 2008b<sup>a</sup>).

Supercooling of palm stearin fat by  $\Delta T_{\text{sup}} = 20^{\circ}\text{C}$  ( $T_{\text{cool}} = 34^{\circ}\text{C}$ ) and ripening at  $52^{\circ}\text{C}$  showed a  $\beta$  structure formation as soon as the ripening period was started (Fig. 4.12). As observed for the palm mid fraction before,  $\alpha$  to  $\beta'$  solid-solid transformation occurred during initial crystallization, while the process was accelerated by application of high shear (Fig. 4.13).  $\beta'$  to  $\beta$  transformation was induced almost immediately after temperature increase during ripening. A solid-solid transformation can not be approved by the data, as shown later for further  $\beta$  modifications. There was no peak shift, but a parallel decrease of  $\beta'$  and increase of  $\beta$  crystals determined. Exclusively triclinic  $\beta$  crystals were formed during subsequent seed-crystallization. The  $\beta'$  structure is therefore clearly an unstable form (Fig. 4.14). However, even the  $\beta$  peak pattern was modified in the solid state during this final treatment. The two low ranged initial short spacing values ( $d_{\text{XRS}} < 0.4 \text{ nm}$ ), formed during ripening ( $\beta_1$ ), were decreased by  $0.002 \text{ nm}$  after the second crystallization started, before finally the formation of double peaks was observed ( $\beta_{\text{mix}}$ ).

<sup>a</sup>Including personal discussion of the presented results.

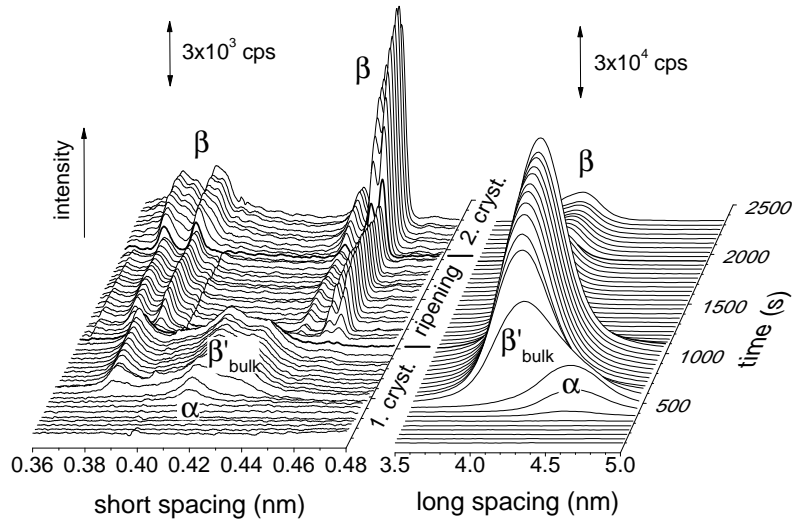


Figure 4.12.: Development of palm stearin d-spacing pattern at  $T_{\text{cool}} = 34^{\circ}\text{C}$  ( $\Delta T_{\text{sup}} = 20^{\circ}\text{C}$ ) by application of high shear ( $\dot{\gamma} = 1000 \text{ s}^{-1}$ ) including intermediate ripening at  $52^{\circ}\text{C}$ .

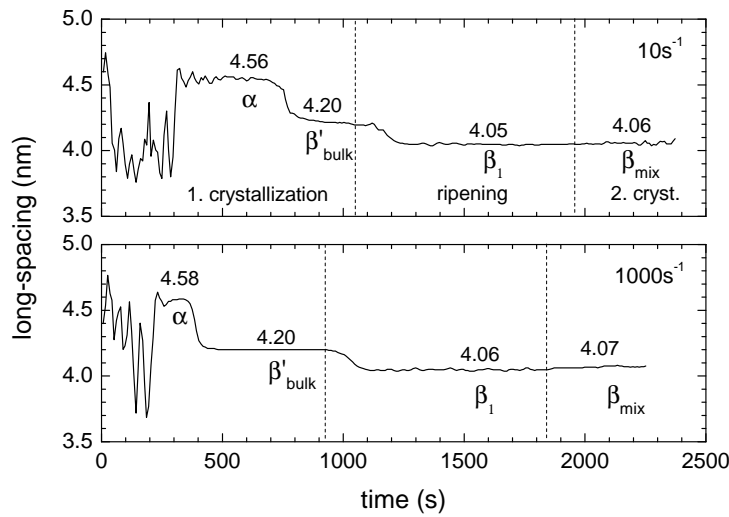


Figure 4.13.: Development of palm stearin long spacing peak value at  $T_{\text{cool}} = 34^{\circ}\text{C}$  ( $\Delta T_{\text{sup}} = 20^{\circ}\text{C}$ ) including intermediate ripening at  $52^{\circ}\text{C}$  by variation of shear rate.

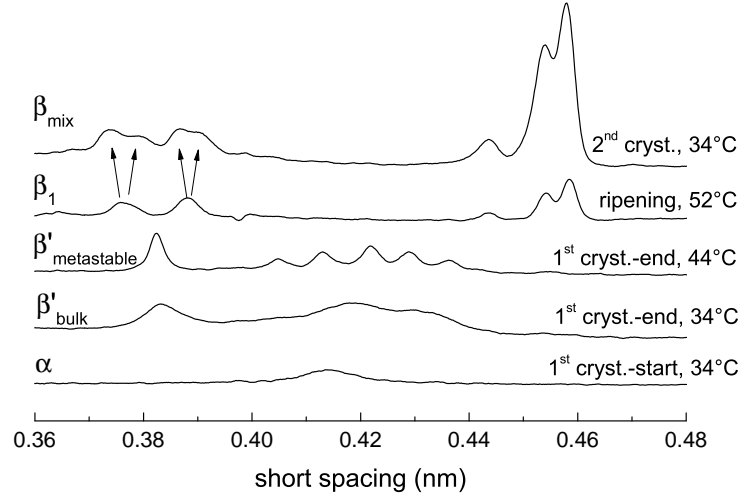


Figure 4.14.: Snap shots of short spacing pattern for palm stearin fat; crystallographic modification by cooling temperature and ripening;  $\dot{\gamma} = 1000 \text{ s}^{-1}$ .

We concluded, that similar to the fractionated solidification after  $\beta'$  ripening of the palm mid fraction, a fractionated  $\beta$  crystallization process was carried out during the final seed crystallization of palm stearin. There is no information found in literature about a modification of the palm stearin  $\beta$  structure so far. To get sufficient information about the geometric nature of the corresponding single crystal subcell modifications of palm stearin fat, further classification of crystallographic planes of a single crystal for a much wider range of scattering angles ( $2\theta$ ) has to be performed. Nevertheless, it is undoubtable that the crystal lattice constants are somehow affected by the temperature/shear treatment applied here, since the results were reproducible. As for the other fats, orientation of the palm stearin crystals was detected for seed crystallization at strong supercooling conditions and high shear application.

In principle, the behavior of palm super stearin is similar to that of palm stearin. Due to two fractionation steps during fat production (palm  $\rightarrow$  palm stearin  $\rightarrow$  palm super stearin), the compatibility of triglycerides is generally enhanced. However, the effect of peak shifting as well as  $\beta$  sub-fractionation was even more pronounced. Overall crystallization kinetics were accelerated compared to single fractionated palm stearin. Furthermore, directly  $\beta$  crystals were formed for  $\Delta T_{\text{sup}} = 10^\circ\text{C}$  rather fast and to a high extent, overshooting the maximum torque measurable by the rheometer setup. The additional fractionation step seems to improve the compatibility within the subfractions but not of the whole triacylglyceride mixture itself. Due to the narrow melting range of palm super stearin fat, the nominal ripening temperature

was risen to  $60.5^\circ\text{C}$  ( $\Delta T_{\text{sup}} = 0.5^\circ\text{C}$ ) to achieve a crystal suspension state. The initial  $\beta$  form ( $\beta_2$ ) was modified by an overall peak shift and peak transformations into a more stable conformation ( $\beta_1$ ) during ripening (peak 1-6, Fig. 4.15). Different to palm stearin,  $\beta$  restructuring was clearly observed during ripening and affected the position of every major peak in the short spacing pattern. The lower stable  $\beta_2$  structure recurred during final seed crystallization, while further shifting of the high stable peaks was observed, which can not be explained so far. However, the results were very well reproducible. Finally a mixed pattern of two  $\beta$  forms was detected ( $\beta_{\text{mix}}$ , Fig. 4.16). For  $\Delta T_{\text{sup}} = 20^\circ\text{C}$  and low shear, direct crystallization in the  $\beta'$  state was noted, while a short  $\alpha$  sequence was noticed for high shear application, rapidly transforming into  $\beta'$  during crystal growth. For both shear conditions at this temperature,  $\beta'$  to  $\beta$  transformation including  $\beta$  shift occurs during ripening (data not shown).

It is assumed that the distinction of characteristic five-finger-print  $\beta^V$  and the four-finger-print  $\beta^{VI}$  short spacing patterns of cocoa butter are based on very similar phenomena of main crystal structure subfractionation, as observed here for both palm stearin fats (Arishima and Sato, 1989; Langevelde *et al.*, 2001b; Peschar *et al.*, 2004). Crystal orientation by high shear application was verified for both crystallization temperatures.

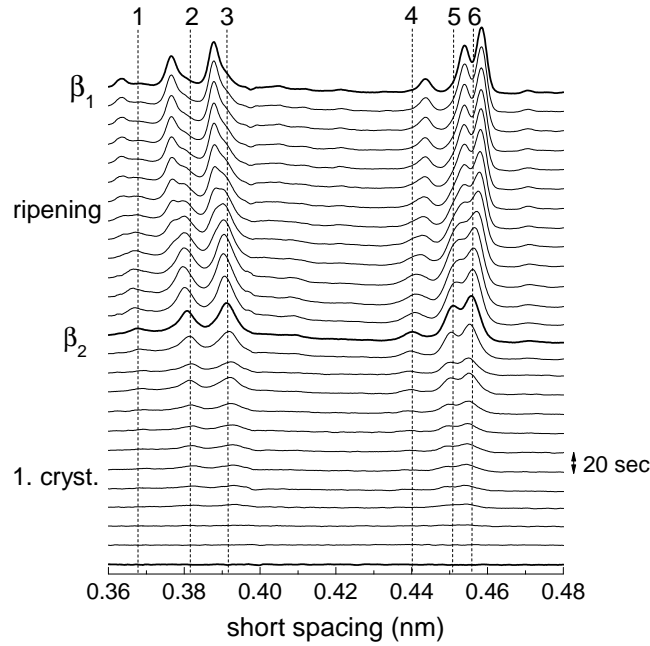


Figure 4.15.: Chronological short spacing of palm super stearin crystallizing at  $T_{\text{cool}} = 51^\circ\text{C}$  ( $\Delta T_{\text{sup}} = 10^\circ\text{C}$ ) by application of low shear ( $\dot{\gamma} = 10\text{s}^{-1}$ ) including ripening at  $60.5^\circ\text{C}$ .

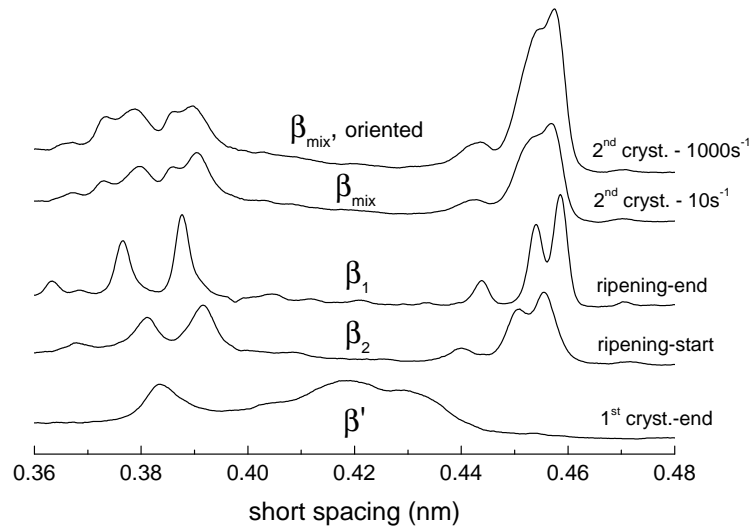


Figure 4.16.: Variation of short spacing pattern for palm super stearin crystals formed during and after shear crystallization at  $T_{\text{cool}} = 41^\circ\text{C}$  ( $\Delta T_{\text{sup}} = 20^\circ\text{C}$ ) including intermediate ripening at  $60.5^\circ\text{C}$ .

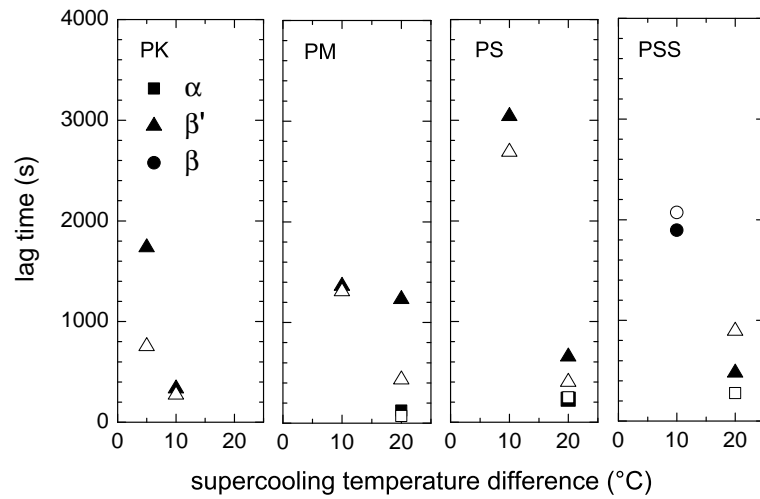


Figure 4.17.: Crystallization lag times of palm fat polymorphs under shear evaluated by x-ray scattering intensities; solid symbols:  $\dot{\gamma} = 10\text{ s}^{-1}$ , open symbols:  $\dot{\gamma} = 1000\text{ s}^{-1}$ .

Nucleation time was approximated by analysis of the long spacing pattern development. It was defined as the point in time of a stable peak maximum position over time (see for example Fig. 4.13). The reduction of nucleation time by high shear application was verified for PK, PM and PS (Fig. 4.17). The molecular mobility is improved by high shear and thereby the probability of nucleation. Crystallization lag time was rather prolonged than reduced at low supercooling condition ( $\Delta T_{\text{sup}} = 10^\circ\text{C}$ ) for PSS. As stated before, straight crystallization into the  $\beta$  form was achieved here. In general, the conformation of the triclinic form is most dense and the Gibbs free energy of activation the highest compared to  $\alpha$  and  $\beta'$  structures (Fig. 2.3). Generally, mechanical energy input by viscous friction under shear flow conditions results in heat dissipation in the media and depends on shear rate by

$$\dot{E}_{\text{diss}} = \tau \dot{\gamma} = \eta \dot{\gamma}^2, \quad (4.2)$$

where  $\tau$  denotes the shear stress and  $\eta$  the dynamic viscosity which is in general Newtonian for a melted fat.

Local reheating effects reduce the crystallization pressure. In the case of PSS, it predominated the positive, nucleation enhancing shear effect. Consequently, the nucleation process for  $\beta$  structures was even slightly delayed.

The rather long lag time for PS nucleation at low supercooling ( $\Delta T_{\text{sup}} = 10^\circ\text{C}$ ) can be explained by a reduced, effective supercooling temperature difference as indicated in Figure 4.17. As verified by XRS,  $\beta'$  crystals nucleated while the supercooling temperature difference on the abscissa is based on the maximal  $\beta$  melting point ( $T_{\text{melt}}(\beta') < T_{\text{melt}}(\beta)$ ). In contrast, the fat specific most stable form nucleated for PK, PM at both temperatures tested as well as for PSS at low supercooling conditions. Consequently the driving force PS supercooled by  $\Delta T_{\text{sup}} = 10^\circ\text{C}$  was reduced compared to the all other fats investigated.

For strong supercooling, the accelerating effect of shear for the  $\alpha$  to  $\beta'$  transformation was shown for PM and PS (Fig. 4.8 and 4.13). Furthermore high shear could even influence the polymorphic structure nucleating as shown for PSS ( $\Delta T_{\text{sup}} = 20^\circ\text{C}$ ).

Detailed information about the long and short spacing values and corresponding crystallization conditions for each single polymorphic form are listed in the appendix (Tab. B.1-B.3).

##### Palm based Fat Blends

**Approach:** Besides the polymorphic properties of fat nuclei and its transformation kinetics during further crystal growth influenced by high shear application and temperature treatment, the macrostructural aspects are also of importance for a comprehensive characterization of a crystal network development.

In that context, the effect of fat blending commonly used in industry for designing filling masses was studied. Hardening was investigated by blending a palm mid fraction (PM) with high stable palm super stearin fat (PSS). Softening was achieved by addition of hazelnut oil to refined palm oil.

The methodologies applied were the same as for series 1. Fat samples were crystallized first either under almost static or dynamic conditions. During the ripening period, the highest stable polymorphs are formed. In a second crystallization step, their seeding capability was tested at static conditions for all variations. Polymorphic as well as structural developments were analyzed. Seed production temperature was constant at 25°C, while final solidification of the seed slurry was performed at 20°C. Ripening temperature was set to 40°C with the exception of pure PM (35°C), since its maximal melting point (melting endset) was 37°C. For each sample reference measurements were performed by direct crystallization at 20°C without precrystallization. In contrast to series 1, low shear crystallization was modified to oscillatory shear (*static*), while high shear condition was again simulated in the rotational rheometer (*dynamic*, Chap. 3.3.6). By the use of oscillatory analysis during the 2<sup>nd</sup> crystallization after ripening, details in structure development were better detectable than by steady shear, rotational analysis.

**Results:** The kinetic and polymorphic advantage by seeding of PM is demonstrated in Figure 4.18. The crystalline structure was built up immediately and showed a homogenous single-stage crystallization, if seeded, while a lag time and double-stage characteristics were observed for the non-seeded fat. The initial increase of  $G'$  ( $t < 500$  s) is caused by temperature dilatation of the liquid fat only. Nucleation is detected more sensitive by  $G''$  at  $t \approx 500$  s. In correlation with the x-ray scattering analysis  $\alpha$  nucleation and growth can be denoted for the first period (Fig. 4.19). The double-stage behavior is based on subsequent transformation into a  $\beta'$  form and further crystal growth. The scattering intensity of the most representative short spacing value of  $\beta'$  is different to zero during  $\alpha$  crystal growth and vice versa, since their d-values are close to each other (Fig. 4.20).



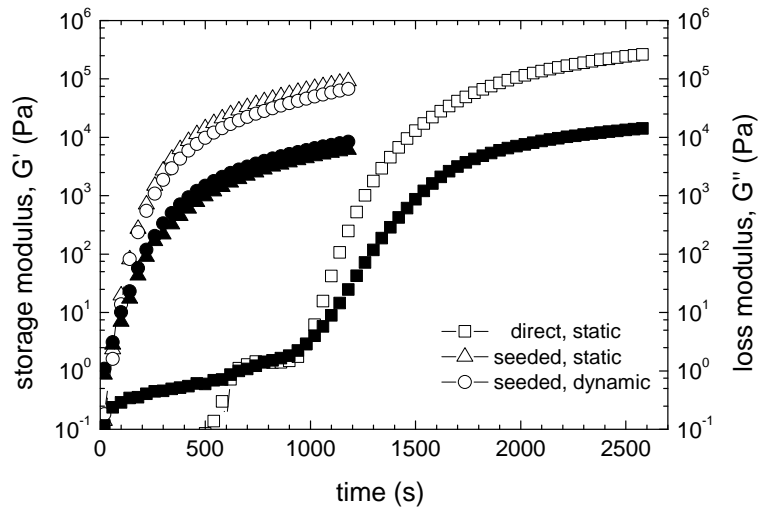


Figure 4.18.: Crystallization kinetics of PM crystallized without precrystallization (direct) and from a seed suspension state (static, dynamic) at 20°C, monitored by oscillatory shear rheometry; open symbols:  $G'$ , solid symbols:  $G''$ .

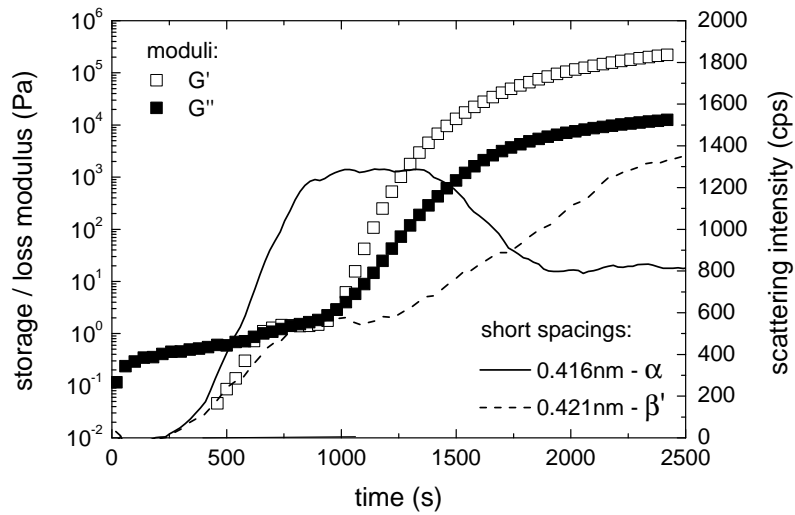


Figure 4.19.: Correlation of double stage solidification ( $G'$ ,  $G''$ ) to crystallographic  $\alpha$  and  $\beta'$  subcell growth of a palm mid fraction crystallized at 20°C without precrystallization, short spacings of corresponding subcell structure peak listed.

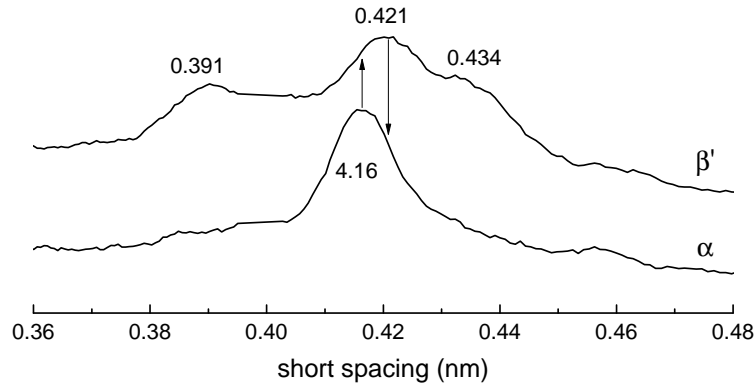


Figure 4.20.: Short spacing pattern of crystallographic  $\alpha$  and  $\beta'$  subcell structures of a palm mid fraction.

Blending  $\beta$  stable PSS into PM fat did not effect the crystallographic, but the kinetic and structural situation for crystallization at 20°C without precrystallization. The double-stage crystallization form of PM was maintained, while the nucleation period was consistently reduced and the network was strengthened by the PSS fraction ( $G'$ ,  $G'' \uparrow$ ; Fig. 4.21). At elevated temperature (25°C), the lower kinetics of pure PM were compensated by the addition of PSS (Fig. 4.22). Moreover, shear additionally reduced nucleation as well as transformation periods. The rheometer was almost as sensitive to the nucleation as the x-ray detector. Only for slow kinetics an advantage of the XRS method became evident.

During ripening of the fat blends transformation into a  $\beta$  form was achieved (Fig. 4.23,  $t = 3000s$ ). Nevertheless crystal growth during the final crystallization step did not result in a pure  $\beta$  crystal growth, but a parallel  $\beta'$  development instead ( $t > 400s$ ). Crystallographic compatibility of PM and PSS was therefore not given. However, the seed effect was positive from a kinetic perspective, since lag time was equal to zero after ripening at 40°C (Fig. 4.24). In terms of macroscopic texture, the fat crystal network formed by seeding was also more plastic compared to the non-seeded fat blend ( $G' \downarrow, G'' \uparrow$ ). It is concluded, that the seed crystal surface area of PSS  $\beta$  nuclei promoted  $\beta'$  nucleation by reducing the integrative surface tension compared to nucleation without seed nuclei. The positive effect on kinetics by adding PSS is off-set by a hardening microstructure. This has to be kept in mind when replacing hydrogenated fats by blends of natural fat fractions to minimize the trans fatty acid content.

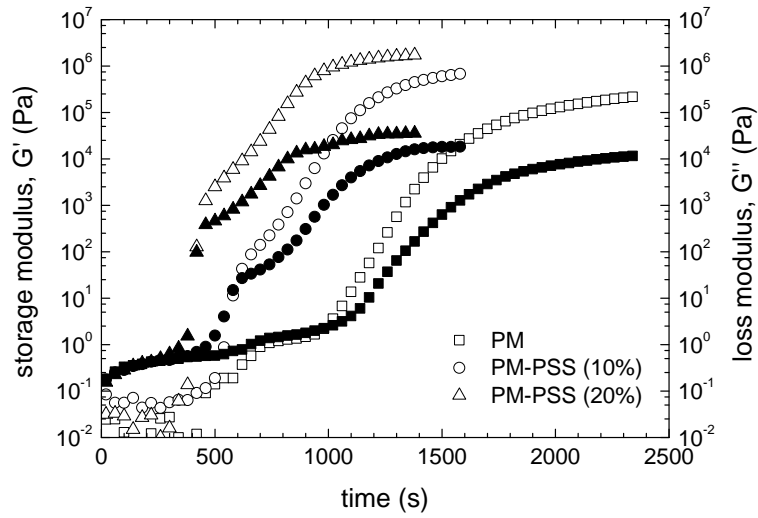


Figure 4.21.: Effect of palm super stearin (PSS) blending on the structure development of statically crystallizing palm mid fraction (PM) without precrySTALLIZATION;  $T_{\text{cryst}} = 20^\circ\text{C}$ , open symbols:  $G'$ , solid symbols:  $G''$ .

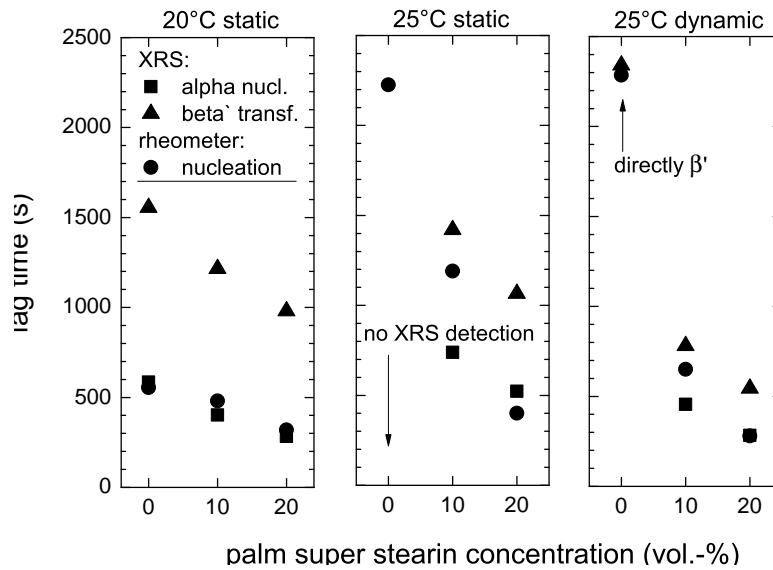


Figure 4.22.: Absolute lag time of nucleation (nucl.) and polymorphic transformation (transf.) for palm mid/palm super stearin fat blends as affected by boundary conditions; nucl.: nucleation, transf.: transformation, dynamic:  $\dot{\gamma} = 540 \text{ s}^{-1}$ .

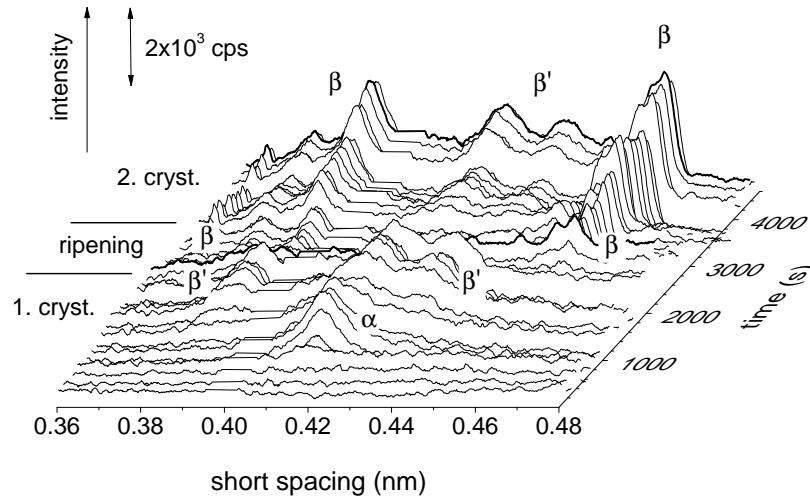


Figure 4.23.: Short spacing pattern of a palm mid / palm super stearin fat blend (80:20) during crystallization at 25°C, ripening at 40°C and final solidification at 20°C under high shear ( $540 \text{ s}^{-1}$ ).

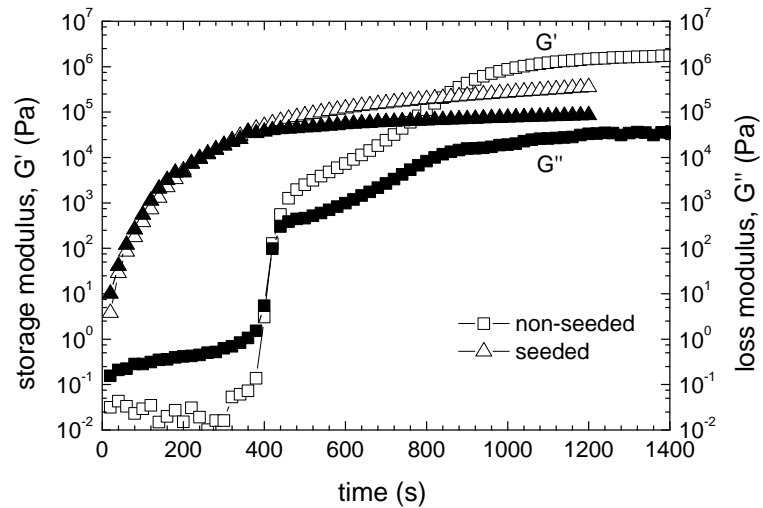


Figure 4.24.: Seeding effect of PSS based  $\beta$  crystals on the structuring kinetics of the PM-PSS (80%-20%) by oscillatory rheometry;  $T_{\text{cryst}} = 20^\circ\text{C}$ .

Hazelnut oil is frequently used in fat based confectionery fillings. By blending palm oil (PO) with hazelnut oil (HO), the positive effect of shear induced crystallization on pure palm fat and the negative effect of the liquid oil decelerating the kinetics are superimposed as shown in Figure 4.25. Furthermore, the final crystalline  $\beta$  fraction of the blends after ripening was disproportionately reduced relative to the hazelnut oil content (Fig. 4.26). Moreover, the pre-crystallization temperature of hazelnut oil blends should be reduced, since the negative impact by mechanical heat dissipation (Eqn. 4.2) is enhanced as shown in Figure 4.27 in case of high shear crystallization (25°C, dynamic). Besides the retardation of nucleation by blending hazelnut oil to PO, it also effected the polymorphic structure of crystal nuclei within a critical temperature range. For pure palm fat, the  $\alpha$  form was favored, while  $\beta'$  nucleation was observed for an HO oil fraction of 20 % at 25°C. In the first case, the  $\alpha$  melting point was well above the cooling temperature. But for the fat blend it was close or even below this value resulting in prolonged nucleation into the next more stable polymorphic form ( $\beta'$ ). The conclusions are supported by the findings of Zeng (2000) and Nattress *et al.* (2004), where consistently reduced melting points were stated for seeded cocoa butter or dark chocolate mixed with hazelnut oil.

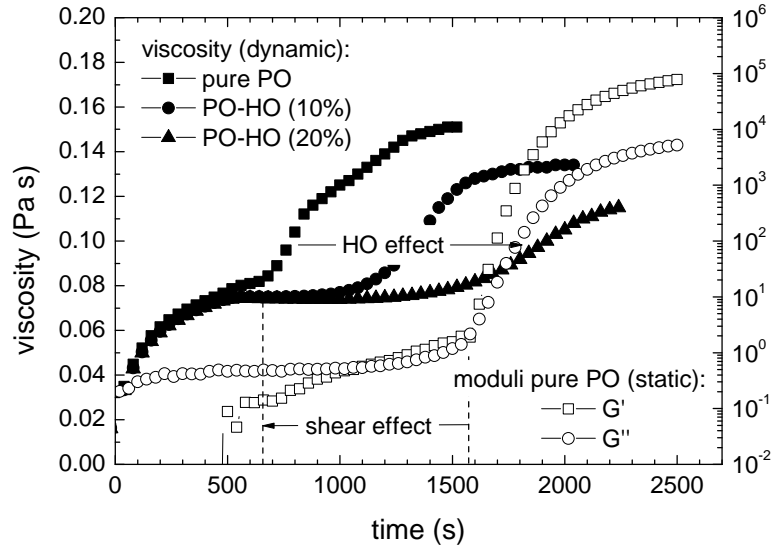


Figure 4.25.: Kinetic retardation for dynamic crystallization (viscosity) of palm fat / hazelnut oil blends compared to static crystallization (moduli) of pure palm oil,  $T_{cryst} = 25^{\circ}\text{C}$ .

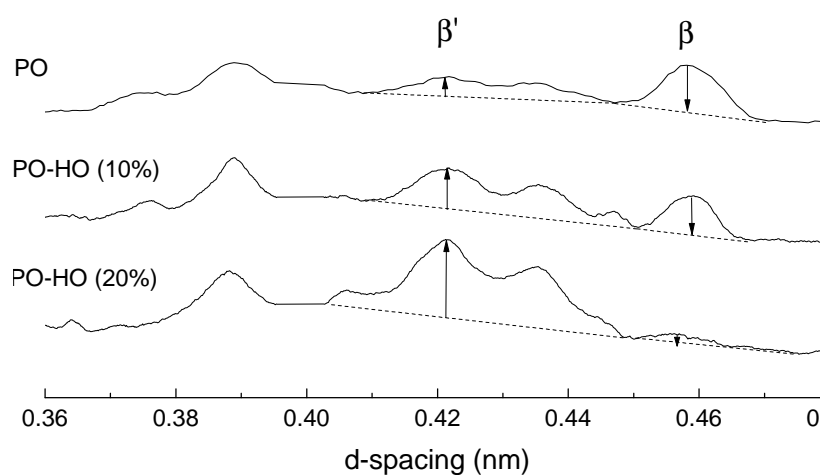


Figure 4.26.: Effect of hazelnut oil concentration (HO) on relative fraction of  $\beta$  transformation of unfractionated palm fat (PO) illustrated by short spacing pattern after final (=2<sup>nd</sup>) seed crystallization.

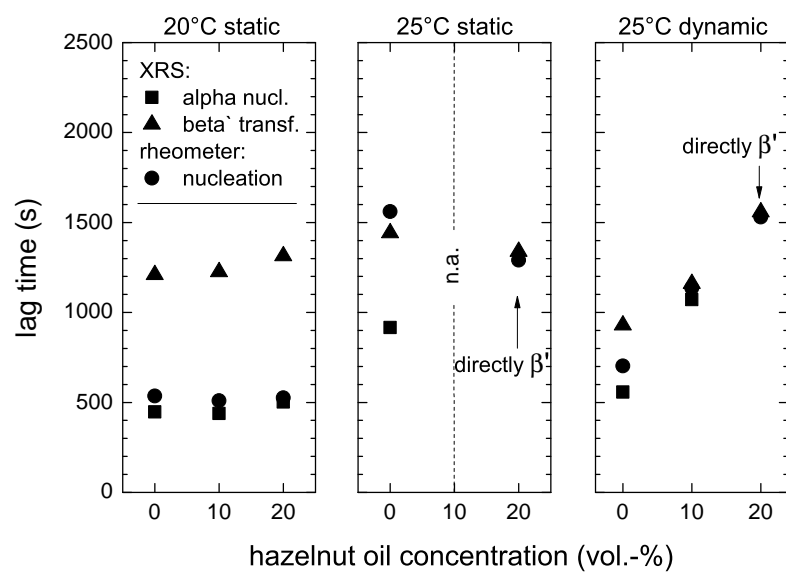


Figure 4.27.: Absolute lag time of nucleation and polymorphic transformation for palm fat / hazelnut oil blends as affected by boundary conditions; nucl.: nucleation, transf.: transformation, dynamic:  $\dot{\gamma} = 540 \text{ s}^{-1}$ .

### Summary:

The nucleation kinetics (lag time) and the polymorphic structure of the nuclei ( $\alpha$ ,  $\beta'$ ,  $\beta$ ) depend on fat type (triglyceride mixture) and super cooling temperature. Minor concentrations of corresponding seed crystals are sufficient to overcome the nucleation phase. Application of high shear during crystallization reduces the nucleation period and in particular the transformation phase ( $\alpha$  to  $\beta'$ ). However, above a fat specific temperature limit, shear can even prolong the nucleation period due to mechanical energy dissipation.

Palm kernel fat crystallizes rather fast into the  $\beta'$  form, which is stable during any ripening phase. Palm mid fraction (PM) is characterized by a double stage crystallization that is based on separated  $\alpha$  and  $\beta'$  crystal growth sequences, respectively. This behavior is comparable to non-seeded cocoa butter (Padar *et al.*, 2008). It could be shown, that PM undergoes different  $\beta'$  modifications induced by ripening at an elevated temperature. Single-stage crystallization is observed for all other fats. Hardening of PM with PSS does not alter the double stage crystallization characteristics. Nonetheless, crystallization kinetics are accelerated and the structure is strengthened. Polymorphic purification of high stable fat fractions is observed during temperature induced ripening.

Palm stearin (PS) and palm super stearin (PSS) are  $\beta$  stable. Polymorphic modifications of  $\beta'$  and  $\beta$  forms are results of controlled temperature fluctuations. The lag times for  $\beta'$  nucleation of both fats are higher than for  $\beta'$ -stable fats (e.g. PM, PK) at a constant absolute supercooling level, since the effective  $\beta'$  supercooling of palm stearin fats, is reduced.

Unfractionated palm oil is highly polymorphic ( $\alpha$ ,  $\beta'$ ,  $\beta$ ). By addition of hazelnut oil, crystallization kinetics decelerated, fat crystal network softened and fractional transformation into  $\beta$  crystals during ripening of unfractionated palm oil is suppressed.

## 4.2. Quantitative Seed Effects on Solidification

To optimize energy efficiency of a cooling process, the effect of a seeding technique for crystallization of different fats is investigated in the following subchapters. A minor fraction of the pure fat component is therefore pretreated separately (Chap. 3.2.1) and finally mixed into the bulk mass before cooling is applied.

### 4.2.1. Crystallization Kinetics

**Approach:** Crystallization kinetics are crucial for minimizing cooling times of chocolate products. For reduction of cooling time fat specific seed crystals are of interest for both, equipment and product manufacturer. Kinetics of various fats in a non-seeded and seeded state at different temperatures were investigated by time-resolved SFC measurements. For non-seeded material, a nucleation phase is expected especially for low supercooling temperatures. Since accuracy of SFC values by NMR technique is rather low for SFC values below 0.005 and nucleation results in concentrations below this detection limit, this period is denoted *lag time* instead.

The crystallization theory by Avrami is based on isothermal crystallization without any precrystallization. Since cooling temperatures were rather low, crystallization often started before the sample mass reached its target cooling temperature. Nevertheless, fitting with the crystal growth models of Avrami was performed. As boundary conditions of the theoretical approach were not strictly fulfilled, fitting parameters are therefore discussed in a more general way. Minimum temperatures for stringent compliance of isothermal condition of the presented setup are noted in the result tables. For a comprehensive comparison and approximation of the overall crystallization time for non-seeded as well as seeded fats, absolute growth rate  $g_{abs}$  (crystallizing mass fraction per minute, Eqn. 3.3), relative growth rate  $g_{rel}$  (ratio of absolute fraction to maximal fraction crystallized per minute, Eqn. 3.4) and an approximated crystallization time  $t_{approx}$  (Eqn. 3.5 to 3.7) were determined and are further discussed.

For cocoa butter positive effects in terms of crystallization kinetics and crystallographic quality by seed application were already determined empirically by confectionary manufacturers and also from a science perspective by several authors (Hachiya *et al.*, 1989; Padar *et al.*, 2008; Zeng, 2002). Since the nucleation period is replaced by the addition of seed, crystallization starts immediately when reaching moderate supercooling conditions. Consequently, this situation no longer conforms to the boundary conditions of the Avrami theory. Nevertheless, the robust and well fitting nature of *Avrami's Approximate Equation* (Eqn. 2.14) can be used for comparison of relative solidification velocity within the pool of fat types investigated.

**Results:** The absence of any lag phase (=immediate SFC increase) and mostly the acceleration of solidification speed (=slope) at low supercooling conditions are characteristic for crystallization by seeding. For cocoa butter (CB), these effects were best visible (Fig. 4.28). For  $T_{cool} = 25^{\circ}\text{C}$  there was no crystallization observed without precrystallization, while seeded CB was converging to an equilibrium state of  $SFC \geq 0.4$ . Furthermore, the double-stage crystallization at  $T_{cool} = 20^{\circ}\text{C}$  for non-seeded CB turns into a steady exponential rate when using seeds. Cooling to  $15^{\circ}\text{C}$  and  $10^{\circ}\text{C}$  resulted in a crossing of the crystallization curves (seeded vs. non-seeded), leading to slightly higher SFC values for non-seeded CB. As shown elsewhere (Fig.



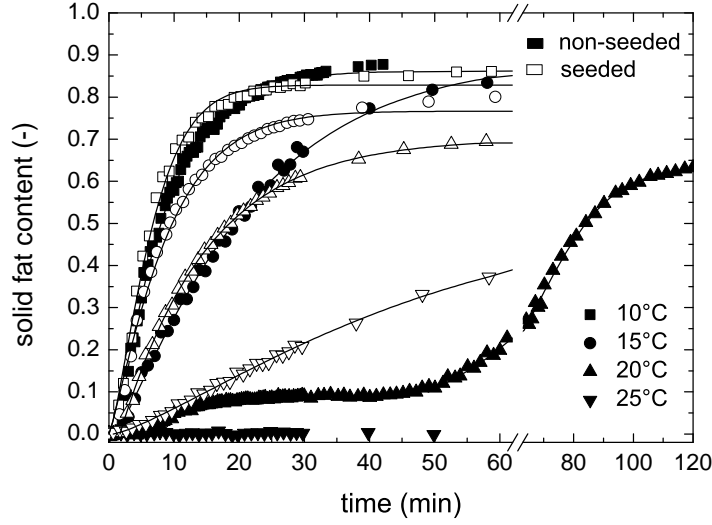


Figure 4.28.: Solidification curves of non-seeded ( $T_{\text{start}} = 50^\circ\text{C}$ ) and seeded ( $T_{\text{start}} = 31.5^\circ\text{C}$ ) cocoa butter at various temperatures; solid lines: Avrami fitting (Approximate Equation).

5.5), the enhanced SFC values of the non-seeded samples decrease during subsequent storage, converging towards the stable SFC of the seeded probes. Higher end SFC, as well as the double-stage solidification at elevated temperatures are based on an  $\alpha/\beta'$  mixture generated during crystallization in the non-seeded case (Fig. 5.3 A), followed by a transformation process towards the  $\beta$  state during storage (Fig. 5.6). Padar *et al.* (2008) and Mazzanti *et al.* (2005) reported similar results. On the other hand, seeded CB solidifies straight into the  $\beta$  state (see Fig. 5.3 B). Since the melting point of CB  $\beta'$  crystals is still above the maximum cooling temperature tested ( $T_{\text{melt}}(\beta') = 28^\circ\text{C} > 25^\circ\text{C} = T_{\text{cool,max}}(\text{CB})$ ), there was no  $\beta$  crystallization observed for low supercooling of non-seeded CB fat.

Palm super stearin (PSS) was the other  $\beta$  structuring fat investigated (Fig. 4.29). It showed similar behavior for cooling temperatures below the melting range of corresponding  $\beta'$  crystals ( $40^\circ\text{C} < T_{\text{melt}}(\beta') < 50^\circ\text{C}$ ). In contrast to nucleation of CB at  $T_{\text{cool}} \geq 20^\circ\text{C}$  (low supercooling), PSS crystallized directly into  $\beta$  at  $T_{\text{cool}} \geq 50^\circ\text{C}$  out of the non-seeded state. This is indicated by merging SFC equilibrium values for seeded and non-seeded samples and confirmed by synchrotron radiation data (Chap. 4.1.2).

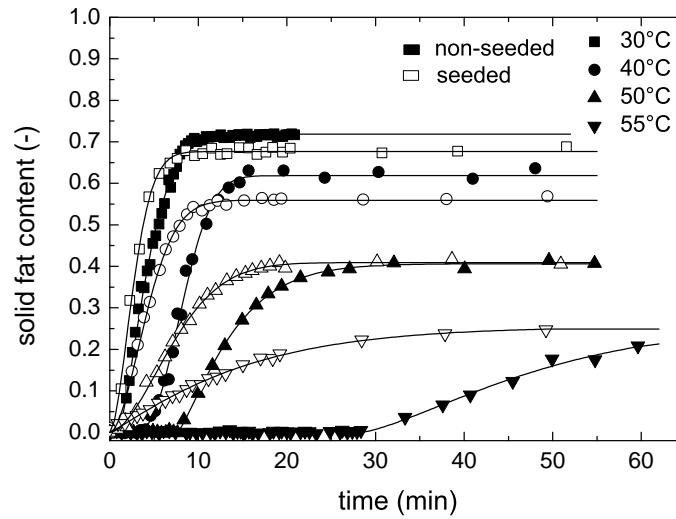


Figure 4.29.: Solidification curve of non-seeded ( $T_{\text{start}} = 70^{\circ}\text{C}$ ) and seeded ( $T_{\text{start}} = 61^{\circ}\text{C}$ ) palm super stearin at various temperatures; solid lines: Avrami fitting (Approximate Equation).

For palm mid fraction (PM), a double-stage crystallization kinetic was generally observed (Fig. 4.30). For kinetic model fitting, the crystallization curves were split into two parts at the inflection point of the interim SFC plateau. Model parameters were determined for each stage individually. The explanatory power of the Avrami parameter of the second crystallization stage is thereby lost, because nucleation is no longer part of the data but is part of the Avrami assumptions. Consequently, fitting results in a mathematical term reflecting the experimental data only. Based on scattering analysis before (Fig. 4.7) and observations by Padar *et al.* (2009) on two-stage crystallization of non-seeded cocoa butter, the first stage represents  $\alpha$  nucleation and growth, while the second stage stands for  $\beta'$  growth after  $\alpha$  to  $\beta'$  transformation. PM did react on seed crystals by lag phase neutralization, but overall kinetic acceleration was not observed. Seeding temperature, amount of PM seed as well as seed material (besides PM: PKS -  $\beta'$ , CB, PSS -  $\beta$ ) showed no significant effect on crystal growth rate of the seeded PM sample (results not shown). To avoid seed remelting, a highly concentrated palm mid fat seed suspension was spray chilled (Chap. 3.2.5). Powder seeding was performed at room temperatures around  $20^{\circ}\text{C}$ . Nevertheless, no significant effect on subsequent solidification could be observed (results not shown). It is assumed that there exists another trigger regulating the crystallization event such as surface active substances.

For lauric fats like palm kernel (PK, Fig. 4.31), palm kernel stearin (PKS) and Laurina (LA), seeding had generally positive impact on the kinetics, reducing required cooling time, but did not change the polymorphic structure formed ( $\beta'$ ).

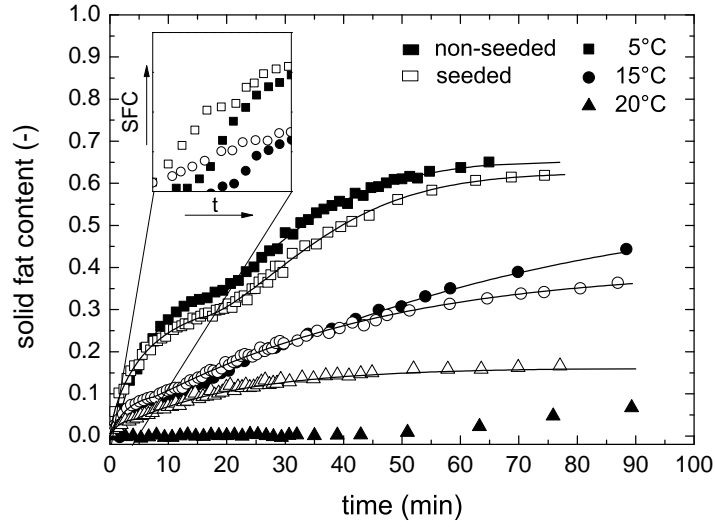


Figure 4.30.: Solidification curve of non-seeded ( $T_{\text{start}} = 50^{\circ}\text{C}$ ) and seeded ( $T_{\text{start}} = 27^{\circ}\text{C}$ ) palm mid fraction at various temperatures; solid lines: Avrami fitting (Approximate Equation).

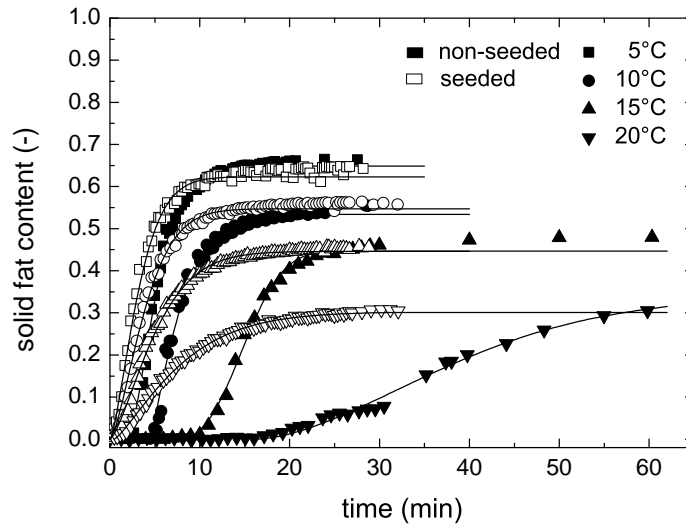


Figure 4.31.: Solidification curve of non-seeded ( $T_{\text{start}} = 50^{\circ}\text{C}$ ) and seeded ( $T_{\text{start}} = 25.5^{\circ}\text{C}$ ) palm kernel fat at various temperatures, solid lines: Avrami fitting (Approximate Equation).

In the following, first non-seeded crystallization and second seeded crystallization kinetics are discussed in further detail.

**Non-seeded:** Nucleation lag time and supercooling temperature of non-seeded fat samples reveal a general correlation (Fig. 4.32). From theory, nucleation phase is correlated to supercooling by Equation 2.8. Neglecting the differences of fat specific parameters ( $T_f$ ,  $\Delta H_{m,f}$ ) and using an averaged absolute cooling temperature ( $T_{cool,ave}$ ), one can simplify to Equation 4.3. The fit quality (all fats) is poor ( $R^2 = 0.55$ ) due to the simplifications, but still mirrors the trend well.

$$t_{ind} = D^* T^{-0.5} \exp F^* / (T \Delta T^2) \quad (4.3)$$

$$\begin{aligned} \text{with } D^* &= \frac{1}{(4\sigma k_B)^{1/2}} v_{mol}^{-1/3} h = 33.31 \text{ minK}^{-1/2}, \\ F^* &= \frac{16\pi\sigma^3 T_f^2 V_f^2}{3k_B \Delta H_{m,f}^2} = 45\,437.95 \text{ K}^3, \\ T &= T_{cool,ave} = 292 \text{ K}, \end{aligned}$$

Supercooling by  $\Delta T \geq 25^\circ\text{C}$ , generally resulted in lag times of  $t_{ind} < 2 \text{ min}$ . For  $\Delta T < 25^\circ\text{C}$ , the lag time increased up to 28 min. Each fat type is a mixture of triglycerides of different fractions. Additionally minor components (mono-, di-glycerides) influence nucleation kinetics (Gordon and Rahman, 1991). For more detailed explanation of fat specific differences, further work should be performed either by multiple fractionation processing or by variation of pure triglyceride combinations.

For a mechanistic approach, the Avrami coefficients (*Approximate Equation*, Eqn. 2.14) of the non-seeded samples are discussed in the following. The quality of the fits is good ( $R^2 \geq 0.98$ , Fig. 4.28-4.31). Considering the isothermal boundary conditions, mostly a sporadic nucleation and needle like (1D) crystal growth is revealed, since values for  $m_A$  are close to 2 and the 1D model fits only (Eqn. 2.11; Appendix, Tab. B.4). The accelerating effect of lower cooling temperatures is visualized in Figure 4.33. A reduction of  $m_A$  represents a shift from sporadic to instantaneous nucleation. Higher  $k_A$  values mirror an increase in crystallization kinetics.

Laurina represents the classical behavior, as the exponential factor  $m$  is reduced with increasing supercooling temperature while the factor  $k_A$  is increasing exponentially. However, the reduction of  $m_A$  has not been observed but stays nearly constant for the other lauric fats as well as CB, while the increase of  $k_A$  is similar to that for LA (Appendix, Tab. B.4). This reduces the informative value of the fitting parameters by the *Approximate Equation*. However, for palm super stearin, the development of

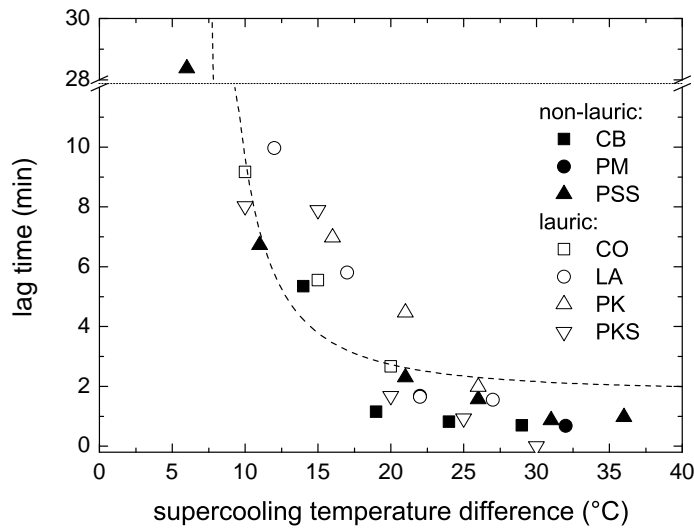


Figure 4.32.: Crystallization lag phase as function of supercooling temperature difference for all fats investigated; solid symbols: non-lauric, open symbols: lauric fats, dashed line: Rousset fitting (Eqn. 4.3),  $R^2 \approx 0.55$ .

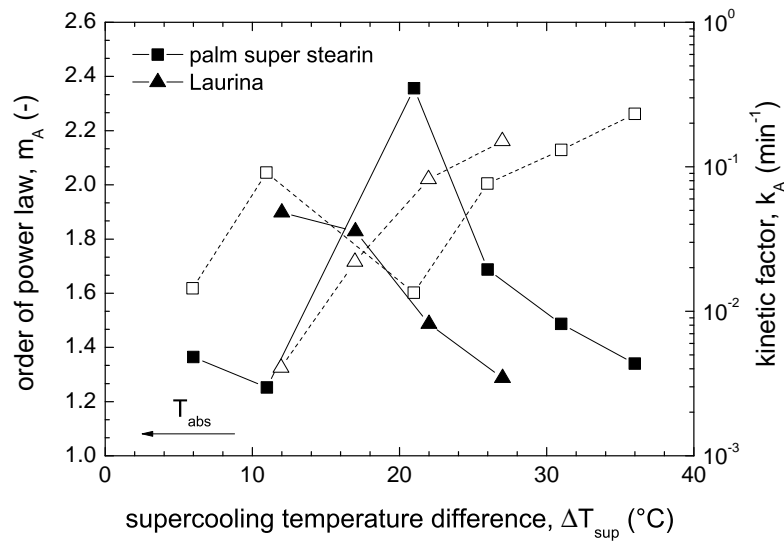


Figure 4.33.: Avrami *Approximate Equation*:  $m_A$  (solid symbols) and  $k_A$  (open symbols) as function of supercooling temperature.

both values is clearly unsteady between  $11^\circ\text{C} < \Delta T < 21^\circ\text{C}$ . This temperature range matches the conclusion about the predominant polymorphic form growing as stated before. For  $\Delta T \leq 11^\circ\text{C}$  ( $T_{\text{cool}} \geq 50^\circ\text{C}$ ) crystallization occurred in the stable  $\beta$  form, and for  $\Delta T \geq 21^\circ\text{C}$  ( $T_{\text{cool}} \leq 40^\circ\text{C}$ ) in the unstable  $\beta'$  form. Therefore  $m_A$  is re-raised and  $k_A$  reset when supercooling is shifted from  $11^\circ\text{C}$  to  $21^\circ\text{C}$ .

These findings are explained on a physical basis by corresponding 1D Avrami fitting values in Figure 4.34. The probability of nuclei growth per unit time  $p_A$  increased as crystallization pressure was enhanced by supercooling as shown for LA. The 1D-Avrami constant  $D_1$  is the product of (i) the cross-sectional area of needle-like crystals ( $A_1$ ), (ii) the average rate of relative growth ( $\dot{l}$ ) and (iii) the initial number of nuclei ( $N_0$ , see also Eqn. 2.11).  $D_1$  increases for higher supercooling temperatures, meaning that a higher number of nuclei, growing faster, overcome the effect of a probably smaller cross-sectional area of a single rod-like crystal compared to crystallization at low supercooling conditions. The tendencies explained for LA and other fats were different for PSS. For  $11^\circ\text{C} \leq \Delta T \leq 26^\circ\text{C}$  both parameters drop by more than 60 % resulting in a general deceleration of the crystallization process. The polymorphic switch from  $\beta$  to  $\beta'$  crystal growth occurring exactly in this temperature range is therefore also noticed by an unsteady fitting parameter development of the dimensional Avrami fitting (1D) as a function of supercooling temperature.

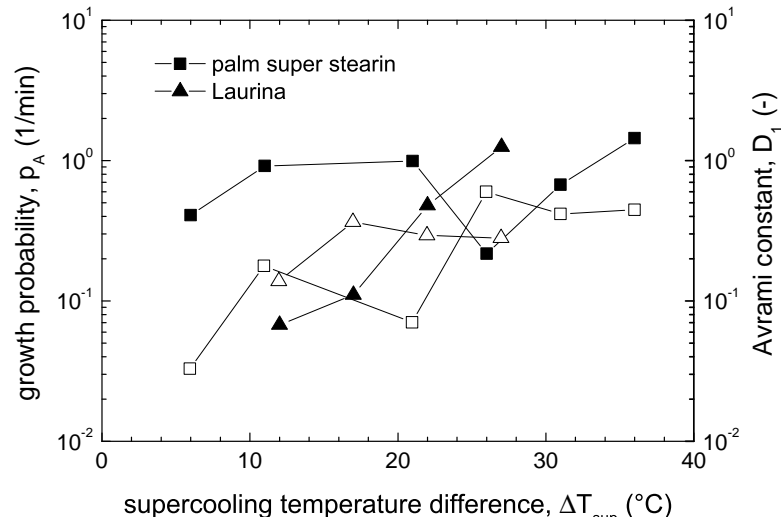


Figure 4.34.: Avrami 1D: Growth probability ( $p_A$ , solid symbols) and Avrami constant ( $D_1$ , open symbols) as function of supercooling temperature.

**Effect of seed:** The differentiation into instantaneous and sporadic nucleation by interpretation of the Avrami factor  $m_A$  (*Approximate Equation*) or the probability of nuclei growth  $p_A$  (1D) respectively is incorrect in the case of seeded samples, since addition of seed crystals simulate always instantaneous nucleation. Therefore the boundary conditions of Avrami's theory are fulfilled and the focus was set on crystal growth seed effects. The absolute crystal growth factor ( $g_{\text{abs}}$ , Eqn. 3.3) was calculated on the basis of the fitting parameters (*Approximate Equation*, Eqn. 2.14) for both, seeded and non-seeded fats. They correlate with cooling temperature. The values differ as a function of fat type due to a variation of corresponding melting ranges (Fig. 4.35 A-B). For single fats (LA, CB and partly PSS), an accelerating seed effect can be seen. For CB and PSS, this can be explained by  $\beta'$  crystallization for non-seeded and  $\beta$  crystallization for seeded fats. The driving force  $\Delta T$  is higher for a  $\beta$  compared to a  $\beta'$  crystal of the very same fat at a constant cooling temperature and thereby accelerates the crystal growth rate (Rousset, 2002). In contrast, consistent  $\beta'$  crystallization was detected for LA (non-seeded and seeded). The positive seed effect is therefore not driven by polymorphism and has to be further examined. Seeding at low supercooling of PSS (direct  $\beta$  crystallization) and crystallization of PK and PKS in general ( $\beta'$  stable) did not accelerate the kinetics as the polymorphic form did not change.

The fitting data of PM is not discussed here, since the comparison of single-stage double-stage crystallization is not meaningful. Furthermore CO was not investigated in the seeded state, since with PK, PKS and LA already three lauric fats were analyzed that showed very similar kinetics to CO in the non-seeded state.

Displaying the same data by supercooling temperature and relative growth rates ( $g_{\text{rel}}$ , Eqn. 3.4), a general trend of the crystallization kinetics of fats is derived (4.35 C-D). CB shows a different behavior compared to all other fat types confirming the statement by Koch (1973) about the uniqueness of the cocoa butter triglyceride composition. At the same time, CB is the only representative of a confirmed triple-chain length (3L) in its stable  $\beta$  form (Langevelde *et al.*, 2001a). In contrast, for the  $\beta'$  subcell structure of PK (Fig. 4.6), but also for the  $\beta$  form of PSS (equal to PS Fig. 4.12) a double-chain length (2L) was determined by x-ray scattering before. Further investigations by the examination of a series of triglyceride systems of both classes (3L, 2L) are required to confirm this possible explanation.

The normalized crystal growth factors  $g_{\text{rel}}$  are in good agreement with an empirical linear fit ( $g_{\text{rel}} = -0.015 \text{ min}^{-1} + 0.0073 \Delta T$ ,  $R^2 = 0.93$ ), based on the data of seeded fats except CB. Besides CB, non-seeded LA shows a singularity by reduced crystal growth rates in contrast to the other non-seeded fats and the general fit.  $\beta'$  stability is given in this case. In the case of CB, it seems, that the incorporation of triglycerides into a 3-L packing is more complex than into a 2-L packing as for all other fats. However, crystallized Laurina does consist of a 2-L  $\beta'$  structure, but still shows slower kinetics than in the seeded case. Therefore it is assumed, that a limiting factor for

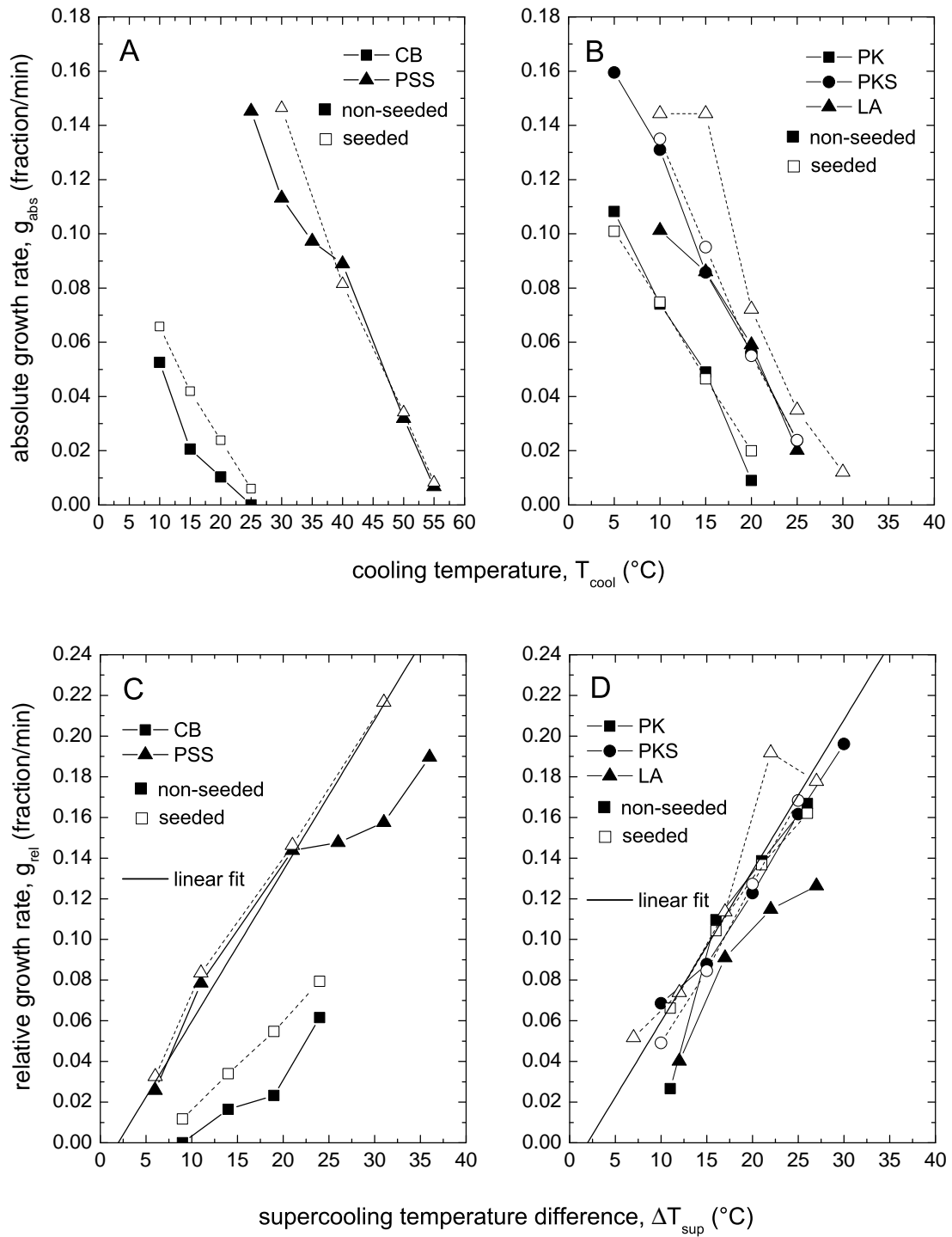


Figure 4.35.: Absolute crystal growth rate ( $g_{abs}$ ) as function of absolute temperature (A, B) and relative crystal growth rate ( $g_{rel}$ ) as function of supercooling temperature difference (C, D) of non-lauric (A, C) and lauric (B, D) fats;  $R^2(\text{fit}) \approx 0.93$ .



growth is not only the mechanism of triglyceride incorporation into a crystal surface, but can also be related to the macroscopic crystal network development (fractional dimensions; Marangoni and Ollivon, 2007; Narine and Marangoni, 1999a,d).

The presented normalization can serve as a general classification into fast ( $g_{\text{rel}}(\Delta T) > g_{\text{master-curve}}$ ), regular ( $= g_{\text{master-curve}}$ ) or slow crystallization properties ( $< g_{\text{master-curve}}$ ) of confectionery fats.

Approximation of total crystallization times according to Equations 3.5 - 3.7 is illustrated as a function of the supercooling condition in Figure 4.36.  $\beta$  stable non-lauric fats show longer crystallization times than the  $\beta'$  stable lauric fats at low supercooling conditions in the non-seeded state. Seeding reduces overall crystallization time by elimination of lag time and crystallographic transformation periods. This advantage seems negligible for non-lauric fats at  $\Delta T \geq 25^\circ\text{C}$ , while the overall time reduction is still observed for lauric fats.

It is important to note, that any solidification data depends also on the heat transfer conditions. Even when assuming an infinite cooling capacity of the tempered metal block holding the NMR-tubes (glas,  $d_{\text{tube}} = 10\text{ mm}$ ,  $m_{\text{sample}} \approx 4\text{ g}$ ), the removal of specific and latent heat is still delayed compared to DSC analysis in an aluminum pans ( $V_{\text{pan}} = 40\text{ }\mu\text{l}$ ,  $m_{\text{sample}} \leq 10\text{ mg}$ ) or microscopical investigations (Himawan *et al.*, 2006; Tewkesbury *et al.*, 2000).

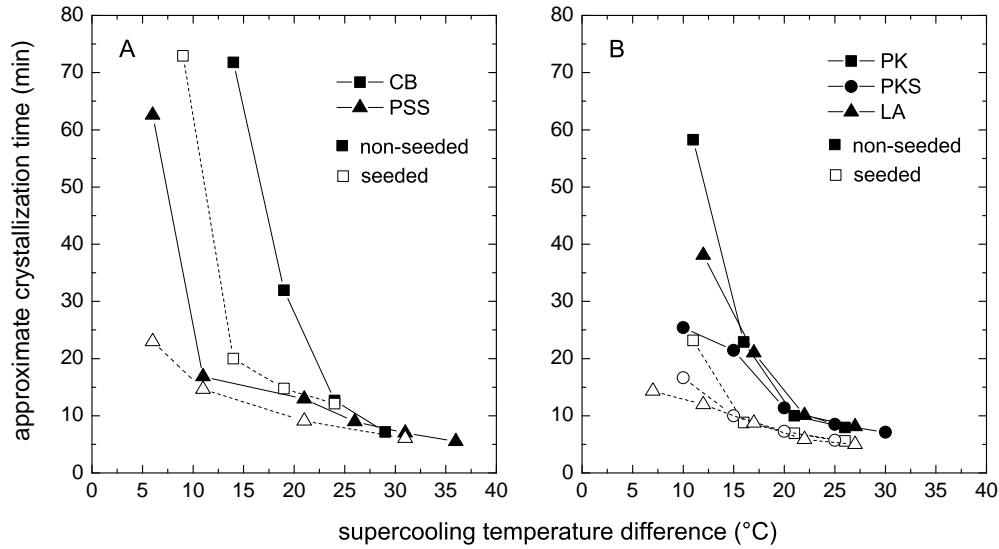


Figure 4.36.: Approximate crystallization time of non-seeded and seeded non-lauric (A) and lauric fats (B) with single-stage crystallization properties,  $SFC(t_{\text{approx}}) \geq SFC_{\text{rel,ave}} = 0.84$ .

**Summary:** Analysis of solidification kinetics of fats by pNMR technique for several confectionery fats has revealed two major findings. On the one hand, crystallization kinetics are individual for each fat as a function of absolute cooling temperature, since they have different melting temperature ranges as well as maximum melting temperatures. On the other hand, the similarities and singularities of fats can be evaluated by correlation of normalized crystal growth rates and approximated crystallization times to the supercooling temperature difference, representing the driving force. Furthermore crystal growth in an unstable  $\beta'$  form of  $\beta$  stable fats can be determined by a non-linear relationship between relative growth rate and supercooling temperature without any XRD evaluation. This crystallographic variation by crossing the melting temperature of a lower stable polymorph can be also detected by evaluating kinetic parameters according to Avrami (1940) (Eqn. 2.14).

#### 4.2.2. Contraction Kinetics

**Approach:** Contraction, as one of the related effects to crystallization of confectionery fat systems, was investigated for various vegetable fats by a so-called *normal force approach*. Details of this method are described in Chapter 3.3.4. Contraction behavior over time of melted cocoa butter (CB), palm super stearin (PSS), palm mid fraction (PM), palm kernel stearin (PKS) and Laurina<sup>®</sup> (LA) was monitored combined with a rheological oscillatory structure analysis. In general, development of the contraction and structure, as well as related final properties were of interest. Cooling temperature was varied.

Additionally, the effect of fat specific seed material on contraction characteristics was investigated. Starting temperature corresponded to seed crystal production ( $T_{ripe}$ ) in the pilot plant scale device (Chap. 3.2.1). Crystallization temperature was fixed to  $T_{cool} = 15^{\circ}\text{C}$  except for the high melting PSS ( $40^{\circ}\text{C}$ ). Supplementary CB, PKS and PM were tested at  $20^{\circ}\text{C}$ .

The corresponding solid fat content was determined separately via NMR (Chap. 4.2.1).

**Non-seeded, temperature variation:** Figure 4.37 shows exemplarily the development of cocoa butter contraction. In general, it is also characterized by a contraction lag time. Within this time period, the melted fat is cooled down and crystal nuclei are formed, which is comparable to the lag time analyzed by the NMR approach. As soon as crystal size and number are reaching a critical limit, the particle structure is detectable by rheological moduli ( $G', G''$ ) apart from temperature related oil thickening. Contraction start is observed parallel or shortly after, as growing crystals start to interact, resulting in agglomeration and structural network formation, that is able to transfer forces to the adjacent plates of the rheometer gap. Therefore, contraction

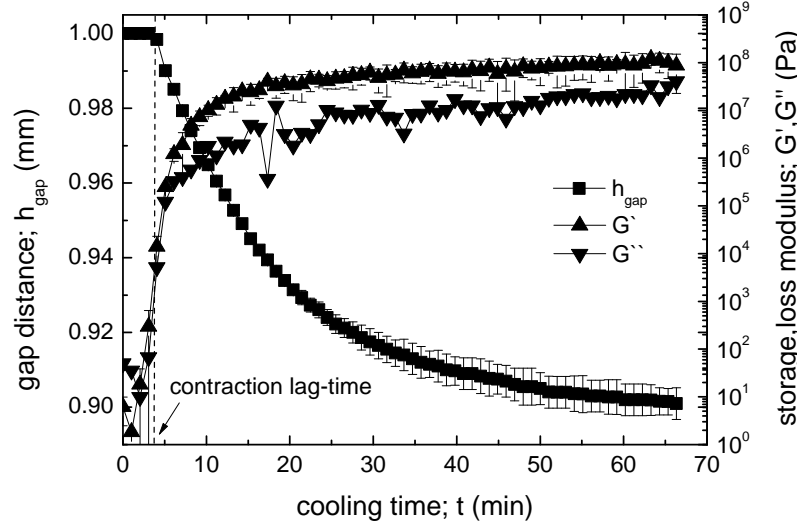


Figure 4.37.: Contraction analysis and structural development of non-seeded cocoa butter fat crystallizing,  $T = 15^{\circ}\text{C}$ .

lag time is higher than crystallization lag time based on SFC evaluation by definition. Contraction rate is fast in the beginning and slows down towards the state of thermodynamic equilibrium (Fig. 4.37). In most cases, the final crystal network is rather hard ( $G', G'' > 10^8$ ). The last ten values of a single run were averaged for further evaluation.

Cooling temperature reduction resulted in shorter lag times and increased gap reduction, as shown for PM in Figure 4.38. The double stage crystallization phenomenon for PM (general) and CB ( $20^{\circ}\text{C}$ ), as observed by NMR-kinetic experiments earlier (Fig. 4.30 and 4.28), is generally reflected by contraction and structure development (Fig. 4.39). All other fats showed consistently single stage contraction as during NMR evaluation before.

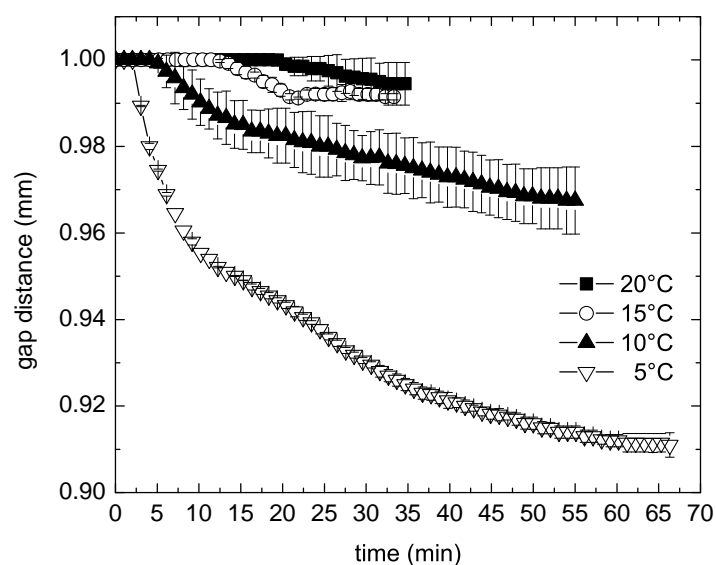


Figure 4.38.: Contraction development of non-seeded palm mid fraction (PM) by variation of cooling temperature (no correction of plate/plate steel dilatation).

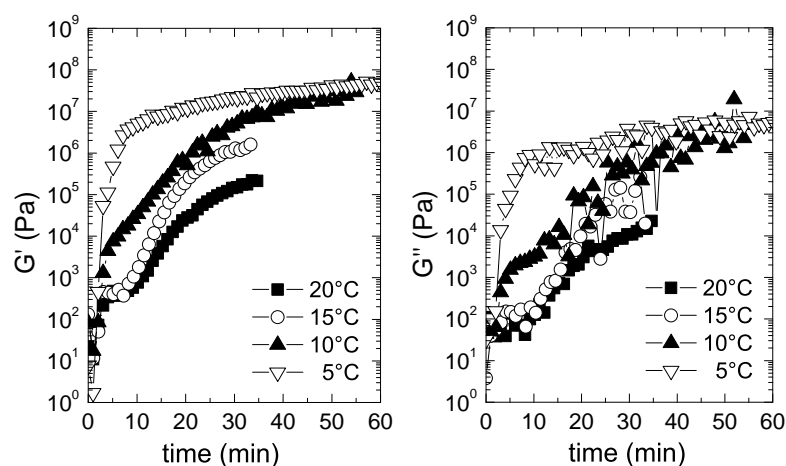


Figure 4.39.: Structure development of non-seeded palm mid fraction (PM) by variation of cooling temperature.

The final contraction and rheometric structure properties of different fats are given in Figure 4.40. LA (A) and PM (B) showed a comprehensible behavior. Solid fat content, contraction as well as storage and loss moduli ( $G'$ ,  $G''$ ) increased with decreasing cooling temperature. PKS and PSS followed this trend (Appendix, Fig. B.1, B.2). Results of cocoa butter are different in several aspects (Fig. 4.40 C). Contraction at 20°C was almost non-existent at a medium SFC, which is comparable to PM (B) at  $T = 15^\circ\text{C}$ . The contraction of CB reached the maximum of all fats at  $T = 15^\circ\text{C}$ . A critical temperature limit was between  $10^\circ\text{C} - 20^\circ\text{C}$  with an optimal time-temperature-history at  $T = 15^\circ\text{C}$ , so that the contraction was maximized. From a polymorphic point of view, the metastable range of the  $\alpha$  form is within this temperature range (Tab. 2.3). Therefore, an instantaneous nucleation and single-stage crystal growth was observed at  $15^\circ\text{C}$ , while sporadic nucleation and double-stage growth occurred at  $20^\circ\text{C}$  (see also Fig. 4.28). Cooling at lower temperatures reduced the contraction, while the corresponding SFC value was further increased. The inconsistency in contraction development over cooling temperature was also observed for  $G'$ ,  $G''$ . The parallel formation of  $\gamma$  nuclei is possible for  $T_{\text{cool}} < 15^\circ\text{C}$ . Consequently it is assumed, that the enhanced kinetics and the lower density of the  $\gamma$  nuclei result in a loose packing of crystals and thereby to a reduced contraction.

Figure 4.41 summarizes the contraction ability of the fats investigated. Lauric fats (LA, PKS) show intermediate values, while effective PM contraction occurs only at rather low temperatures. Fractionated PSS is characterized by a shift to high temperatures, as its melting range is significantly increased by the fractionation process with respect to unfractionated palm oil. CB shows generally the best contraction ability as discussed before but its development as function of cooling temperature is less predictable.

Nevertheless, a general correlation of contraction and solid fat content exists (4.42). Almost no contraction was detected for a solid fat content below 0.5, while cocoa butter showed the best contraction at maximal solid fat fractions ( $>0.8$ ). Timms (2003a) suggested a linear correlation of SFC and contraction value with fitting parameters based on Hannewijk's data (1964). This can not be confirmed by the present work. Instead, a critical SFC threshold is assumed, where crystal-crystal interactions lead to an initial network enabling the alignment of any contraction forces. A simple, exponential fit illustrates the non-linear, general trend but also the influence by fat type variation ( $R^2 = 0.59$ ).

#### 4. Nucleation and Crystallization Kinetics of Fats

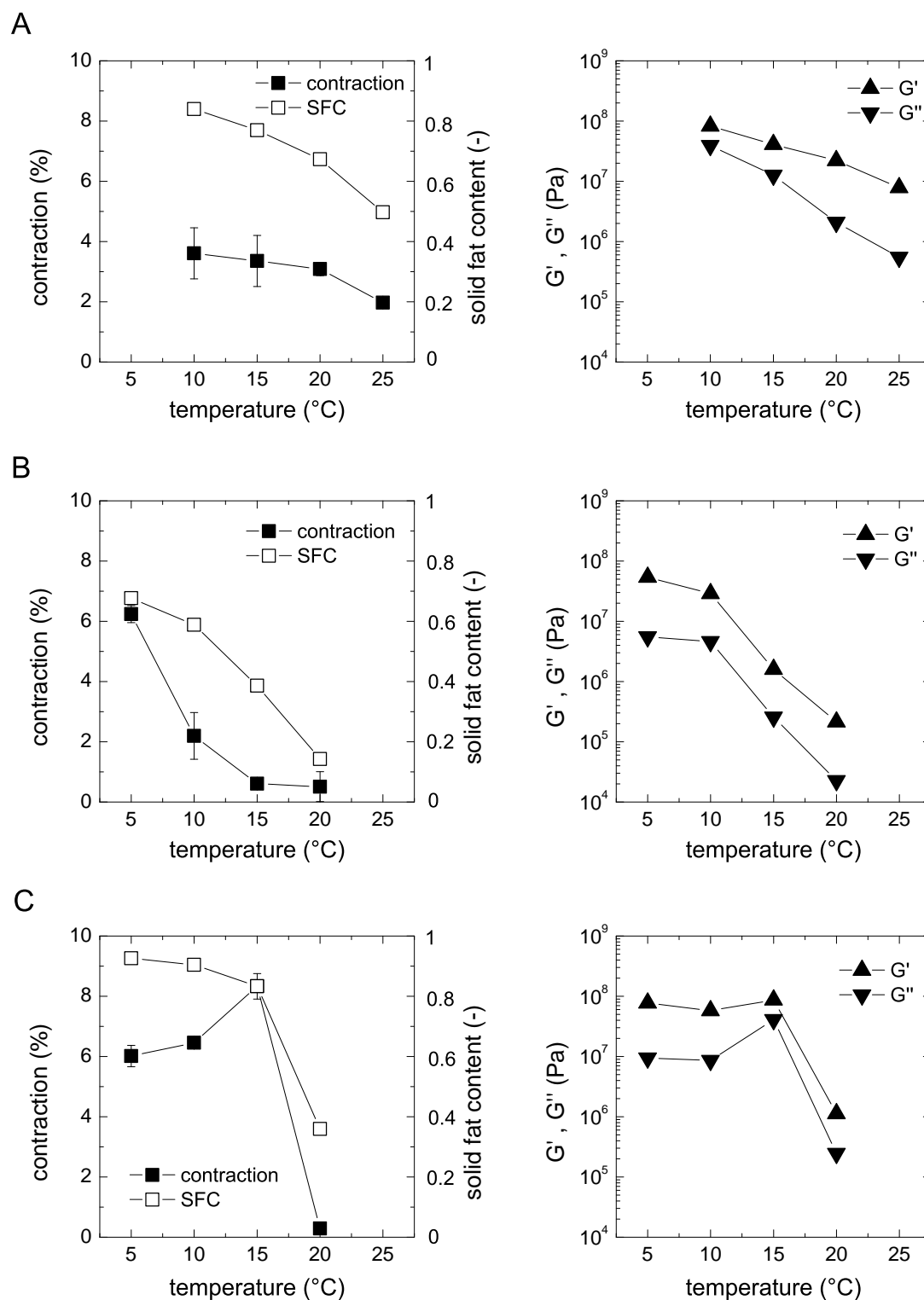


Figure 4.40.: Final contraction, solid fat content and storage/loss moduli ( $G'$ ,  $G''$ ) of non-seeded fats: Laurina (A), pam mid fraction (B) and cocoa butter (C) by variation of absolute cooling temperature.

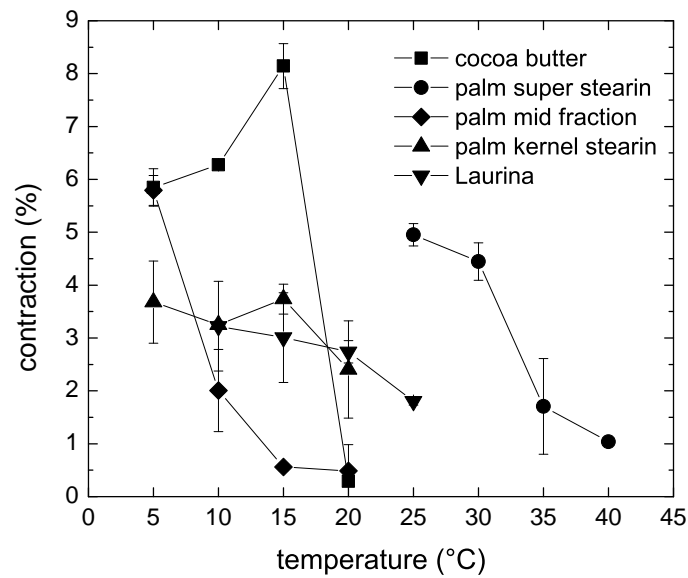


Figure 4.41.: Contraction of non-seeded fats as function of absolute temperature.

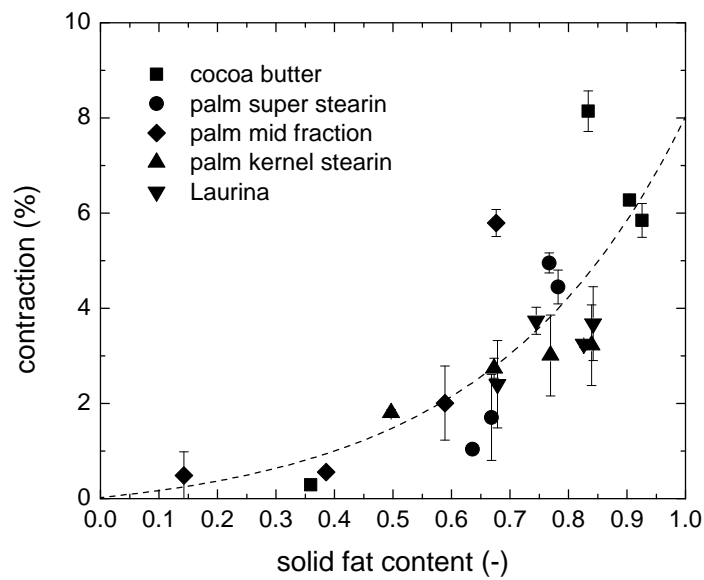


Figure 4.42.: Contraction as function of solid fat content, dashed line: exponential best fit.

**Effect of seed:** In contrast to the elimination of any lag time until crystal growth by seeding (Chap. 4.2.1), the contraction lag time was only reduced (Fig. 4.43). As explained before, a minimum amount of crystallized material is required before a crystal network is formed and tensile forces can be transferred by the system. Therefore lag times of SFC and contraction analysis are not equivalent ( $t_{\text{lag}}(\text{SFC}) < t_{\text{lag}}(\text{contraction})$ ). In general, contraction lag times of seeded fats were reduced by 45 % in average compared to non-seeded ( $T_{\text{cool}} = 15^\circ\text{C}$ ).

Contraction and SFC development of non-seeded and seeded cocoa butter during cooling is shown in Figure 4.44. At  $20^\circ\text{C}$  (A), the seeding effect was most evident. The small amount of unstable  $\beta'$  crystals formed ( $\text{SFC} \approx 0.1$ ) was not sufficient for a continuous crystal network in the non-seeded case. Contraction did not occur within time of analysis. In contrast, seeded cocoa butter crystallized directly into the  $\beta$  state onto the seed crystal surface area. Thereby, the SFC of the thermodynamic equilibrium state was reached much faster in the seeded case. Contraction and SFC increased simultaneously. At  $15^\circ\text{C}$  (B), the non-seeded sample showed contraction as well. By seeding, an increase of the crystal growth rate and the contraction rate was observed. Furthermore the absolute contraction value was increased, even though the final solid fat content was lower compared to the non-seeded state. As explained before (Chap. 4.2.1), a difference in the final SFC is an indicator for different polymorphic structures formed. Lower stable polymorphs ( $\alpha$ ,  $\beta'$ ) temporarily crystallize

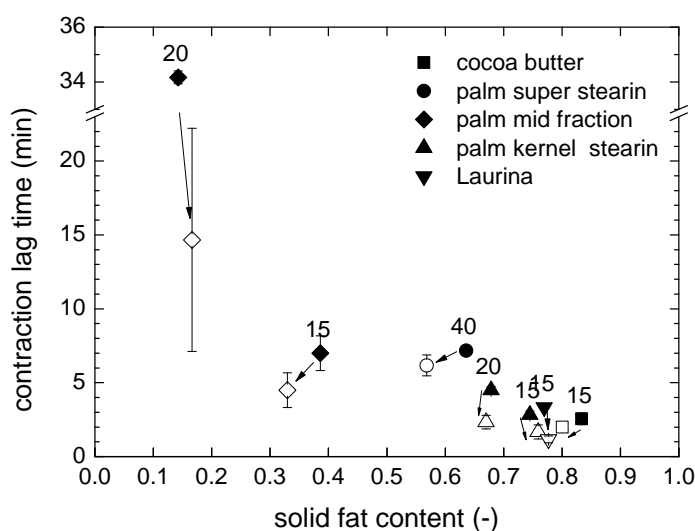


Figure 4.43.: Contraction lag times as a function of solid fat content (SFC); solid symbols: non-seeded, open symbols: seeded, numbers indicate cooling temperature in  $^\circ\text{C}$ .



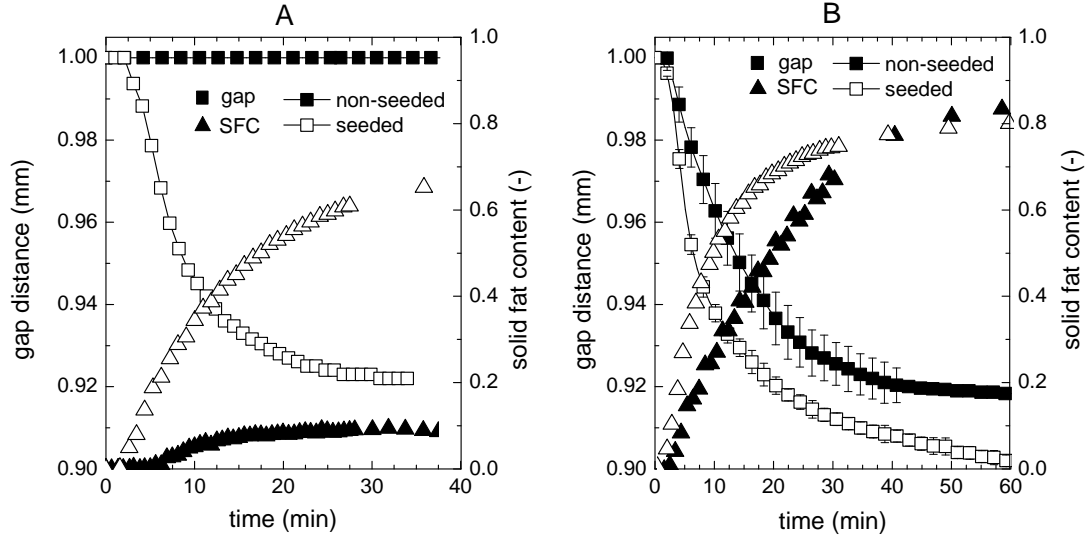


Figure 4.44.: Time-resolved gap contraction in relation to NMR solidification analysis of cocoa butter; A:  $T_{\text{cool}} = 20^{\circ}\text{C}$ , B:  $T_{\text{cool}} = 15^{\circ}\text{C}$ .

to a higher extent than stable forms (here  $\beta^V$ ), before the solid-solid transformation takes place on storage. The same qualitative characteristics were found for palm super stearin at  $40^{\circ}\text{C}$  (data not shown).

The results hereby confirm the hypothesis that contraction is not solely a function of solid fat content, but also depends on the crystalline structure forming. At the same time the final, high contraction values of non-seeded cocoa butter implies a good detachment of non-seeded chocolate, which is not the case from a practical point of view (Beckett, 2009). Mehrle (2007) showed, that the contraction kinetics of confectionery masses are reduced dependent on the cocoa butter content. The absolute increase in contraction of seeded compared to non-seeded masses was also small but the kinetics differed significantly. The contraction development of seeded compared to non-seeded samples was more homogeneous, which is in good agreement with our data. It is therefore assumed, that the detachment is not only dependent on the absolute contraction but also on the kinetics influencing the internal structure network development.

In general, the initial matrix of a fat crystal network is based on the nuclei or seed crystals, respectively, and their interconnection during crystal growth. Quantity and size distribution of the nuclei, but also crystal growth kinetics can be therefore decisive for the network formation and affect the contraction ability during cooling. Nuclei number density and size can not be predicted in the non-seeded state and are time-temperature dependent, while they are controlled by application of seed crystals. In the present study, not the individual parameter, but their product was

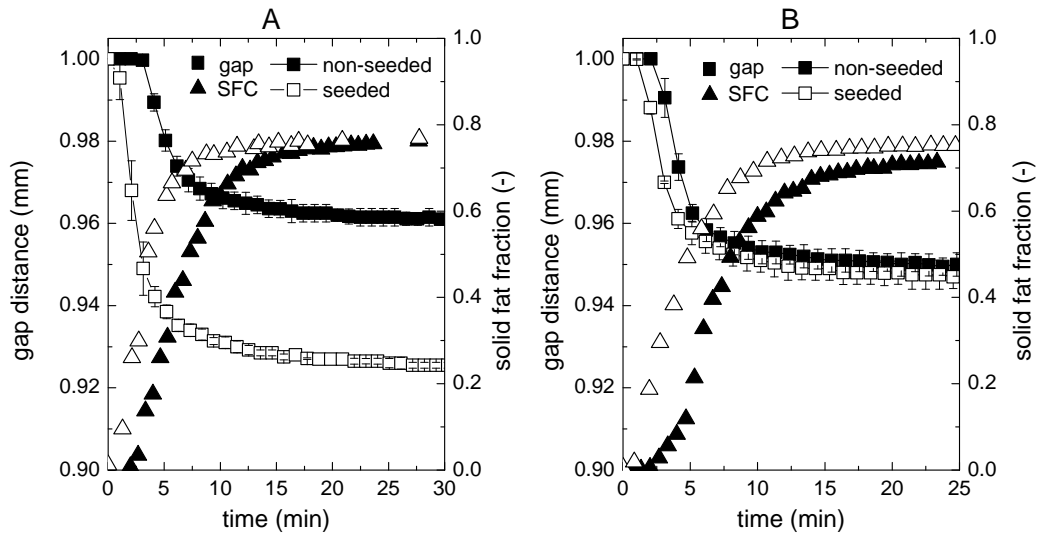


Figure 4.45.: Time-resolved gap contraction in relation to NMR solidification analysis of lauric fats at 15°C; A: Laurina, B: palm kernel stearin.

controlled ( $c_{\text{seeds}} = 0.5\text{weight-\%}$  (pure fat sample) = const.). Crystal growth kinetics have been investigated previously in Chapter 4.2.1). Laurina showed slow crystallization kinetics in the non-seeded state compared to the other lauric fats before (Fig. 4.35). Similar to CB, seeding of Laurina accelerated growth as well as contraction kinetics and improved explicitly the absolute contraction (Fig. 4.45 A). Since this fat crystallized consistently into a  $\beta'$  form, the network formation has to contribute to the overall contraction ability.

On the other hand, seeding of palm kernel stearin fat did not improve the contraction significantly, while the kinetics were accelerated mainly by elimination of the nucleation lag time (Fig. 4.45 B). Based on the theory presented, this can only be achieved, if the nuclei amount and size in the non-seeded case is somehow similar to the seed crystals. Further experiments with palm kernel fat at higher temperatures (less supercooling) are proposed to verify this assumption. In general the separation of seed quantity and seed crystal size should be considered for future investigations on this subject.

Figure 4.46 summarizes the contraction improvement by seeding using exponential trendlines, taking several fats into account. The seed effect on palm mid was small as the SFC at 15–20°C stayed below 0.5. Contraction values of non-seeded CB in the range of 6–8 % seem rather high on the first view, but are consistent with observations by Hannewijk *et al.* (1964). In his work the melting expansion of solidified fats was investigated by dilatometry. By recalculation of the data into volume contraction

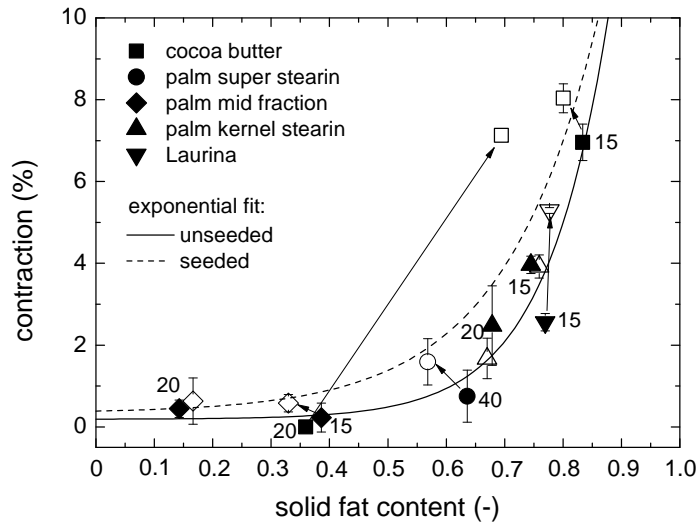


Figure 4.46.: Contraction of non-seeded (solid) and seeded (open) fats; numbers indicate cooling temperature in °C, arrows indicate the corresponding seeded sample.

values, 5.8% for rapid cooling and 7.9% for *stabilized* cooling are reported for CB at 10°C excluding the liquid oil dilatation effect. The notation *stabilized* Hannewijk *et al.* (1964) is not directly explained and stands either for a manual tempering step at 25°C after primary solidification ( $\rightarrow \beta$  quality) or a low cooling rate. Furthermore, the corresponding solid fat content values are not given. Timms (2003a) proposed a simple triplication of the linear contraction analysis by Lovegren and Feuge (1965) resulting in a corresponding volume contraction of 4.5–6.6% for  $14^\circ\text{C} < T < 22^\circ\text{C}$ , which is in good agreement with the present work. The extrapolated contraction data of different cocoa butter polymorphs referred to by Timms (2003a) are not clearly retraceable. Boundary conditions and analysis method are also unknown. The volume contractions were listed to 5.7% for  $\alpha$ , 7.3% for  $\beta'$  and 8.4% for  $\beta$  crystallization. The most comprehensible work was published by Arishima *et al.* (1995), where the mass density of different polymorphs of the triglycerides POP, POS and SOS and the corresponding liquid phase were determined. They represent about 83% of all triglycerides. Averaging results in a volume contraction of 7.2% for  $\alpha$ , 10.7% for  $\beta'$  and 11.2% for  $\beta$  structures. The performance of pure TAG systems is reduced in mixtures such as natural fats. Therefore, the presented contraction values of 6.9% for non-seeded ( $\approx \beta' + \alpha$ ) and 8.0% for seeded CB ( $\approx \beta$ ) are reduced.

Mehrle (2007) presented contraction data of chocolate masses (dark, milk, hazelnut filling). The seeded chocolate masses contracted up to 12% (dark), 9% (milk) and 7% (hazelnut filling), respectively, on the basis of the pure fat phase only. Non-

seeded masses contracted less (e.g. dark: 10.9 %). These values are rather high, even exceeding the maximal performance of the pure triglyceride systems by Arishima *et al.* (1995). Nevertheless it was demonstrated, that the contraction was improved by seeding. Milk fat and especially hazelnut oil fraction reduced the contraction performance significantly.

Hannevijk *et al.* (1964) investigated also the contraction ability of palm oil. For unfractionated palm oil, contraction by 2.3–3.3 % was presented at  $T_{\text{cool}} = 20 \rightarrow 10^\circ\text{C}$  for rapid cooling and up to 4.1 % for cooling after tempering. This fat was not investigated here, but it demonstrates the generally reduced contraction ability compared to cocoa butter of regular palm fats. Finally, a single value published by the same author for a palm mid fraction (6.7 % at  $0^\circ\text{C}$ ) is also in agreement with our data (5.8 % at  $5^\circ\text{C}$ , Fig. 4.41) considering the deviation in cooling temperature.

Present data are mainly in agreement with literature. Variations by analysis method and fat composition are inevitable in this context. The benefit of the present method is the time-resolved analysis of the contraction development (=contraction kinetics).

**Summary:** It is summarized that contraction of pure fats can be analyzed by a normal force controlled apparatus, as introduced by Schantz and Linke (2001) for chocolate. The rheological method of normal force control and superimposed oscillatory analysis is sensitive for multi-stage crystallization kinetics. This observation is consistent with the findings in the solidification kinetic analysis (Chap. 4.2.1). Fat contraction depends mainly on the solid fat content. However, it can vary significantly by fat type for SFC values  $>0.5$ . Contraction values of up to 8% were achieved for cocoa butter ( $SFC = 0.8$ ) and 3–6 % for the other fats ( $SFC = 0.65 - 0.8$ ). Enhanced contraction by seed application was achieved for  $\beta$  stable (CB, PSS) as well as  $\beta'$  fats (PM, LA). Contraction ability depends not solely on the crystalline subcell structure formed. It is suggested that initial number and size of crystal nuclei as well as crystallization kinetics are decisive for the final network structure. By seeding the first two parameters can be controlled. Therefore an expansion of analysis methods by determination of the fractal dimensions within a fat crystal network by variation of the seed quantity is advised for future investigations (Marangoni and Hartel, 1998; Marangoni and Ollivon, 2007; Narine and Marangoni, 1999c; Vreeker *et al.*, 1992).

## 5. Knowledge Transfer to Industrial Cooling Concepts

### 5.1. Structure Density of Cocoa Butter

So far, studies on confectionery fat crystallization properties were performed with lab scaled equipment only. Sample geometry and mass as well as cooling conditions were comparable within a single, analytical method, but partly differed between them. Furthermore they do not necessarily match the conditions in confectionery industry, as they were restricted to the tool options and boundary conditions. In preparation of a process oriented study (Chap. 5.2), the crystallization (SFC development) and contraction behavior of pure cocoa butter for different precrystallization conditions in praline moulds cooled at a certain temperature under controlled air flow velocity were of interest. Thereby the scale up from lab to pilot plant dimensions was tested.

**Approach** The precrystallization conditions investigated were *non-seeded*, conventionally *tempered* and *seeded*. For preparation of non-seeded samples, cocoa butter was simply cooled down from 50°C to 34°C in a jacketed beaker while stirred. For seeding, seed crystal suspension prepared by the *Seed Master* device was used. A seeding temperature of 34°C was chosen to assure pure  $\beta^{VI}$  seeding. 3.6 % of the suspension was mixed for 10 min into the temperature controlled, molten cocoa butter, resulting in a seed crystal concentration of 0.2 % within the product. This amount was tested in advance to be sufficient for cocoa butter. Tempering was performed by low shear and temperature variation according to Chapter 3.2.2. To vary the crystallographic quality of the seed crystals, the tempered crystals ( $\beta^V$ ) were mixed into pre-cooled, molten cocoa butter at 31°C to the very same, final seed concentration of 0.2 %. Moulding was performed by hand into single praline moulds (Chap. 3.2.3). The filled moulds were stored on a rack and placed into a pilot plant scale cooling tunnel (Chap. 3.2.4). This was operated at different target temperatures ( $T_{tunnel} = 10^\circ\text{C}, 13^\circ\text{C}, 17^\circ\text{C}, 20^\circ\text{C}$ ) at a constant air speed of  $v_{tunnel} = 7.2 \text{ m/s}$ , resulting in a laminar boundary layer flow on top of the moulds ( $Re_{max} = 1.5 \cdot 10^4 < Re_{crit}$ ). The core temperature development was monitored during cooling. Additionally three NMR tubes were prepared and placed in front of the praline rack. Solid fat content

was analyzed every 10 min for 1 h until an equilibrium was reached. The trials were performed separately for each type of precrystallization.

The solidified cocoa butter samples were de-moulded and stored at 18°C along with the NMR samples for one week. Density and solid fat content were analyzed directly after cooling (= 0 d) as well as after 1 day and 7 days of storage. NMR tubes were re-used each time while praline samples had to be disposed after single analysis. For both methods triplicates were evaluated.

## Results

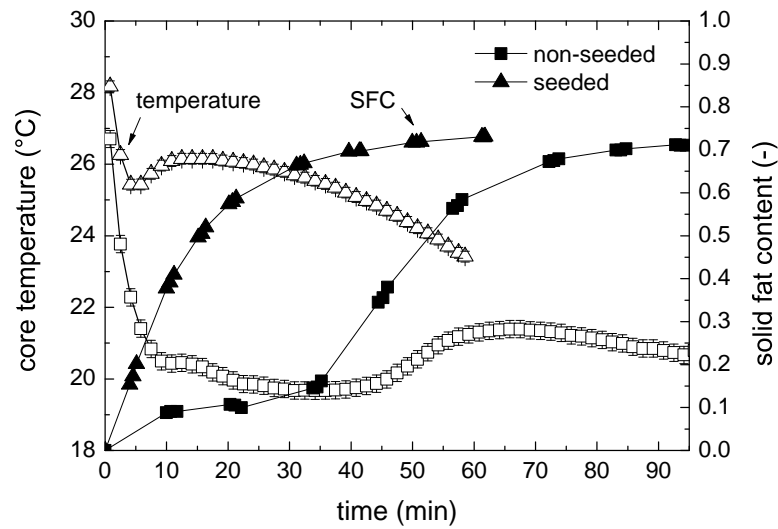


Figure 5.1.: SFC and core temperature development of cocoa butter samples in single praline moulds during crystallization by air cooling;  $T_{cool} = 20^{\circ}\text{C}$ ,  $v = 7.2 \text{ m/s}$ .

As the effects of bench-top tempering and  $\beta^{VI}$  seeding are similar, results of both types are shown only, if they significantly differ from each other. The effect of seeding on the solidification kinetics (SFC) in the cooling tunnel is comparable to the kinetic analysis from the lab scale experiments (Fig. 5.1, compare Fig. 4.28). Seed crystals induce instant crystallization and lead to a homogeneous single stage crystallization at an increased temperature (temperature curve inflection point). At the same time, the final contraction of seeded fat was increased, as indicated by density analysis (Fig. 5.2). Moreover,  $\beta^{VI}$  seeding was more effective than  $\beta^V$  tempering at low cooling temperatures. The lowest SFC value for seeded fats at a constant cooling temperature demonstrates the optimized stability of the crystals formed as discussed before in the context of  $\beta$  stable fats (Chap. 4.2.1).

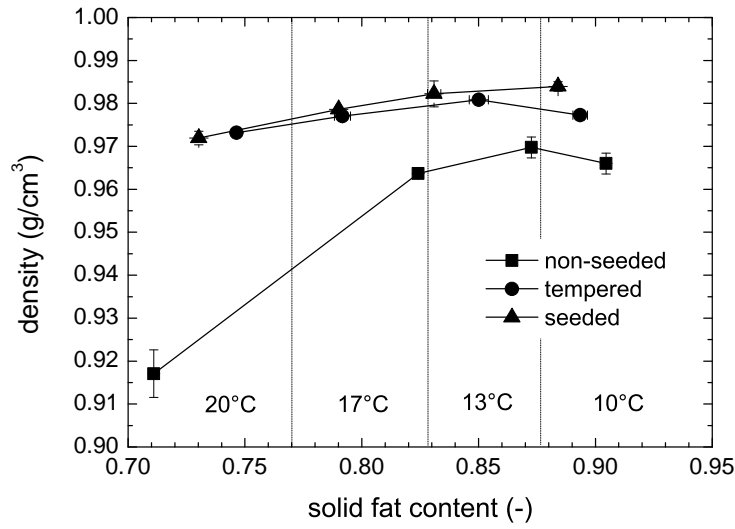


Figure 5.2.: Volume density of cocoa butter pralines directly after demoulding as function of solid fat content; related cooling temperature indicated.

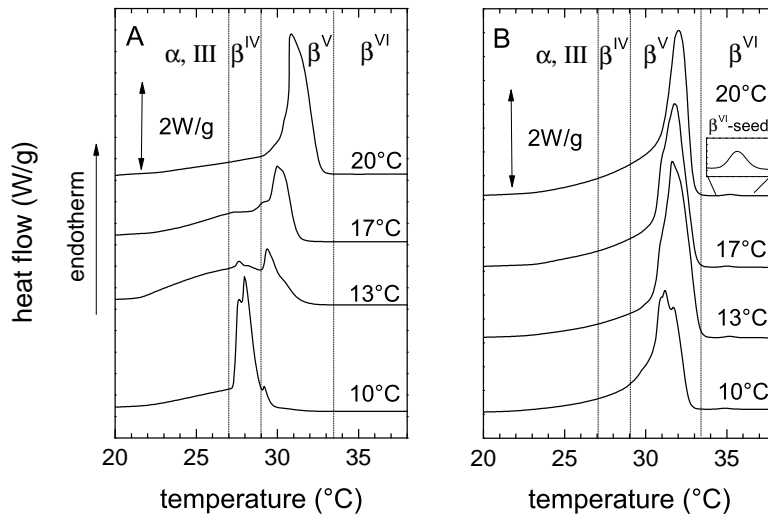


Figure 5.3.: Melting characteristics of non-seeded (A) and  $\beta^{VI}$  seeded (B) cocoa butter immediately after demoulding by variation of solidification temperature;  $\beta^{VI}$  melting peak magnified.

DSC analysis reveals the crystallographic imperfection for non-seeded fat (Fig. 5.3). The quality is reduced with decreasing cooling temperature. However, almost pure  $\beta$  crystals were detected for cooling at 20°C. This is not in agreement with results by Padar *et al.* (2008) and Mazzanti *et al.* (2005) for time-resolved x-ray analysis, where the double stage crystallization ended up in a  $\beta'$  form instead. Polymorphic transformation ( $\beta' \rightarrow \beta$ ) within the time period from solidification in the tunnel until DSC analysis (up to 1h) is therefore assumed especially with increasing cooling temperature. In contrast to the non-seeded state, the presence of  $\beta^{VI}$  seed crystals strictly promoted  $\beta^V$  growth and were detectable within the seeded fats. According to Zeng (2002),  $\beta^{VI}$  crystals of cocoa butter are formed only diffusion controlled but not directly, even if the sample is seeded with it. In general, the  $\beta$  quality of seeded samples (melting homogeneity and temperature) was only slightly reduced for strong cooling ( $T_{cool} = 10^\circ\text{C}$ ).

Final evaluation of absolute contraction on the basis of liquid cocoa butter density at 31.5°C ( $\rho = 0.9005 \text{ g/cm}^3$ ) results in similar values for seeded and tempered fat (Fig. 5.4). The contraction increased (7.4%  $\rightarrow$  8.5%) with decreasing cooling temperature mainly by thermal dilatation. The contraction ability of non-seeded samples is generally reduced by approximately 1% compared to seeded samples. As mentioned before, cooling to only 20°C results in very poor contraction. This observation supports the assumption of subsequent polymorphic transformation after the cooling process. It shows further that recrystallization does not improve the contraction after the crystal network has been already developed. The contraction values based on the *Archimedes* principle are in good agreement with the values by rheometer determination presented in Chapter 4.2.1 (open symbols in Fig. 5.4).

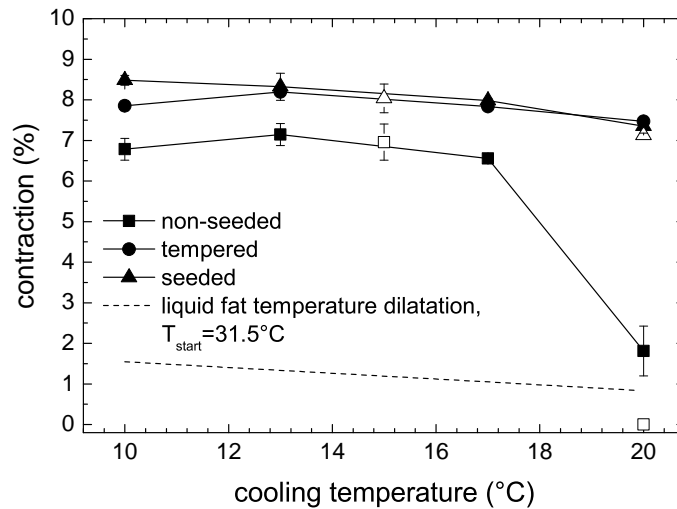


Figure 5.4.: Absolute contraction of cocoa butter immediately after demoulding; closed symbols: Archimedes principle, open symbols: rheometric method.



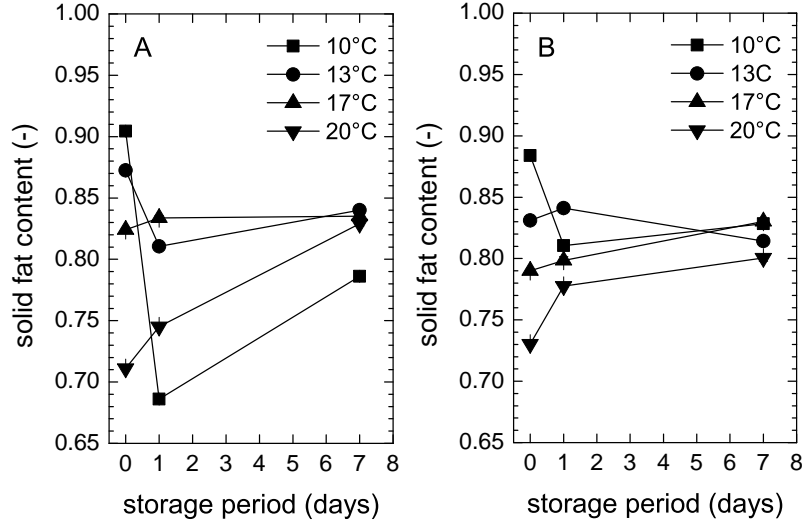


Figure 5.5.: Storage effect on solid fat content (SFC) of non-seeded (A) and  $\beta^{VI}$  seeded cocoa butter (B) by variation of solidification temperature;  $T_{stor} = 18^\circ\text{C}$ .

Post-storage crystallization affected several parameters. As storage temperature was different to cooling temperatures, the SFC values were generally aligning around  $0.82 \pm 0.015$  (Fig. 5.5). Melt-mediated re-crystallization is observed for strong cooling conditions ( $T_{cool} = 10^\circ\text{C}, 13^\circ\text{C}$ ) especially for non-seeded masses indicating crystallographic re-structuring. DSC results confirm the polymorphic transformation process ( $\beta^{IV} \rightarrow \beta^V$ ) for non-seeded and minor  $\beta^V$  perfection for seeded fats (Fig. 5.6).

Different to the fluctuating SFC development, the density generally increased during storage (Fig. 5.7). This was less pronounced for non-seeded fats and less homogeneous compared to seeded fat. The exceptional low density of non-seeded fat at  $20^\circ\text{C}$  stayed constant even though post-crystallization by  $\Delta SFC > 0.1$  was observed. It is concluded, that the the initial crystal network formed in the cooling tunnel confines the potential of post-contraction on storage. Non-seeded crystallization at different temperatures results in a variation of crystalline matrices, while number and size of nuclei are controlled and constant for all temperatures if seeded. Thereby, final density values are higher and its variation smaller than for non-seeded fat. Figure 5.8 summarizes exemplarily the effect of seeding and tempering ( $T_{cool} = 10^\circ\text{C}$ ) in terms of structure density ( density + SFC) development during storage. Strong supercooling of non-seeded cocoa butter leads to enhanced melt-mediated restructuring (SFC fluctuation) and decreased density compared to conventionally tempered cocoa butter, while seeding leads to the most dense and most stable structure.

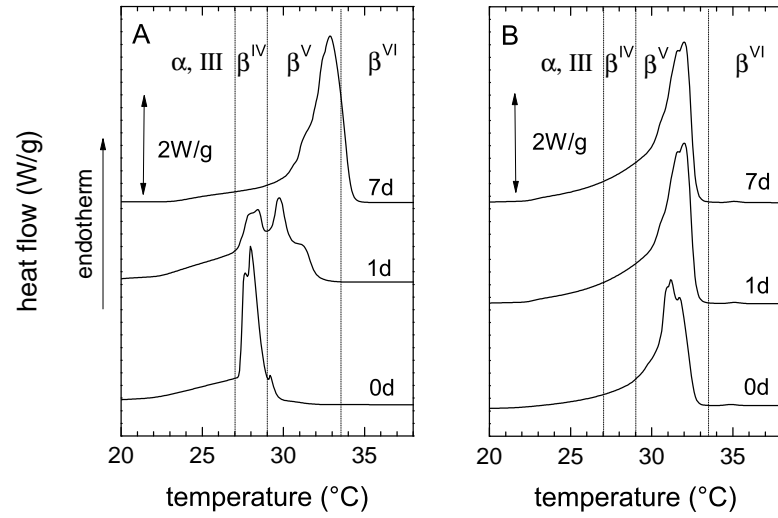


Figure 5.6.: Storage effect on melting profile stability of non-seeded (A) and  $\beta^{VI}$  seeded cocoa butter (B);  $T_{cool} = 10^\circ\text{C}$ ,  $T_{stor} = 18^\circ\text{C}$ .

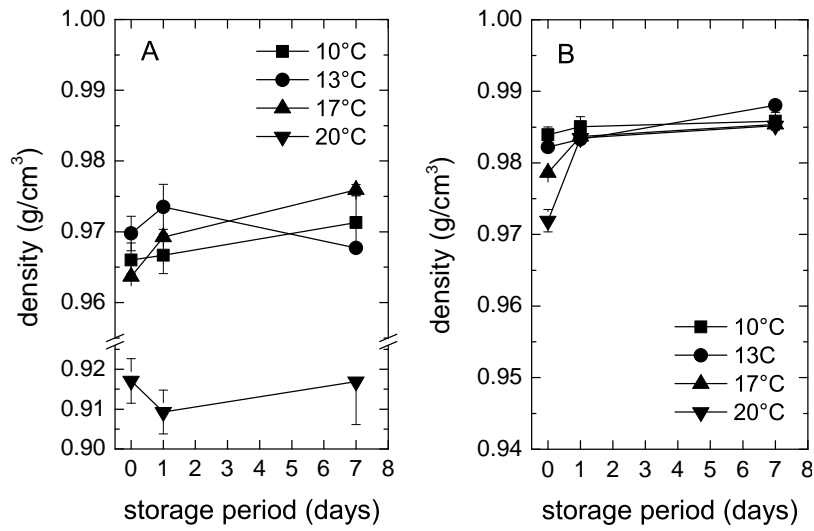


Figure 5.7.: Storage effect on density of non-seeded (A) and  $\beta^{VI}$  seeded (B) cocoa butter by variation of solidification temperature;  $T_{cool} = 10^\circ\text{C}$ ,  $T_{stor} = 18^\circ\text{C}$ .

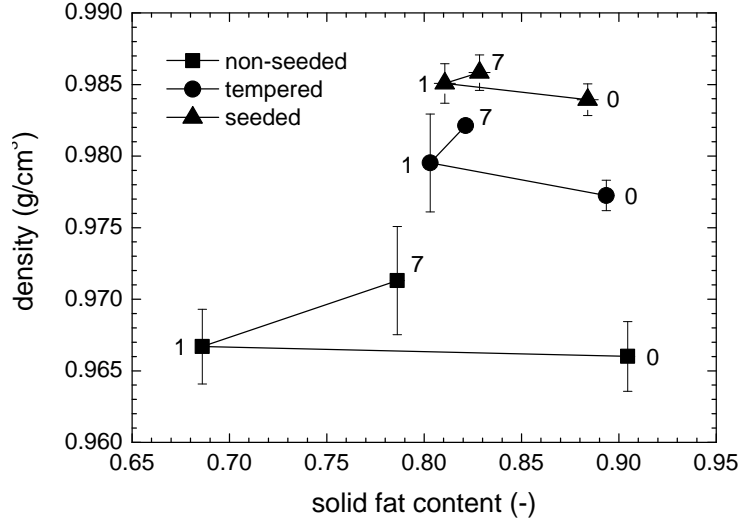


Figure 5.8.: Structure development of cocoa butter solidified at 10°C by correlation of solid fat content and density; numbers indicate days of storage at  $T_{\text{stor}} = 18^\circ\text{C}$ .

Results concerning absolute density of specific crystal forms of cocoa butter are in good agreement with literature. Vaeck (1960) presented melting dilatation results of the major crystallographic structures leading to specific densities of  $0.972\text{ g/cm}^3$  for  $\alpha$ ,  $0.990\text{ g/cm}^3$  for  $\beta'$  and  $1.003\text{ g/cm}^3$  for  $\beta$  phases while Timms (2003a) deduced out of work by Hannewijk *et al.* (1964) values of  $0.968\text{ g/cm}^3$  for  $\alpha$ ,  $0.985\text{ g/cm}^3$  for  $\beta'$  and  $0.997\text{ g/cm}^3$  for  $\beta$  crystals.

Taking the corresponding SFC into account for linear extrapolation, a density range from  $0.992\text{ g/cm}^3 \rightarrow 1.003\text{ g/cm}^3 \pm 0.002\text{ g/cm}^3$  was evaluated for  $\beta^V$  structures in our study. For the  $\beta'$  form,  $0.971\text{ g/cm}^3$  was determined. While the  $\beta$  density is in good agreement with literature, the  $\beta'$  values are in the  $\alpha$  range of published data. As Arishima *et al.* (1995) mentioned for density studies of pure triglycerides (POS, POP, SOS), not only the crystallographic nanostructure, but also the time-temperature history of crystallization and storage influences the overall density. This observation is confirmed here by the deviation in density of  $\beta$  crystal networks in all three cases of precrystallization after storing. Based on the findings of Padar (2009) and Mazzanti *et al.* (2005) the macroscopic network is based on  $\alpha$  crystals forming during cooling of non-seeded cocoa butter. Even though transformation to a  $\beta^V/\beta^{VI}$  mixture took place on storage, crystal density stayed rather low  $<0.98\text{ g/cm}^3$  and did not increase at all for the specific case of double-stage crystallization at  $20^\circ\text{C}$  ( $0.920\text{ g/cm}^3$ , Fig. 5.7). The density determination of polymorphic structures is therefore additionally a function of the fractal dimensions of the initial network.

**Summary:** It is concluded, that contraction behavior is improved and postcrystallization effects are reduced especially by  $\beta^{VI}$  seeding. Non-seeded cocoa butter fat still reaches  $\approx 7\%$  in volume contraction, but crystallization kinetics and the crystal network formed are not homogeneous as indicated by SFC and density analysis. This may cause poor de-moulding behavior and rough product surface area typical for non-seeded confectionery products containing cocoa butter. In contrast, conventionally tempered cocoa butter contracts straight up to  $\approx 8\%$ . The smaller crystal size and the high temperature stability of  $\beta^{VI}$  seeds produced by high-shear crystallization stabilize and improve further the contraction ability (up to 8.5%) at low cooling temperatures.

### 5.2. Cooling Limits for Praline Production

In Chapter 4, different aspects of individual fat crystallization were investigated on a qualitative as well as quantitative scale. However, in the process of chocolate manufacturing, all these parameters are interdependent and contribute to the final properties of a fat based confectionery product. Therefore pralines were crystallized in a convective cooling tunnel while monitoring several variables in parallel. Especially for filled product, an insight into the solidification process was of interest, facing the complex situation of different solidification kinetics of shell and filling mass.

**Approach** An application trial was carried out solidifying nougat pralines produced by a *One Shot* depositer (Chap. 3.2.3) at variable air cooling conditions. Thereby, the previously gained knowledge of pure cocoa butter crystallization could be extended by evaluation of convective cooling on realistic products. The pralines were stored for fat bloom analysis. The recipes of chocolate shell mass and hazelnut filling are given in 3.1.2. Tempering was performed by seeding technique (*Seed-Master*) with pure cocoa butter suspension (Chap. 3.2.1). Dark chocolate shell mass was seeded with 0.5% and hazelnut filling by 1% of seed suspension at 32°C. Seeding was performed separately for each trial. A regular tempercurve analysis was performed for every batch.

The theoretical flow regime (=overflowing plain) in the cooling tunnel above the rack (Chap. 3.2.4) had a laminar boundary layer with  $Re_{min} = 2.1 \cdot 10^4$  and  $Re_{max} = 4.7 \cdot 10^5$  for the range of process conditions chosen (Appendix, Tab. B.6).

Reference trials with pure dark chocolate shell mass were performed to differentiate between oil migration driven or crystallographic transformation driven fat bloom development. The effect of filling precrystallization was investigated by an additional trial performed with non-seeded filling mass ( $T_{cool} = 12^\circ\text{C}$ ,  $v_{air} = 1 \text{ m/s}$ ).

A toolbox for parallel monitoring of several product properties during the cooling process as well as long-term storage was employed to assess the solidification kinetics from different perspectives. For the detection of product temperature during active cooling (*=real-time tempercurve*), a thermocouple setup was adjusted on top of a single mold (Chap. 3.2.4). Solidification was monitored by multiple texture analysis (needle penetration) as explained in Chapter 3.3.9. Contraction of confectionery masses was analyzed on a single mould by the ultrasound technique *DetachLog* (Chap. 3.3.8) developed within the work of Mehrle (2007) and further optimized within the present studies.

Texture analysis (TA) was applied to assess long-term storage (24 weeks) effects. Melting profiles of each trial were analyzed by DSC method in duplicates (3.3.1). Initial analysis by TA and DSC was performed directly after demoulding. Due to post-crystallization effects on storage (Chap. 5.1), the pralines were stored initially at 18°C for a period of two weeks. Storage temperature was finally elevated ( $T_{\text{stor}} = 23^\circ\text{C}$ ) compared to regular storage temperatures of chocolates (18°C-20°C) for acceleration of temperature dependent kinetics such as filling oil diffusion and polymorphic transformations. On the other hand temperature was still kept below the melting ranges of  $\beta'$  and  $\beta$  crystals to maintain the crystal network. All other methods were applied after the stabilization period and shipping, since the analysis was performed by several scientific partners organized in a European project frame.

Visual fat bloom analysis was performed by photographic evaluation (*DigiEye*, as well as by human eye (Chap. 3.3.10). Structural changes were monitored by confocal laser scanning microscopy (CLSM, Chap. 3.3.11).

The presentation of the results is separated into (i) inline analysis during cooling in the air streamed cooling tunnel and to (ii) extended methods applied during storage.

## Results

**Cooling Tunnel** The effect of cooling temperature and air velocity on inline product temperature profile progression (*real-time tempercurve*) of pralines was determined. Real-time tempercurves of the most extreme cooling parameter combinations are shown in Figure 5.9. They were evaluated by determination of the inflection point values ( $t_{\text{inf}}$ ,  $T_{\text{inf}}$ ,  $s_{\text{inf}}$ ). Maximal spread of total cooling time until main crystallization ( $t_{\text{inf}}$ ) was between 300s and 800s. Main crystallization temperatures ( $T_{\text{inf}}$ ) varied from 22°C (shell) to 7°C (filling). Furthermore, slope values  $s_{\text{inf}}$  at inflection points of the shell sensor (3) were generally lower than those of the core sensor (1), because locally conducted heat flow increased from core to shell position due to increasing local temperature gradients with radial distance from the core. This is most obvious at strong cooling ( $T_{\text{cool}} = -10^\circ\text{C}$ ). Generally, the inflection slope is a result of superimposed crystallization rate (heat generation), heat conduction coefficient,

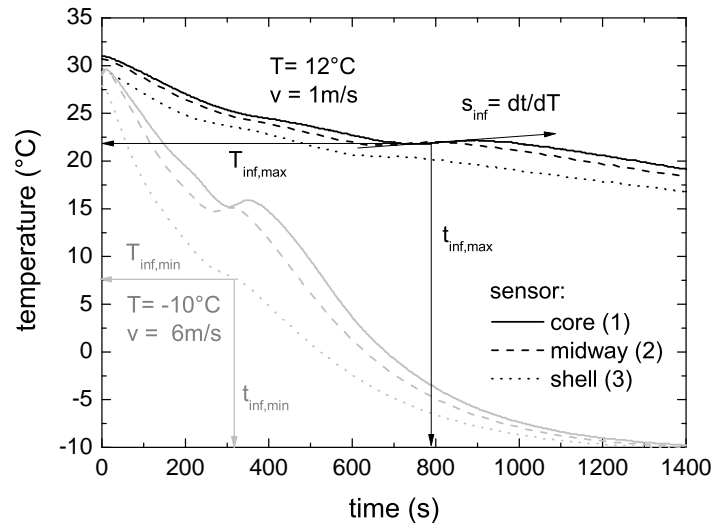


Figure 5.9.: Real-time tempercurve development of air cooled dark chocolate nougat pralines for the most extreme cooling conditions investigated.

product geometry and cooling conditions (heat transfer coefficient). The slope value increases with increasing crystallization kinetic as well as total latent heat released (SFC) and decreases with increasing local cooling capacity within the system. The comparison of offline temper-test results (Fig. 5.10) and the real-time tempercurves point out that fat crystallization, and therefore final product structure, is not only defined by precrystallization but the combination of both process steps, tempering and cooling. The inner temperature sensors (1, 2) are related to the praline filling mass. The outer sensor (3) is positioned at the interface of filling and shell mass. Thereby, the crystallization events of both masses are directly monitored. Details of the shell and filling crystallization are highlighted in Figure 5.11 during cooling at  $T_{\text{cool}} = 12^{\circ}\text{C}$  and  $v_{\text{air}} = 1 \text{ m/s}$ . The crystallization of the chocolate shell mass took place after 300 s at  $24^{\circ}\text{C}$  (A). For a filled praline the inflection point was less developed, since the filling did not contribute to the latent heat release within this time period (B1). The seed effect in the filling is detectable by the development of a second inflection point (B1 vs. C,  $t = 600 \text{ s}$ ). Even though only the filling temperature is monitored by sensor 1 (B2), shell crystallization is mirrored time-delayed ( $t = 350 \text{ s}$ ) in the temperature progression of the core prior to its crystallization ( $t = 750 \text{ s}$ ).

As crystallization of the chocolate shell occurred well in advance of filling solidification and showed therefore higher inflection temperatures, these values were less critical in terms of polymorphic product quality or process time optimization. Consequently the crystallization of the filling mass is discussed in more detail.

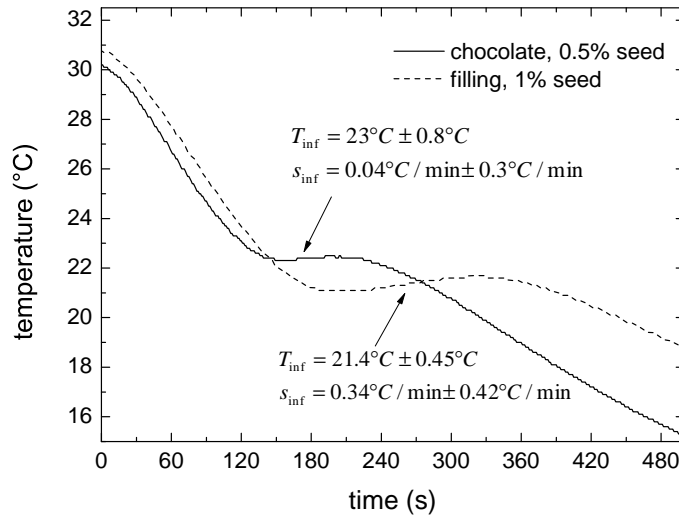


Figure 5.10.: Representative tempercurve development (offline) of dark chocolate and hazelnut filling after  $\beta^{VI}$  seeding, averaged inflection point values indicated.

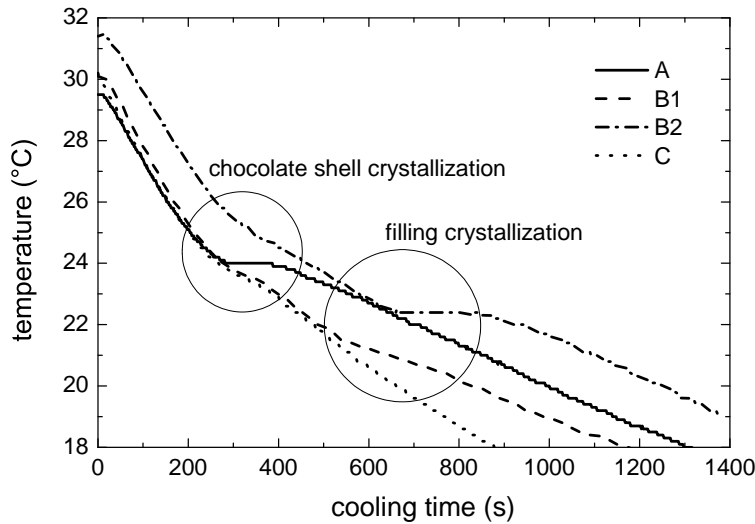


Figure 5.11.: Real-time tempercurves at the shell region (sensor 3: A, B1, C) and core (sensor 1: B2) of seeded, pure chocolate (A), a well seeded praline (B) and a praline with non-seeded filling (C);  $T_{cool} = 12^{\circ}\text{C}$ , and  $v_{air} = 1 \text{ m/s}$ .

The time period, until filling crystallization was observed, decreased from core to shell due to an increasing local product temperature gradient by external cooling (data not shown). The inflection temperature ( $T_{\text{inf}}$ ) decreased as well (Appendix, B.7), because crystallization is not instantaneous when reaching a critical temperature but is triggered by kinetics as a function of supercooling temperature and time (see also Fig. 4.35). Consequently the crystallization kinetic is the limiting factor for a crystallization process optimization in this case.

Cooling temperature reduction ( $T_{\text{cool}} \downarrow$ ) generally reduced all values ( $t_{\text{inf}}$ ,  $T_{\text{inf}}$ ,  $s_{\text{inf}}$ ) and enhanced the gradual span from core to shell sensor (Appendix, B.7). The acceleration of the air velocity ( $v_{\text{air}} \uparrow$ ) had the same effect on  $t_{\text{inf}}$  and  $T_{\text{inf}}$ . However, heat accumulation is observed at the praline core, since the local  $s_{\text{inf}}$  was even increased. In this case, not the kinetics but heat conduction became the limiting factor for solidification.

Taking general theory of heat transfer for flow over a flat plate into account, the following statements can be made for the temperature progression until crystallization starts. According to Equations 5.1 and 5.2, parameters influencing the level of heat flux are cooling temperature  $T_{\text{cool}}$ , heat transfer coefficient  $\alpha_{\text{HT}}$ , heat conductivity coefficient  $\lambda_{\text{HT,prod}}$  and product dimension  $s_{\text{HT,prod}} = h_{\text{plain}}/2$ . The product mean temperatures at core ( $T_1$ ) and shell ( $T_3$ ) are then defined by Equation 2.15.

$$\dot{q}_{\text{cond}} \approx \frac{\lambda_{\text{HT,prod}}}{s_{\text{HT,prod}}} (T_1 - T_3) \quad (5.1)$$

$$\dot{q}_{\text{trans}} \approx \alpha_{\text{HT}} (T_3 - T_{\text{cool}}) \quad (5.2)$$

With decreasing cooling temperature, the temperature gradient for heat transfer is initially increased. Consequently, the conducted heat flux is enhanced, as  $T_3(t)$  decreases faster. Since the temperature profile within the praline was approximately parabolic, even for the most gentle cooling conditions (12°C, 1 m/s), the heat conduction coefficient limits the cooling process ( $BI > 1$ , Wagner, 2011), as concluded before.  $\lambda_{\text{product}}$  is a material property of the confectionary mass (and mold material). It can be seen as a constant for the temperature range of interest (e.g.,  $\lambda_{\text{fat}} = 0.15 \text{ W/(mK)}$ ,  $\lambda_{\text{sugar}} = 0.58 \text{ W/(mK)}$ ; Tscheuschner, 2004) and is rather small compared to water ( $\lambda_{\text{water}} \approx 600 \text{ W/(mK)}$ ). Only by variation of the product recipe this factor can be modified, giving a first boundary condition for the discussion of cooling optima of confectionery products. However, heat transfer coefficient  $\alpha_{\text{HT}}$  for convection is dependent on the cooling air velocity (Eqn. 2.21, 2.22). Triplication of  $v_{\text{air}}$  leads to an enhanced heat transfer for the entire cooling period with an increase of  $\alpha_{\text{HT}}$  by 73 % (145 % for sixfold air velocity; VDI, 2006). In comparison, a decrease in cooling temperature from 12°C to 7°C at a product molding temperature of 30°C increases the heat transfer by 28 % (122 % for −10°C), but declines proportional to the temperature gradient  $T_3 - T_{\text{cool}}$  with cooling time.



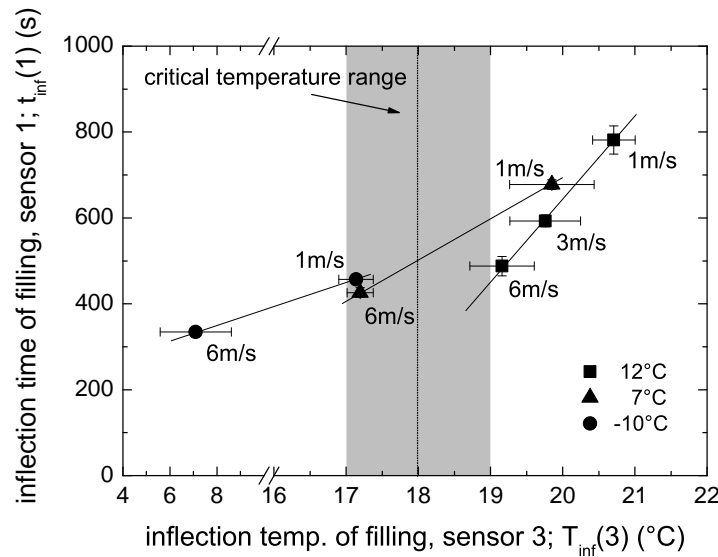


Figure 5.12.: Correlation of inflection time of the praline center and crystallization temperature of filling mass at the shell region by variation of cooling conditions.

Goals of chocolate solidification by cooling are the effective removal of latent heat and a sufficient mass contraction for product detachment, which is correlated to the controlled  $\beta$  crystallization of the whole product. A first estimation of minimal cooling time is therefore given by the inflection time of the product center (sensor 1). Correlation of  $t_{\text{inf}}$  at the center (sensor 1) with  $T_{\text{inf}}$  close to the shell (sensor 3) as a quality parameter is given in Figure 5.12. 17°C-19°C is the minimum melting range of cocoa butter  $\alpha$  crystals and is therefore seen as a critical limit ( $\Delta T = 0$ ) for main crystallization to avoid uncontrolled nucleation of unstable  $\alpha$  crystals. Furthermore, Malssen *et al.* (1996) showed, that  $\alpha$  but also  $\beta'$  nucleation of non-seeded cocoa butter does not occur above 19°C even at very low cooling rates. An increase of air velocity reduced the cooling time until core crystallization more efficiently than cooling temperature reduction with respect to a constant polymorphic quality ( $T_{\text{inf}}(3)$ ). The velocity increase from 1 m/s to 3 m/s at  $T_{\text{cool}} = 12^\circ\text{C}$  reduced cooling time by 24 % compared to 13 % for a temperature decrease from 12°C to 7°C at  $v_{\text{air}} = 1 \text{ m/s}$ .

Both actions resulted in similar inflection point temperatures (= quality) throughout the praline profile (Tab. B.7), that is correlated with the polymorphic quality. With further increase of air velocity (6 m/s,  $T_{\text{cool}} = 12^\circ\text{C}=\text{const.}$ ), cooling time was finally reduced by a total of 38 %. The evaluated process time reduction is generally

lower than by theoretical approximation for a laminar flow regime. First of all, heat transfer of confectionery products is generally limited by internal heat conduction ( $BI > 1$ ; Tewkesbury *et al.*, 2000). Therefore enhanced cooling conditions are less effective for the product center than for its surface layer. Secondly, the actual product temperature of center crystallization was generally reduced due to stronger cooling conditions, as discussed before. Therefore, additional removal of specific heat has to be considered. This has not been considered here so far. Several authors (Franke, 1998; Révérend *et al.*, 2010; Stapley *et al.*, 1999; Tewkesbury *et al.*, 2000) discussed this rather complex situation for the simulation of chocolate crystallization. They all are attempts on a numerical base requiring intensive data acquisition for each confectionery mass intended to be used.

Crystallization temperature of the filling mass close to the shell was finally decreased to approximately 19°C ( $T_{\text{cool}} = 12^\circ\text{C}$ ,  $v_{\text{air}} = 6 \text{ m/s}$ ), which is close to the polymorphic limit. All other parameter sets ( $T_{\text{cool}} = -10^\circ\text{C}$ ;  $T_{\text{cool}} = 7^\circ\text{C} + v_{\text{air}} = 6 \text{ m/s}$ ) led to temperatures below the critical value and are therefore not recommended for this particular product from a crystallographic point of view.

Demoulding characteristics analyzed by ultrasound technique (*DetachLog*) for  $T_{\text{cool}} = 12^\circ\text{C}$  are shown in combination with real-time tempercurves in Figure 5.13. The origin of the initial, significant signal fluctuation is not clear yet. By data comparison of reference trials with pure chocolate and chocolate bars in tablet moulds, it is assumed, that the mould geometry (half-sphere, less product) causes this phenomenon. Since the final detachment after main crystallization was of interest, the reason for this observation was not further investigated for now.

Overall, the patterns are consistent with increasing air velocity and show an amplitude minimum (=damping maximum) shortly before the core crystallization was detected. Detachment was achieved after the temperature inflection point was reached. This is plausible, since contraction is caused by crystallization and a critical contraction limit has to be reached before detachment is completed. Approximation of the minimal cooling time required was therefore corrected based on the *DetachLog* data (Fig. 5.14 compare with Fig. 5.12)). The general advantage of air velocity increase compared to cooling temperature reduction is no longer obvious. Instead, the evaluated minimal cooling times by cooling temperature reduction and air flow increase tested as a function of potential crystal quality are rather similar. Nevertheless, the results point out, that the control of air velocity is at least as important as the regulation of cooling temperature in a convective cooling tunnel.

For the most extreme cooling conditions ( $T_{\text{cool}} = -10^\circ\text{C}$ ) the advantage of the *DetachLog* system compared to temperature sensors in terms of mould detachment is demonstrated. Cooling period until center crystallization was reduced by velocity increase (Fig. 5.12). However, contraction behavior of the pralines was less effective than for low air speed (Fig. 5.14). This was caused by the inflection temperature of the chocolate shell mass. It dropped to 15.5°C and thereby below the critical range

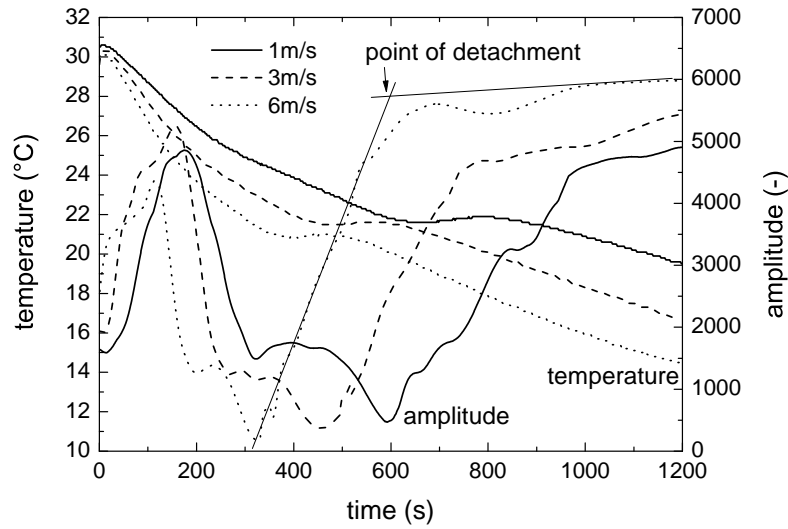


Figure 5.13.: Real-time tempercurves at the praline center and corresponding *Detach-Log* signals for cooling at 12°C and variation of air speed.

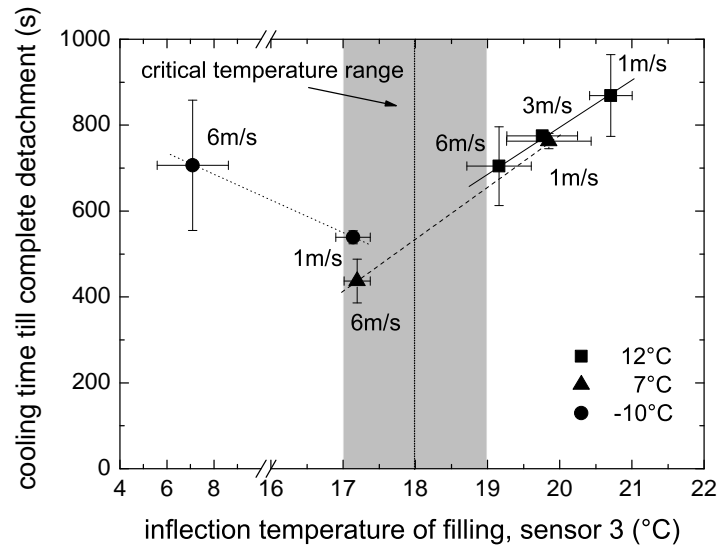


Figure 5.14.: Correlation of cooling time until complete detachment to crystallization temperature of filling mass at the shell region of pralines by variation of cooling conditions.

for  $\alpha$  nucleation at  $v_{\text{air}} = 6 \text{ m/s}$  only (Appendix, Tab. B.8) Analysis of cocoa butter contraction behavior (Chap. 4.2.2 and 5.1) showed that unstable polymorphs reduce the contraction ability. It is therefore concluded, that a homogeneous contraction of the shell mass by controlled  $\beta$  crystal growth is even more important than contraction of the filling in terms of mould detachment.

Texture analysis during cooling by needle penetration was not reproducible for filling masses. Cracks were observed within the first 15 min of cooling as soon as the needle passed the chocolate-filling interface. Filling mass was still soft while the shell had already crystallized. Therefore the shell hardness was evaluated only. Solidification started simultaneously to the onset of the chocolate shell crystallization (Fig. 5.15). The consistent hardening process was slowed down by the latent heat release of the filling mass. This effect was evident for cooling temperature variation at a constant air velocity of  $v_{\text{air}} = 1 \text{ m/s}$  and for air velocity variation at a constant cooling temperature of  $T_{\text{cool}} = 12^\circ\text{C}$  (Fig. 5.16). It was not observed for stronger cooling conditions, as the increased cooling capacity could compensate the additional heat release much faster. Hardening was accelerated by increased air velocities, leading to plateau values after approximately 20 min of cooling.

DSC of seeded shell and filling mass directly after cooling showed consistently  $\beta$  quality, while non-seeded filling resulted in a polymorphic mixture (Fig. 5.17). Nucleation of proportional, unstable crystals ( $< \beta^{IV}$ ) within seeded masses and at strong cooling conditions (e.g.  $-10^\circ\text{C}$ ) was therefore not confirmed here.

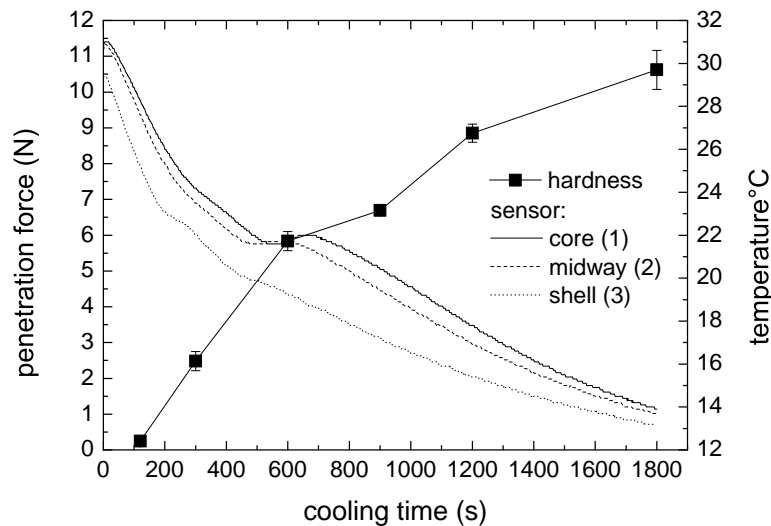


Figure 5.15.: Shell hardness and real-time temperature development of a filled praline during solidification;  $T_{\text{cool}} = 12^\circ\text{C}$ ,  $v_{\text{air}} = 3 \text{ m/s}$ .

A side-effect of relative contraction differences was observed for strong cooling to

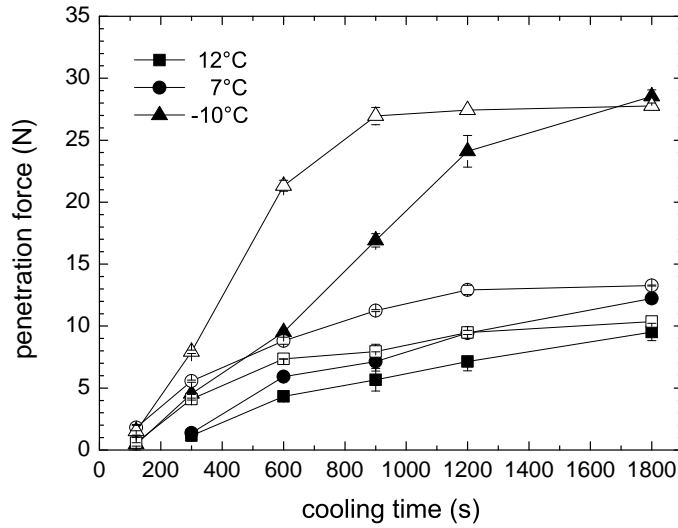


Figure 5.16.: Solidification development of chocolate shell (filled pralines) during solidification; solid symbols:  $v = 1$  m/s, open symbols:  $v = 6$  m/s.

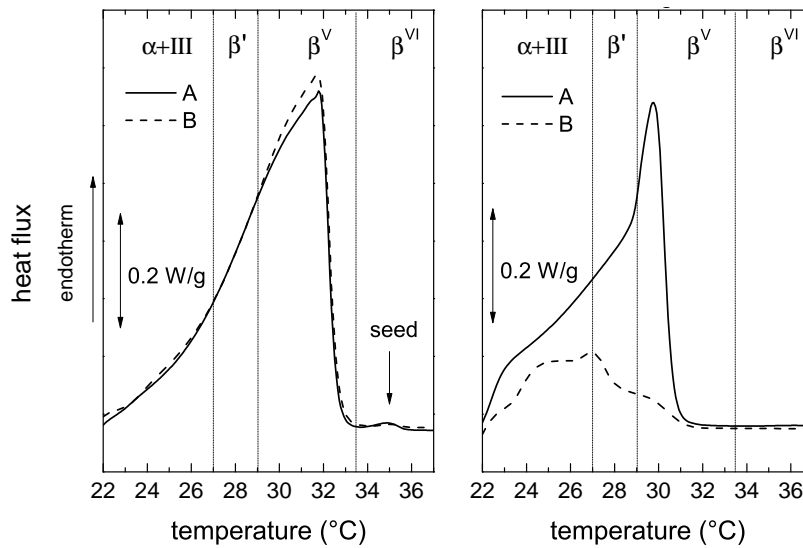


Figure 5.17.: Melting curves of pralines with a seeded chocolate shell and seeded (A) or non-seeded (B) hazelnut filling mass ,  $T_{\text{cool}} = 12^\circ\text{C}$ ,  $v_{\text{air}} = 1$  m/s.

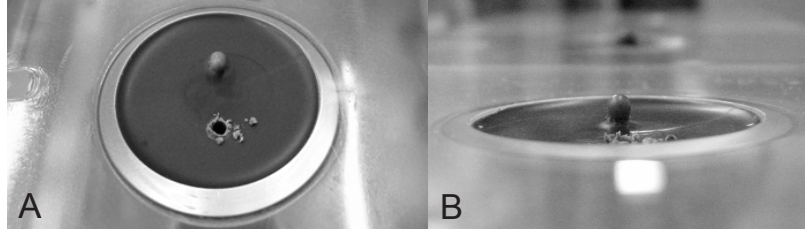


Figure 5.18.: Filling mass extruded out of penetration hole as observed for harsh cooling conditions or non-seeded filling within the initial 5 min of cooling; A - top view, B - side view.

$-10^{\circ}\text{C}$ . While chocolate shell (32% fat) contracts rather fast up to 3% by crystallization (Chap. 4.2.2 and Mehrle, 2007), the filling is still liquid at this point and is thereby squeezed out of the first hole of texture analysis after  $t_{cool} = 2$  min (Fig. 5.18). This phenomenon was also observed for non-seeded filling cooled at regular conditions ( $T_{cool} = 12^{\circ}\text{C}$ ,  $v_{air} = 1$  m/s). Even though contraction kinetics of the seeded chocolate are reduced at  $12^{\circ}\text{C}$ , the contraction of the non-seeded filling is almost non-existent. Consequently the shell and filling contraction were still very different, resulting in an overpressure. This effect is observed on filled products moulded by co-extrusion only (*One-Shot*) and is a potential factor for enhanced oil migration. For conventional or frozen cone moulding techniques the contraction of the shell mass is almost finished after the first cooling step before the filling is introduced into the system.

**Fat Bloom Stability** Visual fat bloom analysis during storage of praline products by a human panel and by *DigiEye* were very similar as shown later. The trials can be clustered in 1 and 2 according to the real-time tempercurves inflection data according to:

$$T_{inf,3}(\text{cluster 1}) < 18^{\circ}\text{C} < T_{inf,3}(\text{cluster 2}) \quad (5.3)$$

The reference pralines out of pure chocolate form a 3<sup>rd</sup> cluster.

- cluster 1:  $T_{cool} = -10^{\circ}\text{C}$ ,  $v_{air} = 1, 6$  m/s;  $T_{cool} = 7^{\circ}\text{C}$ ,  $v_{air} = 6$  m/s,
- cluster 2:  $T_{cool} = 12^{\circ}\text{C}$ ,  $v_{air} = 1, 3, 6$  m/s;  $T_{cool} = 7^{\circ}\text{C}$ ,  $v_{air} = 1$  m/s,
- cluster 3: plain chocolate reference pralines,  $T_{cool} = 12, 7, -10^{\circ}\text{C}$ ,  $v_{air} = 1$  m/s.

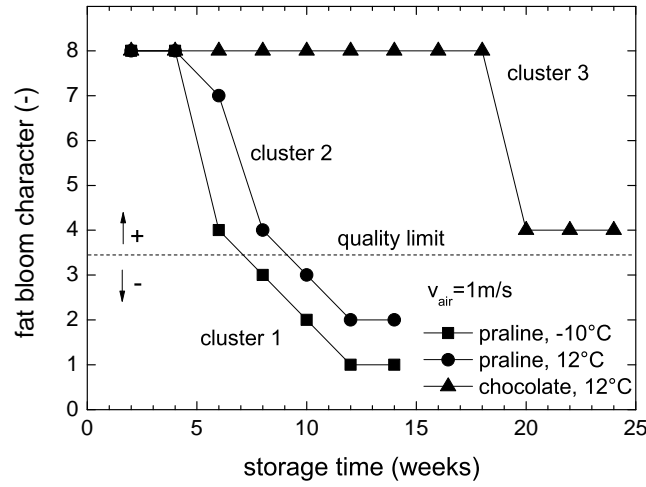


Figure 5.19.: Fat bloom evaluation by a human panel, representative single trials for three quality clusters; cluster 1:  $T_{\text{inf},3} < 18^\circ\text{C}$ , cluster 2:  $T_{\text{inf},3} > 18^\circ\text{C}$ , cluster 3: plain chocolate as reference.

Quality deficiency was recognized by human eye after 6 weeks of storage for cluster 1 (Fig. 5.19). The appearance for more gently cooled pralines stayed almost perfect at this point (cluster 2). Unacceptable fat bloom of cluster 1 was finally reached after 8 weeks. Cluster 2 followed this trend with a retardation of two weeks. Cluster 3 started to bloom after 14 weeks ( $T_{\text{cool}} = -10,7^\circ\text{C}$ ) and 20 weeks ( $T_{\text{cool}} = 12^\circ\text{C}$ ), respectively. Evaluation of several sets of pralines at different storage temperatures with the very same confectionery masses in prior studies revealed a minimal time scaling factor of 2.5 for unacceptable quality deficiency on storage at  $23^\circ\text{C}$  compared to  $20^\circ\text{C}$ . Hence, actual fat bloom stability was 20 weeks (cluster 1) and 25 weeks (cluster 2) for the pralines and 50 weeks for plain chocolate, respectively. The values are representative for equivalent, commercial products as discussed with industrial partners.

Results by *DigiEye* evaluation were in good agreement with human eye (Fig. 5.20). The critical range for unacceptable fat bloom ( $WI_{\text{crit}} = 29 - 30$ ) was evaluated in advance (Chap. 3.3.10). This value was reached for cluster 1 after 6 weeks of storage, while cluster 2 showed minor bloom development. After 12 weeks bloom had been further developed for cluster 1, while cluster 2 showed unacceptable fat bloom on a lower level, too. Plain chocolate (cluster 3) was still of good quality.

The high fat bloom stability of plain chocolate as reference material in contrast to filled pralines reveals the negative effect of hazelnut filling. It is thereby proven that fat bloom development on the pralines was driven by oil migration (Galdamez *et al.*, 2009; Motwani *et al.*, 2011) instead of polymorphic cocoa butter transformation.

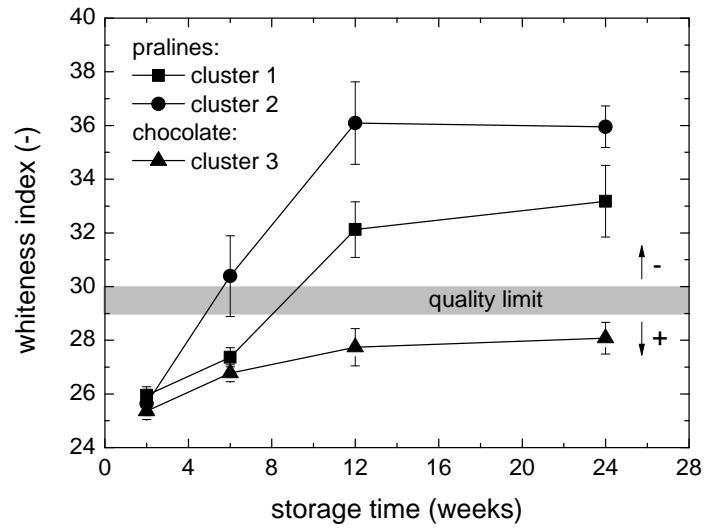


Figure 5.20.: Fat bloom evaluation by *DigiEye* technique based on whiteness indexing (L-a-b system); cluster 1:  $T_{\text{inf},3} < 18^\circ\text{C}$ , cluster 2:  $T_{\text{inf},3} > 18^\circ\text{C}$ , cluster 3: plain chocolate as reference.

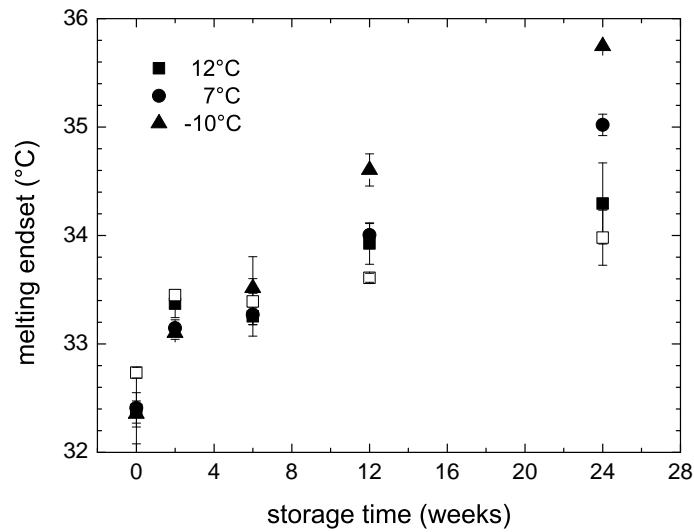


Figure 5.21.: Melting endset of the chocolate surface of pralines (solid symbols) and plain chocolate (open symbols) on storage as function of cooling temperature;  $T_{\text{stor}} = 23^\circ\text{C}$ ,  $v = 1 \text{ m/s}$ .



Melting behavior of chocolate shell (surface) and filling (core) mass was analyzed by DSC. In literature, fat bloom is linked to the formation of  $\beta^{VI}$  fat crystals at the surface (Cebula and Ziegler, 1993; Peschar *et al.*, 2004; Sonwai and Rousseau, 2008). As  $\beta^{VI}$  crystals exhibit a 2–3°C higher melting range compared to  $\beta^V$ , the melting endset temperature was used for the evaluation of  $\beta^{VI}$  crystals. In general a steady increase and a narrowing of the melting ranges were observed with storage time. The endset of seeded filling converged from 30.5°C to 33°C on storage independently of the cooling conditions (data not shown). The melting endset of the chocolate surface increased faster with decreasing cooling temperature (Fig. 5.21). It raised from 32.5°C to almost 36°C for strong cooling (−10°C, cluster 3). Overall, the migration of hazelnut oil enhanced the formation of high stable fat crystals compared to plain chocolate.

In general, there is a correlation of melting endset of the chocolate surface and fat bloom development evaluated by the whiteness indexing (Fig. 5.22). In average (linear trend), unacceptable fat bloom development corresponded to a melting endset of approximately 34°C. However, the scattering along the trendline is rather strong ( $R^2 = 0.746$ ). Furthermore, the sample quantity for DSC analysis is very small (<10 mg). Representative sampling of the chocolate surface is therefore difficult. It can only be improved by multiple repetition of analysis. Evaluation of fat bloom by DSC analysis only is therefore not recommended.

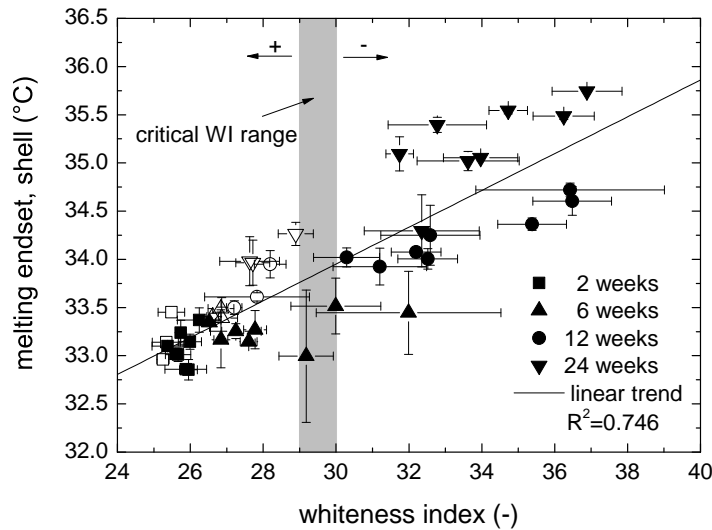


Figure 5.22.: Correlation of chocolate melting endset to whiteness index (fat bloom scale) of pralines (solid symbols, all cooling parameters) and plain chocolate (open symbols) on storage (23°C).

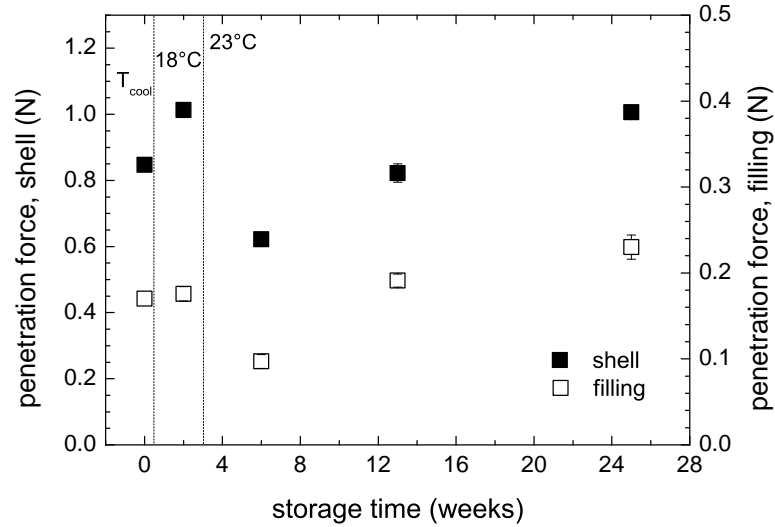


Figure 5.23.: Needle penetration force of chocolate shell and hazelnut filling on long-term storage;  $T_{\text{cool}} = 12^{\circ}\text{C}$ ,  $v_{\text{air}} = 1 \text{ m/s}$ .

The hardness of the chocolate shell was increased in the first two weeks of storage by post-crystallization (Fig. 5.23). The texture of both masses was softened due to the increase of the final storage temperature from  $18^{\circ}\text{C}$  to  $23^{\circ}\text{C}$ . The texture developments of seeded masses after 6 weeks correlate well with the melting endset increase for both confectionery masses (chocolate: Fig. 5.24, filling: Fig. 5.25). This correlation is dependent on the precrystallization state. Non-seeded filling mass exhibits high endset values in relation to its hardness, that was exceptionally low (0.08 N) right after cooling compared to seeded filling (0.17 N) at the same cooling conditions (data not shown). It is concluded, that the reduced structure density (TA) and crystal quality (DSC) of the non-seeded filling after cooling enhances the crystallographic transformation process of the filling (endset and hardness increase, Fig. 5.25) compared to a seeded filling.

By confocal laser scanning microscopy the fractional nature of chocolate masses becomes visible (Fig. 5.26). The liquid fraction of the continuous fat phase is lucid green (fluorescence marker: *Bodipy*), while the solidified network is colored dark-green. Cocoa particles are red (*Texas Red*), but mostly covered by fat layers. The black, edged particles are sugar crystals, the main ingredient of chocolate. The general picture (B) was similar for all trials after post-crystallization (2 weeks at  $18^{\circ}\text{C}$ ). After six month of storage spherical, liquid fat inclusions were detected. They were visible in the chocolate shell close to the filling of all pralines (A, C). However, they were only detected close to the chocolate surface of heavily bloomed samples (D, cluster 3). It is assumed, that migrated oil is represented by theses inclusions. This would support

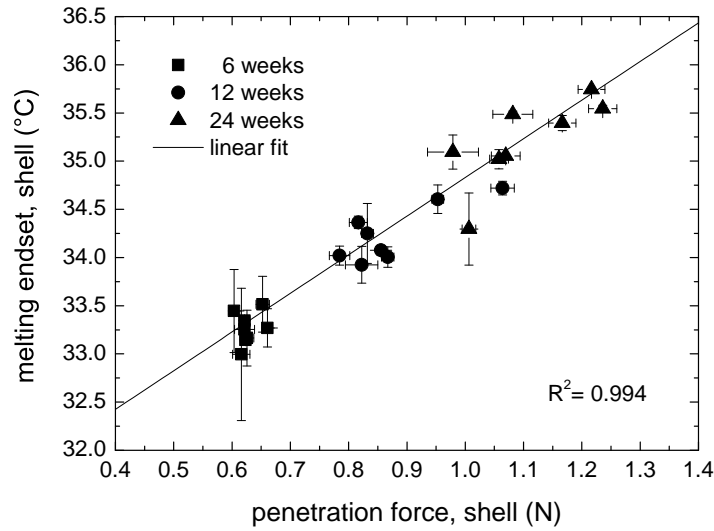


Figure 5.24.: Correlation of melting endset and penetration force for the chocolate praline shell during storage;  $T_{\text{stor}} = 23^\circ\text{C}$ .

the theory, that supercooling beyond a critical limit leads to a permanently reduced

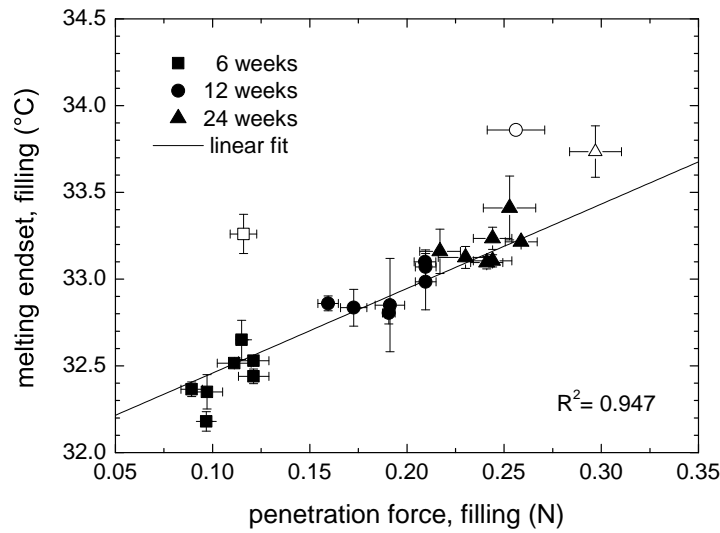


Figure 5.25.: Correlation of melting endset and penetration force for the praline filling during storage;  $T_{\text{stor}} = 23^\circ\text{C}$ ; solid symbols: seeded, open symbols: non-seeded.

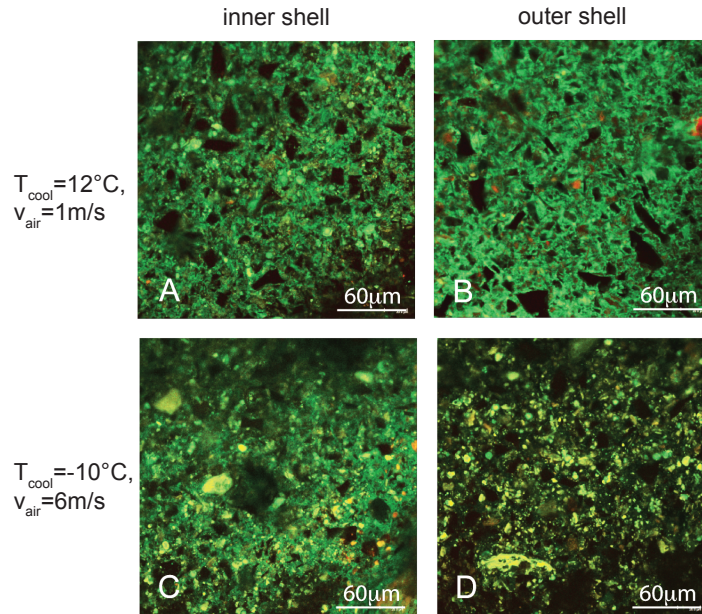


Figure 5.26.: CLSM micrographs of the dark chocolate shell of pralines at defined radial spots after 6 months of storage at 23°C, stained with *Bodipy* (green) and *Texas Red* (red).

structure density by nucleation of unstable fat crystals. The oil migration out of the filling, but also through the chocolate shell is thereby accelerated. However, oil inclusions were detected not before fat bloom has been developed. Hence, CLSM can be used on a qualitative basis for a bloomed product, but not as a predictive tool prior to any fat bloom development.

**Summary:** By analysis of real-time tempercurve data of filled confectionery, crystallization kinetics of both masses, but also the qualitative properties of the crystal network formed can be evaluated. It is a useful tool to screen cooling parameters for individual products. The minimal cooling time until detachment can be determined by the *DetachLog* system. Fat bloom analysis confirmed the hypothesis that cocoa butter based masses, crystallizing below the melting onset of  $\alpha$  crystals, developed fat bloom crystals faster and to a higher extent than at crystallization temperatures above this range. Hence, the praline trials are split into two different quality clusters (clusters 1, 2). Furthermore, the negative effect of hazelnut filling mass on overall fat bloom stability of a praline is strong by comparison to the reference quality of plain chocolate (cluster 3). Fat bloom development comes along with an increase in maximum melting temperature of the shell surface and is correlated to the hardness of the chocolate.

## 5.3. Seed Powder Processing

**Introduction:** The conventional way of chocolate tempering is performed by supercooling and partly re-melting of the whole chocolate mass to a final temperature around 29–32°C under low shear (Chap. 3.2.2). The alternative to this energy consuming process, high shear crystallization of pure cocoa butter generating a seed crystal suspension, was explained, applied and adapted for non-cocoa butter fat systems (Chap. 3.2.1, 4.2.1 and 4.2.2). A third option of chocolate precrystallization is the application of cocoa butter seed powders. The advantage of powder is the decoupling of seed production and final application resulting in more flexibility for a production line. Furthermore it is a simple, but reproducible method for hand made products in smaller batches, as produced by bakeries or professional confectioners. On the other hand, the homogeneous distribution of seed powder into molten chocolate is difficult. During the past 15 years spray chilling (*prilling*) of cocoa butter fat was investigated in the context of an optimization of chocolate precrystallization methods at the Laboratory of Food Process Engineering of ETH Zurich. Wagner (1997) performed experiments in the context of general studies on prilling of different food liquids. A pressure nozzle system was generally used. Temperature distribution over the spray tower height was in the range of –20°C to –50°C. Besides molten cocoa butter, precrystallized material (35°C) was also used. However, the precrystallization method was poor and of less quality than the bench-top temper method applied in Chapter 5.1. The powder out of non-seeded but also of precrystallized cocoa butter initially showed a mixture of  $\alpha$ ,  $\beta'$  and  $\beta^V$  crystals. The author did not explain the unexpected detection of  $\beta^V$  crystals, even though the feed material was not seeded in most cases. Transformation to highly thermally-stable forms was observed on subsequent storage. Powder flow properties degraded due to sintering effects at elevated storage temperatures.

Zeng (2000) picked up this topic and focused on the transformation kinetics on storage rather than varying process conditions. He finally proposed a controlled storage for 2–3 days at 11–13°C in order to enable the transformation process to the desired  $\beta^V$  structure while minimizing the sintering effect. Further, diffusion controlled transformation into the  $\beta^{VI}$  form could be achieved only at storage temperatures above 28°C. Therefore, the production of a cocoa butter powder with acceptable flow properties containing a significant fraction of stabilizing  $\beta^{VI}$  has not been realized so far.  $\beta^{VI}$  seed crystals showed an improved contraction behavior and product storage stability and would be therefore of advantage if present in seed powder. The industrial production of cocoa butter seed powder in the  $\beta^V$  only was developed separately by Uelzena AG (Uelzen, Germany) and Barry Callebaut (Zurich, Switzerland) and is commercially available.

**Approach:** In the present study the high shear crystallization concept and the prilling process were combined. By the use of a well defined cocoa butter seed suspension as starting material for prilling, the seed effect on main crystallization at extreme conditions ( $T_{cryst} \ll 0^\circ\text{C}$ ,  $d_{max} < 500\ \mu\text{m}$ ) was tested. The goal was to achieve a high stable powder ( $\beta^V/\beta^{VI}$ ) directly after production. If successful, the sintering effect on storage can be avoided, because the powder melting range is well above regular storage temperatures of confectionery products. Non-seeded cocoa butter was also prilled as a reference. A two-component jet system was used to decouple product flow rate and atomization energy (Chap. 3.2.5). The effect of main process parameters (cooling temperature, product flow rate, dispersing air pressure) were investigated with respect to polymorphic quality and powder particle size distribution.

**Results:** Prilling of non-seeded cocoa butter resulted in an unstable mixture of  $\alpha$  and  $III$  crystals, as expected. Crystals transformed into the  $\beta^V$  form via  $\beta'$  within one week of storage at  $10^\circ\text{C}$  (Fig. 5.27). In contrast, prilling of the concentrated seed suspension ( $c_{seed} = 10\%$ ) led to a  $\beta^V/\beta^{VI}$  mixture ( $\approx 80 : 20$  by melting enthalpy), that was stable in this conformation for at least one month of storage (Fig. 5.28). The difference in  $\beta$  quality was confirmed by XRD analysis after long-term storage (Fig. 5.29)..

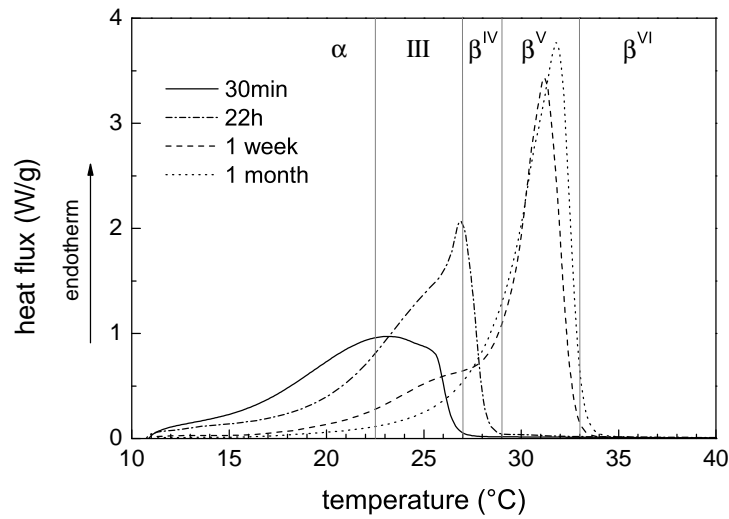


Figure 5.27.: Powder melting characteristics chilled of non-seeded cocoa butter;  $T_{cool} = -30^\circ\text{C}$ ,  $p = 2\text{ bar}$ ,  $\dot{V} = 180\text{ ml/min}$ .

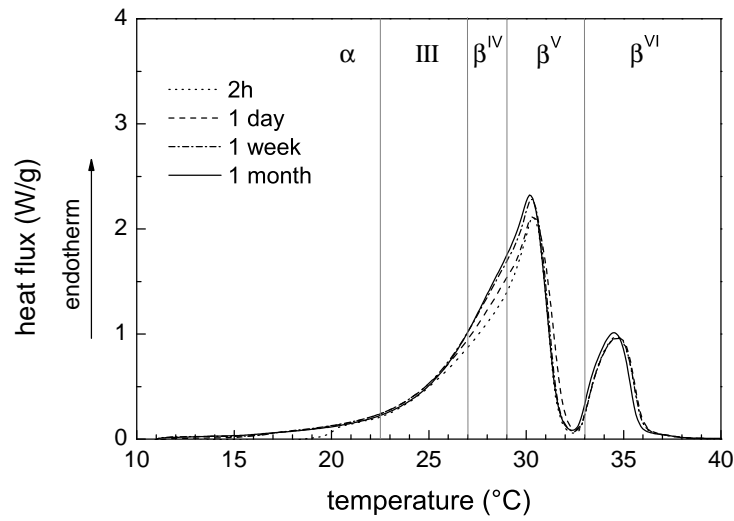


Figure 5.28.: Melting characteristics of cocoa butter powder out of seed suspension;  $T_{cool} = -30^{\circ}\text{C}$ ,  $p = 2 \text{ bar}$ ,  $\dot{V} = 180 \text{ ml/min}$ .

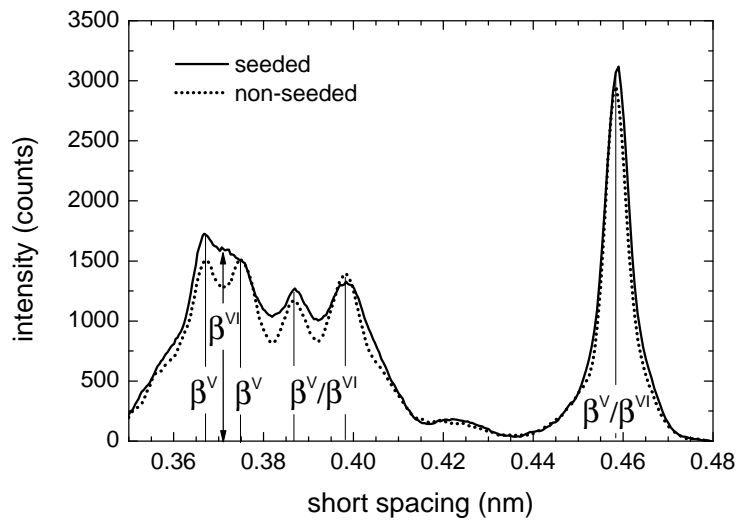


Figure 5.29.: X-ray powder diffraction pattern of prilled cocoa butter out of a seeded (solid) and an non-seeded state (dots) after one month of storage at  $10^{\circ}\text{C}$ .

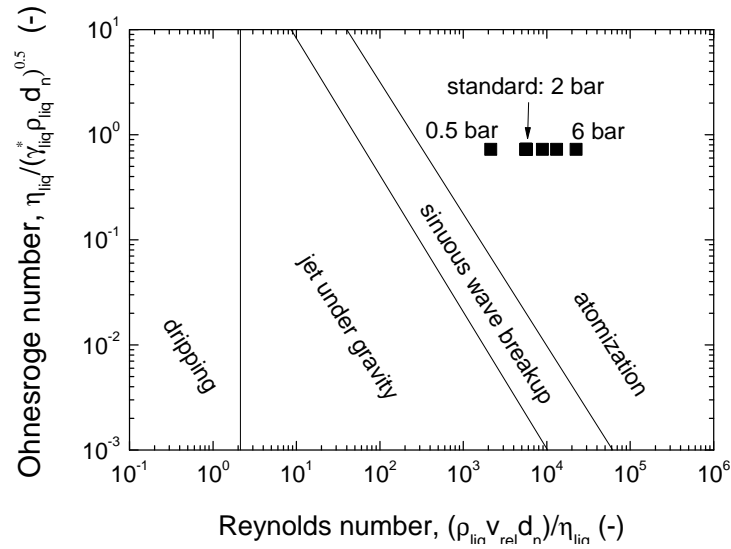


Figure 5.30.: Classification of the breakup mechanism of cocoa butter seed suspension by variation of dispersing pressure according to Ohnesorge (1936).

According to the breakup categories by Ohnesorge (1936), prilling was performed in the atomization process range only (Fig. 5.30). As the Ohnesorge number of a Newtonian fluid is solely a function of its physical parameters, variation of process parameter effecting the Reynolds number leads to a horizontal shift only assuming Newtonian behavior for the corresponding high shear rates in the nozzle. The apparent horizontal spread was achieved by variation of dispersing air pressure. The effect of product flow rate variation on the Reynolds number was rather small, while the effect of cooling temperature variation could be neglected in this context. Standard parameter were defined to:  $T_{cool} = -30^\circ\text{C}$ ,  $\dot{V}_{feed} = 180 \text{ ml/min}$ ,  $p_{air} = 2 \text{ bar}$  (S1, Appendix: Tab. B.10).

Variation of cooling temperature ( $-10^\circ\text{C}$  to  $-70^\circ\text{C}$ ) did not influence polymorphic quality of the bulk material (data not shown). This fact highlights the strong seeding effect of the concentrated crystal suspension. By analysis of mass specific melting energy, a general post crystallization was determined during storage (Fig. 5.31). For  $T_{cool} = -10^\circ\text{C}$ ,  $-20^\circ\text{C}$  the residence time of free fall in the tower was insufficient for a complete solidification. The specific melting energy was therefore reduced and an enhanced post-crystallization of 8 % (by melting energy) and 5.5 % respectively was observed during the first week of storage. For non-seeded cocoa butter sprayed at  $-30^\circ\text{C}$ , post crystallization was even more pronounced (19 %). However, not only an incomplete crystallization due to slow crystallization kinetics but also the reduced, specific melting enthalpy of unstable crystals may have contributed to the low specific melting enthalpy ( $< 130 \text{ J/g}$ ). The high value after one month of storage ( $< 160 \text{ J/g}$ ) was based on an increased solid fat content compared to the suspension sprayed



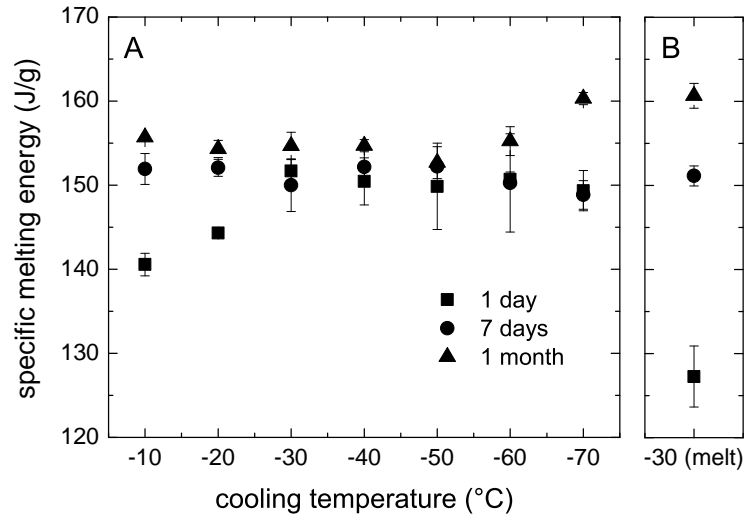


Figure 5.31.: Melting enthalpy development of cocoa butter seed powder stored at 10°C for one month analyzed by DSC; A: seeded, B: non-seeded,  $SFC(1 \text{ month} = 0.88 \pm 0.005$ .

powders ( $SFC_{\text{non-seeded}} = 0.915 > 0.88 = SFC_{\text{seeded}}$ ).

Results of particle size analysis show a minor reduction of the coarse fraction after long-term storage (Fig. 5.32). As there was generally post crystallization observed on storage, it is assumed, that mechanical de-agglomeration in methanol during sample preparation for particle size determination was hindered by the presence of a bigger fraction of liquid fat films for high cooling temperatures compared to stored products. Aside from this, the risk of water condensation during product transfer from the tower into the storage containers increased with decreasing cooling temperature. This might be the reason for the increase of the coarse particle sizes for very low cooling temperatures. Condensating water at the container lids during storage was generally observed.

Keeping the feed stream constant the effect of dispersing air pressure is shown in Figure 5.33 ( $p_{\text{max}}/p_{\text{min}} = 12$ ). Absolute particle size distribution (PSD) is most effectively reduced up to a medium pressure of  $p = 3$  bar. Overall,  $x_{90,3}$  was decreased from 650  $\mu\text{m}$  to 150  $\mu\text{m}$  while corresponding span (Eqn. 3.21) ranged from 2.80 to 2.05. The pressure-PSD correlation is of negative exponential nature.

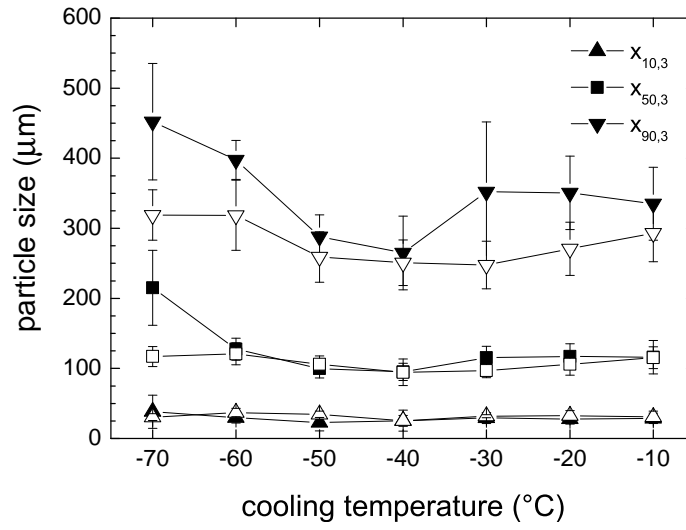


Figure 5.32.: Particle size distribution of cocoa butter powder by variation of cooling temperature;  $p = 2$  bar,  $\dot{V} = 180$  ml/min, solid symbols: 1 day storage, open symbols: 1 month storage.

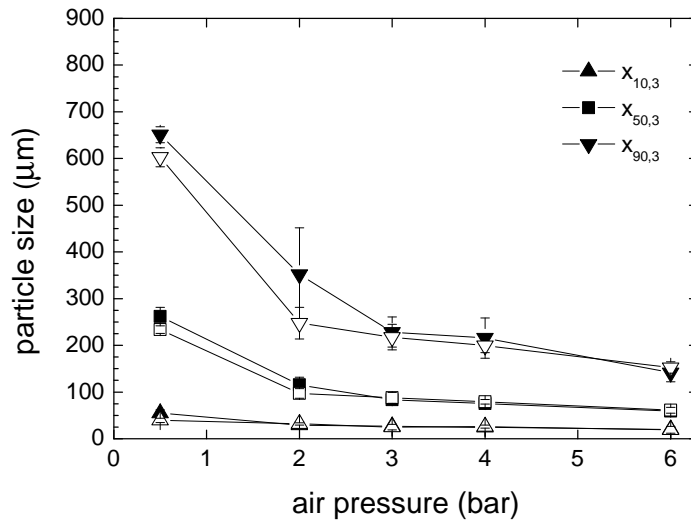


Figure 5.33.: Particle size distribution of cocoa butter powder by variation of air pressure;  $T = -30$  °C,  $\dot{V} = 180$  ml/min, solid symbols: 1 day storage, open symbols: 1 month storage.

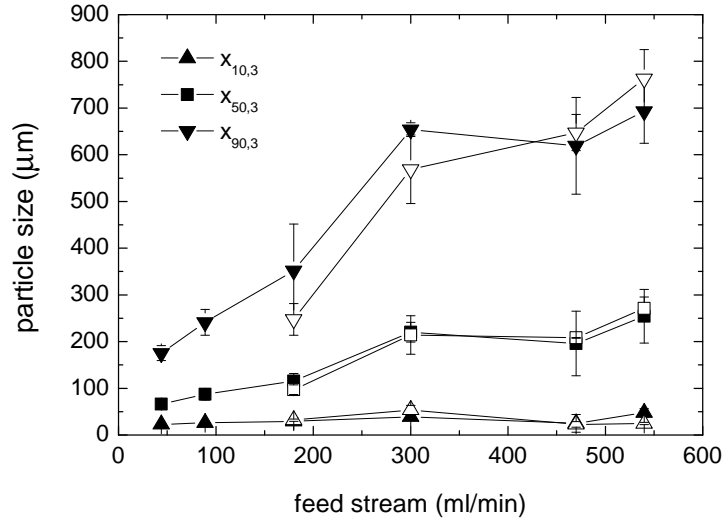


Figure 5.34.: Particle size distribution of cocoa butter powder by variation of feed stream;  $T = -30^{\circ}\text{C}$ ,  $p = 2\text{ bar}$ , solid symbols: 1 day storage, open symbols: 1 month storage.

Finally the volume flow rate of cocoa butter feed was varied from 45 ml/min to 540 ml/min ( $\dot{V}_{max}/\dot{V}_{min} = 12$ ). Minimal and maximal PSD parameters were similar to the ranges of air pressure variation (Fig. 5.34). The span was reduced from 3.0 to 2.3. Based on the data, a linear correlation of PSD to feed flow rate is feasible ( $R^2 < 0.89$ ).

Several correlations of material properties or dimensionless numbers exist to the mean or the sauter diameter of sprayed liquids (Gramlich *et al.*, 2011; Lefebvre, 1989; Schroeder *et al.*, 2012; Walzel, 1990, 2011). However, the corresponding fit functions are mainly empirical driven and linked to specific boundary conditions. A comprehensive prediction of a PSD for a given liquid system and a selected atomizer is therefore not possible so far. Since the mechanism of seed slurry jets and droplets was not in the focus of the present work, this was not further investigated.

In contrast to the needle-like clustered structure of crystals for static growth (Marangoni, 2003; Narine and Marangoni, 1999b), the morphology of powder particles is dominated by spherical or streamlined geometries and smooth surfaces throughout the different PSD ranges (Fig. 5.35). This reflects the typical atomization process particle shape and an immediate solidification of the liquid after dispersion (Wagner, 1997).

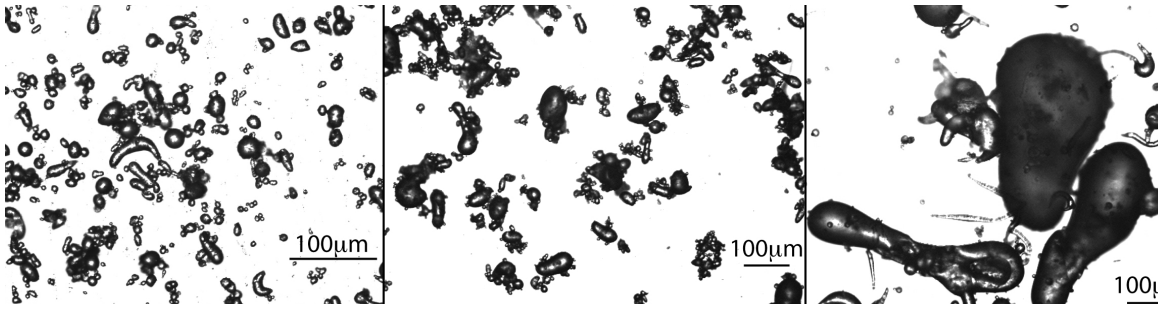


Figure 5.35.: Light microscopy images of cocoa butter seed powder; A: 6 bar, B: 2 bar, C: 0.5 bar,  $\dot{V}_{\text{feed}} = 180 \text{ ml/min}$ ,  $T_{\text{cool}} = -30^\circ\text{C}$ .



Figure 5.36.: Prilled cocoa butter seed powder by variation of atomizing air pressure; left -  $p = 6 \text{ bar}$  ( $x_{90,3} = 150 \mu\text{m}$ ), right -  $p = 0.5 \text{ bar}$  ( $x_{90,3} = 650 \mu\text{m}$ ).

For characterization of seed powder flow behavior the products with smallest and biggest particle sizes were selected (Fig. 5.36) in addition to the standard powder *S1* (Appendix, Tab. B.10). The ratio of consolidation stress to yield strength ( $ff_c$ ) is typically used for determination of powder flowability based. Results are listed in Table 5.1 and show very cohesive properties for the finest and the medium sized powder ( $1 < ff_c < 2$ ) and a less cohesive characteristic for the most coarse powder ( $2 < ff_c < 4$ ). Overall the first impressions by manual handling of the powders were confirmed. Bigger particle sizes improve the flowability. But even at  $10^\circ\text{C}$  the fat particles show mostly strong cohesion. Since the fat particles are deformable and will partly remelt under pressure, storage in bigger volumes is not supposed to improve the flow property as for other materials (Schulze, 2008).

**Application:** A test application was performed for practical verification and comparison of the concept of  $\beta^V/\beta^{VI}$  powder seeding to the regular tempering process. A commercially available, dark chocolate ( $c_{\text{fat}} = 33\%$ ) was used.

Table 5.1.: Results of seed powder analysis on flowability by  $ff_c$  determination after ten weeks of storage at 10°C, consolidation stress  $\sigma_n = 2000$  Pa.

trial	particle size distribution			ff <sub>c</sub> values	
no.	$x_{10,3}$	$x_{50,3}$	$x_{90,3}$	mean	SD
	$\mu m$	$\mu m$	$\mu m$	-	-
S13	19	61	153	1.21	0.13
S1	31	96	248	1.36	0.16
S9	24	271	763	3.5	0.1

Seed concentration was adjusted according to the temper curve analysis, resulting in 0.8 % ( $SFC_{\text{powder}}=0.88$ ) by mass mixed into the molten chocolate annealed to 31°C (Fig. 5.37). Taking the corresponding powder melting range into account, a total seed crystal concentration of  $c_{\text{crystal}} = 0.18$  % (mainly  $\beta^{VI}$ ) was applied, which is in good agreement with findings of Wagner (1997) for cocoa butter powder seeding of dark chocolate. Tempercurve slope values ( $s_{\text{target}} = 0^\circ\text{C}/\text{min}$ ) of seeded ( $0.2^\circ\text{C}/\text{min}$ ) and tempered chocolate ( $0.24^\circ\text{C}/\text{min}$ ) were of good quality and consistent. Inflection point temperature was decreased for the powder seeded product by  $0.65^\circ\text{C}$  implying a less optimal precrystallization state by practical experience. Nonetheless, the powder seeding effect is obvious in direct comparison to the temperature progression of non-seeded chocolate (Fig. 5.37). The seed was stable, as indicated by repetitive temper curve analysis after tablet moulding.

Chocolate tablets were cooled at  $14^\circ\text{C}$  for 30 min and stored in a cabinet at  $18^\circ\text{C}$ . The demoulding ability after cooling was good for tempered and seeded masses and bad for non-seeded. Surface gloss was very good for regular tempered (Fig. 5.38 A-top), good for seeded (B-top) and bad (C-top) for non-seeded chocolate. Strong fat bloom development of the non-seeded samples was observed on storage within 15 days while the quality of the seeded chocolate was constant. Even after 9 months of storage (3 months at  $18^\circ\text{C}$ , 3.-9. month at  $10^\circ\text{C}$ ) there was no degradation of quality visible by naked eye (not shown).

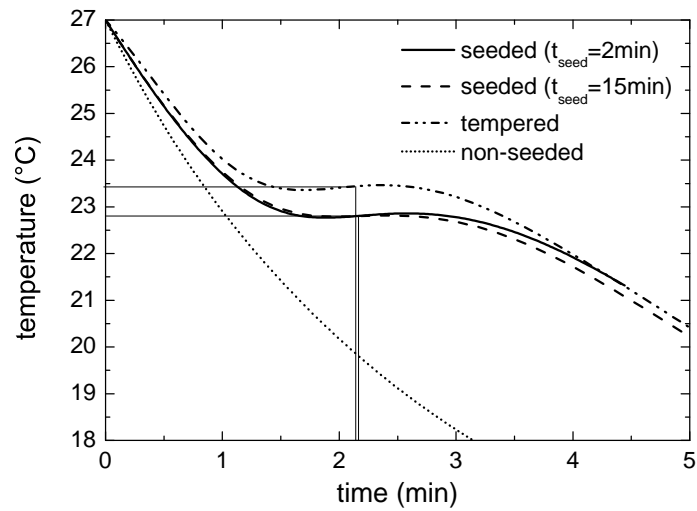


Figure 5.37.: Tempercurve development of seeded, tempered and non-seeded dark chocolate, stability of powder seeded batch indicated by double measurement.

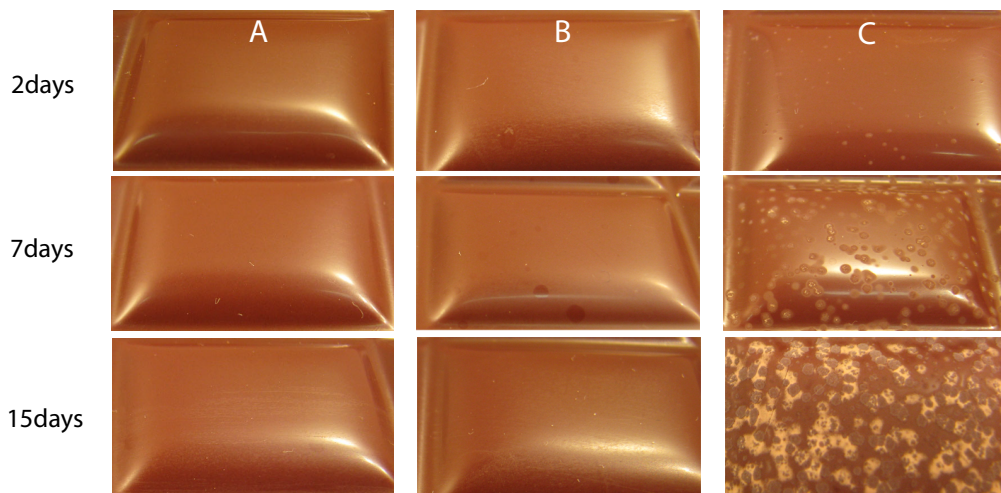


Figure 5.38.: Fat bloom development on seeded (A), conventionally tempered (B) and non-seeded (C) dark chocolate by digital imaging.

**Summary:** Prilling of highly concentrated cocoa butter seed suspension results in a  $\beta$  stable crystalline powder. The  $\beta^{VI}$  fraction depends on its initial concentration in the seed suspension. The powder can be used for precrystallization of cocoa butter based, confectionery masses. The process parameters of a pneumatic nozzle system can be adjusted to the required particle size distribution. The PSD mean values are significantly reduced with increasing, dispersing pressure and/or decreasing feed flow rate. Cocoa butter particles below  $200\mu\text{m}$  ( $x_{50,3} = 60\mu\text{m}$ ) can be produced at low pressure ( $<10\text{bar}$ ). Cooling conditions around  $-40^\circ\text{C}$  seem optimal from a crystallization kinetics point of view. The powder shows strong cohesion behavior, when stored in big containers, and has to be handled with care to maintain its flowability. Based on the strong seed potential of concentrated seed suspension we derive the following hypothesis: Proper  $\beta^V$  crystallization during rapid cooling can be achieved by excessive seeding (over-seeding). However, for moulded confectionery products a sufficient contraction ability and the initial surface gloss have to be maintained, so that a limiting, maximum seed concentration might be also given.





## 6. Conclusions

Precrystallization is generally performed for chocolate manufacturing (cocoa butter) by traditional tempering as well as novel seeding applications. By transfer of the seeding concept to non-cocoa butter fats, polymorphic but also kinetic and macro-structural improvements were determined. Lauric and palm fats as well as cocoa butter were successfully analyzed during crystallization out of a non-seeded as well as seeded state.

Seed material was produced individually from each fat type by high-shear crystallization and subsequent temperature induced ripening. Crystallographic investigations on the moment of crystal nucleation at high-shear conditions as well as during the ripening phase were realized by a rheometer *Searle* geometry in combination with synchrotron radiation. The nucleation time is significantly reduced with increasing shear rate. Lauric fats show short nucleation times compared to palm fats. Depending on supercooling temperature and fat type,  $\alpha$ ,  $\beta'$  or even  $\beta$  nucleation is observed. Only for unfractionated palm and palm stearin fats,  $\beta$  forms exist as for cocoa butter. This molecular alignment is most efficiently achieved by temperature driven transformation out of lower stable forms. All other fats (cocos, palm kernel, palm kernel stearin, Laurina, palm mid fraction) are  $\beta'$  stable. Especially for palm stearin  $\beta$  forms, but also for palm mid  $\beta'$  forms subcell modifications are evident within its main subcell structure reflecting action of fractional, polymorphic purification.

For general classification of the crystallization kinetics of fats, the Avrami model was successfully fitted to NMR-data of non-seeded samples. Mostly, one dimensional, single-stage crystal growth is concluded. The probability of nuclei growth is higher with increasing supercooling temperature difference. Palm mid fat (generally) and cocoa butter (for low supercooling) show a double-stage crystallization. The same effect can be observed by combined rheological and x-ray scattering analysis (XRS). A separation of the  $\alpha$  nucleation and the  $\beta'$  crystal growth with an intermediate polymorphic transformation process is thereby detected.

By application of fat specific seed material, the nucleation lag phase is generally erased. Furthermore, final SFC of  $\beta$  stable fats is lower than in the non-seeded case (e.g. palm *super* stearin, cocoa butter) concerning the short-term quasi-equilibrium state (1<sup>st</sup> hour of solidification). On a long term, partial remelting and transformation of non-seeded fat crystals into the highest stable form reduces the SFC reaching

the stable value of the corresponding seeded sample. The double-stage character of cocoa butter at high cooling temperatures was avoided, as direct  $\beta$  crystallization was induced by the presence of the seed crystals. The boundary conditions of the Avrami model are not valid for solidification out of a seeded state. However, fitting is still possible from a mathematical point of view. Thereby a representative crystal growth factor was defined. By normalization to the final SFC, a linear master curve is achieved for relative crystal growth as a function of supercooling temperature difference. This is valid for non-seeded as well as seeded samples as long as the subcell structure during main crystal growth represents the highest stable form of the individual fat. In return, the normalized growth value of non-seeded fats is reduced, if generally a  $\beta$  stability exists but  $\beta'$  crystal growth is predominant. In this case, the actual supercooling temperature difference for  $\beta'$  is reduced compared to the stated one based on the  $\beta$  form, whereby crystal growth is decelerated. Cocoa butter does not match the master curve for unknown reasons, while the polymorphic seed effect is clearly stated by enhanced kinetics.

Besides time-resolved crystallization analysis by NMR, rheological and XRS techniques, dynamic contraction was analyzed using a normal force controlled rheometer device with a plate/plate geometry. The contraction progress during steady cooling is generally consistent with the SFC development of corresponding NMR measurements including double-stage crystallization. In general, contraction ability is a function of SFC. Nonetheless, the correlation details are fat specific and contraction is improved by seeding. Even though, the individual contraction increase for cocoa butter by seeding seems rather small, the detachment of seeded chocolate is improved. Besides the positive effect on absolute contraction, seeding also accelerates and homogenizes (single-stage crystallization) the contraction kinetics compared to non-seeded cocoa butter. It is concluded, that not solely the absolute contraction ability, but also the kinetic of this process and the macrostructural matrix of the crystal network forming have an impact on the final structure density.

The crystallization characteristics of cocoa butter (polymorphism, kinetic, contraction, storage stability) determined on lab scale devices are also representative for realistic cooling conditions by convective cooling. The crystallization behavior of fat based product can be monitored online by temperature and detachment sensors. The crystallization kinetics and the contraction ability are reduced for a hazelnut filling mass of a praline in relation to the chocolate shell layer. Cooling time reduction is a matter of optimized heat transfer by preservation of product quality. In this context, the installation of controlled air flow velocities (heat transfer coefficient) in direct contact with the product is of importance. The product quality is less negatively effected by controlled regulation of the heat transfer coefficient by air flow speed compared to an ordinary reduction of the cooling temperature. For cocoa butter based masses, the main crystallization temperature should stay above 18°C. Otherwise, nucleation

---

of less dense, unstable  $\alpha$  crystals is enabled. In solid chocolate bars or tablets, the polymorphic transformation process at the products surface is enhanced. In pralines, there it leads to an enhanced potential of oil migration from the filling center to the chocolate shell surface. Both actions lead to fat bloom development. Furthermore, the formation of unstable crystals results in reduced volume contraction and thereby in poor mould detachment.

Fat bloom development is generally correlated with an increase of maximal melting temperature (DSC) and hardening of the chocolate surface (needle penetration). Confocal laser scanning microscopy is a supplementary tool for the visualization of the migration phenomenon but so far not helpful for quantitative evidence.

By application of seed powder instead of temperature sensitive seed suspension, confectioners and small enterprises can also profit from the seeding concept, since the acquisition costs of a tempering or a suspension seeding device are very high. By prilling of highly concentrated seed suspensions, the seed powder can be enriched with  $\beta^{VI}$  crystals up to 20 %. Furthermore this powder shows pure  $\beta$  quality ( $\beta^V + \beta^{VI}$ ) directly after production and does not have to be stored at controlled conditions to induce the polymorphic transformation process from unstable to stable crystals after processing as done so far.

The particle size distribution (PSD) of the powder is generally a function of the seed suspension viscosity and its surface tension for constant process boundary conditions. It can be varied by the pressure of dispersing air and/or the feed flow rate of a pneumatic nozzle system. A mean particle size of 60  $\mu\text{m}$  (span: 2,05) was achieved at a dispersing pressure of 6 bar. Further reduction of the PSD seems possible by combination of both parameter extremes. Overall production rate can be increased by injection with a multiple set of spray nozzles. The quality and stability of a powder seeded chocolate bar is comparable to that of a conventional tempered mass.

In summary, not only for chocolate, but also for non-cocoa butter filling masses, the application of a seed suspension is beneficial for the homogenization of a fat crystal network forming during the cooling process. It also improves the contraction behavior and reduces the required cooling time as it effects the crystallization kinetics.



# Bibliography

- AOCS: *AOCS Official Method Cd 16-81: Solid Fat Content (SFC) by Low-Resolution Nuclear Magnetic Resonance, the indirect method*. American Oil Chemists' Society, 1999a.
- AOCS: *AOCS Official Method Cd 16b-93: Solid Fat Content (SFC) by Low-Resolution Nuclear Magnetic Resonance, the direct method*. American Oil Chemists' Society, 1999b.
- Arishima, T. and K. Sato: *Polymorphism of POP and SOS: 3. Solvent crystallization of beta-2-poymorphs and beta-1-polymorphs*. Journal of the American Oil Chemists' Society, 66(11):1614–1617, 1989.
- Arishima, T., N. Sagi, H. Mori, and Sato K.: *Density Measurements of the Polymorphic Forms of POP, POS and SOS*. Journal of Japan Oil Chemists' Society, 44:15–21, 1995.
- Avrami, M: *Kinetics of phase change i - General theory*. Journal of Chemical Physics, 7(12):1103–1112, 1939.
- Avrami, M: *Kinetics of phase change II - Transformation-time relations for random distribution of nuclei*. Journal of Chemical Physics, 8:212–224, 1940.
- Beckett, S.T. (editor): *Industrial Chocolate Manufacturer and Use*. Wiley-Blackwell, Oxford, 4th edition, 2009.
- Berg, T.G.O. and U.I. Brimberg: *Kinetics of fat crystallization*. Fette Seifen Anstrichmittel, 85(4):142–149, 1983.
- Bezard, J.A.: *Component triglycerides of palm-kernel oil*. Lipids, 6(9):630–634, 1971.
- Bolliger, S., B. Breitschuh, M. Stranzinger, T. Wagner, and E. J. Windhab: *Comparison of precrystallization of chocolate*. Journal of Food Engineering, 35(3):281–297, 1998.
- Braipson-Danthine, Sabine and Veronique Gibon: *Comparative analysis of triacylglycerol composition, melting properties and polymorphic behavior of palm oil and fractions*. European Journal of Lipid Science and Technology, 109(4):359–372, 2007.

- Buckle, E.R.: *Studies on freezing of pure liquids: 2. Kinetics of homogeneous nucleation in supercooled liquids*. Proceedings of the Royal Society of London Series A - Mathematical and Physical Sciences, 261(1305):189–196, 1961.
- Calliauw, G, I Foubert, W De Greyt, P Dijckmans, M Kellens, and K Dewettinck: *Production of cocoa butter substitutes via two-stage static fractionation of palm kernel oil*. Journal of the American Oil Chemists Society, 82(11):783–789, 2005.
- Cebula, D. J. and G. Ziegleder: *Studies of bloom formation using x-ray-diffraction from chocolates after long-term storage*. Fett Wissenschaft Technologie - Fat Science Technology, 95(9):340–343, 1993.
- Chaiseri, S and P. S. Dimick: *Lipid and hardness characteristics of cocoa butters from different geographic regions*. Journal of the American Oil Chemists Society, 66(12):1771–1776, 1989.
- Chawla, P. and J. M. Deman: *Measurement of the size distribution of fat crystals using a laser particle counter*. Journal of the American Oil Chemists Society, 67(5):329–332, 1990.
- Che Man, Y. B., T. Haryati, H. M. Ghazali, and B. A. Asbi: *Composition and thermal profile of crude palm oil and its products*. Journal of the American Oil Chemists Society, 76(2):237–242, 1999.
- Christian, J.W. (editor): *The theory of transformations in metals and alloys*. Elsevier Science Ltd., 3rd edition, 2002.
- De Graef, V., I. Foubert, K. W. Smith, F. W. Cain, and K. Dewettinck: *Crystallization behavior and texture of trans-containing and trans-free palm oil based confectionery fats*. Journal of Agricultural and Food Chemistry, 55(25):10258–10265, 2007.
- De Graef, V., B. Goderis, P. Van Puyvelde, I. Foubert, and K. Dewettinck: *Development of a rheological method to characterize palm oil crystallizing under shear*. European Journal of Lipid Science and Technology, 110(6):521–529, 2008.
- De Graef, V., P. van Puyvelde, B. Goderis, and K. Dewettinck: *Influence of shear flow on polymorphic behavior and microstructural development during palm oil crystallization*. European Journal of Lipid Science and Technology, 111(3):290–302, 2009.
- Deffense, E.: *Fractionation of palm oil*. Journal of the American Oil Chemists Society, 62(2):376–385, 1985.
- Dimick, P.S. and D.M. Manning: *Thermal and compositional properties of cocoa butter during static crystallization*. Journal of the American Oil Chemists' Society, 64(12):1663–1669, 1987.

- D'Souza, V., J. M. Deman, and L. Deman: *Short spacings and polymorphic forms of natural and commercial solid fats - a review*. Journal of the American Oil Chemists Society, 67(11):835–843, 1990.
- Foubert, I.: *Modelling isothermal cocoa butter crystallization: Influence of temperature and chemical composition*. PhD thesis, University of Gent, 2003.
- Foubert, I., P. Vanrolleghem, O. Thas, and K. Dewettinck: *Influence of chemical composition on the isothermal cocoa butter crystallization*. Journal of Food Science, 69(9):E478–E487, 2004.
- Franke, K.: *Modelling the cooling kinetics of chocolate coatings with respect to final product quality*. Journal of Food Engineering, 36(4):371–384, 1998.
- Fredrick, E., I. Foubert, J. Van De Sybe, and K. Dewettinck: *Influence of monoglycerides on the crystallization behavior of palm oil*. Crystal Growth & Design, 8(6):1833–1839, 2008.
- Galdamez, J.R., K. Szlachetka, J.L. Duda, and G.R. Ziegler: *Oil migration in chocolate: A case of non-fickian diffusion*. Journal of Food Engineering, 92(3):261–268, 2009.
- Garti, N. and K. Sato (editors): *Crystallization processes in fats and lipid systems*. Marcel Dekker, New York - Basel, 2001.
- Ghotra, B.S., S.D. Dyal, and S.S. Narine: *Lipid shortenings: a review*. Food Research International, 35(10):1015–1048, 2002.
- Gibon, V., F. Durant, and C. Deroanne: *Polymorphism and intersolubility of some palmitic, stearic and oleic triglycerides - PPP, PSP and POP*. Journal of the American Oil Chemists Society, 63(8):1047–1055, 1986.
- Goertzel, G.: *An algorithm for the evaluation of finite trigonometric series*. The American Mathematical Monthly, 65:34–35, 1958.
- Gordon, M. H. and I. A. Rahman: *Effects of minor components on the crystallization of coconut oil*. Journal of the American Oil Chemists Society, 68(8):577–579, 1991.
- Graf, M.: *Übertragung des konzepts der scherinduzierten impfvorkristallisation auf laurische fettsysteme*. Master's thesis, ETH Zurich, 2006.
- Gramlich, S., A. Mescher, M. Piesche, and P. Walzel: *Modelling and experimental investigation of the gas-induced breakup of liquid threads stretched by gravity*. Chemie Ingenieur Technik, 83(3):273–279, 2011.
- Gunstone, F.D. (editor): *Vegetable Oils in Food Technology*. Wiley-Blackwell, 2011.

- Guth, O. J., J. Aronhime, and N. Garti: *Polymorphic transitions of mixed triglycerides, SOS, in the presence of sorbitan monostearate*. Journal of the American Oil Chemists Society, 66(11):1606–1613, 1989.
- Hachiya, I, T Koyano, and K Sato: *Observation of seeding effects on fat bloom of dark chocolate*. Food Microstructure, 8(2):257–261, 1989.
- Hachiya, I., T. Koyano, and K. Sato: *Seeding effects on solidification behavior of cocoa butter and dark chocolate .1. kinetics of solidification*. Journal of the American Oil Chemists' Society, 66(12):1757–1762, 1989a.
- Hachiya, I., T. Koyano, and K. Sato: *Seeding effects on solidification behavior of cocoa butter and dark chocolate .2. physical-properties of dark chocolate*. Journal of the American Oil Chemists' Society, 66(12):1763–1770, 1989b.
- Hammond, C.: *The basics of crystallography and diffraction*. Oxford Science Publications, 3rd edition, 2009.
- Hannewijk, J., Haighton A.J., and Hendrikse P.W.: *Oils, Fats and Fat Products*, volume 1, chapter Dilatometry of Fats. John Wiley & Sons Ltd, Interscience Publishers, 1964.
- Heller, H.: *Kombi-technik: Giessmaschine und one-shot*. Zucker- und Süßwaren Wirtschaft, 6:170–172, 2000.
- Himawan, C., V. M. Starov, and A.G.F. Stapley: *Thermodynamic and kinetic aspects of fat crystallization*. Advances in Colloid and Interface Science, 122(1-3):3–33, 2006.
- Ibrahim, N.A., A. Kuntom, T.T. Sue, and Lin W.L.: *Current status of malaysian crude palm kernel oil characteristics*. Oil Palm Bulletin, 47:15–27, 2003.
- James, Bryony J. and Bronwen G. Smith: *Surface structure and composition of fresh and bloomed chocolate analysed using x-ray photoelectron spectroscopy, cryo-scanning electron microscopy and environmental scanning electron microscopy*. LWT - Food Science and Technology, 42(5):929–937, 2009.
- Jin, Qingzhe, Ting Zhang, Liang Shan, Yuanfa Liu, and Xingguo Wang: *Melting and solidification properties of palm kernel oil, tallow, and palm olein blends in the preparation of shortening*. Journal of the American Oil Chemists' Society Society, 85(1):23–28, 2008.
- Juul, B.: *Beat migration bloom by optimizing your process*. The Manufacturing Confectioner, pp. 68–75, 2010.
- Kawamura, K.: *DSC thermal-analysis of crystallization behavior in palm oil*. Journal of the American Oil Chemists' Society, 56(8):753–758, 1979.



- Kenny, J.M., A. Maffezzoli, and L. Nicolais: *A new kinetic-model for polymer crystallization derived by calorimetric analysis*. *Thermochimica Acta*, 227:83–95, 1993.
- Khanna, Y.P. and T.J. Taylor: *Comments and recommendations on the use of the AVRAMI-equation for physicochemical kinetics*. *Polymer Engineering and Science*, 28(16):1042–1045, 1988.
- Kloek, W, P Walstra, and T van Vliet: *Nucleation kinetics of emulsified triglyceride mixtures*. *Journal of the American Oil Chemists'*, 77(6):643–652, 2000.
- Koch, J.: *The natural rate of solidification of chocolate*. *Confectionery Production*, 39(2):67–70, 1973.
- Koyano, T., I. Hachiya, T. Arishima, K. Sato, and N. Sagi: *Polymorphism of POP and SOS: 2. Kinetics of melt crystallization*. *Journal of the American Oil Chemists Society*, 66(5):675–679, 1989.
- Koyano, T., I. Hachiya, and K. Sato: *Fat polymorphism and crystal seeding effects on fat bloom stability of dark chocolate*. *Food Structure*, 9(3):231–240, 1990.
- Langevelde, A. van, K. van Malssen, E. Sonneveld, R. Peschar, and H. Schenk: *Crystal packing of a homologous series beta'-stable triacylglycerols*. *Journal of the American Oil Chemists' Society*, 76(5):603–609, 1999.
- Langevelde, A. van, R. Driessen, W. Molleman, R. Peschar, and H. Schenk: *Cocoa-butter long spacings and the memory effect*. *Journal of the American Oil Chemists' Society*, 78(9):911–918, 2001a.
- Langevelde, A. van, K. Van Malssen, R. Peschar, and H. Schenk: *Effect of temperature on recrystallization behavior of cocoa butter*. *Journal of the American Oil Chemists' Society*, 78(9):919–925, 2001b.
- Larsson, K.: *Classification of glyceride crystal forms*. *Acta Chemica Scandinavica*, 20(8):2255–2260, 1966.
- Larsson, K.: *Molecular arrangement in glycerides*. *Fette Seifen Anstrichmittel Verbunden Mit Der Zeitschrift Die Ernährungsindustrie*, 74(3):136–142, 1972.
- Larsson, K.: *Lipids - Molecular organization, physical functions and technical applications*, chapter Lipid functionality in foods, pp. 173–212. Bell and Bain Ltd., 1994.
- Laureles, L. R., F. A. Rodriguez, C. E. Reano, G. A. Santos, A. C. Laurena, and E. M. T. Mendoza: *Variability in fatty acid and triacylglycerol composition of the oil of coconut (cocos nucifera l.) hybrids and their parentals*. *Journal of Agricultural and Food Chemistry*, 50(6):1581–1586, 2002.
- Lefebvre, A.H.: *Atomization and Sprays*. Hemisphere Publishing Corporation, 1989.

- Lorén, N.: *Understanding and controlling the microstructure of complex foods*, chapter Confocal fluorescence microscopy (CLSM) for food structure characterisation, pp. 233–260. Woodhead Publishing Limited and CRC Press LLC, 2007.
- Lovegren, N.V and R.O. Feuge: *Solidification of cocoa butter*. Journal of the American Oil Chemists' Society, 42(4):308–312, 1965.
- Lovegren, N.V., M.S. Gray, and R.O. Feuge: *Effect of liquid fat on melting-point and polymorphic behavior of cocoa butter and a cocoa butter fraction*. Journal of the American Oil Chemists' Society, 53(3):108–112, 1976.
- Lutton, E.S.: *Review of the polymorphism of saturated even glycerides*. Journal of the American Oil Chemists' Society, 27(7):276–281, 1950.
- MacMillan, S. D., K. J. Roberts, A. Rossi, M. A. Wells, M. C. Polgreen, and I. H. Smith: *In situ small angle X-ray scattering (SAXS) studies of polymorphism with the associated crystallization of cocoa butter fat using shearing conditions*. Crystal Growth & Design, 2(3):221–226, 2002.
- Maleky, F. and A. G. Marangoni: *Process development for continuous crystallization of fat under laminar shear*. Journal of Food Engineering, 89(4):399–407, 2008.
- Malssen, K. van: *Real-Time X-Ray Powder Diffraction Applied to Cocoa Butter and Graphite Intercalates*. PhD thesis, University van Amsterdam, The Netherlands, 1994.
- Malssen, K. van, R. Peschar, and H. Schenk: *Real-time x-ray powder diffraction investigations on cocoa butter. 1. temperature-dependent crystallization behavior*. Journal of the American Oil Chemists' Society, 73(10):1209–1215, 1996.
- Malssen, K. van, A. van Langevelde, R. Peschar, and H. Schenk: *Phase behavior and extended phase scheme of static cocoa butter investigated with real-time x-ray powder diffraction*. Journal of the American Oil Chemists' Society, 76(6):669–676, 1999.
- Mandelkern, L., F.A. Quinn, and P.J. Flory: *Crystallization kinetics in high polymers: 1. Bulk polymers*. Journal of Applied Physics, 25(7):830–839, 1954.
- Manning, D.M. and P.S. Dimick: *Crystal morphology of cocoa butter*. Food Microstructure, 4(2):249–265, 1985.
- Marangoni, AG: *On the use and misuse of the avrami equation in characterization of the kinetics of fat crystallization (vol 75, pg 1465, 1998)*. Journal of the American Oil Chemists' Society, 76(2):281–281, 1999.
- Marangoni, A.G.: *Relationship between crystallization behaviour and structure in cocoa butter*. Crystal Growth & Design, 3:95–108, 2003.

- Marangoni, A.G.: *Fat crystal network*, chapter Crystallization kinetics. Marcel Dekker, Inc., New York, 2005.
- Marangoni, A.G. and R.W. Hartel: *Visualization and structural analysis of fat crystal networks*. Food Technology, 52(9):46–51, 1998.
- Marangoni, A.G. and M. Ollivon: *Fractal character of triglyceride spherulites is a consequence of nucleation kinetics*. Chemical Physics Letters, 442(4-6):360–364, 2007.
- Mazzanti, G.: *Soft Materials - Structure and Dynamics*, chapter Crystallization of Bulk Fats under Shear. Marcel Dekker, 2005.
- Mazzanti, G., S. E. Guthrie, E. B. Sirota, A. G. Marangoni, and S. H. J. Idziak: *Orientation and phase transitions of fat crystals under shear*. Crystal Growth & Design, 3(5):721–725, 2003.
- Mazzanti, G., A. G. Marangoni, and S. H. J. Idziak: *Modeling phase transitions during the crystallization of a multicomponent fat under shear*. Physical Review E, 71(4):12, 2005.
- Mechelen, J.B. van, K. Goubitz, M. Pop, R. Peschar, and H. Schenk: *Structures of mono-unsaturated triacylglycerols. v. the beta '(1)-2, beta '-3 and beta(2)-3 polymorphs of 1,3-dilauroyl-2-oleoylglycerol (laola) from synchrotron and laboratory powder diffraction data*. Acta Crystallographica Section B - Structural Science, 64:771–779, 2008a.
- Mechelen, J.B. van, R. Peschar, and H. Schenk: *Structures of mono-unsaturated triacylglycerols. iv. the highest melting beta '-2 polymorphs of trans-mono-unsaturated triacylglycerols and related saturated tags and their polymorphic stability*. Acta Crystallographica Section B - Structural Science, 64:249–259, 2008b.
- Mechelen, J.B. van, R. Peschar, and H. Schenk: *Structures of mono-unsaturated triacylglycerols. II. The beta(2) polymorph*. Acta Crystallographica Section B - Structural Science, 62(Part 6):1131–1138, 2006.
- Mehrle, Y.: *Solidification and contraction of confectionary systems in rapid cooling processing*. PhD thesis, ETH Nr. 17442, Food Process Engineering, ETH Zurich, 2007.
- Minato, A, S Ueno, J Yano, K Smith, H Seto, Y Amemiya, and K Sato: *Thermal and structural properties of sn-1,3-dipalmitoyl-2-oleoylglycerol and sn-1,3-dioleoyl-2-palmitoylglycerol binary mixtures examined with synchrotron radiation x-ray diffraction*. Journal of the American Oil Chemists' Society Society, 74(10):1213–1220, 1997.

- Motwani, T., W. Hanselmann, and R.C. Anantheswaran: *Diffusion, counter-diffusion and lipid phase changes occurring during oil migration in model confectionery systems*. Journal of Food Engineering, 104(2):186–195, 2011.
- Narine, S. S. and A. G. Marangoni: *Mechanical and structural model of fractal networks of fat crystals at low deformations*. Physical Review E, 60(6):6991–7000, 1999a.
- Narine, S. S. and A. G. Marangoni: *Fractal nature of fat crystal networks*. Physical Review E, 59(2):1908–1920, 1999b.
- Narine, SS and AG Marangoni: *Relating structure of fat crystal networks to mechanical properties: a review*. Food Research International, 32(4):227–248, 1999c.
- Narine, SS and AG Marangoni: *Microscopic and rheological studies of fat crystal networks*. Journal of Crystal Growth, 198:1315–1319, 1999d.
- Nattress, L.A., G.R. Ziegler, R. Hollender, and D.G. Peterson: *Influence of hazelnut paste on the sensory properties and shelf-life of dark chocolate*. Journal of Sensory Studies, 19(2):133–148, 2004.
- Nopens, I., I. Foubert, V. De Graef, D. Van Laere, K. Dewettinck, and P. Vanrolleghem: *Automated image analysis tool for migration fat bloom evaluation of chocolate coated food products*. LWT-Food Science and Technology, 41(10):1884–1891, 2008.
- Ohnesorge, W.V.: *Die bildung von tropfen an düsen und die auflösung flüssiger strahlen*. ZAMM - Zeitschrift für Angewandte Mathematik und Mechanik, 16(6):355–358, 1936.
- Padar, S.: *Optimization of a Co-Injection Process for Confectionera Systems aided by Flow Simulation and Experiment*. PhD thesis, ETH Nr. 18381, Food Process Engineering, ETH Zurich, 2009.
- Padar, S., S. A. K. Jeelani, and E. J. Windhab: *Crystallization kinetics of cocoa fat systems: Experiments and modeling*. Journal of the American Oil Chemists’ Society, 85(12):1115–1126, 2008.
- Padar, S., Y. E. Mehrle, and E. J. Windhab: *Shear-induced crystal formation and transformation in cocoa butter*. Crystal Growth & Design, 9(9):4023–4031, 2009.
- Pantzaris, T.P. and Y. Basiron: *Vegetable Oils in Food Technology: Composition, Properties and Uses*, chapter The lauric oil (coconut and palmkernel) oils, pp. 157–202. Blackwell Publishing Ltd., Oxford, 2002.

- Peschar, R., MM Pop, DJA De Ridder, JB van Mechelen, RAJ Driessen, and H Schenk: *Crystal structures of 1,3-distearoyl-2-oleoylglycerol and cocoa butter in the beta(v) phase reveal the driving force behind the occurrence of fat bloom on chocolate*. Journal of Physical Chemistry B, 108(40):15450–15453, 2004.
- Reddy, SY, N Full, PS Dimick, and GR Ziegler: *Tempering method for chocolate containing milk-fat fractions*. Journal of the American Oil Chemists Society, 73(6): 723–727, 1996.
- Révérend, B.J.D. Le, P. J. Fryer, and S. Bakalis: *Modelling crystallization and melting kinetics of cocoa butter in chocolate and application to confectionery manufacturing*. Soft Matter, 5(4):891–902, 2009.
- Révérend, B.J.D. Le, B.J.D. Le, I. Smart, P.J. Fryer, and S. Bakalis: *Modelling the rapid cooling and casting of chocolate to predict phase behaviour*. Chemical Engineering Science, 66(6):1077–1086, 2010.
- Riiner, Ü.: *Investigation of the polymorphism of fats and oils by temperature programmed x-ray diffraction*. Lebensmittel-Wissenschaft und Technologie - Food Science and Technology, 3(6):101–106, 1970.
- Rohm, H., B. Böhme, and G. Ziegler: *Haltbarkeit von One-Shot-Pralinen - Einfluss von Füllungsart und Füllungsviskosität*. Süßwaren, 4, 2007.
- Rohm H., Böhme B., Ziegler G.: *Haltbarkeit von One-Shot-Pralinen - Einfluss von Füllungsart und Füllungsviskosität*. Süßwaren, 9:13–15, 2005.
- Rohsius, C, S. Elwers, and R. Lieberei: *Cocoa atlas*. Technical report, German Cocoa and Chocolate Foundation, Hamburg/Bonn, 2010.
- Rousseau, D.: *Understanding and controlling the microstructure of complex foods*, chapter The microstructure of chocolate, pp. 233–260. Woodhead Publishing Limited and CRC Press LLC, 2007.
- Rousset, P.: *Physical Properties of Lipids*, chapter Modeling Crystallization Kinetics of Triacylglycerols. Marcel Dekker, 2002.
- Sato, K.: *Crystallization behaviour of fats and lipids - a review*. Chemical Engineering Science, 56(7):2255–2265, 2001.
- Sato, K., T. Arishima, Z.H. Wang, K. Ojima, N. Sagi, and H. Mori: *Polymorphism of pop and sos .1. occurrence and polymorphic transformation*. Journal of the American Oil Chemists Society, 66(5):664–674, 1989.
- Schanda, János (editor): *Colorimetry: Understanding the CIE System*. John Wiley & Sons, Inc., 2007.

- Schantz, B. and L. Linke: *Messmethoden für Erstarrung und Kontraktion*. Zucker- und Süßwaren Wirtschaft, (12):15–17, 2001.
- Schroeder, Jewe, Agnes Kleinhans, Yvonne Serfert, Stephan Drusch, Heike P. Schuchmann, and Volker Gaukel: *Viscosity ratio: A key factor for control of oil drop size distribution in effervescent atomization of oil-in-water emulsions*. Journal of Food Engineering, 111(2):265–271, 2012.
- Schulze, D.: *Powders and Bulk Solids*. Springer-Verlag Berlin Heidelberg, 2008.
- Sharples, A.: *Introduction to Polymer Crystallization*. Edward Arnold Ltd., London, 1966.
- Sonoda, T., Y. Takata, S. Ueno, and K. Sato: *Dsc and synchrotron-radiation x-ray diffraction studies on crystallization and polymorphic behavior of palm stearin in bulk and oil-in-water emulsion states*. Journal of the American Oil Chemists' Society Society, 81(4):365–373, 2004.
- Sonwai, S. and M. R. Mackley: *The effect of shear on the crystallization of cocoa butter*. Journal of the American Oil Chemists' Society, 83(7):583–596, 2006.
- Sonwai, Sopark and Derick Rousseau: *Structure evolution and bloom formation in tempered cocoa butter during long-term storage*. European Journal of Lipid Science and Technology, 108(9):735–745, 2006.
- Sonwai, Sopark and Derick Rousseau: *Fat crystal growth and microstructural evolution in industrial milk chocolate*. Crystal Growth & Design, 8(9):3165–3174, 2008.
- Spieß, L., G. Teichert, R. Schwarzer, H. Behnken, and C. Genzel: *Moderne Röntgenbeugung*. Vieweg + Teubner, 2nd edition, 2009.
- Stapley, A. G. F., H. Tewkesbury, and P. J. Fryer: *The effects of shear and temperature history on the crystallization of chocolate*. Journal of the American Oil Chemists' Society Society, 76(6):677–685, 1999.
- Talbot, G.: *Industrial Chocolate Manufacturer and Use*, chapter Vegetable fats, pp. 415–433. Wiley-Blackwell, 2009.
- Tang, T.S., C.L. Chong, and M.S.A. Yusoff: *Malaysian palm kernel stearin, palm kernel olein and their fractionated products*. PORIM Technology, 16:1–19, 1995.
- Tarabukina, E., F. Jégou, J.-M. Haudin, P. Navard, and E. Peuvrel-Disdier: *Effect of shear on the rheology and crystallization of palm oil*. Journal of Food Science, 74(8):E405–E416, 2009.
- Tewkesbury, H., A. G. F. Stapley, and P. J. Fryer: *Modelling temperature distributions in cooling chocolate moulds*. Chemical Engineering Science, 55(16):3123–3132, 2000.

- Timms, R.E.: *Confectionery Fats Handbook*, volume 14 of *The Oily Press Lipid Library*. P.J. Barnes & Associates, Bridgewater, 1st edition, 2003a.
- Timms, R.E.: *Confectionery Fats Handbook*, chapter Applications, pp. 295–328. The Oily Press Lipid Library. P.J. Barnes & Associates, Bridgewater, 1st edition, 2003b.
- Tipler, P.A. and G. Mosca: *Physics for scientists and engineers*. Freeman, New York, 5th edition, 2003.
- Tscheuschner, H.D.: *Grundzüge der Lebensmittelverfahrenstechnik*. Behr's, Hamburg, 2004.
- Turnbull, D. and J.C. Fisher: *Rate of nucleation in condensed systems*. Journal of Chemical Physics, 17(1):71–73, 1949.
- Unruh, T., K. Westesen, P. Bosecke, P. Lindner, and M. H. J. Koch: *Self-assembly of triglyceride nanocrystals in suspension*. Langmuir, 18(5):1796–1800, 2002.
- Vaeck, S.V.: *Cacao butter and fat bloom*. The Manufacturing Confectioner, 40:35–74, 1960.
- VDI: *Einführung in die Lehre von der Wärmeübertragung*, chapter A, pp. 1–54. VDI, Düsseldorf, 10th edition, 2006.
- Vreeker, R., L. L. Hoekstra, D. C. Denboer, and W. G. M. Agterof: *The fractal nature of fat crystal networks*. Colloids and Surfaces, 65(2-3):185–189, 1992.
- Wagner, T.: *Kaltsprühen ein- und mehrphasiger Flüssigkeiten*. PhD thesis, ETH Nr. 12442, Food Process Engineering, ETH Zurich, 1997.
- Wagner, W.: *Wärmeübertragung*. Vogel, Würzburg, 2011.
- Walker, J.H.: *Industrial Chocolate Manufacturer and Use*, chapter Cold Forming Technologies. Wiley-Blackwell, 2009.
- Walzel, P.: *Ullmann's Encyclopedia of Industrial Chemistry*, chapter Spraying and Atomizing of Liquids. Wiley VCH Verlag GmbH & Co. KGaA, 2009.
- Walzel, Peter: *Zerstäuben von flüssigkeiten*. Chemie Ingenieur Technik, 62(12):983–994, 1990.
- Walzel, Peter: *Influence of the Spray Method on Product Quality and Morphology in Spray Drying*. Chemical Engineering & Technology, 34(7, SI):1039–1048, 2011.
- Wille, R. L. and E. S. Lutton: *Polymorphism of cocoa butter*. Journal of the American Oil Chemists' Society, 43(8):491, 1966.
- Windhab, E.: *Industrial Chocolate Manufacturer and Use*, chapter Tempering, p. 276. Wiley-Blackwell, Oxford, 2009.

- Windhab, E.J.: *New developments in crystallization processing*. Journal of Thermal Analysis and Calorimetry, 57(1):171–180, 1999.
- Windhab, E.J. and Y. Zeng: *Method of producing seed crystal suspension based on melted fat*. patent, W0 0072695, 12 2000.
- Windhab, E.J., L. Rolfes, and H. Rohenkohl: *Shear-induced effects on crystallization from molten fats*. Chemie Ingenieur Technik, 63(4):385–385, 1991.
- Wright, AJ, RW Hartel, SS Narine, and AG Marangoni: *The effect of minor components on milk fat crystallization*. Journal of the American Oil Chemists' Society, 77 (5):463–475, 2000.
- Yap, P. H., J. M. Deman, and L. Deman: *Polymorphism of palm oil and palm oil products*. Journal of the American Oil Chemists' Society, 66(5):693–697, 1989.
- Zeng, Y.: *Impf- und Scherkristallisation von Schokoladen*. PhD thesis, ETH Nr. 13798, Food Process Engineering, ETH Zurich, 2000.
- Zeng, Y.: *Tempering Continuous precrystallization of chocolate with seed cocoa butter crystal suspension*. The Manufacturing Confectioner, pp. 71–80, 2002.
- Ziegleder, G.: *Dsc-thermal analysis and kinetics of cocoa butter crystallization*. Fett Wissenschaft Technologie-Fat Science Technology, 92(12):481–485, 1990.
- Ziegleder, G and I. Schwingshandl: *Kinetics of fat migration within chocolate products. part iii: fat bloom*. Fett-Lipid, 100(9):411–415, 1998.
- Ziegleder, G., C. Moser, and J. Geier-Greguska: *Kinetics of fat migration within chocolate products. Part I: Principles and analytics*. Fett-Lipid, 98(6):196–199, 1996a.
- Ziegleder, G., C. Moser, and J. Geier-Greguska: *Kinetics of fat migration within chocolate products. Part II: Influence of storage temperature, diffusion coefficient, solid fat content*. Fett-Lipid, 98(7-8):253–256, 1996b.
- Ziegler, G.R.: *Crystallization and Solidification Properties of Lipids*, chapter Solidification processes in chocolate confectionary manufacture, pp. 215–224. AOCS Press, Champaign, IL, 2001.
- Zwietering, M.H., I. Jongenburger, F.M. Rombouts, and K. Vantriet: *Modeling of the bacterial-growth curve*. Applied and Environmental Microbiology, 56(6):1875–1881, 1990.



# Appendix



## A. Methods

Table A.1.: Overview of solidification kinetic evaluation of vegetable fats: non-seeded.

fat type	solidification temperature [°C ]					
	5	10	15	20	25	30
cocoa butter	x	x	x	x	-	-
cocos	x	x	x	x	-	-
palm kernel	x	x	x	x	x	-
palm kernel stearine	-	x	x	x	x	-
laurina	-	x	x	x	x	x
palm mid fraction	x	-	x	-	x	-
palm super stearine	25	30	35	40	50	55

Table A.2.: Overview of solidification kinetic evaluation of vegetable fats: seeded.

fat type	solidification temperature [°C ]					
	5	10	15	20	25	30
cocoa butter	-	x	x	x	x	-
palm kernel	x	x	x	x	-	-
palm kernel stearine	-	x	x	x	x	-
laurina	-	x	x	x	x	x
palm	x	x	x	x	-	-
palm mid fraction	x	-	x	x	-	-
palm super stearine	-	30	-	40	50	55

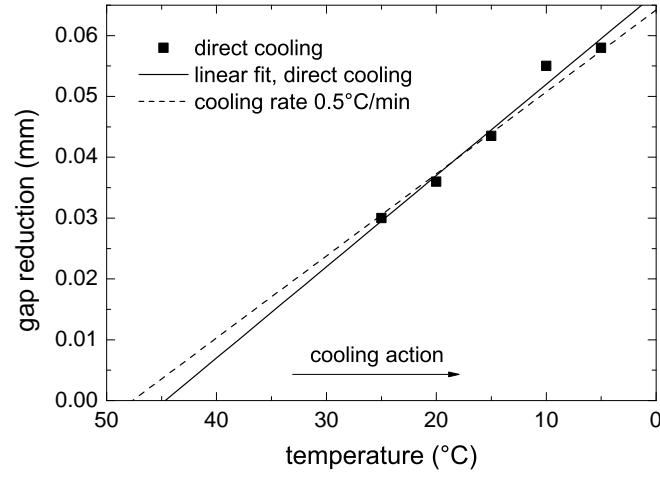


Figure A.1.: Contraction of the plate/plate-geometry due to temperature dilatation, comparison of gradual and direct cooling.

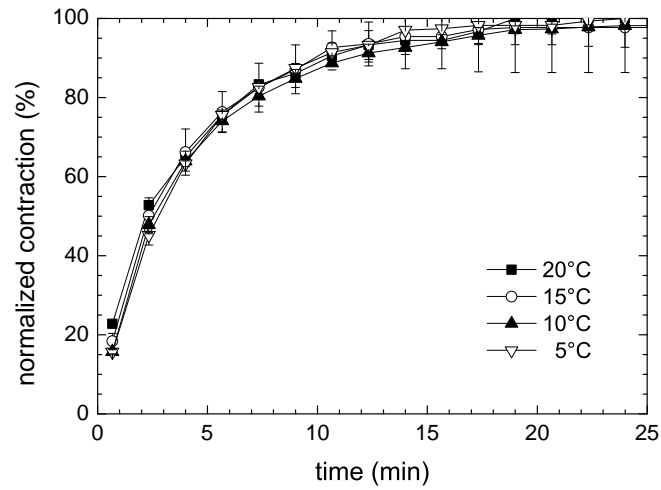


Figure A.2.: Normalized contraction development of plate/plate-geometry as function of cooling time, direct cooling from 50°C to set temperature.

Table A.3.: Fat types and temperatures tested for contraction analysis out of the melt.

fat	cooling temperature [°C ]							
	5	10	15	20	25	30	35	40
CB	x	x	x	x				
PM	x	x	x	x				
PKS		x	x	x	x			
LA		x	x	x	x			
PSS					x	x	x	x

Table A.4.: Fat types, start and cooling temperatures tested for contraction analysis of seeded melts,  $SFC_{seeded} = 0.5\%$ .

fat	seeding temperature [°C ]	cooling temperature [°C ]
CB	31.5	10, 15, 20
PM	27	10, 15, 20
PKS	30.5	15, 20
LA	36	15
PSS	60	40

Table A.5.: Fats and corresponding experimental parameters of series 1: temperature, shear rate.

vegetable fat	$T_{pre}$ [°C]	$T_{cryst}$ [°C]	$T_{rip}$ [°C]	$\dot{\gamma}$
palm kernel	38	23	26	10, 1000
		18		10, 1000
palm mid	47	27	35	10, 1000
		17		10, 1000
palm stearin	64	44	52	10, 1000
		34		10, 1000
palm super stearin	71	51	60.5	10, 1000
		41		10, 1000

Table A.6.: Fats and corresponding experimental parameters of series 2: temperatures, shear condition.

vegetable fat	$T_{\text{cryst},1}$ [°C]	$T_{\text{rip}}$ [°C]	$T_{\text{cryst},2}$ [°C]	condition
PM	20	-	-	static
	25	35	20	static
	25	35	20	dynamic
PM-PSS 10%	20	40	20	static
	25	35	20	static
	25	40	20	dynamic
PM-PSS 20%	20	35	-	static
	25	40	20	static
	25	40	20	dynamic
PO	20	40	-	static
	25	40	20	static
	25	40	20	dynamic
PO-HO 10%	25	35	-	static
	25	40	20	dynamic
PO-HO 20%	20	40	20	static
	25	40	20	static
	25	40	20	dynamic

## B. Results

Table B.1.: X-ray scattering peak values (d-spacing) of palm kernel fat and palm mid fraction, main polymorphic forms and polymorph modifications as detected during crystallization (series 1; see 4.1.2).

fat type	polymorph	long spacing nm	short spacing nm	condition
palm kernel	$\beta'$	3.43 (vs)	0.441 (w), 0.424 (m), 0.403 (w), 0.382 (s)	$T_{crist} = 23^\circ\text{C}$ , $\Delta T^a = -5^\circ\text{C}$ , $\dot{\gamma} = 10\text{ s}^{-1}$
		3.42 (m)	0.440 (m), 0.423 (m), 0.403 (w), 0.381 (vs)	$T_{crist} = 18^\circ\text{C}$ , $\Delta T = -10^\circ\text{C}$ , $\dot{\gamma} = 1000\text{ s}^{-1}$
	$\alpha$	4.70-4.74 (vs)	0.414 (vw)	$T_{crist} = 17^\circ\text{C}$ , $\Delta T = -20^\circ\text{C}$
	$\beta'_2$	4.25-4.28 (vs)	0.432-0.434 (m), 0.389 (m)	1 <sup>st</sup> crystallization, $T_{crist} = 17^\circ\text{C}$ , $\dot{\gamma} = 1000\text{ s}^{-1}$
palm mid fraction	$\beta'_1$	4.25-4.28 (vs)	0.432-0.434 (m), 0.385 (m)	1 <sup>st</sup> crystallization, $T_{crist} = 17^\circ\text{C}$ , $\dot{\gamma} = 10\text{ s}^{-1}$
	$\beta'_{\text{mix}}$	4.25-4.28 (vs)	0.432-0.434 (m), 0.383 (m)	$T_{rip} = 26^\circ\text{C}$ , $\Delta T = -2^\circ\text{C}$
		4.25-4.28 (vs)	0.432-0.434 (m), 0.379-0.388 (w)	2 <sup>nd</sup> crystallization, $T_{crist} = 17^\circ\text{C}$

<sup>a</sup> supercooling temperature difference

peak intensity: vs - very strong, s - strong, m - medium, w - weak, vw - very weak



Table B.2.: X-ray scattering peak values (d-spacing) of palm stearin fat, main polymorphic forms and polymorph modifications as detected during crystallization procedure (series 1; see 4.1.2).

polymorph	long spacing nm	short spacing nm	condition
$\alpha$	4.56-4.66 (vs)	0.414-0.415 (vw)	$T_{cryst} = 34^\circ\text{C}$ , $\Delta T^a = -20^\circ\text{C}$
$\beta'_{\text{meta}}$	4.18 (vs)	0.436 (w), 0.429 (w), 0.422 (m), 0.413 (w), 0.405 (w), 0.383 (s)	1 <sup>st</sup> crystallization, $T_{cryst} = 44^\circ\text{C}$ , $\Delta T = -10^\circ\text{C}$ , $\dot{\gamma} = 1000 \text{ s}^{-1}$
$\beta'$	4.2 (vs)	0.430 (w), 0.419 (m), 0.383 (w)	1 <sup>st</sup> crystallization, $T_{cryst} = 34^\circ\text{C}$
$\beta_1$	4.05-4.06 (vs), 3.96-3.98 (vs)	0.459 (s), 0.454 (s), 0.444 (w), 0.388 (s), 0.377 (m), 0.364 (w)	$T_{rip} = 52^\circ\text{C}$ , $\Delta T = -2^\circ\text{C}$
$\beta_{\text{mix}}$	4.05-4.06 (vs), 3.96-3.98 (vs)	0.458 (s), 0.454 (s), 0.443 (w), 0.390 (s), 0.379-0.380 (m), 0.366 (w)	2 <sup>nd</sup> crystallization, $T_{cryst} = 44^\circ\text{C}$ , $\dot{\gamma} = 1000 \text{ s}^{-1}$
	4.05-4.06 (vs), 3.96-3.98 (vs)	0.459 (s), 0.454 (s), 0.444 (w), 0.389 (m), 0.387 (m), 0.377 (m), 0.373 (m), 0.367-0.368 (vw)	2 <sup>nd</sup> crystallization, $T_{cryst} = 44^\circ\text{C}$ , $\dot{\gamma} = 10 \text{ s}^{-1}$
	4.05-4.06 (s), 3.96-3.98 (s)	0.458 (s), 0.454 (s), 0.444 (w), 0.391 (m), 0.387 (m), 0.379 (m), 0.374 (m), 0.367-0.368 (vw)	2 <sup>nd</sup> crystallization, $T_{cryst} = 34^\circ\text{C}$ , $\dot{\gamma} = 1000 \text{ s}^{-1}$

<sup>a</sup> supercooling temperature difference

peak intensity: vs - very strong, s - strong, m - medium, w - weak, vw - very weak

Table B.3.: X-ray scattering peak values (d-spacing) of palm super stearin fat, main polymorphic forms and polymorph modifications as detected during crystallization procedure (series 1; see 4.1.2).

polymorph	long spacing nm	short spacing nm	condition
$\alpha$	4.55 (vs)	0.415 (vw)	$T_{crist} = 41^\circ\text{C}$ , $\Delta T^a = -20^\circ\text{C}$
$\beta'$	4.19-4.20 (vs)	0.430 (w), 0.419-0.420 (m), 0.383 (m)	1 <sup>st</sup> crystallization, $T_{crist} = 41^\circ\text{C}$
$\beta_2$	4.03-4.06(vs), 3.95 (vs)	0.455 (s), 0.451 (s), 0.440 (w), 0.392 (s), 0.381 (m), 0.368 (w)	1 <sup>st</sup> crystallization, $T_{crist} = 51^\circ\text{C}$ , $\Delta T = -10^\circ\text{C}$ , $\dot{\gamma} = 1000\text{ s}^{-1}$
$\beta_1$	4.03-4.06 (vs), 3.95 (vs)	0.459 (s), 0.454 (s), 0.444 (w), 0.387 (s), 0.376 (m), 0.362 (w)	$T_{rip} = 60.5^\circ\text{C}$ , $\Delta T = -0.5^\circ\text{C}$
$\beta_{mix}$	4.03-4.06 (vs), 3.95 (vs)	0.458 (s), 0.454 (s), 0.444 (w), 0.389 (s), 0.377 (m), 0.364 (w)	2 <sup>nd</sup> crystallization, $T_{crist} = 51^\circ\text{C}$
	4.03-4.06 (vs), 3.95 (vs)	0.458 (s), 0.454 (s), 0.443 (w), 0.390 (s), 0.386 (m), 0.379 (m), 0.373 (w), 0.368 (w), 0.361 (vw)	2 <sup>nd</sup> crystallization $T_{crist} = 41^\circ\text{C}$

<sup>a</sup> supercooling temperature difference

peak intensity: vs - very strong, s - strong, m - medium, w - weak, vw - very weak

Table B.4.: Parameters of Avrami's Approximate Equation applied on the solidification curves of several fats out of the melt by variation of cooling temperature,  $R_{ave} \geq 98.5\%$

fat	temperature °C	supercooling temp. °C	$t_0$ min	$SFC_{max}$ -	$k$ $min^{-n}$	$m$ -
CB	5	29	0.7	0.90	0.159	1.26
	10	24	1.3	0.86	0.121	1.04
	15	19	1.2	0.89	0.032	1.13
	20 (a) *	14	5.4	0.09	0.147	1.02
	20 (b)	14	-	0.59	0.001	2.03
PM	5 (a)	39	0.7	0.36	0.152	1.02
	5 (b)	39	-	0.31	0.030	1.21
	15 (a)	29	1.7	0.09	0.376	1.32
	15 (b)	29	-	0.46	0.010	1.13
PSS	25	36	1.0	0.77	0.232	1.34
	30	31	0.9	0.72	0.131	1.49
	35	26	1.6	0.66	0.076	1.69
	40 *	21	2.3	0.62	0.013	2.36
	50	11	6.7	0.41	0.091	1.25
	55	6	28.4	0.26	0.014	1.36
CO	5	20	2.7	0.74	0.052	1.75
	10 *	15	5.6	0.58	0.028	1.90
	15	10	9.2	0.52	0.013	1.60
PK	5	26	2.0	0.65	0.132	1.52
	10	21	4.5	0.53	0.205	1.20
	15 *	16	7.0	0.45	0.003	2.70
PKS	10	25	0.9	0.81	0.058	1.87
	15	20	1.7	0.70	0.038	1.83
	20 *	15	7.9	0.64	0.021	1.83
	25	10	8.0	0.35	0.015	1.86
LA	10	30	1.6	0.80	0.150	1.29
	15	25	1.7	0.75	0.082	1.49
	20 *	20	5.8	0.65	0.022	1.83
	25	15	10.0	0.50	0.007	1.74

\* - minimum temperature at which crystallization starts after reaching set temperature.

Table B.5.: Parameters of Avrami's Approximate Equation applied on the solidification curves of several seeded fats by variation of cooling temperature,  $R_{ave} \geq 98\%$

fat	temperature °C	supercooling temp. min	t <sub>ind</sub> -	SFC <sub>max</sub> min <sup>-n</sup>	k -	m
CB	10	24	0	0.83	0.070	1.35
	15	19	0	0.77	0.075	1.16
	20	14	0	0.70	0.073	1.01
	25 *	9	0.7	0.52	0.007	1.28
PM	5 (a)	39	0	0.34	0.225	0.76
	5(b)	39		0.35	0.007	1.55
	15 (a)	29	0	0.10	0.336	0.96
	15 (b)	29		0.30	0.020	1.06
	20	24	0	0.13	0.050	0.99
PSS	31	30	0	0.68	0.136	1.73
	40	21	0	0.56	0.053	1.83
	50	11	0	0.41	0.023	1.76
	55	6	0	0.25	0.046	1.13
PK	5	26	0	0.62	0.160	1.43
	10	21	0	0.55	0.111	1.47
	15	16	0	0.45	0.085	1.42
	20	11	0.48	0.30	0.071	1.26
PKS	10	25	0	0.80	0.143	1.51
	15	20	0	0.75	0.111	1.42
	20	15	0	0.65	0.085	1.31
	25	10	0	0.49	0.047	1.27
LA	10	27	0	0.81	0.195	1.38
	15	22	0	0.75	0.106	1.75
	20	17	0	0.64	0.073	1.53
	25	12	0	0.47	0.061	1.36
	30	7	0	0.23	0.089	1.08

\* - minimum temperature at which crystallization starts after reaching set temperature.

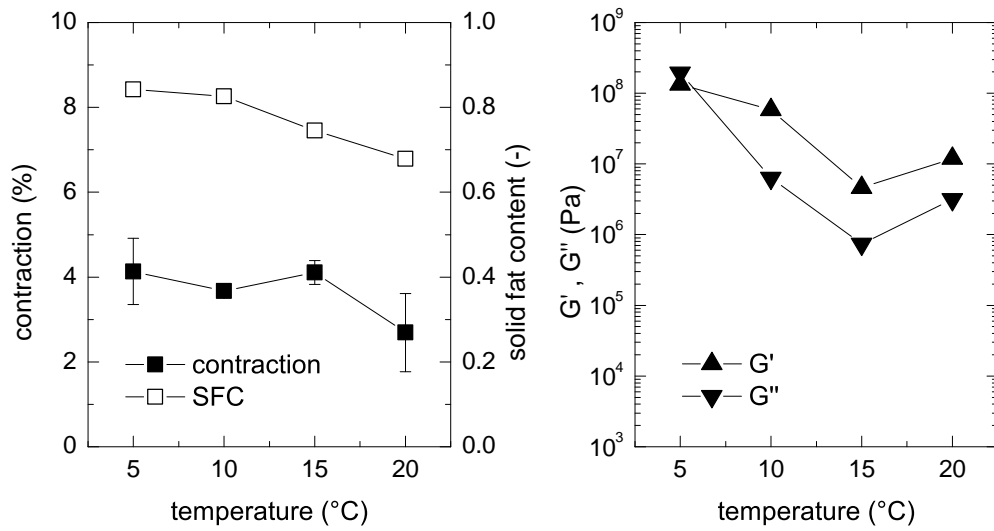


Figure B.1.: Final contraction, solid fat content and structure resistance of palmkernel stearin by variation of cooling temperature.

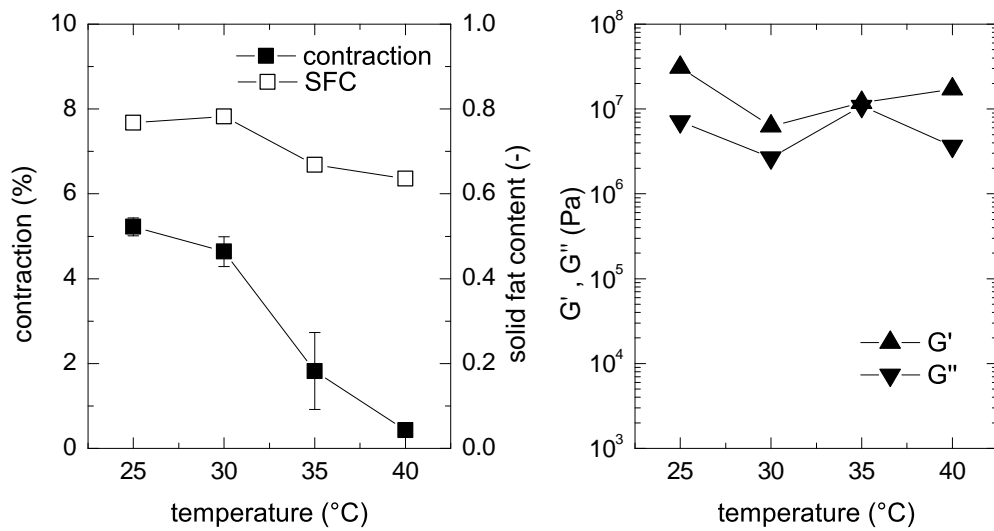


Figure B.2.: Final contraction, solid fat content and structure resistance of palm super stearin by variation of cooling temperature.

## B. Results

Table B.6.: Cooling parameter combinations applied on praline production by air stream cooling including reference trials.

confectionery masses	air velocity m/s	cooling temperature °C		
		12	7	-10
seeded chocolate - seeded filling	1	x	x	x
	3	x	-	-
	6	x	x	x
seeded chocolate - non-seeded filling	1	x	-	-
seeded chocolate	1	x	x	x

Table B.7.: Characteristic inflection point values of real-time tempercurves for praline filling mass by variation of process parameters.

$T_{\text{cool}}$ °C	$v_{\text{cool}}$ m/s	sensor no.	$T_{\text{inf}}$ °C	SD $T_{\text{inf}}$ °C	$s_{\text{inf}}$ °C/min	SD $s_{\text{inf}}$ °C/min	$T_3$ for $t_{\text{inf},1}$ °C
12	1	1	22.2	0.3	0.13	0.10	20.2
		2	22.1	0.3	0.06	0.13	
		3	20.7	0.3	-0.19	0.11	
12	3	1	21.8	0.4	0.05	0.3	19.1
		2	21.7	0.3	-0.07	0.22	
		3	19.8	0.5	-0.34	0.12	
12	6	1	21.3	0.3	0.18	0.14	18.2
		2	21.3	0.1	0.04	0.10	
		3	19.2	0.4	-0.32	0.10	
7	1	1	21.7	0.3	0.07	0.15	18.7
		2	21.6	0.4	-0.02	0.18	
		3	19.8	0.6	-0.38	0.13	
7	6	1	20.0	0.2	0.29	0.26	15.7
		2	19.9	0.1	-0.16	0.30	
		3	17.2	0.2	-0.62	0.32	
-10	1	1	19.6	0.2	-0.14	0.16	14.1
		2	19.8	0.2	-0.50	0.15	
		3	17.1	0.2	-1.17	0.11	
-10	6	1	15.2	0.4	0.97	0.15	7.0
		2	14.2	1.0	0.23	0.43	
		3	7.1	1.5	-1.42	0.31	

Table B.8.: Characteristic inflection point values of real-time tempercurves for praline shell mass by variation of process parameters.

$T_{\text{cool}}$ °C	$v_{\text{cool}}$ m/s	$T_{\text{inf}}$ °C	SD $T_{\text{inf}}$ °C	$s_{\text{inf}}$ °C/min	SD $s_{\text{inf}}$ °C/min
12	1	23.8	0.1	-0.50	0.08
12	3	22.8	0.2	-0.64	0.17
12	6	22.0	0.2	-0.63	0.22
7	1	23.11	0.3	-0.7	0.17
7	6	21.1	0.30	-0.94	0.40
-10	1	20.8	0.54	-1.23	0.39
-10	6	15.5	0.87	-2.49	0.26

Table B.9.: Characteristic inflection point values of real-time tempercurves for praline shaped plain chocolate by variation of cooling temperature,  $v = 1$  m/s.

$T_{\text{cool}}$ °C	sensor no.	$T_{\text{inf}}$ °C	SD $T_{\text{inf}}$ °C	$s_{\text{inf}}$ °C/min	SD $s_{\text{inf}}$ °C/min	$T_3$ for $t_{\text{inf}}$ (sensor 1) °C
12	1	25.1	0.3	0.08	0.03	23.6
	2	25.0	0.2	0.08	0.01	
	3	23.9	0.1	0.0	0.05	
7	1	24.7	0.0	0.11	0.13	22.7
	2	24.6	0.0	0.13	0.08	
	3	23.2	0.0	-0.10	0.03	
-10	1	22.6	0.0	0.08	0.02	18.8
	2	22.7	0.1	-0.11	0.06	
	3	21.3	0.1	-0.34	0.04	

Table B.10.: Process parameter variation of cocoa butter prilling investigations, S1: standard parameter.

no.	cocoa source	cooling temperature [°C]	flow rate [ml/min]	air pressure [bar]
S0	<b>melt</b>	-30	180	2
<b>S1</b>	<b>slurry</b>	<b>-30</b>	<b>180</b>	<b>2</b>
S2	suspension	<b>-10</b>	180	2
S3	suspension	<b>-20</b>	180	2
S4	suspension	<b>-40</b>	180	2
S5	suspension	<b>-50</b>	180	2
S6	suspension	<b>-60</b>	180	2
S14	suspension	<b>-70</b>	180	2
D4	suspension	-30	<b>45</b>	2
D3	suspension	-30	<b>90</b>	2
S7	suspension	-30	<b>300</b>	2
S8	suspension	-30	<b>470</b>	2
S9	suspension	-30	<b>540</b>	2
S10	suspension	-30	180	<b>0.5</b>
S11	suspension	-30	180	<b>3</b>
S12	suspension	-30	180	<b>4</b>
S13	suspension	-30	180	<b>6</b>



# Curriculum Vitae

Daniel Ehlers



## Personal Data

date of birth 9<sup>th</sup> April 1982  
place of birth Meppen, Germany  
citizen of Germany

## Education and Work Experience

- 2008-2013 PhD student and research assistant at the Laboratory of Food Process Engineering; IFNH, ETH Zurich, Switzerland
- 2002-2008 Diploma studies in Biological Engineering, Technical University of Karlsruhe (today: Karlsruhe Institute of Technology, KIT), Germany  
  
Major fields of study: Food Process Engineering, Technical Refrigeration Engineering, Thermal Process Engineering  
  
Semester thesis abroad (five months), Schulich School of Engineering, University of Alberta, Calgary, Canada  
  
Student research assistant (two years), Technical University of Karlsruhe
- 2001-2002 Emergency Medical Technician, German Red Cross, Uelzen, Germany
- 2001 Abitur, Herzog-Ernst-Gymnasium, Uelzen, Germany